

11-2011

Development of Alternative Wood-Post MGS Approach Guardrail Transition

Scott K. Rosenbaugh

University of Nebraska-Lincoln, srosenbaugh2@unl.edu

Kevin D. Schrum

University of Nebraska-Lincoln, kevin.schrum@huskers.unl.edu

Ronald K. Faller

University of Nebraska - Lincoln, rfaller1@unl.edu

Karla A. Lechtenberg

University of Nebraska - Lincoln, kpolivka2@unl.edu

Dean L. Sicking

University of Nebraska - Lincoln, dsicking1@unl.edu

See next page for additional authors

Follow this and additional works at: <http://digitalcommons.unl.edu/ndor>



Part of the [Transportation Engineering Commons](#)

Rosenbaugh, Scott K.; Schrum, Kevin D.; Faller, Ronald K.; Lechtenberg, Karla A.; Sicking, Dean L.; and Reid, John D., "Development of Alternative Wood-Post MGS Approach Guardrail Transition" (2011). *Nebraska Department of Transportation Research Reports*. 139.

<http://digitalcommons.unl.edu/ndor/139>

This Article is brought to you for free and open access by the Nebraska LTAP at DigitalCommons@University of Nebraska - Lincoln. It has been accepted for inclusion in Nebraska Department of Transportation Research Reports by an authorized administrator of DigitalCommons@University of Nebraska - Lincoln.

Authors

Scott K. Rosenbaugh, Kevin D. Schrum, Ronald K. Faller, Karla A. Lechtenberg, Dean L. Sicking, and John D. Reid



TESTING CERT # 2937.01

*Midwest States Regional Pooled Fund Research Program
Fiscal Year 2009 (Year 19)
Research Project Number TPF-5(193)
NDOR Sponsoring Agency Code RFP-09-03*

DEVELOPMENT OF ALTERNATIVE WOOD-POST MGS APPROACH GUARDRAIL TRANSITION

Submitted by

Scott K. Rosenbaugh M.S.C.E., E.I.T.
Research Associate Engineer

Kevin D. Schrum, B.S.C.E., E.I.T.
Graduate Research Assistant

Ronald K. Faller, Ph.D., P.E.
Research Assistant Professor

Karla A. Lechtenberg, M.S.M.E., E.I.T.
Research Associate Engineer

Dean L. Sicking, Ph.D., P.E.
Professor and MwRSF Director

John D. Reid, Ph.D.
Professor

MIDWEST ROADSIDE SAFETY FACILITY

Nebraska Transportation Center
University of Nebraska-Lincoln
2200 Vine Street
130 Whittier Research Center
Lincoln, Nebraska 68583-0583
(402) 472-0965

Submitted to

MIDWEST STATES REGIONAL POOLED FUND PROGRAM

Nebraska Department of Roads
1500 Nebraska Highway 2
Lincoln, Nebraska 68502

MwRSF Research Report No. TRP-03-243-11

November 28, 2011

TECHNICAL REPORT DOCUMENTATION PAGE

1. Report No. TRP-03-243-11	2.	3. Recipient's Accession No.	
4. Title and Subtitle Development of Alternative Wood-Post MGS Approach Guardrail Transition		5. Report Date November 28, 2011	
		6.	
7. Author(s) Rosenbaugh, S.K., Schrum, K.D., Faller, R.K., Lechtenberg, K.A., Sicking, D.L., and Reid, J.D.		8. Performing Organization Report No. TRP-03-243-11	
9. Performing Organization Name and Address Midwest Roadside Safety Facility (MwRSF) Nebraska Transportation Center University of Nebraska-Lincoln 2200 Vine Street 130 Whittier Research Center Lincoln, Nebraska 68583-0853		10. Project/Task/Work Unit No.	
		11. Contract © or Grant (G) No. TPF-5(193)	
12. Sponsoring Organization Name and Address Midwest States Regional Pooled Fund Program Nebraska Department of Roads 1500 Nebraska Highway 2 Lincoln, Nebraska 68502		13. Type of Report and Period Covered Final Report: 2009 – 2011	
		14. Sponsoring Agency Code RFPF-09-03	
15. Supplementary Notes Prepared in cooperation with U.S. Department of Transportation, Federal Highway Administration.			
16. Abstract (Limit: 200 words) <p>The objective of this study was to develop a wood-post MGS approach transition system that is equivalent to the simplified steel-post, MGS stiffness transition recently developed at the Midwest Roadside Safety Facility. An extensive literature review was conducted on wood and steel post performance comparisons through either dynamic component testing or full-scale crash testing. This review concluded that 6-ft (1.8-m) long W6x9 (W152x13.4) steel posts and 6-in. x 8-in. (152-cm x 203-mm) wood posts provide similar force vs. deflection characteristics during rotation through soil. However, no such data was available concerning dynamic testing on larger transition posts located adjacent to the bridge rail. Therefore, a dynamic testing program was undertaken to evaluate W6x15 (W152x22.3) steel posts and various sizes of wood posts. At the conclusion of the testing program, an 8-in. x 10-in. (203-mm x 254-mm) wood post was chosen as the best equivalent to the W6x15 (W152x22.3) steel post due to similar post-soil resistances as well as a reduced propensity to fracture when compared to smaller post cross sections.</p> <p>A BARRIER VII computer model was then used to evaluate the wood-post stiffness transition against a calibrated model of the original steel post transition system. When subjected to identical impacts, the wood-post system was shown to reduce system deflections, vehicle pocketing angles, and the potential for wheel snag. Therefore, the wood-post MGS stiffness transition was recommended for use as a MASH TL-3 safety barrier.</p>			
17. Document Analysis/Descriptors Highway Safety, Dynamic Test, Bogie Tests, Roadside Appurtenances, MASH, Wood Post, Approach Guardrail Transition, MGS		18. Availability Statement No restrictions. Document available from: National Technical Information Services, Springfield, Virginia 22161	
19. Security Class (this report) Unclassified	20. Security Class (this page) Unclassified	21. No. of Pages 158	22. Price

DISCLAIMER STATEMENT

This report was completed in part through funding from the Federal Highway Administration, U.S. Department of Transportation. The contents of this report reflect the views and opinions of the authors who are responsible for the facts and the accuracy of the data presented herein. The contents do not necessarily reflect the official views or policies of the state highway departments participating in the Midwest States Regional Pooled Fund Program nor the Federal Highway Administration, U.S. Department of Transportation. This report does not constitute a standard, specification, regulation, product endorsement, or an endorsement of manufacturers.

UNCERTAINTY OF MEASUREMENT STATEMENT

The Midwest Roadside Safety Facility (MwRSF) has determined the uncertainty of measurements for several parameters involved in standard full-scale crash testing and non-standard testing of roadside safety features. Information regarding the uncertainty of measurements for critical parameters is available upon request by the sponsor and the Federal Highway Administration.

The Independent Approving Authority (IAA) for the data contained herein was Mr. Curt Meyer, Research Associate Engineer.

ACKNOWLEDGEMENTS

The authors wish to acknowledge several sources that made a contribution to this project:

(1) the Midwest States Regional Pooled Fund Program funded by the Illinois Department of Transportation, Iowa Department of Transportation, Kansas Department of Transportation, Minnesota Department of Transportation, Missouri Department of Transportation, Nebraska Department of Roads, Ohio Department of Transportation, South Dakota Department of Transportation, Wisconsin Department of Transportation, and Wyoming Department of Transportation for sponsoring this project; and (2) MwRSF personnel for conducting the dynamic tests.

Acknowledgement is also given to the following individuals who made a contribution to the completion of this research project.

Midwest Roadside Safety Facility

J.C. Holloway, M.S.C.E., E.I.T., Test Site Manager
R.W. Bielenberg, M.S.M.E., E.I.T., Research Associate Engineer
C.L. Meyer, B.S.M.E., E.I.T., Research Associate Engineer
A.T. Russell, B.S.B.A., Shop Manager
K.L. Krenk, B.S.M.A., Maintenance Mechanic
A.T. McMaster, Former Laboratory Mechanic
Undergraduate and Graduate Research Assistants

Illinois Department of Transportation

David Piper, P.E., Highway Policy Engineer

Iowa Department of Transportation

David Little, P.E., Assistant District Engineer
Deanna Maifield, P.E., Methods Engineer
Chris Poole, P.E. Litigation/Roadside Safety Engineer

Kansas Department of Transportation

Ron Seitz, P.E., Bureau Chief
Rod Lacy, P.E., Metro Engineer
Scott King, P.E., Road Design Leader

Minnesota Department of Transportation

Michael Elle, P.E., Design Standard Engineer

Missouri Department of Transportation

Joseph G. Jones, P.E., Engineering Policy Administrator

Nebraska Department of Roads

Amy Starr, P.E., Research Engineer
Phil TenHulzen, P.E., Design Standards Engineer
Jodi Gibson, Research Coordinator

Ohio Department of Transportation

Dean Focke, P.E., Road Safety Engineer (Retired)
Michael Blin, P.E., Standards and Geometrics Engineer

South Dakota Department of Transportation

David Huft, Research Engineer
Bernie Clocksin, Lead Project Engineer

Wisconsin Department of Transportation

Jerry Zogg, P.E., Chief Roadway Standards Engineer
John Bridwell, P.E., Standards Development Engineer
Erik Emerson, P.E., Standards Development Engineer

Wyoming Department of Transportation

William Wilson, P.E., Architectural and Highway Standards Engineer

Federal Highway Administration

John Perry, P.E., Nebraska Division Office
Danny Briggs, Nebraska Division Office

TABLE OF CONTENTS

TECHNICAL REPORT DOCUMENTATION PAGE i

DISCLAIMER STATEMENT ii

UNCERTAINTY OF MEASUREMENT STATEMENT ii

ACKNOWLEDGEMENTS iii

TABLE OF CONTENTS v

LIST OF FIGURES vii

LIST OF TABLES x

1 INTRODUCTION 1

 1.1 Background 1

 1.2 Objective 2

 1.3 Research Approach 2

2 WOOD POST EQUIVALENT FOR THE 6-FOOT (1.8-METER) LONG W6x9 (W152x13.4) POST 3

 2.1 Dynamic Component Testing 3

 2.2 Full-Scale Testing 6

 2.3 Conclusions 7

3 COMPONENT TEST CONDITIONS 8

 3.1 Purpose 8

 3.2 Scope 8

 3.3 Weather Conditions 9

 3.4 Equipment and Instrumentation 9

 3.4.1 Bogie 9

 3.4.2 Accelerometers 10

 3.4.3 Pressure Tape Switches 12

 3.4.4 Digital Cameras 12

 3.5 End of Test Determination 18

 3.6 Data Processing 19

4 COMPONENT TESTING RESULTS AND DISCUSSION 20

 4.1 Results 20

 4.1.1 Test No. MGSATB-1 21

 4.1.2 Test No. MGSATB-2 23

 4.1.3 Test No. MGSATB-3 25

 4.1.4 Test No. MGSATB-4 27

 4.1.5 Test No. MGSATB-5 29

 4.1.6 Test No. MGSATB-6 31

 4.1.7 Test No. MGSATB-7 33

4.1.8 Test No. MGSATB-8.....	35
4.1.9 Test No. MGSATB-9.....	37
4.1.10 Test No. MGSATB-10.....	39
4.1.11 Test No. MGSATB-11.....	41
4.1.12 Test No. MGSATB-12.....	43
4.1.13 Test No. MGSATB-13.....	45
4.1.14 Test No. MGSATB-14.....	47
4.1.15 Test No. MGSATB-15.....	49
4.1.16 Test No. MGSATB-16.....	51
4.1.17 Test No. MGSATB-17.....	53
4.1.18 Test No. MGSATB-18.....	55
4.1.19 Test No. MGSATB-19.....	57
4.1.20 Test No. MGSATB-20.....	59
4.2 Discussion.....	61
4.2.1 W6x15 (W152x22.3) Steel Posts, 7 ft (2.1 m) Long.....	64
4.2.2 8-in. x 8-in. (203 mm x 203 mm) Wood Posts, 7 ft (2.1 m) Long.....	65
4.2.3 Wood 8-in. x 10-in. and 10-in. x 10-in. Posts, 7 ft Long.....	66
4.2.4 6-in. x 10-in. (152-mm x 254-mm) Wood Posts, 7 ft (2.1 m) Long.....	68
4.2.5 8-in. x 10-in. (203-mm x 254-mm) Wood Posts, 6.5 ft (2.0 m) Long.....	69
4.3 Bogie Testing Conclusions.....	70
5 BARRIER VII ANALYSIS OF WOOD POST SYSTEM.....	74
5.1 Calibration of Steel Post Transition Model.....	74
5.2 Wood-Post Transition Model.....	75
5.2.1 6-in. x 8-in. (152-mm x 203-mm) Wood Post, 6 ft (1.8 m) Long.....	75
5.2.2 8 in. x 10 in. (203-mm x 254-mm) Wood Post, 6.5 (2.0 m) ft Long.....	76
5.2.3 General Comments.....	77
5.3 Evaluation Criteria.....	78
5.4 BARRIER VII Analysis and Results.....	78
6 DESIGN DRAWINGS.....	81
7 SUMMARY, CONCLUSIONS, AND RECOMMENDATIONS.....	88
8 STIFFNESS TRANSITION ADAPTATION RECOMMENDATIONS.....	91
8.1 Adaptation for Transition to TL-4 Glulam Bridge Rail.....	91
8.2 Adaptation for Iowa Transition to New Jersey Safety Shape Concrete Parapet.....	92
8.3 Adaptations to Other Thrie Beam Transitions.....	92
9 REFERENCES.....	95
10 APPENDICES.....	98
Appendix A. Soil Batch Sieve Analyses.....	99
Appendix B. EDR-3 Equivalency to Approved Transducer.....	101
Appendix C. Material Specifications.....	106
Appendix D. Bogie Test Results.....	107
Appendix E. BARRIER VII Input Decks.....	146
Appendix F. Tabulated BARRIER VII Simulation Results.....	155

LIST OF FIGURES

Figure 1. W6x16 (W152x23.8) Steel and 6-in. x 8-in. (152-mmx203-mm) Wood Posts in Highly Compacted Soil.....	6
Figure 2. Bogie Testing Setup	14
Figure 3. Rigid Frame Bogie on Pipe Guide Track System	17
Figure 4. Rigid Frame Bogie on B-beam Guide Track System.....	17
Figure 5. Force vs. Deflection and Energy vs. Deflection, Test No. MGSATB-1	21
Figure 6. Time Sequential and Post-Impact Photographs, Test No. MGSATB-1	22
Figure 7. Force vs. Deflection and Energy vs. Deflection, Test No. MGSATB-2	23
Figure 8. Time Sequential and Post-Impact Photographs, Test No. MGSATB-2	24
Figure 9. Force vs. Deflection and Energy vs. Deflection, Test No. MGSATB-3	25
Figure 10. Time Sequential and Post-Impact Photographs, Test No. MGSATB-3	26
Figure 11. Force vs. Deflection and Energy vs. Deflection, Test No. MGSATB-4	27
Figure 12. Time Sequential and Post-Impact Photographs, Test No. MGSATB-4.....	28
Figure 13. Force vs. Deflection and Energy vs. Deflection, Test No. MGSATB-5	29
Figure 14. Time Sequential and Post-Impact Photographs, Test No. MGSATB-5	30
Figure 15. Force vs. Deflection and Energy vs. Deflection, Test No. MGSATB-6	31
Figure 16. Time Sequential and Post-Impact Photographs, Test No. MGSATB-6.....	32
Figure 17. Force vs. Deflection and Energy vs. Deflection, Test No. MGSATB-7	33
Figure 18. Time Sequential and Post-Impact Photographs, Test No. MGSATB-7	34
Figure 19. Force vs. Deflection and Energy vs. Deflection, Test No. MGSATB-8	35
Figure 20. Time Sequential and Post-Impact Photographs, Test No. MGSATB-8.....	36
Figure 21. Force vs. Deflection and Energy vs. Deflection, Test No. MGSATB-9	37
Figure 22. Time Sequential and Post-Impact Photographs, Test No. MGSATB-9.....	38
Figure 23. Force vs. Deflection and Energy vs. Deflection, Test No. MGSATB-10	39
Figure 24. Time Sequential and Post-Impact Photographs, Test No. MGSATB-10.....	40
Figure 25. Force vs. Deflection and Energy vs. Deflection, Test No. MGSATB-11	41
Figure 26. Time Sequential and Post-Impact Photographs, Test No. MGSATB-11	42
Figure 27. Force vs. Deflection and Energy vs. Deflection, Test No. MGSATB-12	43
Figure 28. Time Sequential and Post-Impact Photographs, Test No. MGSATB-12	44
Figure 29. Force vs. Deflection and Energy vs. Deflection, Test No. MGSATB-13	45
Figure 30. Time Sequential and Post-Impact Photographs, Test No. MGSATB-13	46
Figure 31. Force vs. Deflection and Energy vs. Deflection, Test No. MGSATB-14	47
Figure 32. Time Sequential and Post-Impact Photographs, Test No. MGSATB-14.....	48
Figure 33. Force vs. Deflection and Energy vs. Deflection, Test No. MGSATB-15	49
Figure 34. Time Sequential and Post-Impact Photographs, Test No. MGSATB-15	50
Figure 35. Force vs. Deflection and Energy vs. Deflection, Test No. MGSATB-16	51
Figure 36. Time Sequential and Post-Impact Photographs, Test No. MGSATB-16.....	52
Figure 37. Force vs. Deflection and Energy vs. Deflection, Test No. MGSATB-17	53
Figure 38. Time Sequential and Post-Impact Photographs, Test No. MGSATB-17	54
Figure 39. Force vs. Deflection and Energy vs. Deflection, Test No. MGSATB-18	55
Figure 40. Time Sequential and Post-Impact Photographs, Test No. MGSATB-18.....	56
Figure 41. Force vs. Deflection and Energy vs. Deflection, Test No. MGSATB-19	57
Figure 42. Time Sequential and Post-Impact Photographs, Test No. MGSATB-19.....	58
Figure 43. Force vs. Deflection and Energy vs. Deflection, Test No. MGSATB-20	59
Figure 44. Time Sequential and Post-Impact Photographs, Test No. MGSATB-20.....	60

Figure 45. Force vs. Deflection Comparison, 7-ft (2.1-m) Long W6x15 (W152x22.3) Steel Posts65

Figure 46. Force vs. Deflection Comparison, 7-ft (2.1-m) Long 8-in. x 8-in. (203-mm x 203-mm) Wood Posts.....66

Figure 47. Force vs. Deflection Comparison, 7-ft (2.1-m) 8-in. x 10-in (203-mm x 254-mm). and 10-in. x 10-in. (254-mm x 254-mm) Wood Posts.....68

Figure 48. Force vs. Deflection Comparison, 7-ft (2.1-m) Long 6-in. x 10-in. (152-mm x 254-mm) Wood Posts.....69

Figure 49. Force vs. Deflection Comparison, 6.5-ft (2.0-m) Long 8-in. x 10-in. (203-mm x 254-mm) Wood Posts70

Figure 50. Design Details, Wood Post MGS Stiffness Transition System Layout.....82

Figure 51. Post Nos. 3 through 15 Rail Attachment Details.....83

Figure 52. Post Nos. 16 through 18 Design Details.....84

Figure 53. Post Nos. 3-15 Design Details.....85

Figure 54. Rail Sections Details.....86

Figure 55. Bill of Materials.....87

Figure 56. Approach Transition to TL-4 Glulam Bridge Rail [13-16].....93

Figure 57. Approach Iowa Transition to NJ Shape Concrete Parapet [17-20].....94

Figure A-1. Sieve Analysis for MGSATB-1 through MGSATB-4.....99

Figure A-2. Sieve Analysis for MGSATB-5 through MGSATB-8.....99

Figure A-3. Sieve Analysis for MGSATB-9 Through MGSATB-17.....100

Figure A-4. Sieve Analysis for MGSATB-18 Through MGSATB-20.....100

Figure B-1. EDR-3 and DTS Equivalency Comparisons, Test No. MGSATB-18.....103

Figure B-2. EDR-3 and DTS Equivalency Comparisons, Test No. DB-1.....104

Figure B-3. EDR-3 and DTS Equivalency Comparisons, Test No. OCF-6105

Figure C-1. Material Test Report for W6x15 (W152x22.3) Steel Posts used in MGSATB-5 and MGSATB-6.....106

Figure D-1. Results of Test No. MGSATB-1 (EDR-3).....108

Figure D-2. Results of Test No. MGSATB-1 (EDR-4).....109

Figure D-3. Results of Test No. MGSATB-1 (DTS).....110

Figure D-4. Results of Test No. MGSATB-2 (EDR-3).....111

Figure D-5. Results of Test No. MGSATB-2 (EDR-4).....112

Figure D-6. Results of Test No. MGSATB-2 (DTS).....113

Figure D-7. Results of Test No. MGSATB-3 (EDR-3).....114

Figure D-8. Results of Test No. MGSATB-3 (EDR-4).....115

Figure D-9. Results of Test No. MGSATB-4 (EDR-3).....116

Figure D-10. Results of Test No. MGSATB-4 (EDR-4).....117

Figure D-11. Results of Test No. MGSATB-5 (EDR-3).....118

Figure D-12. Results of Test No. MGSATB-6 (EDR-3).....119

Figure D-13. Results of Test No. MGSATB-6 (EDR-4).....120

Figure D-14. Results of Test No. MGSATB-7 (EDR-3).....121

Figure D-15. Results of Test No. MGSATB-7 (EDR-4).....122

Figure D-16. Results of Test No. MGSATB-8 (EDR-4).....123

Figure D-17. Results of Test No. MGSATB-9 (EDR-3).....124

Figure D-18. Results of Test No. MGSATB-9 (EDR-4).....125

Figure D-19. Results of Test No. MGSATB-10 (EDR-3).....126

Figure D-20. Results of Test No. MGSATB-10 (EDR-4).....127

Figure D-21. Results of Test No. MGSATB-11 (EDR-3).....128
Figure D-22. Results of Test No. MGSATB-12 (EDR-3).....129
Figure D-23. Results of Test No. MGSATB-13 (EDR-3).....130
Figure D-24. Results of Test No. MGSATB-13 (EDR-4).....131
Figure D-25. Results of Test No. MGSATB-14 (EDR-3).....132
Figure D-26. Results of Test No. MGSATB-14 (EDR-4).....133
Figure D-27. Results of Test No. MGSATB-15 (EDR-3).....134
Figure D-28. Results of Test No. MGSATB-15 (EDR-4).....135
Figure D-29. Results of Test No. MGSATB-16 (EDR-3).....136
Figure D-30. Results of Test No. MGSATB-16 (EDR-4).....137
Figure D-31. Results of Test No. MGSATB-17 (EDR-3).....138
Figure D-32. Results of Test No. MGSATB-17 (DTS).....139
Figure D-33. Results of Test No. MGSATB-18 (EDR-3).....140
Figure D-34. Results of Test No. MGSATB-18 (DTS).....141
Figure D-35. Results of Test No. MGSATB-19 (EDR-3).....142
Figure D-36. Results of Test No. MGSATB-19 (DTS).....143
Figure D-37. Results of Test No. MGSATB-20 (EDR-3).....144
Figure D-38. Results of Test No. MGSATB-20 (DTS).....145
Figure E-1. System Layout Drawing of BARRIER VII Model.....153

LIST OF TABLES

Table 1. Dynamic Test Results for Steel and Wood Posts in Moderately Compacted Soil	4
Table 2. Comparison of Wood and Steel Post from Full-Scale Crash Testing.....	7
Table 3. Dynamic Component-Post Testing Matrix	13
Table 4. Wood Post Details	15
Table 5. Weather Conditions, Test Nos. MGSATB-1 through MGSATB-20.....	16
Table 6. Summary of Accelerometers Used in the Test Matrix	18
Table 7. Dynamic Testing Results	62
Table 8. Bogie Test Result Comparison by Post Size	73
Table 9. Comparison of Test No. MWTSP-2 and BARRIER VII Simulation Results	75
Table 10. Summary of BARRIER VII Simulation Results	79
Table F-1. BARRIER VII Results for Calibrated Steel Post Transition Model	156
Table F-2. BARRIER VII Results for Wood Post Transition Model	157

1 INTRODUCTION

1.1 Background

In 2007, the Midwest States Pooled Fund Program and the Midwest Roadside Safety Facility (MwRSF) began an effort to develop a guardrail stiffness transition between the Midwest Guardrail System (MGS) and thrie beam, bridge rail approach transitions. A stiffness transition had been developed for this situation, and it utilized multiple post sizes [1]. However, the members of the Midwest States Pooled Fund Program desired a stiffness transition utilizing “standard” steel posts at various spacing intervals to gradually increase the system’s lateral stiffness. It was also desired that the stiffness transition have the ability to attach to multiple thrie beam, bridge rail transitions, similar to the original steel-post system. With the rationale that transitioning to a stiff system would be critical and allow for attachment to more flexible systems, the stiffest of the Federal Highway Administration’s (FHWA) accepted bridge rail approach transitions, identified as the transition to Missouri’s thrie beam and channel bridge rail, was selected for use as the downstream end of the stiffness transition [2].

The final system design utilized “standard” W6x9 (W152x13.4) steel guardrail posts at various spacing intervals as well as a combination of W-beam, thrie beam, and a symmetrical W-to-thrie beam guardrail elements to connect the MGS to the stiff bridge rail approach transition [3]. A full-scale crash testing program showed the system satisfied Test Level 3 (TL-3) safety performance criteria presented in the American Association of State Highway and Transportation Officials (AASHTO) *Manual for Assessing Safety Hardware* (MASH) [4]. However, the Midwest States Pooled Fund Program also wanted to have a wood-post variation of this stiffness transition. Therefore, wood post equivalents were needed to replace the steel posts throughout the stiffness transition from MGS to rigid bridge rail.

1.2 Objective

The objective of this project was to determine a wood-post MGS approach transition system that is equivalent to the steel-post MGS stiffness transition. The rail elements of the transition were to remain the same, and only the steel posts were to be altered. Recommendations were to be made regarding the attachment of the stiffness transition to other FHWA-accepted bridge rail transitions consisting of three beam guardrail mounted on wood posts.

1.3 Research Approach

The research objectives were met through a combination of historical data review, physical component testing, and computer simulation and analysis. First, a literature review was conducted on post-soil resistance for both W6x9 (W152x13.4) steel posts and 6-in. x 8-in. (152-mm x 203-mm) wood posts. Conclusions were made regarding these standard post sizes. Next, dynamic component testing was conducted to determine the post-soil resistance characteristics of the larger W6x15 (W152x22.3) steel transition posts embedded 54 in. (1,372 mm) in soil as well as wood posts of multiple cross-sections and embedment depths. After determining equivalent wood posts for both steel post sizes used in the MGS approach transition, BARRIER VII computer simulations were conducted to compare the performance of the wood and steel post systems. The steel-post BARRIER VII model was validated against the full-scale crash testing of the steel-post transition system under MASH safety standards and served as the basis for comparison and evaluation of the wood-post transition system. After the wood-post transition system was determined to be an adequate alternative, the final design drawings were created. Finally, recommendations for the attachment of the stiffness transition to other FHWA accepted bridge rail transitions were specified based on the knowledge obtained during the project.

2 WOOD POST EQUIVALENT FOR THE 6-FOOT (1.8-METER) LONG W6x9 (W152x13.4) POST

For many years the roadside safety community has considered 6-in. x 8-in. (152-mm x 203-mm) wood posts and W6x9 (W152x13.4) steel posts as interchangeable options for 6-ft (1.8-m) long guardrail posts. This philosophy was prominent with previous “standard” strong post W-beam guardrail systems as illustrated in system designator SGR-04a-b found in the *Guide to Standardized Highway Barrier Hardware* [5]. However, the posts in these older systems were embedded 43 in. (1,092 mm) to 44 in. (1,118 mm) in the soil, while MGS posts are embedded only 40 in. (1,016 mm). Blockout depth and splice location differences make the behavior of the MGS different from older W-beam systems. Therefore, a review of previous testing (both post-in-soil component testing and full-scale crash testing) was conducted to compare the performance of 6-in. x 8-in. (152-mm x 203-mm) wood posts and W6x9 (W152x13.4) steel posts when used in the MGS.

2.1 Dynamic Component Testing

During the development of the MGS and its special applications, numerous dynamic component tests were conducted on guardrail posts to gain an understanding of the post-soil resistances [6-8]. Multiple tests utilized 6-ft (1.8-m) long W6x15 (W152x22.3) steel guardrail posts embedded 40 in. (1,016 mm) in AASHTO M147-65 Grade B soil, as recommended by NCHRP Report No. 350 and MASH. Only tests with targeted impact speeds of 20 mph (35 km/h) were compared to control for load rate and inertial effects. Six tests on W6x9 (W152x13.4) steel posts and four tests on 6-in. x 8-in. (152-mm x 203-mm) wood posts met this criterion. The average resistive forces were similar between the two post types, as shown in Table 1. The steel posts showed a slightly higher resistance of 6.8 percent and 11.5 percent at displacements of 15 in. and 20 in. (381 mm and 508 mm), respectively.

Table 1. Dynamic Test Results for Steel and Wood Posts in Moderately Compacted Soil

Test No.	Ref.	Post Type	Embedment Depth, in. (mm)	Impact Height, in. (mm)	Impact Velocity, mph (km/h)	Average Force, kips (kN)	
						@ 15 in. (381 mm)	@ 20 in. (508 mm)
NPG-2	[6]	W6x9 (W152x23.8) Steel	40 (1,016)	24 ⁷ / ₈ (631.8)	21.0 (33.8)	5.78 (25.7)	6.10 (27.1)
NPG-4	[6]	W6x9 (W152x23.8) Steel	40 (1,016)	24 ⁷ / ₈ (631.8)	20.0 (32.2)	6.73 (29.9)	6.66 (29.6)
NPG-9	[6]	W6x9 (W152x23.8) Steel	40 (1,016)	24 ⁷ / ₈ (631.8)	20.8 (33.5)	6.42 (28.6)	6.43 (28.6)
NPG-10	[6]	W6x9 (W152x23.8) Steel	40 (1,016)	24 ⁷ / ₈ (631.8)	21.5 (34.6)	6.99 (31.1)	7.05 (31.4)
MGS2-1B20	[7]	W6x9 (W152x23.8) Steel	40 (1,016)	24 ⁷ / ₈ (631.8)	19.3 (31.1)	6.45 (28.7)	7.13 (31.7)
MGS2-1B21	[7]	W6x9 (W152x23.8) Steel	40 (1,016)	24 ⁷ / ₈ (631.8)	19.8 (31.9)	5.55 (24.7)	6.32 (28.1)
Average (steel):						6.32 (28.1)	6.61 (29.4)
GWB-1	[8]	6 in. x 8 in. (152 mm x 203 mm) Wood	40 (1,016)	24 ⁷ / ₈ (631.8)	20.7 (33.3)	5.18 (23.0)	5.20 (23.1)
GWB-2	[8]	6 in. x 8 in. (152 mm x 203 mm) Wood	40 (1,016)	24 ⁷ / ₈ (631.8)	19.8 (31.9)	6.63 (29.5)	6.41 (28.5)
GWB-6	[8]	6 in. x 8 in. (152 mm x 203 mm) Wood	40 (1,016)	24 ⁷ / ₈ (631.8)	19.6 (31.5)	6.45 (28.7)	6.17 (27.4)
GWB-7	[8]	6 in. x 8 in. (152 mm x 203 mm) Wood	40 (1,016)	24 ⁷ / ₈ (631.8)	19.0 (30.6)	5.67 (25.2)	5.92 (26.3)
Average (wood):						5.98 (26.6)	5.93 (26.4)

4

With the adoption of MASH in 2009, test facilities are now required to follow soil strength guidelines for test article installation in soil in order to ensure consistency among the test facilities. MASH adheres to the general philosophy that testing longitudinal barriers in stiff soil results in higher impact and barrier loads, increased occupant risk values, and increased propensity for rail rupture, pocketing, and snag. Therefore, MASH has established a minimum post-soil resistance force standard to ensure that systems are installed in strong, stiff soil. To satisfy these requirements, MwRSF began to use a high energy, soil compaction method when installing system components (e.g., posts) for compliance testing. As expected, recent bogie testing has shown increased post-soil interaction forces. However, the stiffer soil has not changed the similarity between force vs. deflection curves for the standard MGS guardrail posts. In a recent dynamic testing study, two 6-in. x 8-in. (152-mm x 203-mm) wood posts and two W6x16 (W152x23.8) steel posts were embedded 40 in. (1,016 mm) in a highly compacted soil and impacted at 20 mph (32 km/h) [8]. The W6x16 (W152x23.8) posts have the same flange width and overall depth as a W6x9 (W152x13.4) so the soil resistances for the two posts are the same. Wood and steel posts provided very similar resistances throughout the impact event, as shown by the force vs. deflection curves in Figure 1.

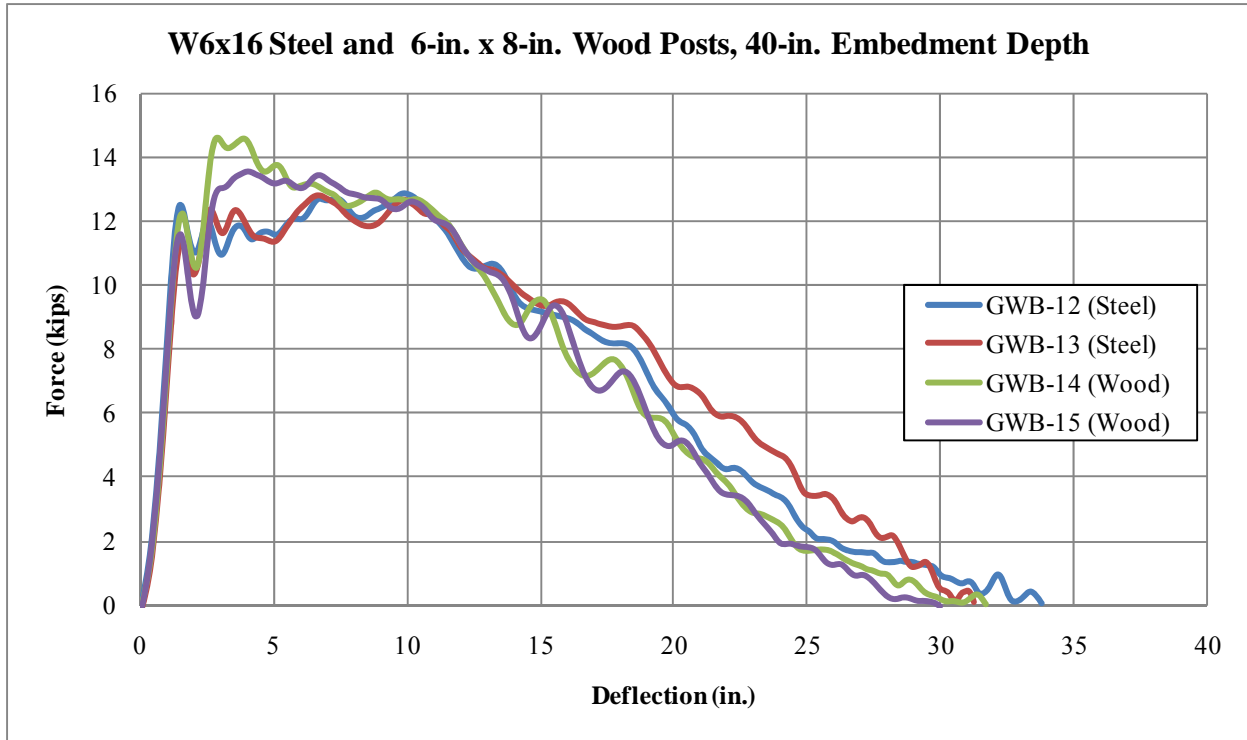


Figure 1. W6x16 (W152x23.8) Steel and 6-in. x 8-in. (152-mmx203-mm) Wood Posts in Highly Compacted Soil

2.2 Full-Scale Testing

Two full-scale crash tests were selected to compare the W6x9 (W152x13.4) steel-post and the 6 in. x 8 in. (152 mm x 203 mm) wood-post performance when installed in the MGS. Test no. 2214MG-2 utilized steel posts [1], while test no. MGSWP-1 utilized the wood posts [10]. Both 181-ft 3-in. (55.2-m) long test installations satisfied all MASH safety performance criteria of test designation no. 3-11. The two systems behaved similarly during the test in terms of maximum dynamic deflection, contact length, and exit conditions, as shown in Table 2. Further, the Occupant Impact Velocities (OIV) and Occupant Ridedown Accelerations (ORA) were very similar, thus suggesting the forces imparted to the vehicle were very similar.

Table 2. Comparison of Wood and Steel Post from Full-Scale Crash Testing

	Test No. 2214MG-2 [1]	Test No. MGSWP-1 [10]
System	181-ft 3-in. (55.2-m) long MGS	181-ft 3-in. (55.2-m) long MGS
Posts	W6x9 (W152x13.4) Steel	Wood 6 in. x 8 in. (152 mm x 203 mm)
Vehicle	2002 Dodge Ram 1500 Quad Cab	2003 Dodge Ram 1500 Quad Cab
Impact Speed	62.8 mph (101.1 km/h)	63.8 mph (102.7 km/h)
Impact Angle	25.5°	25.6°
Exit Speed	39.6 mph (63.7 km/h)	39.6 mph (63.7 km/h)
Exit Angle	13.5°	16.6°
Contact Length	33 ft – 8 in. (10.3 m)	30 ft – 6 in. (9.3 m)
Maximum Dynamic Deflection	43.9 in. (1,115 mm)	46.3 in. (1,176 mm)
System Permanent Set	31 ⁵ / ₈ in. (803 mm)	33 ³ / ₄ in. (857 mm)
Longitudinal OIV	15.32 ft/s (4.67 m/s)	15.27 ft/s (4.65 m/s)
Lateral OIV	15.62 ft/s (4.76 m/s)	16.14 ft/s (4.92 m/s)
Longitudinal ORA	8.23 g's	8.25 g's
Lateral ORA	6.93 g's	10.13 g's

2.3 Conclusions

Similar performance between W6x9 (W152x13.4) steel and 6-in. x 8-in. (152-mm x 203-mm) wood guardrail posts has been documented in both dynamic component testing and full-scale testing. Therefore, 6-in. x 8-in. (152-mm x 203-mm) wood posts were selected as the alternative for the W6x9 (W152x13.4) steel posts found in the MGS to thrie beam stiffness transition. BARRIER VII simulations were used to verify the wood posts did not adversely affect the safety performance of the stiffness transition, as described in Chapter 5.

3 COMPONENT TEST CONDITIONS

3.1 Purpose

In previous research, MwRSF has conducted numerous dynamic component tests of W6x9 (W152x13.4) steel posts and 6-in. x 8-in. (152-mm x 203-mm) wood posts. However, no such tests have been conducted on either W6x15 (W152x22.3) steel posts or large cross section wood posts. Therefore, a series of dynamic component tests were conducted to determine the post-soil interaction force characteristics for these large post sizes in an effort to find an equivalent wood post for the W6x15 (W152x22.3) steel posts utilized in the steel-post MGS stiffness transition to thrie beam.

3.2 Scope

Twenty dynamic component tests were conducted on W6x15 (W152x22.3) steel posts and various wood-post sizes in soil. The target impact conditions for all tests were 20 mph (32 km/h) at an angle of 0 degrees, creating a classical “head-on” or full-frontal impact and strong axis bending. The posts were impacted 24 $\frac{7}{8}$ in. (632 mm) above the ground line. The dynamic component test matrix and the test setup are shown in Table 3 and Figure 2, respectively.

A compacted, coarse, crushed limestone material, as recommended by NCHRP Report No. 350, was utilized for all tests. Soil specifications are shown in Appendix A. Although the soil gradations were similar, the compaction methods were different. Testing began with moderately compacted soil installation methods, but switched to a high-energy lift compaction method after the wood post tests indicated a propensity for post fracture. As previously mentioned, MASH adheres to the general philosophy that testing of longitudinal barriers in stiff soil is critical as it results in higher impact and barrier loads, increased occupant risk values, and increased propensity for rail rupture, vehicle pocketing, and wheel snag. Thus, using heavily compacted soils was justified by MASH. Therefore, test nos. MGSATB-1 through MGSATB-4

utilized moderately compacted soil, while the remainder of the tests utilized heavily compacted soil.

Material specifications, mill certifications, and certificates of conformity for the steel post materials used in test nos. MGSATB-5 and MGSATB-6 are shown in Appendix C. The wood posts were southern yellow pine (SYP) sections. Cross-sectional dimensions, moisture content, weight, and ring density of the posts were recorded, as shown in Table 4. Cross-sectional measurements and moisture content were taken at both ends of the post and at ground line with a pin-type moisture meter [8]. Due to differences in moisture contents, densities, and dimensions, each wood post had a different recorded weight.

3.3 Weather Conditions

Test nos. MGSATB-1 through MGSATB-20 were conducted between October 4, 2007 and October 1, 2010. The weather conditions as per the National Oceanic and Atmospheric Administration (station 14939/LNK) were reported as shown in Table 5. Note station 14939/LNK is at the Lincoln Airport adjacent to MwRSF's testing grounds.

3.4 Equipment and Instrumentation

Various types of equipment and instrumentation were utilized to conduct dynamic post tests and collect and record data. Included were a bogie vehicle, accelerometers, pressure tape switches, high-speed and standard-speed digital video cameras, and still cameras.

3.4.1 Bogie

A rigid frame bogie vehicle was used to impact the posts. A variable height, detachable impact head was used in the testing. The bogie head was constructed using 8-in. (203-mm) diameter, ½-in. (13-mm) thick standard steel pipe, with ¾-in. (19-mm) neoprene belting wrapped around the pipe. The neoprene material was used to prevent the impact head from causing local damage to the post and to prevent large spikes in acceleration. The impact head was bolted to the

bogie vehicle, creating a rigid frame with an impact height of $24\frac{7}{8}$ in. (632 mm). The bogie and attached impact head are shown in Figure 3. The weight of the bogie with the addition of the mountable impact head varied for the tests. The bogie vehicle weight for each test is shown on the individual test summaries provided in Appendix C.

For test nos. MGSATB-1 through MGSATB-16, a pickup truck with a reverse cable tow system was used to propel the bogie to the target impact speed. When the bogie reached the end of the guidance system, it was released from the tow cable, allowing it to be free rolling when it impacted the post. A remote braking system was installed on the bogie allowing it to be brought safely to rest after the test. This setup is shown in Figure 3.

Test nos. MGSATB-17 through MGSATB-20 were conducted using a steel corrugated B-beam guardrail to guide the right-side tires of the bogie as shown in Figure 4. The B-beam is also along the target impact angle. A pickup truck is used to push the bogie to the required impact velocity. As the bogie reaches the end of the guide track, the pickup truck releases and allows the bogie to be “free wheeling” as it exits the guide track and impacts the test article. A remote braking system was installed on the bogie allowing it to be brought safely to rest after the test.

3.4.2 Accelerometers

For MGSATB-1 and MGSATB-2, three accelerometers were mounted on the bogie vehicle. For test nos. MGSATB-3 through MGSATB-7, MGSATB-9, MGSATB-10, and MGSATB-13 through MGSATB-20, two accelerometers were use. For test nos. MGSATB-8, MGSATB-11, and MGSATB-12, only one accelerometer was used. The accelerometers were mounted on the bogie vehicle near its center of gravity to measure the accelerations. The specific accelerometer systems used for each test are shown in Table 6.

The first accelerometer system was a two-arm piezoresistive accelerometer system manufactured by Endevco of San Juan Capistrano, California. Three accelerometers were used to

measure each of the longitudinal, lateral, and vertical accelerations independently at a sample rate of 10,000 Hz. The accelerometers were configured and controlled using a system developed and manufactured by Diversified Technical Systems, Inc. (DTS) of Seal Beach, California. More specifically, data was collected using a DTS Sensor Input Module (SIM), Model TDAS3-SIM-16M. The SIM was configured with 16 MB SRAM memory and 8 sensor input channels with 250 kB SRAM/channel. The SIM was mounted on a TDAS3-R4 module rack. The module rack was configured with isolated power/event/communications, 10BaseT Ethernet and RS232 communication, and an internal backup battery. Both the SIM and module rack were crashworthy. The “DTS TDAS Control” computer software program and a customized Microsoft Excel worksheet were used to analyze and plot the accelerometer data.

The second accelerometer was a triaxial piezoresistive accelerometer system, Model EDR-4 6DOF-500/1200, manufactured by Instrumented Sensor Technology (IST) of Okemos, Michigan and includes three differential channels as well as three single-ended channels. The EDR-4 6DOF-500/1200 was configured with 24 MB of RAM, a range of ± 500 g's, a sample rate of 10,000 Hz, and a 1,677 Hz anti-aliasing filter. The “EDR4COM” and “DynaMax Suite” computer software programs and a customized Microsoft Excel worksheet were used to analyze and plot the accelerometer data.

The third accelerometer, Model EDR-3, was a triaxial piezoresistive accelerometer system developed by IST of Okemos, Michigan. The EDR-3 was configured with 256 kB of RAM, a range of ± 200 g's, a sample rate of 3,200 Hz, and a 1,120 Hz low-pass filter. The “DynaMax 1 (DM-1)” computer software program and a customized Microsoft Excel worksheet were used to analyze and plot the accelerometer data.

MwRSF became ISO 17025 accredited in October, 2009 which predated test nos. MGSATB-18 through 20. At the time of these tests, the EDR-3 was not calibrated by an ISO

17025 approved laboratory due to the lack of an ISO 17025 calibration laboratory with the capabilities of calibrating the unit. However, the EDR-3 was calibrated by IST which provided the traceability for the calibration. Further, MwRSF recognizes that the EDR-3 transducer does not satisfy the minimum 10,000 Hz sample frequency recommended by MASH. Following numerous test comparisons, the EDR-3 has been shown to provide equivalent results to the DTS unit which does satisfy all MASH criteria and has ISO 17025 calibration traceability. Therefore, MwRSF has continued to use the EDR-3 during physical impact testing. The equivalency of the transducers is further explained and comparisons are shown in Appendix B.

3.4.3 Pressure Tape Switches

Three pressure tape switches, spaced at approximately 18-in. (457-mm) intervals and placed near the end of the bogie track, were used to determine the speed of the bogie before impact. As the front tire of the bogie passed over each tape switch, a strobe light was fired sending an electronic timing signal to the data acquisition system. The system recorded the signals and the time each occurred. The speed was then calculated using the spacing between the sensors and the time between the signals. Strobe lights and high-speed video analysis are used only as a backup in the event that vehicle speeds cannot be determined from the electronic data.

3.4.4 Digital Cameras

One AOS VITcam high-speed digital video camera and one JVC digital video camera were used to document each test. The AOS high-speed cameras had frame rates of 500 frames per second and the JVC digital video cameras had frame rates of 29.97 frames per second. All cameras were placed laterally from the post, with a view perpendicular to the bogie's direction of travel. A Nikon D50 digital still camera was also used to document pre- and post-test conditions for all tests.

Table 3. Dynamic Component-Post Testing Matrix

Test No.	Post			Embedment Depth In. (mm)	Bending Axis	Soil and Compaction	Target Impact Velocity mph (km/h)
	Type (Species)	Size in. x in. (mm x mm)	Length ft (m)				
MGSATB-1	Steel	W6x15 (W152x22.3)	7 (2.13)	54 (1,372)	Strong	AASHTO Grade B Moderate Compaction	20 (32)
MGSATB-2	Steel	W6x15 (W152x22.3)	7 (2.13)	54 (1,372)	Strong	AASHTO Grade B Moderate Compaction	20 (32)
MGSATB-3	Wood (SYP)	8 x 8 (203 x 203)	7 (2.13)	54 (1,372)	Strong	AASHTO Grade B Moderate Compaction	20 (32)
MGSATB-4	Wood (SYP)	8 x 8 (203 x 203)	7 (2.13)	54 (1,372)	Strong	AASHTO Grade B Moderate Compaction	20 (32)
MGSATB-5	Steel	W6x15 (W152x22.3)	7 (2.13)	54 (1,372)	Strong	AASHTO Grade B Heavy Compaction	20 (32)
MGSATB-6	Steel	W6x15 (W152x22.3)	7 (2.13)	54 (1,372)	Strong	AASHTO Grade B Heavy Compaction	20 (32)
MGSATB-7	Wood (SYP)	8 x 8 (203 x 203)	7 (2.13)	54 (1,372)	Strong	AASHTO Grade B Heavy Compaction	20 (32)
MGSATB-8	Wood (SYP)	8 x 8 (203 x 203)	7 (2.13)	54 (1,372)	Strong	AASHTO Grade B Heavy Compaction	20 (32)
MGSATB-9	Wood (SYP)	8 x 10 (203 x 254)	7 (2.13)	54 (1,372)	Strong	AASHTO Grade B Heavy Compaction	20 (32)
MGSATB-10	Wood (SYP)	10 x 10 (254 x 254)	7 (2.13)	54 (1,372)	Strong	AASHTO Grade B Heavy Compaction	20 (32)
MGSATB-11	Wood (SYP)	8 x 10 (203 x 254)	7 (2.13)	54 (1,372)	Strong	AASHTO Grade B Heavy Compaction	20 (32)
MGSATB-12	Wood (SYP)	8 x 10 (203 x 254)	7 (2.13)	54 (1,372)	Strong	AASHTO Grade B Heavy Compaction	20 (32)
MGSATB-13	Wood (SYP)	8 x 10 (203 x 254)	6.5 (1.98)	48 (1,219)	Strong	AASHTO Grade B Heavy Compaction	20 (32)
MGSATB-14	Wood (SYP)	8 x 10 (203 x 254)	6.5 (1.98)	48 (1,219)	Strong	AASHTO Grade B Heavy Compaction	20 (32)
MGSATB-15	Wood (SYP)	8 x 10 (203 x 254)	6.5 (1.98)	48 (1,219)	Strong	AASHTO Grade B Heavy Compaction	20 (32)
MGSATB-16	Wood (SYP)	8 x 10 (203 x 254)	6.5 (1.98)	48 (1,219)	Strong	AASHTO Grade B Heavy Compaction	20 (32)
MGSATB-17	Wood (SYP)	8 x 10 (203 x 254)	6.5 (1.98)	48 (1,219)	Strong	AASHTO Grade B Heavy Compaction	20 (32)
MGSATB-18	Wood (SYP)	6 x 10 (152 x 254)	7 (2.13)	52 (1,321)	Strong	AASHTO Grade B Heavy Compaction	20 (32)
MGSATB-19	Wood (SYP)	6 x 10 (152 x 254)	7 (2.13)	52 (1,321)	Strong	AASHTO Grade B Heavy Compaction	20 (32)
MGSATB-20	Wood (SYP)	6 x 10 (152 x 254)	7 (2.13)	52 (1,321)	Strong	AASHTO Grade B Heavy Compaction	20 (32)

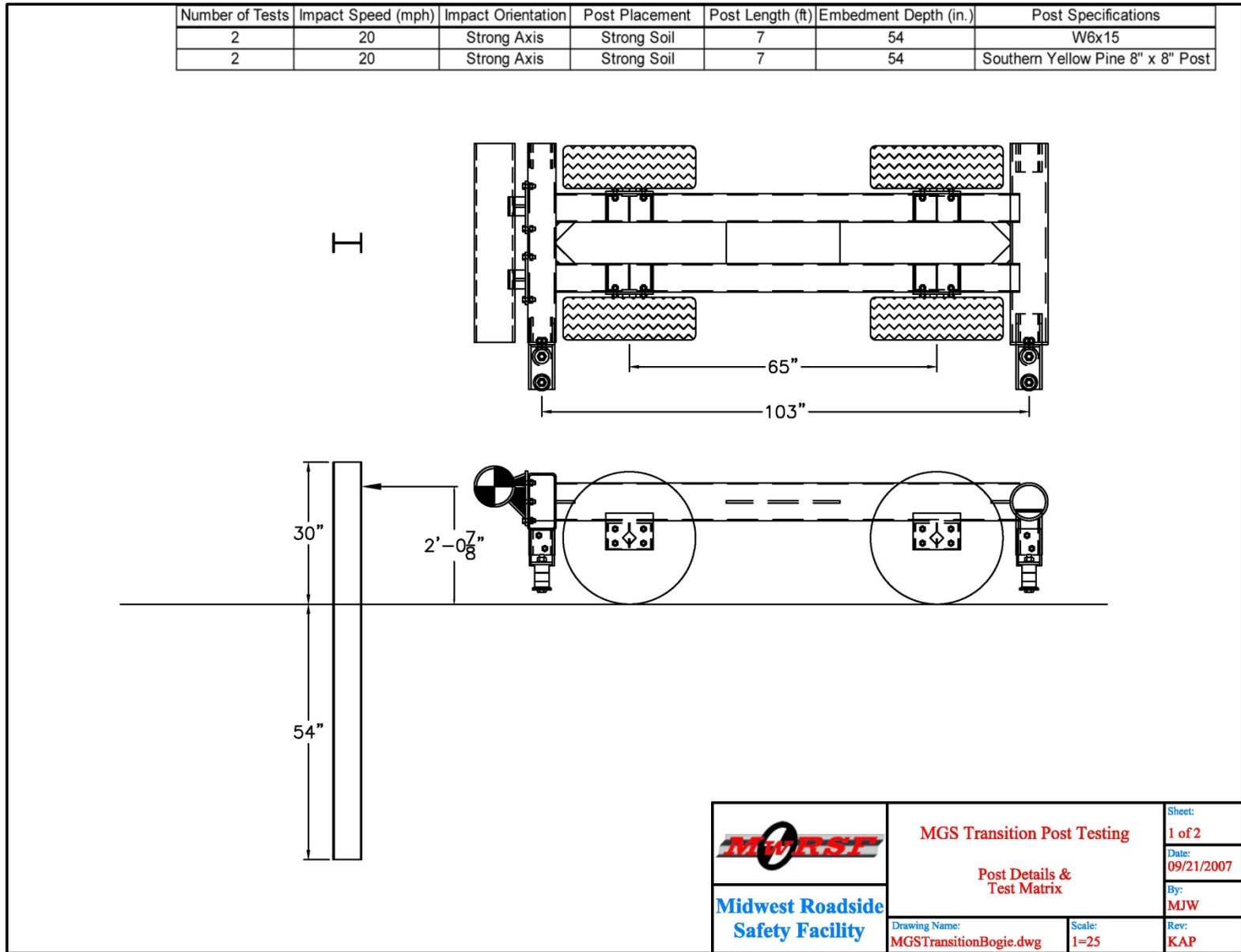


Figure 2. Bogie Testing Setup

Table 4. Wood Post Details

Test No.	Post Dimensions in. x in. (mm x mm)			Length in. (mm)	Weight lb (kg)	Moisture Content (%)			Ring Density rings/in. (rings/cm)
	At Top	At Ground Line	At Bottom			Top	Ground Line	Bottom	
MGSATB-3	8 x 8 (203 x 203)	8 x 8 (203 x 203)	8 x 8 (203 x 203)	84 (2,134)	NA	NA	NA	NA	NA
MGSATB-4	8 x 8 (203 x 203)	8 x 8 (203 x 203)	8 x 8 (203 x 203)	84 (2,134)	NA	NA	NA	NA	NA
MGSATB-7	8 x 7 ⁷ / ₈ (203 x 200)	8 x 8 (203 x 203)	8 ¹ / ₈ x 8 (206 x 203)	84 (2,134)	168 (76)	32	37	32	9 (3.5)
MGSATB-8	8 x 8 (203 x 203)	8 x 8 (203 x 203)	8 x 8 ¹ / ₈ (203 x 206)	84 (2,134)	182 (83)	32	34	44	7 (2.8)
MGSATB-9	8 ³ / ₄ x 10 (210 x 254)	8 ¹ / ₈ x 9 ⁷ / ₈ (206 x 251)	8 ¹ / ₈ x 9 ⁷ / ₈ (206 x 251)	84 (2,134)	152 (69)	35	39	20	3 (1.2)
MGSATB-10	10 x 10 (254 x 254)	10 x 9 ⁷ / ₈ (254 x 251)	10 x 10 ¹ / ₈ (254 x 257)	84 (2,134)	213 (97)	11	16	16	11 (4.3)
MGSATB-11	8 x 9 ³ / ₄ (203 x 248)	8 x 9 ⁷ / ₈ (203 x 251)	8 x 10 (203 x 254)	84 ¹ / ₈ (2,137)	147 (67)	16	15	16	8 (3.1)
MGSATB-12	8 x 10 ¹ / ₈ (203 x 257)	8 ³ / ₈ x 10 ¹ / ₈ (213 x 257)	8 ¹ / ₄ x 10 ¹ / ₄ (210 x 260)	84 ¹ / ₄ (2,140)	181 (82)	15	17	20	4 (1.6)
MGSATB-13	8 x 9 ³ / ₄ (203 x 248)	8 x 9 ⁷ / ₈ (203 x 251)	8 x 9 ⁷ / ₈ (203 x 251)	78 ¹ / ₈ (1,984)	136 (62)	14	15	15	8 (3.1)
MGSATB-14	8 x 10 ¹ / ₈ (203 x 257)	8 x 10 (203 x 254)	8 x 10 ¹ / ₈ (203 x 257)	78 ¹ / ₄ (1,988)	165 (75)	19	16	29	4 (1.6)
MGSATB-15	8 x 9 ³ / ₄ (203 x 248)	8 x 9 ⁷ / ₈ (203 x 251)	8 x 9 ⁷ / ₈ (203 x 251)	78 ¹ / ₈ (1,984)	134 (61)	11	11	12	8 (3.1)
MGSATB-16	8 x 10 ¹ / ₈ (203 x 258)	8 x 10 (203 x 254)	8 x 10 ¹ / ₈ (203 x 258)	78 ¹ / ₄ (1,988)	165 (75)	11	14	NA	4 (1.6)
MGSATB-17	8 ¹ / ₈ x 10 (206 x 254)	8 ¹ / ₈ x 10 (206 x 254)	8 ¹ / ₈ x 10 (206 x 254)	78 (1,981)	148 (67)	12	16	13	8 (3.1)
MGSATB-18	5 ⁷ / ₈ x 9 ⁷ / ₈ (149 x 251)	5 ⁷ / ₈ x 10 (149 x 254)	6 x 9 ⁷ / ₈ (152 x 251)	83 ⁷ / ₈ (2,130)	108 (49)	10	10	10	6 (2.4)
MGSATB-19	6 x 9 ³ / ₄ (152 x 248)	6 x 9 ⁷ / ₈ (152 x 251)	6 x 9 ⁷ / ₈ (152 x 251)	84 ¹ / ₈ (2,137)	105 (48)	8	9	8	NA
MGSATB-20	6 ¹ / ₄ x 10 (159 x 254)	6 x 9 ⁷ / ₈ (152 x 251)	6 x 10 (152 x 254)	84 (2,134)	96 (44)	8	10	17	6 (2.4)

Table 5. Weather Conditions, Test Nos. MGSATB-1 through MGSATB-20

Test No.	Date	Temp. (°F)	Humidity (%)	Wind Speed (mph)	Sky Conditions	Pavement Surface	Previous 3-Day Precipitation (in.)	Previous 7-Day Precipitation (in.)
MGSATB-1	10/4/2007	75	74	7	Overcast	Dry	0.66	1.1
MGSATB-2	10/4/2007	75	74	7	Overcast	Dry	0.66	1.1
MGSATB-3	11/6/2007	43	37	11	Sunny	Dry	0	0
MGSATB-4	11/6/2007	43	37	11	Sunny	Dry	0	0
MGSATB-5	2/17/2009	35	82	15	Sunny	Dry	0	0.36
MGSATB-6	2/23/2009	41	35	15	Sunny	Dry	0	0
MGSATB-7	2/24/2009	48	39	11	Sunny	Dry	0	0
MGSATB-8	2/25/2009	61	38	9	Sunny	Dry	0	0
MGSATB-9	5/20/2009	80	29	25	Sunny	Dry	0	0.28
MGSATB-10	5/20/2009	80	29	25	Sunny	Dry	0	0.28
MGSATB-11	6/11/2009	70	61	14	Overcast	Dry	0.05	2.33
MGSATB-12	6/11/2009	70	61	14	Overcast	Dry	0.05	2.33
MGSATB-13	6/12/2009	67	84	5	Overcast	Wet	0.04	2.33
MGSATB-14	6/15/2009	80	58	9	Overcast	Dry	0.41	0.46
MGSATB-15	6/29/2009	84	31	10	Sunny	Dry	0	0.83
MGSATB-16	6/29/2009	84	31	10	Sunny	Dry	0	0.83
MGSATB-17	7/24/2009	80	54	8	Sunny	Dry	0	0.5
MGSATB-18	7/28/2010	81	74	11	Overcast	Dry	0	0
MGSATB-19	7/28/2010	82	74	10	Overcast	Dry	0	0
MGSATB-20	10/1/2010	78	31	7	Sunny	Dry	0	0.33



Figure 3. Rigid Frame Bogie on Pipe Guide Track System



Figure 4. Rigid Frame Bogie on B-beam Guide Track System

Table 6. Summary of Accelerometers Used in the Test Matrix

Test No.	DTS	EDR-4	EDR-3
MSGATB-1	X	X	X
MSGATB-2	X	X	X
MSGATB-3		X	X
MSGATB-4		X	X
MSGATB-5		X	X
MSGATB-6		X	X
MSGATB-7		X	X
MSGATB-8		X	
MSGATB-9		X	X
MSGATB-10		X	X
MSGATB-11			X
MSGATB-12			X
MSGATB-13		X	X
MSGATB-14		X	X
MSGATB-15		X	X
MSGATB-16		X	X
MSGATB-17	X		X
MSGATB-18	X		X
MSGATB-19	X		X
MSGATB-20	X		X

3.5 End of Test Determination

When the impact head initially contacted the test article, the force exerted by the surrogate test vehicle was directly perpendicular. However, as the post rotates, the surrogate test vehicle's orientation and path moves further from perpendicular. This introduces two sources of error: (1) the contact force between the impact head and the post has a vertical component and (2) the impact head slides upward along the test article. Therefore, only the initial portion of the accelerometer trace may be used since variations in the data become significant as the system rotates and the surrogate test vehicle overrides the system. For this reason, the end of the test needed to be defined.

Guidelines were established to define the end of test time using the high-speed digital video of the crash test. The first occurrence of any one of the following three events was used to determine the end of the test: (1) the test article fractures; (2) the surrogate vehicle overrides/losses contact with the test article; or (3) a maximum post rotation of 45 degrees occurs.

3.6 Data Processing

Initially, the electronic accelerometer data obtained in dynamic testing was filtered using the SAE Class 60 Butterworth filter conforming to the SAE J211/1 specifications [11]. The pertinent acceleration signal was extracted from the bulk of the data signals. The processed acceleration data was then multiplied by the mass of the bogie to get the impact force using Newton's Second Law. Next, the acceleration trace was integrated to find the change in velocity versus time. Initial velocity of the bogie, calculated from the pressure switch data, was then used to determine the bogie velocity, and the calculated velocity trace was integrated to find the bogie's deflection, which is also the deflection of the post. Combining the previous results, a force vs. deflection curve was plotted for each test. Finally, integration of the force vs. deflection curve provided the energy vs. deflection curve for each test.

4 COMPONENT TESTING RESULTS AND DISCUSSION

4.1 Results

The information desired from the component tests was the relation between the applied force and deflection of the post at the impact location. This data was then used to find total energy (the area under the force vs. deflection curve) dissipated during each test.

Although the acceleration data was applied to the impact location, the data came from the center of gravity of the bogie. Error was added to the data since the bogie was not perfectly rigid and sustained vibrations. The bogie may have also rotated during impact, causing differences in accelerations between the bogie center of mass and the bogie impact head. While these issues may affect the data, the data was still valid. Filtering procedures were applied to the data to smooth out vibrations, and the rotations of the bogie during the tests were minor. Significant pitch angles did develop late in some tests as the bogie overrode the post; however, these occurred after the post-bogie interaction of interest. One useful aspect of using accelerometer data was that it included influences of the post inertia on the reaction force. This influence was important as the mass of the post would affect the barrier performance as well as test results.

The accelerometer data for each test was processed in order to obtain acceleration, velocity, and deflection curves, as well as force vs. deflection and energy vs. deflection curves. The values described herein were calculated from the EDR-3 data curves unless otherwise noted. Although the transducers used produced similar results, the EDR-3 has historically provided accurate results, and was the only accelerometer used in all tests except one. Test results for all transducers are provided in Appendix A.

In each of the following dynamic component tests, energy was absorbed by both the post and soil, but for convenience, this report presents the total absorbed energy as post-absorbed energy.

4.1.1 Test No. MGSATB-1

During test no. MGSATB-1, the bogie impacted the post at a speed of 19.2 mph (30.9 km/h). The post rotated through the soil to a maximum deflection of 19.5 in. (495 mm), at which point the bogie vehicle was brought to a stop and then rebounded backward. The post bent backward resulting in yielding and compression flange buckling approximately 6 in. (152 mm) below the ground line.

Force vs. deflection and energy vs. deflection curves created from the EDR-3 accelerometer data are shown in Figure 5. Initially, inertial effects resulted in a force spike of 13.6 kips (60.5 kN) over the first few inches of deflection. The post provided an average resistance force of 13.8 kips (61.4 kN) throughout the impact event, with a peak force of 20.1 kips (89.5 kN). At maximum deflection, the post absorbed 268.5 kip-in. (30.3 kJ) of energy. Time-sequential photographs and post-impact photographs are shown in Figure 6.

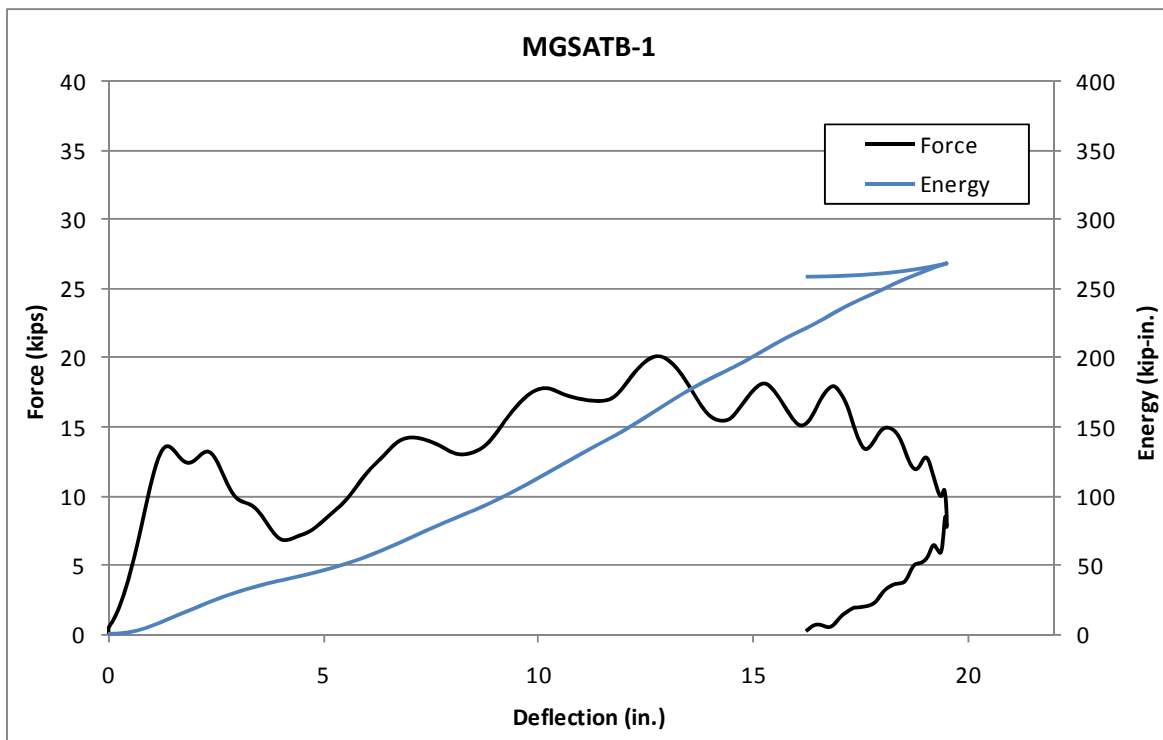
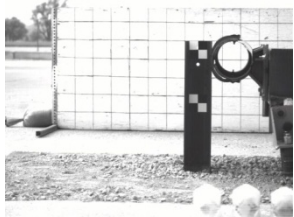
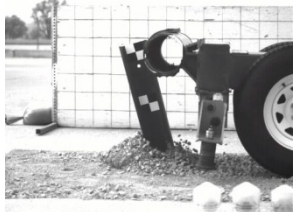


Figure 5. Force vs. Deflection and Energy vs. Deflection, Test No. MGSATB-1



IMPACT



0.050 sec



0.100 sec



0.150 sec



0.200 sec



0.250 sec



Figure 6. Time Sequential and Post-Impact Photographs, Test No. MGSATB-1

4.1.2 Test No. MGSATB-2

During test no. MGSATB-2, the bogie impacted the post at a speed of 19.7 mph (31.7 km/h). The post rotated through the soil to a maximum deflection of 19.3 in. (490 mm) at which point the bogie vehicle was brought to a stop and then rebounded backward. The post bent backward resulting in yielding and compression flange buckling approximately 6 in. (152 mm) below the ground line.

Force vs. deflection and energy vs. deflection curves created from the EDR-3 accelerometer data are shown in Figure 7. Initially, inertial effects resulted in a peak force of 14.2 kips (63.2 kN) over the first few inches of deflection. After a short drop in magnitude, the force increased and remained relatively constant near 19 kips (85 kN) between 10 in. and 18 in. (254 mm and 457 mm) of deflection. The peak force was 19.9 kips (88.5 kN). At the maximum deflection, the post absorbed 282.8 kip-in. (31.9 kJ) of energy. Time-sequential photographs and post-impact photographs are shown in Figure 8.

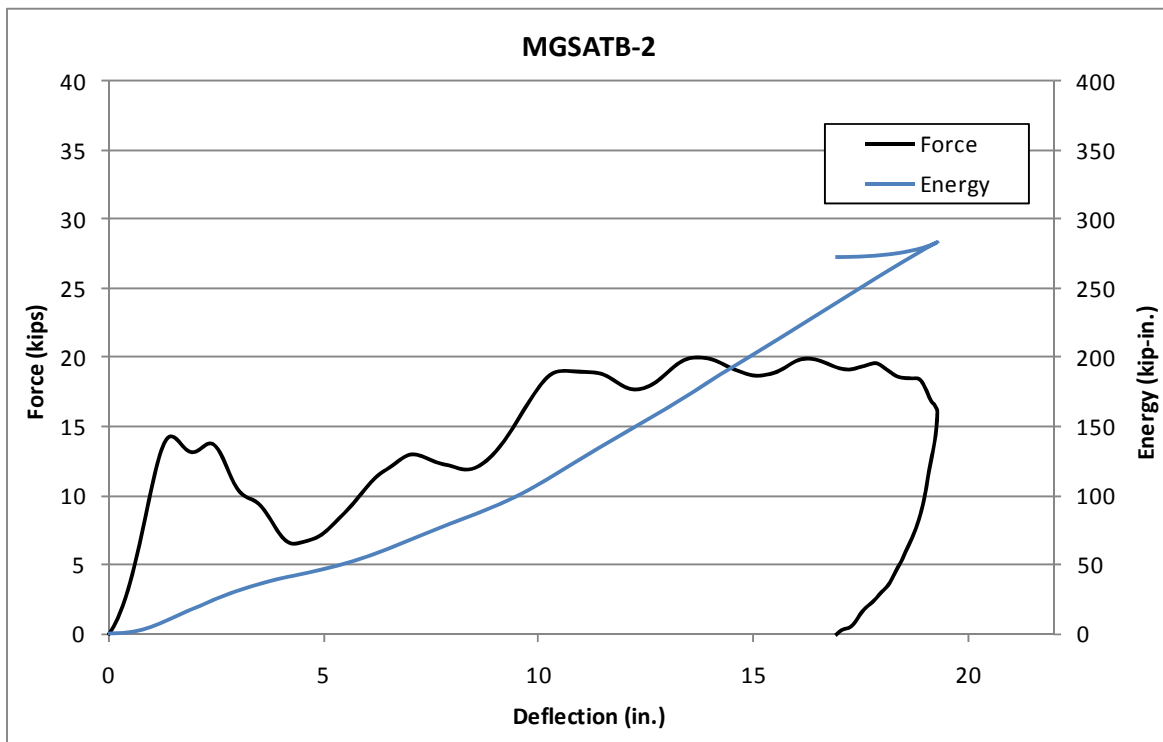


Figure 7. Force vs. Deflection and Energy vs. Deflection, Test No. MGSATB-2



IMPACT



0.050 sec



0.100 sec



0.150 sec



0.200 sec



0.250 sec



Figure 8. Time Sequential and Post-Impact Photographs, Test No. MGSATB-2

4.1.3 Test No. MGSATB-3

During test no. MGSATB-3, the bogie impacted the post at a speed of 18.2 mph (29.3 km/h). The post fractured at a deflection of 10.9 in. (277 mm), and the bogie traveled over the broken post stub. The post fractured approximately 12 in. (305 mm) below the ground line.

Force vs. deflection and energy vs. deflection curves created from the EDR-3 accelerometer data are shown in Figure 9. Initially, inertial effects resulted in a force spike of 12.6 kips (56.0 kN) over the first few inches of deflection. The post began to fracture at a deflection of 8.3 in. (212 mm) and at a peak force of 14.7 kips (65.2 kN). At fracture, the post absorbed 94.6 kip-in. (10.7 kJ) of energy. Time-sequential photographs and post-impact photographs are shown in Figure 10.

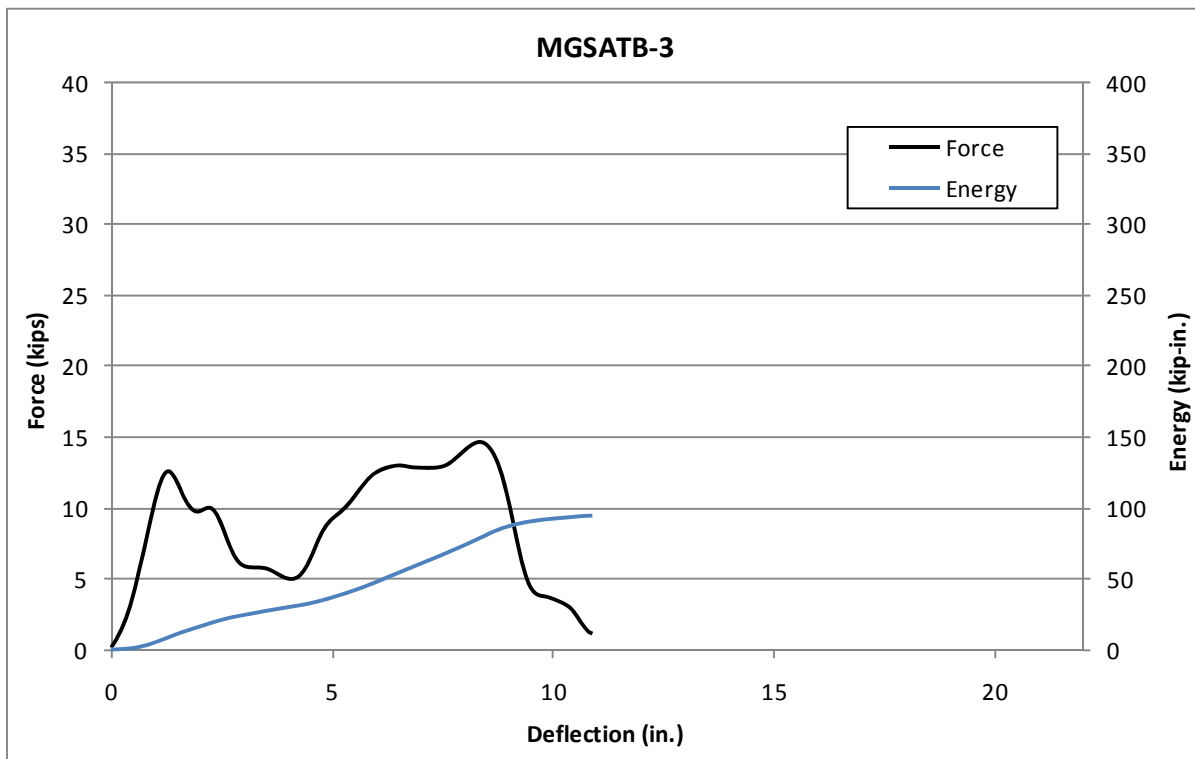
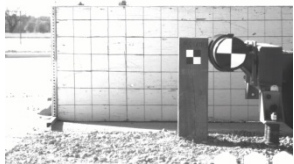
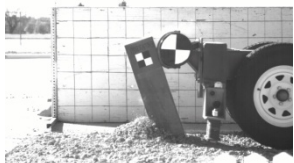


Figure 9. Force vs. Deflection and Energy vs. Deflection, Test No. MGSATB-3



IMPACT



0.050 sec



0.100 sec



0.150 sec



0.200 sec



0.250 sec



Figure 10. Time Sequential and Post-Impact Photographs, Test No. MGSATB-3

4.1.4 Test No. MGSATB-4

During test no. MGSATB-4, the bogie impacted the post at a speed of 18.7 mph (30.1 km/h). The post fractured at a deflection of 13.7 in. (348 mm), and the bogie traveled over the broken post stub. The post fractured approximately 12 in. (305 mm) below the ground line.

Force vs. deflection and energy vs. deflection curves created from EDR-3 accelerometer data are shown in Figure 11. Initially, inertial effects resulted in a force spike of 14.4 kips (64.1 kN) over the first few inches of deflection. The post began to fracture at a deflection of 12.7 in. (323 mm) and a peak force of around 25.4 kips (113 kN). At fracture, the post absorbed 183.7 kip-in. (20.8 kJ) of energy. Time-sequential photographs and post-impact photographs are shown in Figure 12.

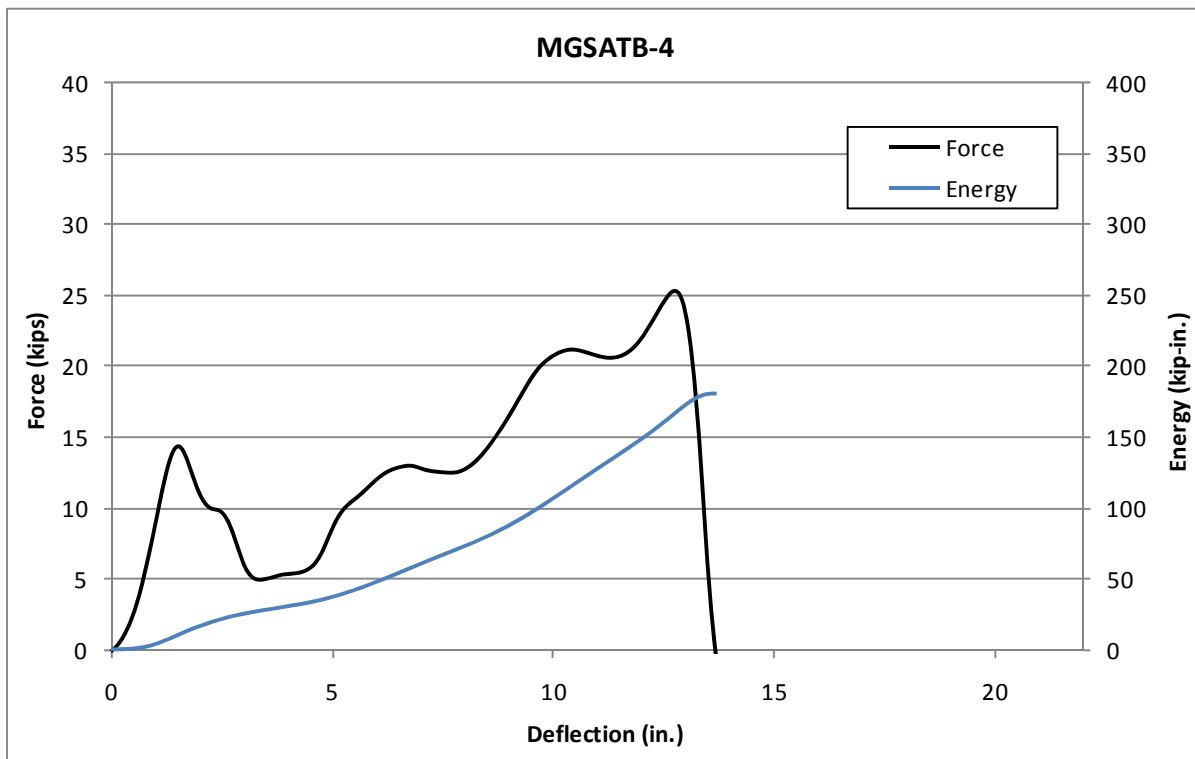
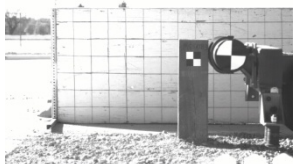
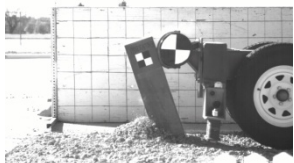


Figure 11. Force vs. Deflection and Energy vs. Deflection, Test No. MGSATB-4



IMPACT



0.050 sec



0.100 sec



0.150 sec



0.200 sec



0.250 sec



Figure 12. Time Sequential and Post-Impact Photographs, Test No. MGSATB-4

4.1.5 Test No. MGSATB-5

During test no. MGSATB-5, the bogie impacted the post at a speed of 21.9 mph (35.2 km/h). The post rotated through the soil to a maximum deflection of 21.4 in. (545 mm) at which point, the bogie vehicle was brought to a stop and then rebounded backward. The post bent backward resulting in yielding approximately 12 in. (305 mm) below the ground line.

Force vs. deflection and energy vs. deflection curves created from the EDR-3 accelerometer data are shown in Figure 13. A peak force of 22.4 kips (99.5 kN) was observed over the first few inches of deflection. The post provided a relatively constant resistance force of about 17 kips (76 kN) throughout the rest of the impact event. At the maximum deflection, the post absorbed 351.0 kip-in. (39.7 kJ) of energy. Time-sequential photographs and post-impact photographs are shown in Figure 14.

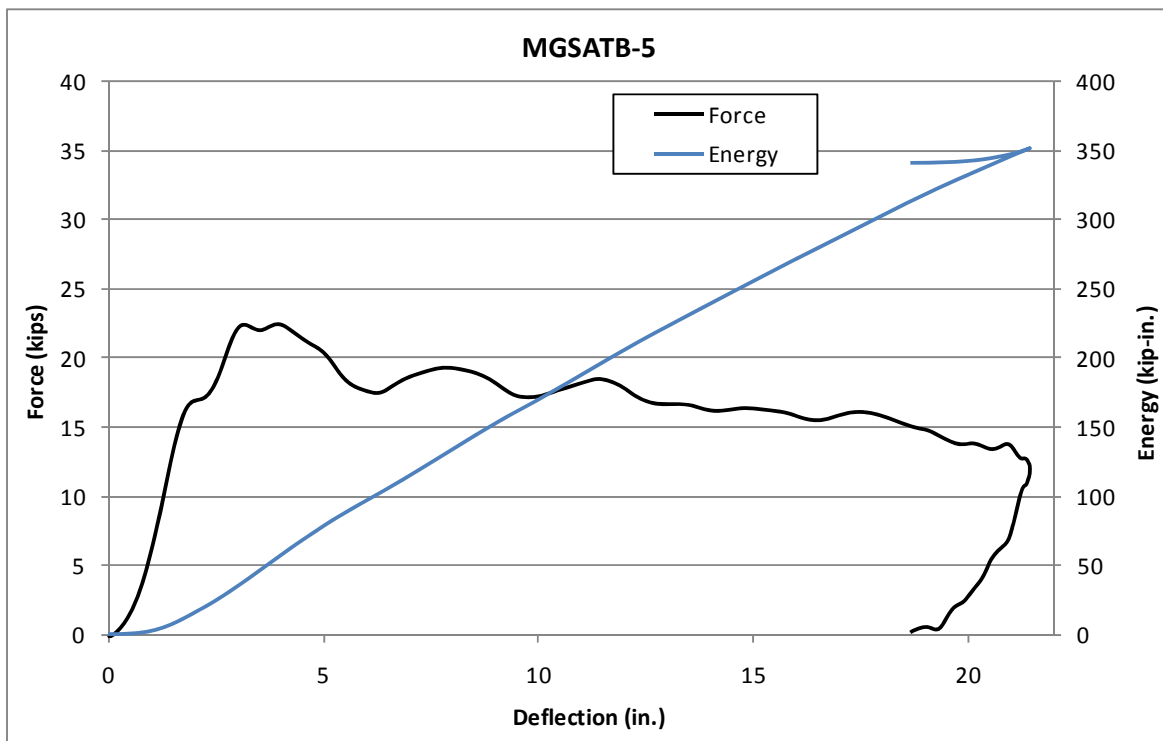


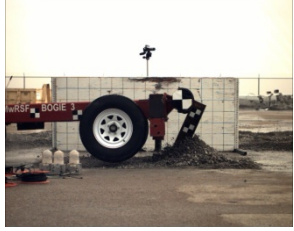
Figure 13. Force vs. Deflection and Energy vs. Deflection, Test No. MGSATB-5



IMPACT



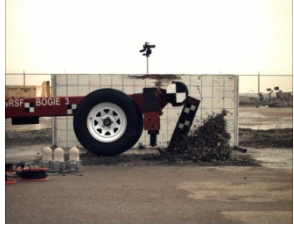
0.050 sec



0.100 sec



0.150 sec



0.200 sec



0.250 sec



Figure 14. Time Sequential and Post-Impact Photographs, Test No. MGSATB-5

4.1.6 Test No. MGSATB-6

During test no. MGSATB-6, the bogie impacted the post at a speed of 21.7 mph (34.9 km/h). As a result, the post rotated through the soil to a maximum deflection of 19.4 in. (493 mm) at which point, the bogie vehicle was brought to a stop and then rebounded backward. The post bent backwards resulting in yielding approximately 12 in. (305 mm) below the ground line.

Force vs. deflection and energy vs. deflection curves created from EDR-3 accelerometer data are shown in Figure 15. A peak force of 22.3 kips (99.3 kN) was observed over the first few inches of deflection. The post provided a relatively constant resistance force of around 18 kips (80 kN) throughout the rest of the impact event. At the maximum deflection, the post absorbed 343.9 kip-in. (38.9 kJ) of energy. Time-sequential photographs and post-impact photographs are shown in Figure 16.

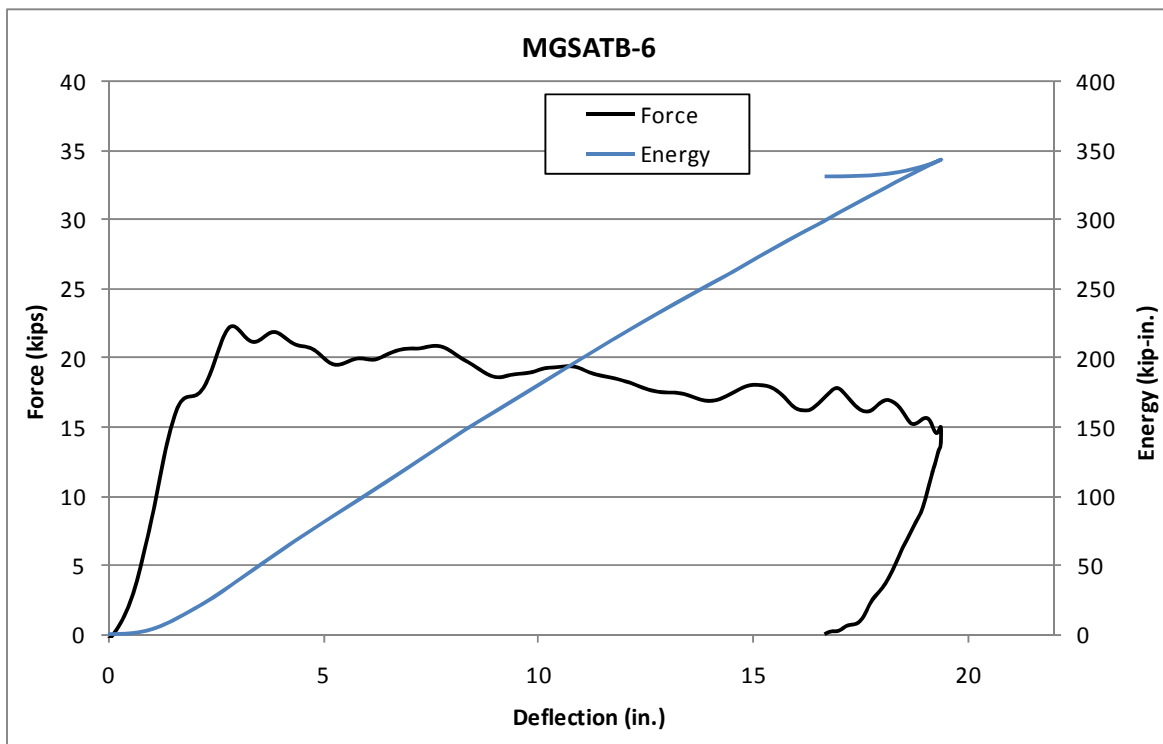


Figure 15. Force vs. Deflection and Energy vs. Deflection, Test No. MGSATB-6



IMPACT



0.050 sec



0.100 sec



0.150 sec



0.200 sec



0.250 sec



Figure 16. Time Sequential and Post-Impact Photographs, Test No. MGSATB-6

4.1.7 Test No. MGSATB-7

During test no. MGSATB-7, the bogie impacted the post at a speed of 21.4 mph (34.4 km/h). As a result, the post fractured at a deflection of 7.9 in. (201 mm), and the bogie traveled over the post stub. The post fractured approximately 4 in. (102 mm) below the ground line. The upper portion of the post split into two pieces when a vertical crack originated at the fracture location and traveled up to the top of the post. This vertical cracking took place 14 msec after impact and at a deflection around 5 in. (127 mm).

Force vs. deflection and energy vs. deflection curves created from EDR-3 accelerometer data are shown in Figure 17. The three force spikes show a systematic fracture of the post throughout the impact event. The post began to fracture at a deflection of 2.0 in. (51 mm), and at a peak force of 17.3 kips (76.9 kN). At fracture, the post absorbed 73.0 kip-in. (8.3 kJ) of energy. Time-sequential photographs and post-impact photographs are shown in Figure 18.

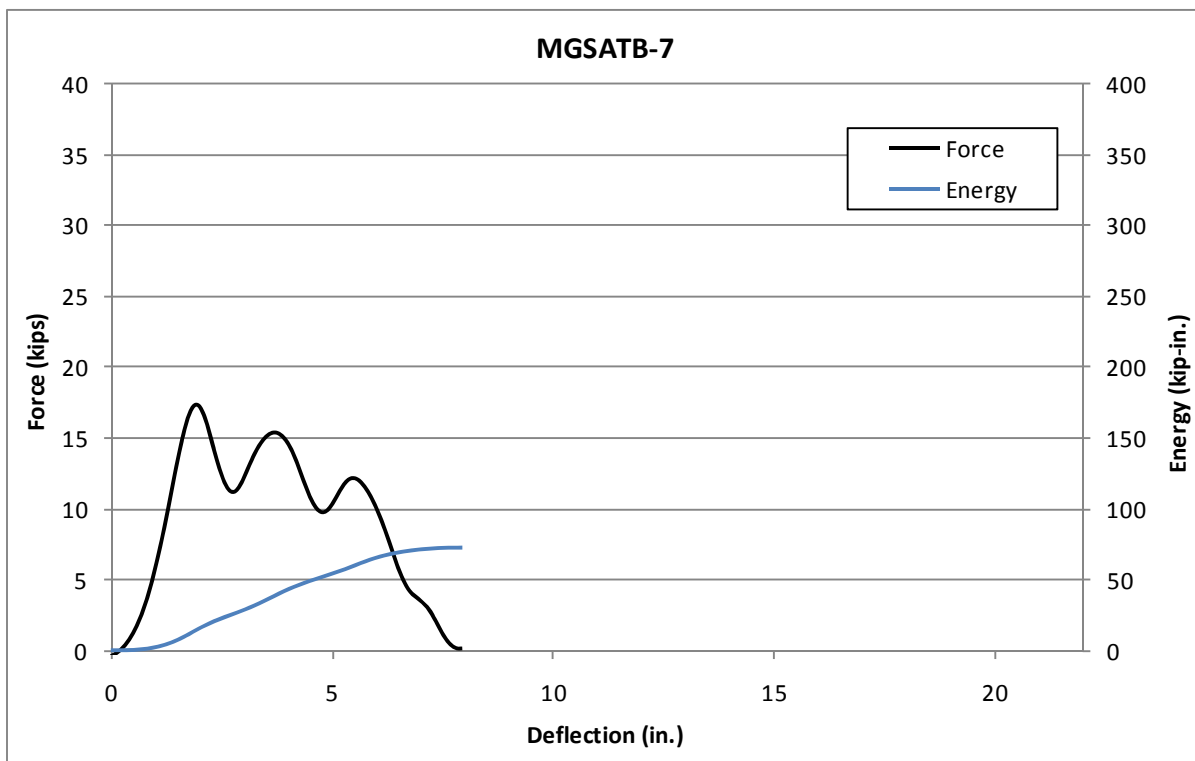
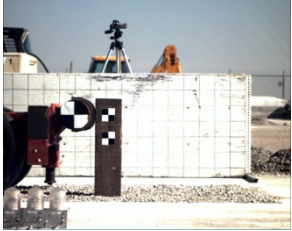


Figure 17. Force vs. Deflection and Energy vs. Deflection, Test No. MGSATB-7



IMPACT



0.050 sec



0.100 sec



0.150 sec



0.200 sec



0.250 sec



Figure 18. Time Sequential and Post-Impact Photographs, Test No. MGSATB-7

4.1.8 Test No. MGSATB-8

During test no. MGSATB-8, the bogie impacted the post at a speed of 21.9 mph (35.2 km/h). As a result, the post experienced a progressive fracture which concluded at a deflection of 5.7 in. (145 mm) with the bogie traveling over the post stub. The post fractured approximately 8 in. (203 mm) below the ground line.

Force vs. deflection and energy vs. deflection curves created from EDR-4 accelerometer data are shown in Figure 19. The two force spikes show a systematic fracture of the post throughout the impact event. A peak force of 24.6 kips (109.3 kN) was observed over the first few inches of deflection. At fracture, the post absorbed 66.8 kip-in. (7.5 kJ) of energy at. Time-sequential photographs and post-impact photographs are shown in Figure 20.

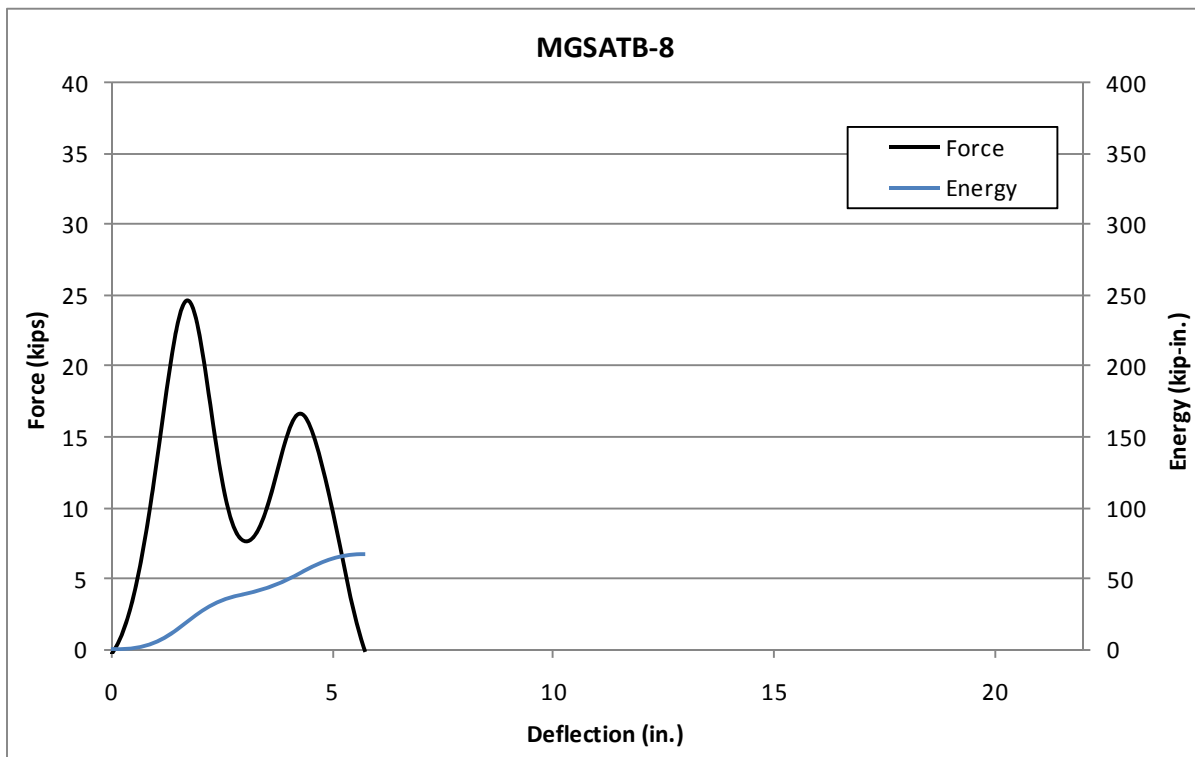


Figure 19. Force vs. Deflection and Energy vs. Deflection, Test No. MGSATB-8



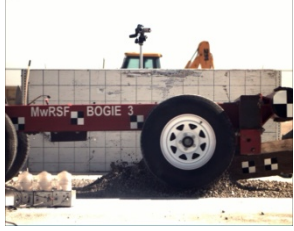
IMPACT



0.050 sec



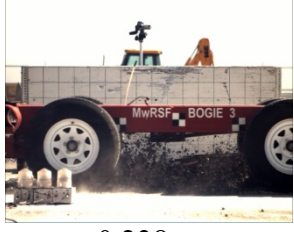
0.100 sec



0.150 sec



0.200 sec



0.238 sec



Figure 20. Time Sequential and Post-Impact Photographs, Test No. MGSATB-8

4.1.9 Test No. MGSATB-9

During test no. MGSATB-9, the bogie impacted the post at a speed of 19.9 mph (32.0 km/h). As a result, the post fractured at a deflection of 4.8 in. (122 mm), and the bogie traveled over the post stub. The post fractured approximately 15 in. (381 mm) below the ground line.

Force vs. deflection and energy vs. deflection curves created from the EDR-3 accelerometer data are shown in Figure 21. A peak force of 15.7 kips (69.8 kN) was observed over the first few inches of deflection. At fracture, the post absorbed 37.3 kip-in. (4.2 kJ) of energy. Time-sequential photographs and post-impact photographs are shown in Figure 22.

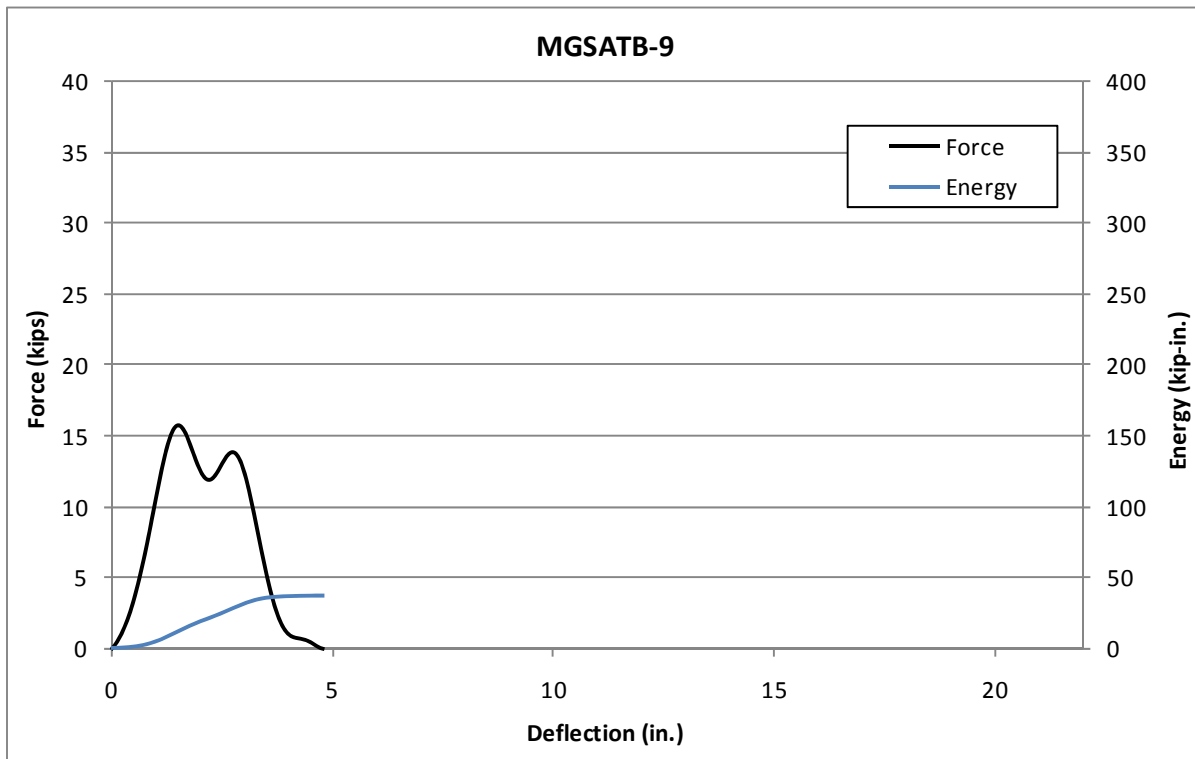


Figure 21. Force vs. Deflection and Energy vs. Deflection, Test No. MGSATB-9



IMPACT



0.050 sec



0.100 sec



0.150 sec



0.200 sec



0.250 sec



Figure 22. Time Sequential and Post-Impact Photographs, Test No. MGSATB-9

4.1.10 Test No. MGSATB-10

During test no. MGSATB-10, the bogie impacted the post at a speed of 20.5 mph (33.0 km/h). As a result, the post rotated through the soil to a maximum deflection of 11.2 in. (284 mm), at which point, the bogie vehicle was brought to a stop and then rebounded backward. The wood post remained undamaged.

Force vs. deflection and energy vs. deflection curves created from the EDR-3 accelerometer data are shown in Figure 23. The forces quickly rose to a peak force of 36.7 kips (163.3 kN) over the first few inches of deflection. The post provided an average resistance force of 28 kips (120 kN) through 10 in. (254 mm) of deflection. The post absorbed 307.4 kip-in. (34.7 kJ) of energy. Time-sequential photographs and post-impact photographs are shown in Figure 24.

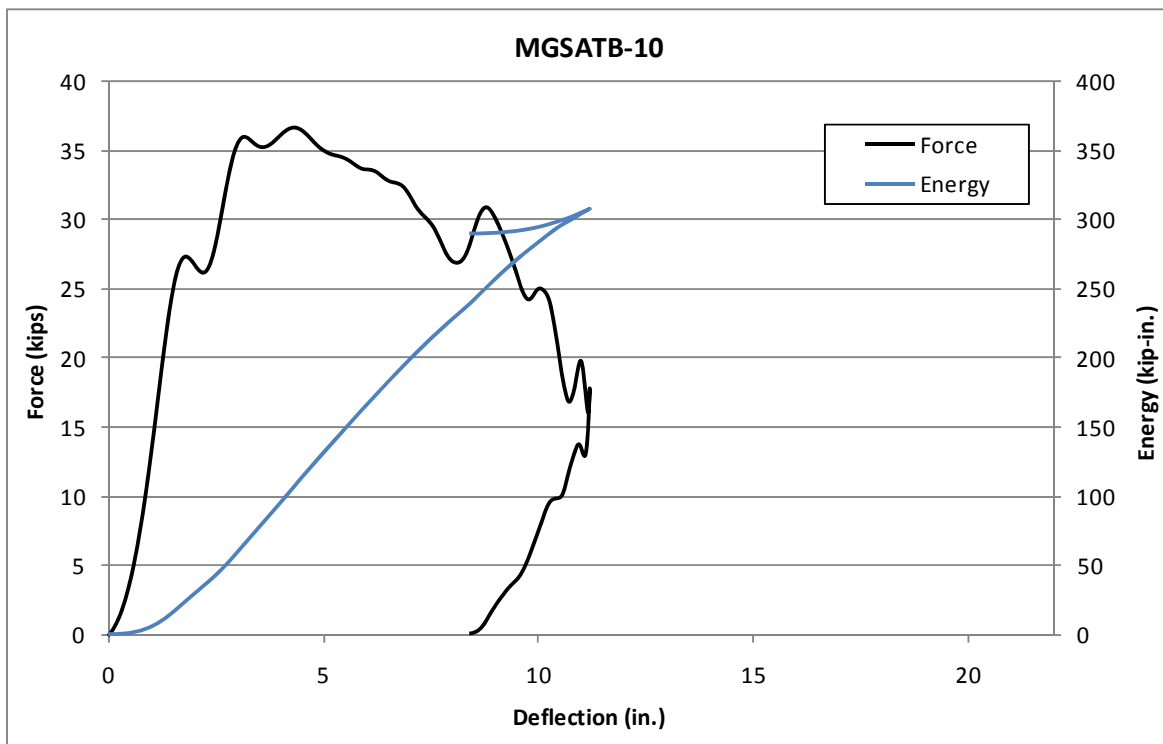


Figure 23. Force vs. Deflection and Energy vs. Deflection, Test No. MGSATB-10



IMPACT



0.050 sec



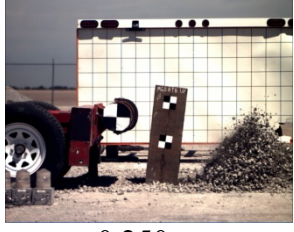
0.100 sec



0.150 sec



0.200 sec



0.250 sec



Figure 24. Time Sequential and Post-Impact Photographs, Test No. MGSATB-10

4.1.11 Test No. MGSATB-11

During test no. MGSATB-11, the bogie impacted the post at a speed of 20.6 mph (33.2 km/h). As a result, the post rotated through the soil to a maximum deflection of 12.9 in. (328 mm), at which point, the bogie vehicle was brought to a stop and then rebounded. The wood post remained undamaged.

Force vs. deflection and energy vs. deflection curves created from the EDR-3 accelerometer data are shown in Figure 25. The force rapidly increased to a peak force of 30.9 kips (137.4 kN) over the first few inches of deflection. The post provided an average resistance force of more than 25 kips (110 kN) through 10 in. (254 mm) of deflection. The post absorbed 311.7 kip-in. (35.2 kJ) of energy. Time-sequential photographs and post-impact photographs are shown in Figure 26.

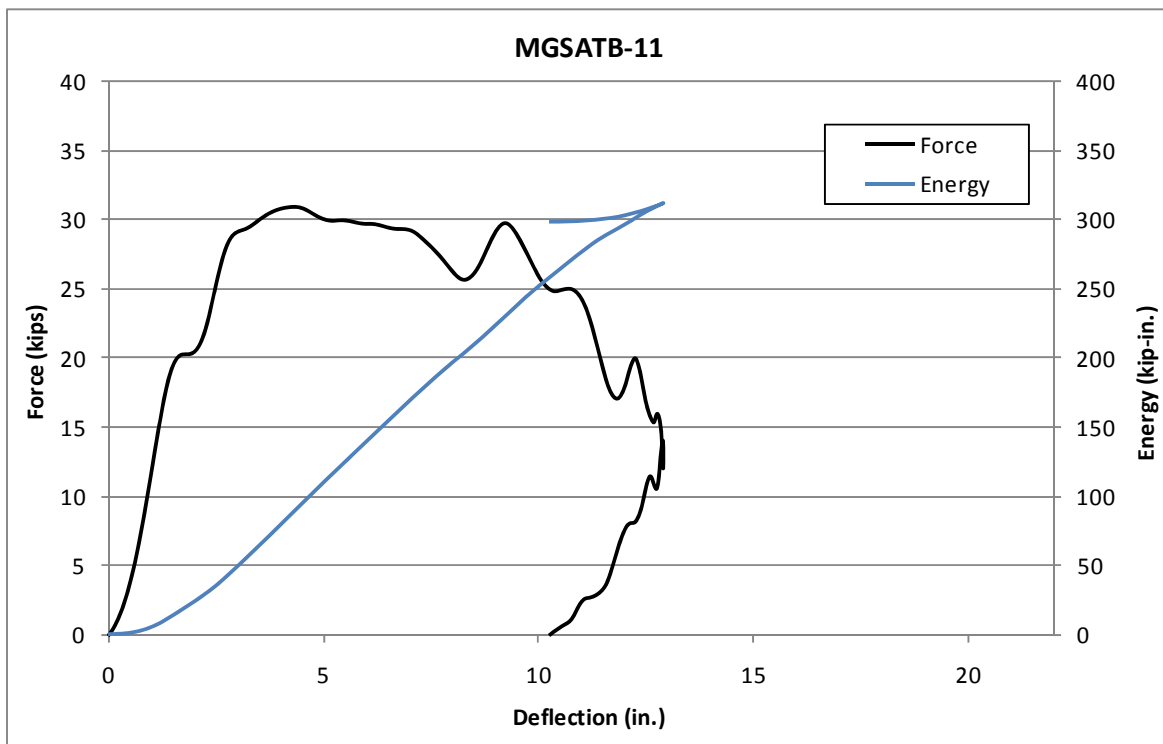


Figure 25. Force vs. Deflection and Energy vs. Deflection, Test No. MGSATB-11



IMPACT



0.050 sec



0.100 sec



0.150 sec



0.200 sec



0.250 sec

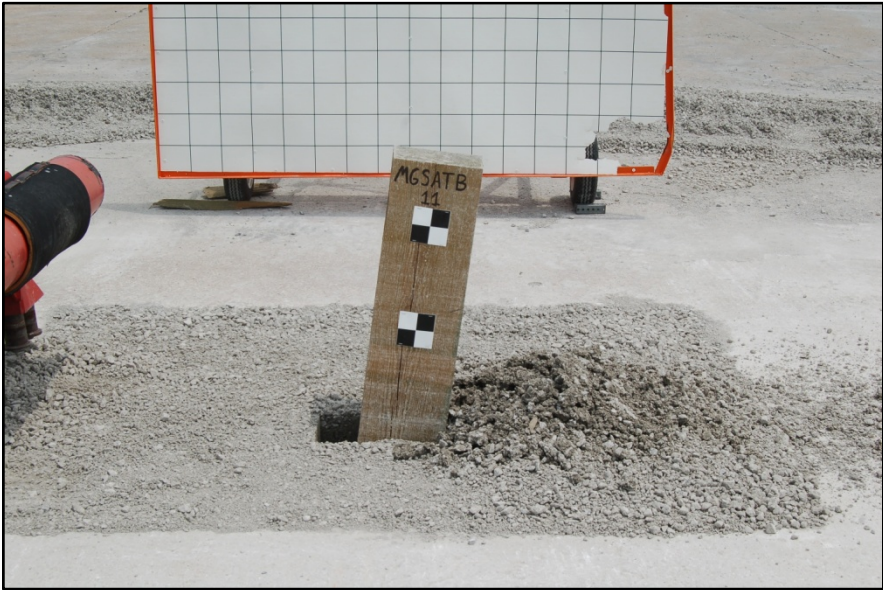


Figure 26. Time Sequential and Post-Impact Photographs, Test No. MGSATB-11

4.1.12 Test No. MGSATB-12

During test no. MGSATB-12, the bogie impacted the post at a speed of 19.4 mph (31.2km/h). As a result, the post rotated through the soil to a maximum deflection of 13.6 in. (345 mm), at which point, the bogie vehicle was brought to a stop and then rebounded backward. The wood post remained undamaged.

Force vs. deflection and energy vs. deflection curves created from the EDR-3 accelerometer data are shown in Figure 27. Initially, the force rapidly increased to a peak force of 25.6 kips (113.7 kN) over the first few inches of deflection. The post provided an average resistance force over 20 kips (90 kN) through 11 in. (279 mm) of deflection. The post absorbed a 275.5 kip-in. (31.1 kJ) of energy. Time-sequential photographs and post-impact photographs are shown in Figure 28.

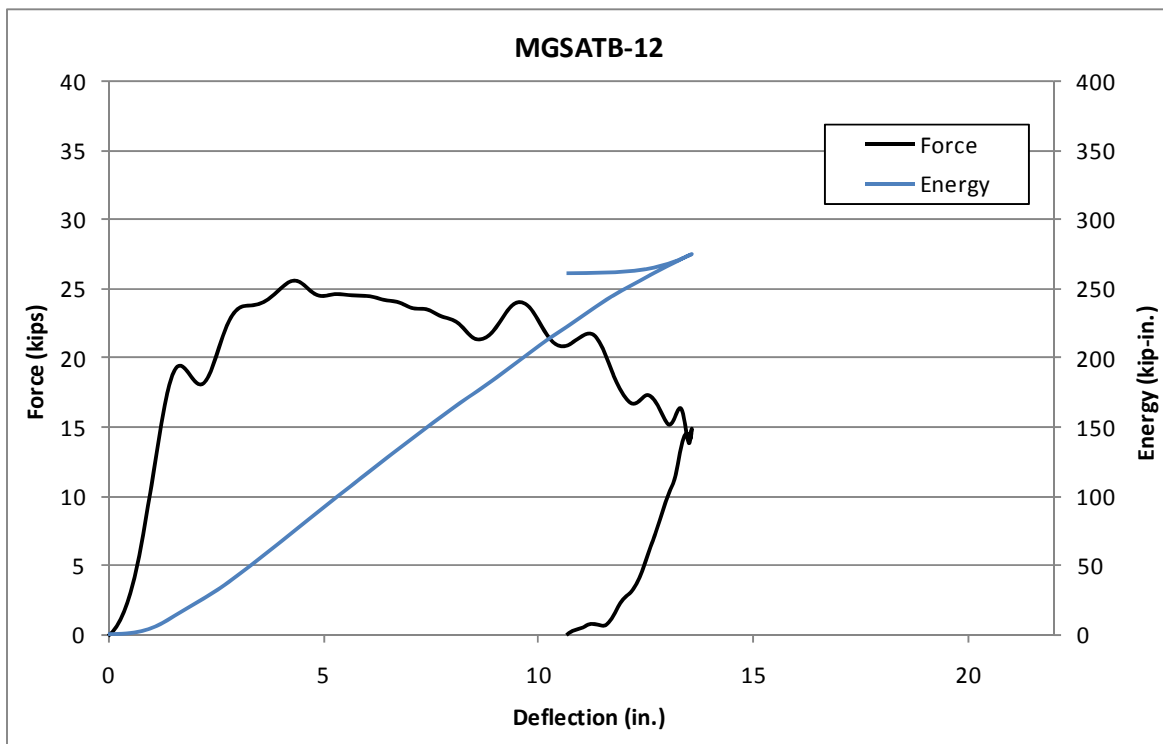


Figure 27. Force vs. Deflection and Energy vs. Deflection, Test No. MGSATB-12



IMPACT



0.050 sec



0.100 sec



0.150 sec



0.200 sec



0.250 sec



Figure 28. Time Sequential and Post-Impact Photographs, Test No. MGSATB-12

4.1.13 Test No. MGSATB-13

During test no. MGSATB-13, the bogie impacted the post at a speed of 20.2 mph (32.6 km/h). As a result, the post rotated through the soil to a maximum deflection of 20.5 in. (522 mm), at which point, the bogie vehicle was brought to a stop and then rebounded backward. The wood post remained undamaged.

Force vs. deflection and energy vs. deflection curves created from the EDR-3 accelerometer data are shown in Figure 29. Initially, inertial effects resulted in a peak force of 19.1 kips (85.0 kN) at a deflection of 1.4 in. (37 mm). The post provided a relatively constant resistance force of around 15 kips (67 kN) through 17 in. (432 mm) of deflection. The post absorbed 298.8 kip-in. (33.8 kJ) of energy. Time-sequential photographs and post-impact photographs are shown in Figure 30.

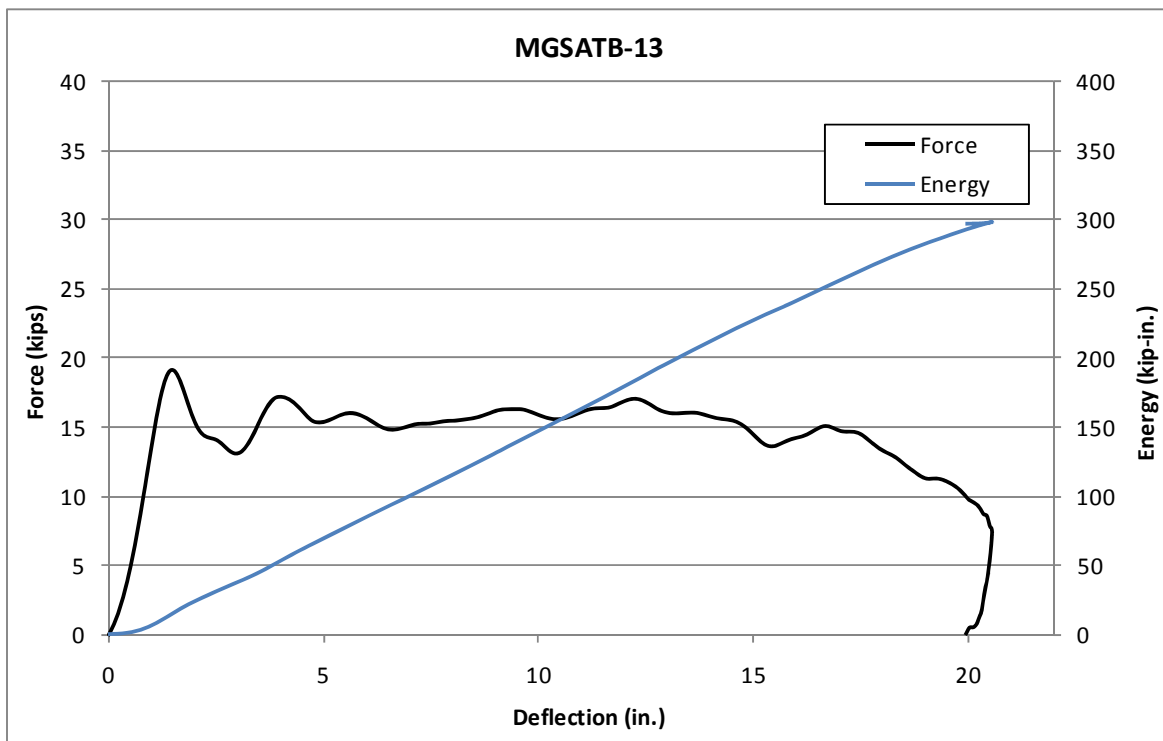


Figure 29. Force vs. Deflection and Energy vs. Deflection, Test No. MGSATB-13



IMPACT



0.050 sec



0.100 sec



0.150 sec



0.200 sec



0.250 sec



Figure 30. Time Sequential and Post-Impact Photographs, Test No. MGSATB-13

4.1.14 Test No. MGSATB-14

During test no. MGSATB-14, the bogie impacted the post at a speed of 19.7 mph (31.7 km/h). As a result, the post rotated through the soil to a maximum deflection of 17.0 in. (432 mm), at which point, the bogie vehicle was brought to a stop and then rebounded backward. The wood post remained undamaged.

Force vs. deflection and energy vs. deflection curves created from the EDR-3 accelerometer data are shown in Figure 31. Initially, the force rapidly increased to a peak force of 20.5 kips (91.2 kN). The post provided an average resistance force of around 19 kips (85 kN) through 11 in. (279 mm) of deflection. The post absorbed 283.5 kip-in. (32.0 kJ) of energy. Time-sequential photographs and post-impact photographs are shown in Figure 32.

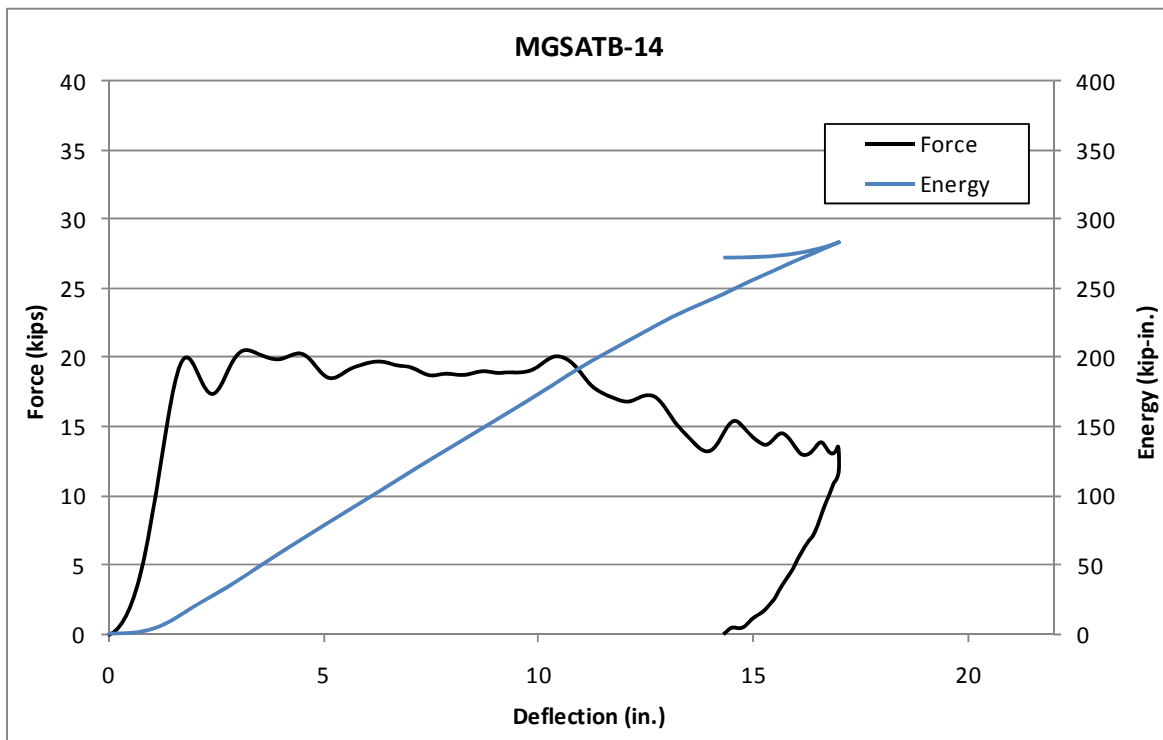
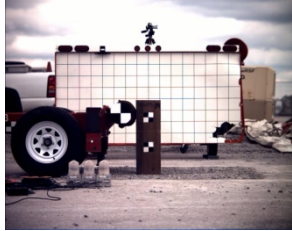


Figure 31. Force vs. Deflection and Energy vs. Deflection, Test No. MGSATB-14



IMPACT



0.050 sec



0.100 sec



0.150 sec



0.200 sec



0.250 sec



Figure 32. Time Sequential and Post-Impact Photographs, Test No. MGSATB-14

4.1.15 Test No. MGSATB-15

During test no. MGSATB-15, the bogie impacted the post at a speed of 21.0 mph (33.8 km/h). As a result, the post rotated through the soil to a maximum deflection of 16.8 in. (427 mm), at which point, the bogie vehicle was brought to a stop and then rebounded backward. The post showed early signs of fracture as cracks were found on the tension side face of the post at 8 in. (203 mm) below the ground line. The post was also bent downstream at this same location.

Force vs. deflection and energy vs. deflection curves created from the EDR-3 accelerometer data are shown in Figure 33. Initially, the force rapidly increased to 35 kips (156 kN) and remained at this magnitude until 9 in. (229 mm) of deflection. The load decrease beyond this deflection was attributed to the cracks that formed on the tension side face of the post. The post absorbed 325.6 kip-in. (36.8 kJ) of energy. Time-sequential photographs and post-impact photographs are shown in Figure 34.

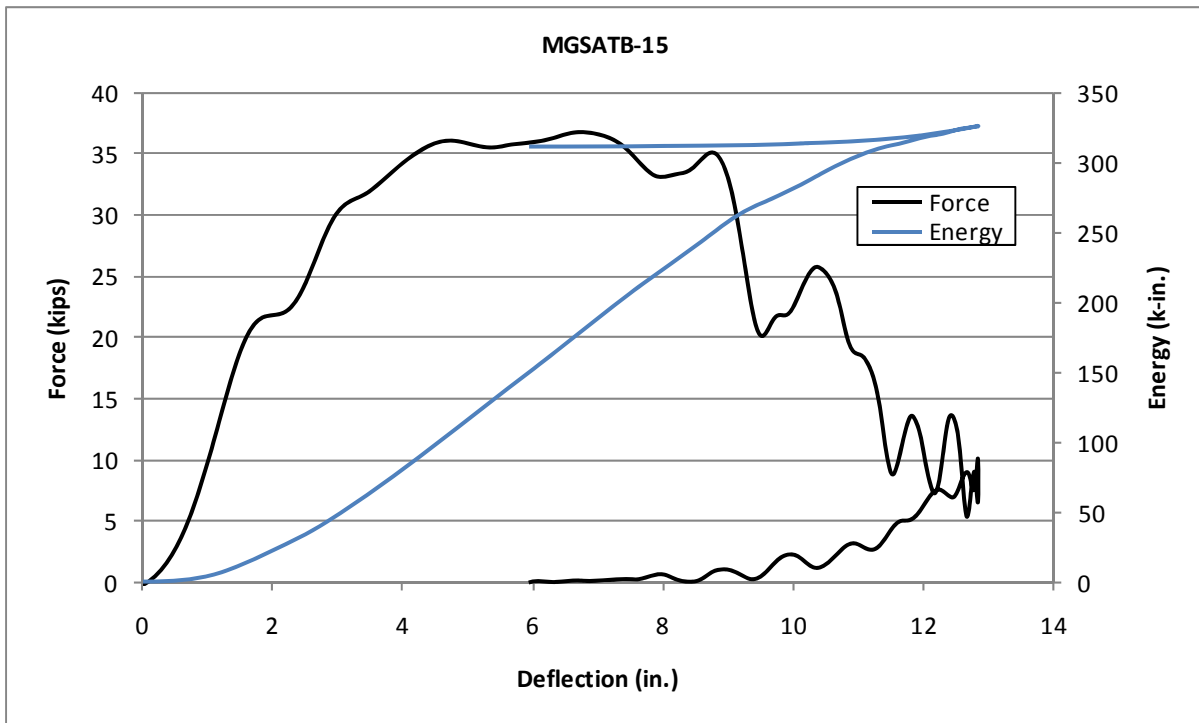


Figure 33. Force vs. Deflection and Energy vs. Deflection, Test No. MGSATB-15



IMPACT



0.050 sec



0.100 sec



0.150 sec



0.200 sec



0.250 sec



Figure 34. Time Sequential and Post-Impact Photographs, Test No. MGSATB-15

4.1.16 Test No. MGSATB-16

During test no. MGSATB-16, the bogie impacted the post at a speed of 20.2 mph (32.5 km/h). As a result, the post began to rotate through the soil but fractured at a displacement of 10.4 in. (264 mm). The post fractured near ground line.

Force vs. deflection and energy vs. deflection curves created from the EDR-3 accelerometer data are shown in Figure 35. The resistance force steadily increased until it reached a peak force of 30.7 kips (136.5 kN) at 6 in. (152 mm) of deflection, when the post began to fracture. At fracture, the post absorbed 194.4 kip-in. (22.0 kJ) of energy. Time-sequential photographs and post-impact photographs are shown in Figure 36.

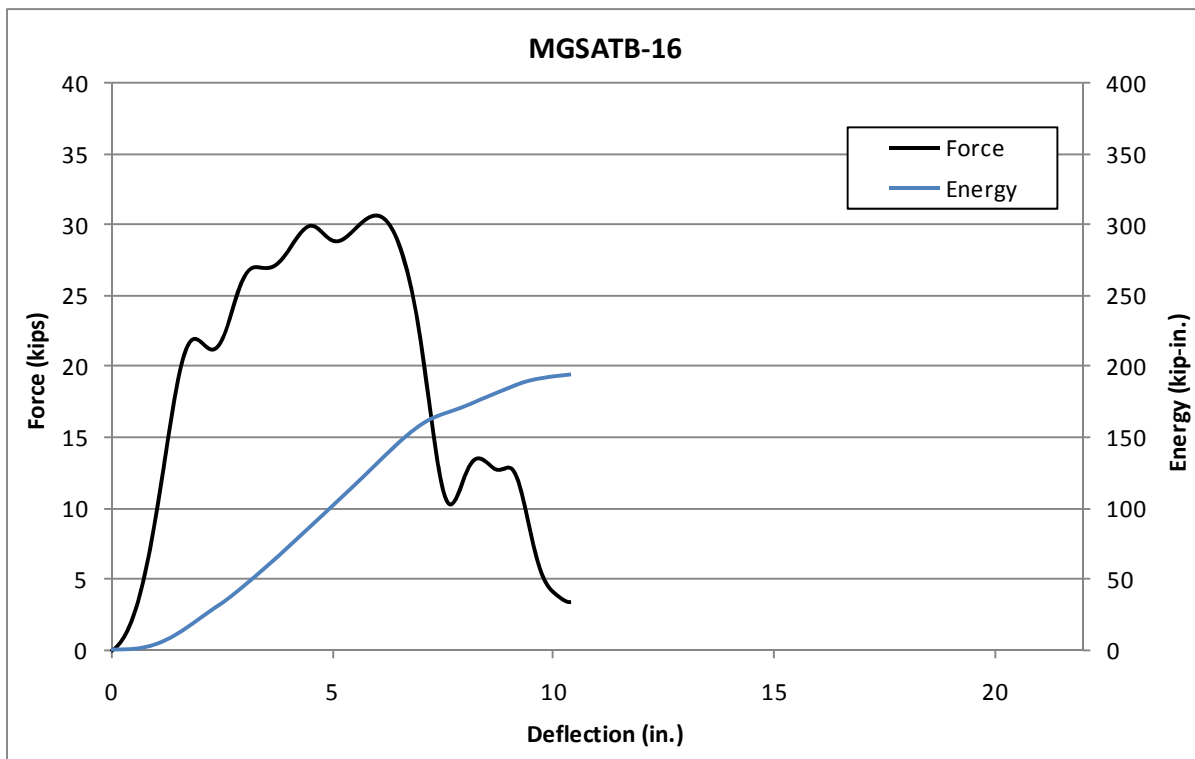


Figure 35. Force vs. Deflection and Energy vs. Deflection, Test No. MGSATB-16



IMPACT



0.050 sec



0.100 sec



0.150 sec



0.200 sec



0.250 sec



Figure 36. Time Sequential and Post-Impact Photographs, Test No. MGSATB-16

4.1.17 Test No. MGSATB-17

During test no. MGSATB-17, the bogie impacted the post at a speed of 19.6 mph (31.5 km/h). As a result, the post rotated through the soil to a maximum deflection of 12.3 in. (312 mm), at which point, the bogie vehicle was brought to a stop and then rebounded backward. The wood post remained undamaged.

Force vs. deflection and energy vs. deflection curves created from the EDR-3 accelerometer data are shown in Figure 37. The resistance increased rapidly to a peak force of 34.8 kips (154.8 kN) over the first few inches of deflection. The post provided an average resistance force of 27.5 kips (122.3kN) through 10 in. (25.4 mm) of deflection. The post absorbed 286.5 kip-in. (32.4 kJ) of energy. Time-sequential photographs and post-impact photographs are shown in Figure 38.

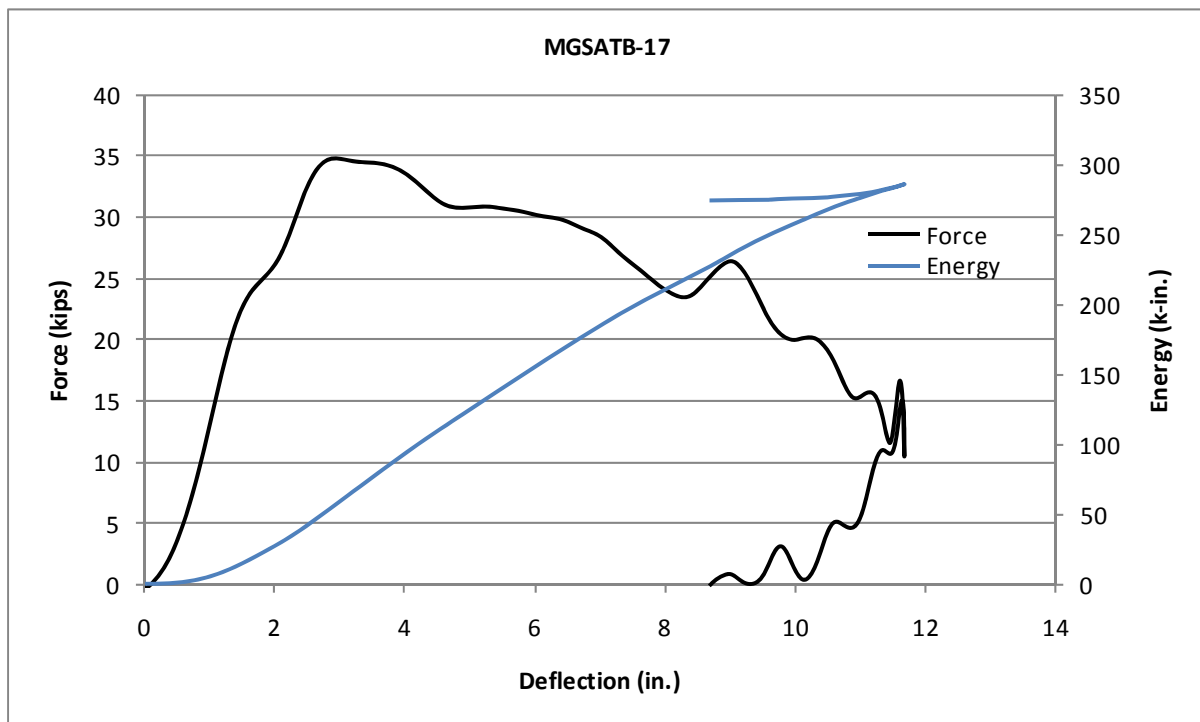


Figure 37. Force vs. Deflection and Energy vs. Deflection, Test No. MGSATB-17



IMPACT



0.050 sec



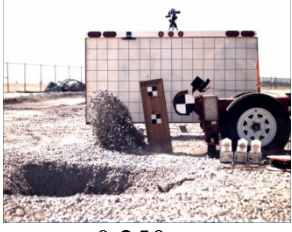
0.100 sec



0.150 sec



0.200 sec



0.250 sec



Figure 38. Time Sequential and Post-Impact Photographs, Test No. MGSATB-17

4.1.18 Test No. MGSATB-18

During test no. MGSATB-18, the bogie impacted the post at a speed of 21.0 mph (33.8 km/h). As a result, the post rotated through the soil to a maximum deflection of 18.0 in. (457 mm), at which point, the bogie vehicle was brought to a stop and then rebounded backward. The wood post remained undamaged.

Force vs. deflection and energy vs. deflection curves created from the EDR-3 accelerometer data are shown in Figure 39. After the initial stiffness increase over the first few inches of deflection, the post provided a relatively constant resistance force of around 20 kips (90 kN). A peak force of 21.8 kips (96.8 kN) was observed at 10 in. (25.4 mm) of deflection. The post absorbed 352.2 kip-in. (36.7 kJ) of energy. Time-sequential photographs and post-impact photographs are shown in Figure 40.

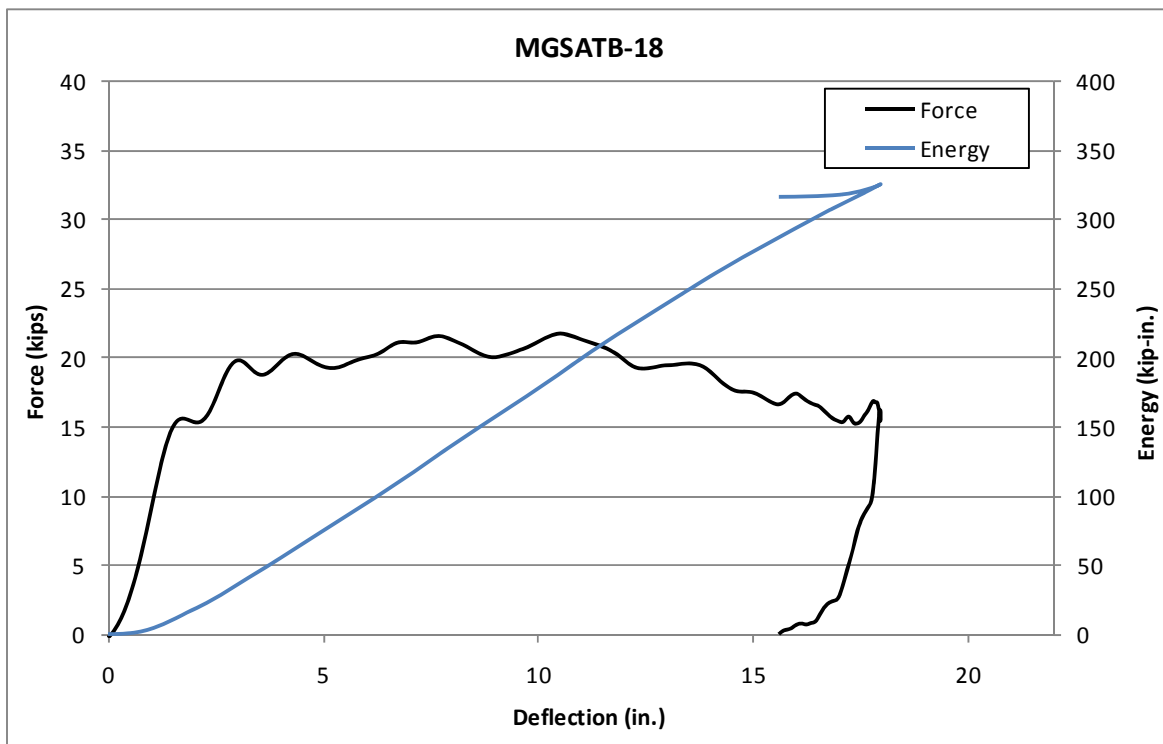


Figure 39. Force vs. Deflection and Energy vs. Deflection, Test No. MGSATB-18



IMPACT



0.050 sec



0.100 sec



0.150 sec



0.200 sec



0.250 sec



Figure 40. Time Sequential and Post-Impact Photographs, Test No. MGSATB-18

4.1.19 Test No. MGSATB-19

During test no. MGSATB-19, the bogie impacted the post at a speed of 19.7 mph (31.7 km/h). As a result, the post fractured into three pieces, and the bogie traveled over the post stub. The upper portion of the post split in to two pieces through a preexisting vertical crack on the left side of the post. After splitting, the upper pieces fractured from the bottom portion of the post at approximately 8 in. (203 mm) below the ground line.

Force vs. deflection and energy vs. deflection curves created from the EDR-3 accelerometer data are shown in Figure 41. Before fracture, the post provided a resistance force of around 15 kips (65 kN) with a peak force of 17.0 kips (75.8 kN) at a deflection of 6.7 in. (170 mm). At fracture, the post absorbed 124.3 kip-in. (14.0 kJ) of energy. Time-sequential photographs and post-impact photographs are shown in Figure 42.

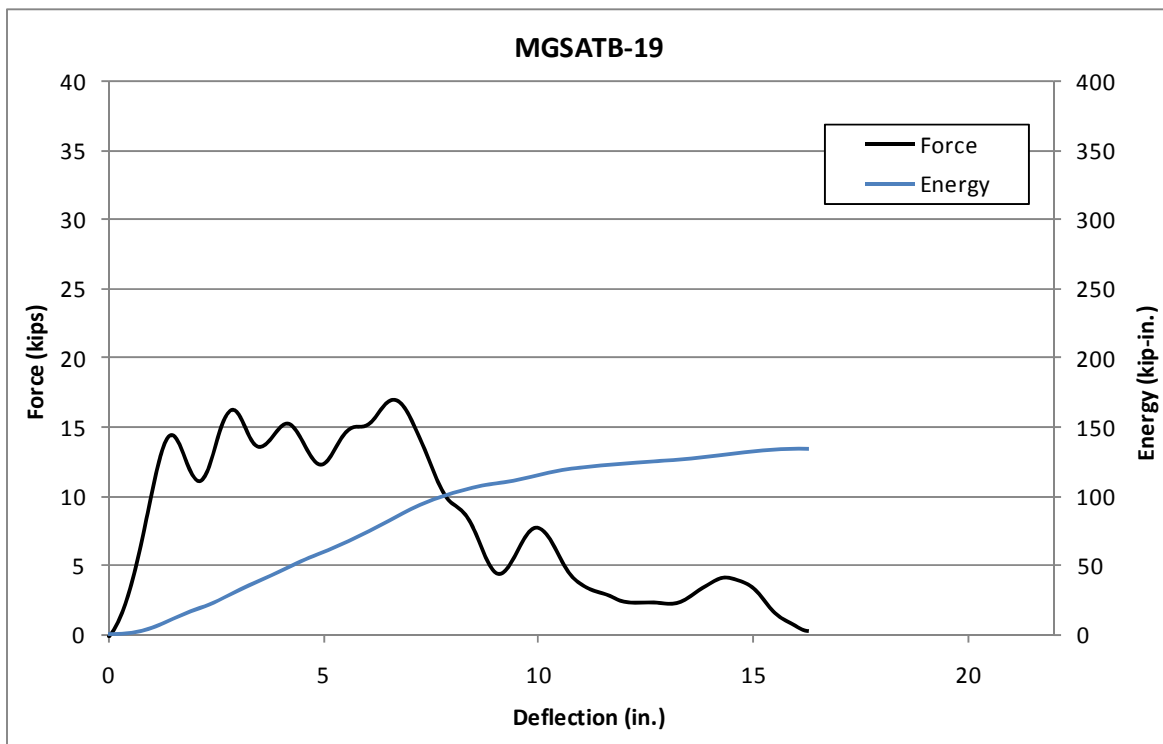


Figure 41. Force vs. Deflection and Energy vs. Deflection, Test No. MGSATB-19



IMPACT



0.050 sec



0.100 sec



0.150 sec



0.200 sec



0.250 sec



Figure 42. Time Sequential and Post-Impact Photographs, Test No. MGSATB-19

4.1.20 Test No. MGSATB-20

During test no. MGSATB-20, the bogie impacted the post at a speed of 24.5 mph (39.5 km/h). As a result, the post fractured at a deflection of 4.2 in. (108 mm), and the bogie traveled over the post stub. The post fractured at approximately 8 in. (20 cm) below the ground line.

Force vs. deflection and energy vs. deflection curves created from the EDR-3 accelerometer data are shown in Figure 43. Due to early post failure, only a single force spike was recorded. The peak force was 13.9 kips (61.9 kN) at a deflection of 1.9 in. (48 kN). The post absorbed 28.5 kip-in. (3.2 kJ) of energy at the time of fracture. Time-sequential photographs and post-impact photographs are shown in Figure 44.

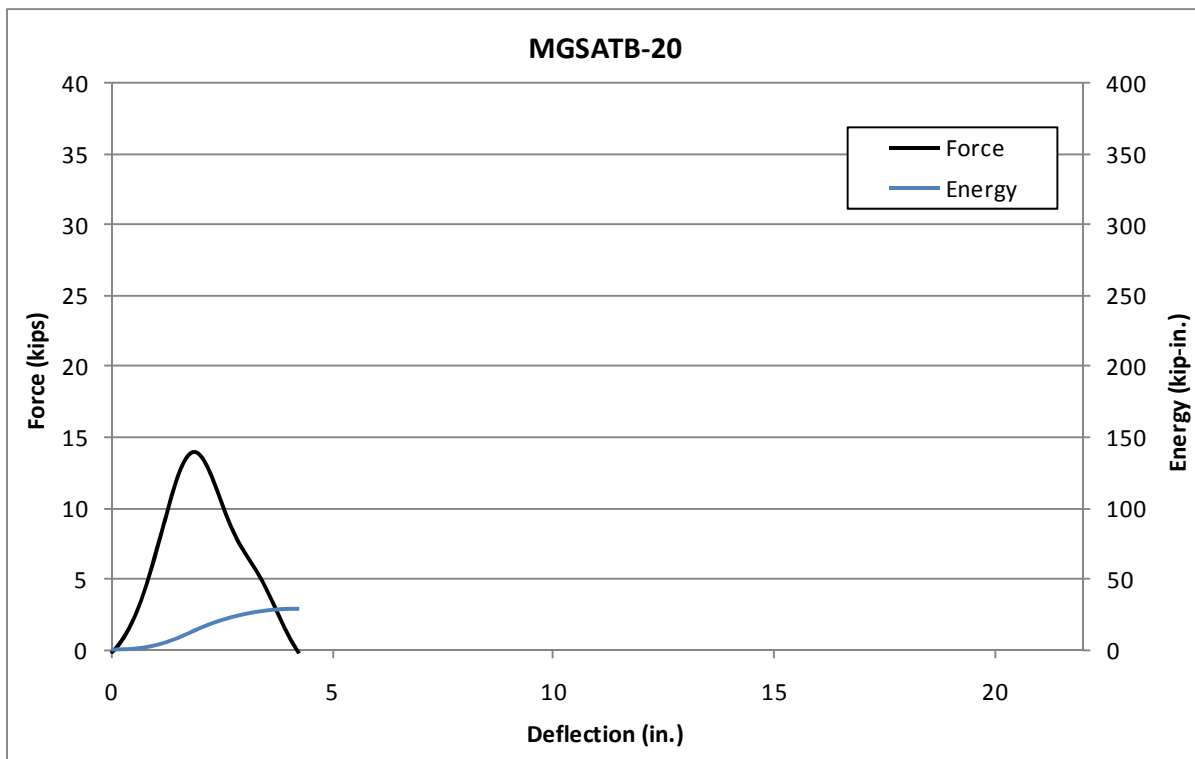
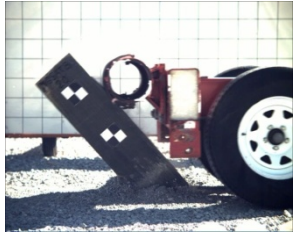


Figure 43. Force vs. Deflection and Energy vs. Deflection, Test No. MGSATB-20



IMPACT



0.050 sec



0.100 sec



0.150 sec



0.200 sec



0.250 sec



Figure 44. Time Sequential and Post-Impact Photographs, Test No. MGSATB-20

4.2 Discussion

The results from the bogie testing matrix are summarized in Table 7. The bogie impact speed was relatively constant throughout the testing matrix with a target impact velocity of 20 mph (32 km/h). Thus, the energy absorption variances were the result of the failure mechanism. Posts that rotated through the soil absorbed all of the kinetic energy of the impacting bogie. Alternatively, posts that fractured experienced a quick and abrupt end to the resistance force, absorbed much less energy, and allowed the bogie vehicle to travel past the impact location.

Setting aside post strength and fracture, the variance in soil resistance forces was attributed to post dimensions and soil compaction. Wider posts and posts with greater embedment depths displace a greater amount of soil as they rotate, resulting in increased resistance forces. Although increasing the depth of the cross section greatly increases the bending strength of the post, it should have virtually no effect on the soil resistance.

Resistance force differences between tests with identical post sizes can be explained by variances in soil compaction and strength. This was best illustrated by comparing the results from test nos. MGSATB-1 and MGSATB-2 with moderately compacted soil to the results from test nos. MSGATB-5 and MGSATB-6 with heavily compacted soil. All four tests were conducted on identical W6x15 (W152x22.3) steel posts. From this comparison, a force increase of roughly 30 percent was observed for the posts placed in heavily compacted soil. This noted increase in soil resistance along with a higher propensity for wood post fracture led the researchers to believe that heavily compacted soils were critical for wood posts. As a result, only the first four tests were conducted with moderately compacted soil while the rest were installed in heavily compacted soil.

Table 7. Dynamic Testing Results

Test No.	Post Type, in. x in. (mm x mm)	Embed. Depth in. (mm)	Bogie Speed mph (km/h)	Average Force			Peak Force kip (kN)	Max Disp. in. (mm)	Failure Type	Max Energy kip-in. (kJ)
				@ 5" kip (kN)	@ 10" kip (kN)	@ 15" kip (kN)				
MGSATB-1	Steel W6x15 (W152x22.3)	54 (1,372)	19.2 (30.9)	9.1 (40.5)	11.2 (49.8)	13.3 (59.4)	20.1 (89.5)	19.5 (496)	Post Yielding & Rotation in Soil	268.5 (30.3)
MGSATB-2	Steel W6x15 (W152x22.3)	54 (1,372)	19.7 (31.7)	9.3 (41.2)	10.6 (47.2)	13.4 (59.7)	19.9 (88.7)	19.3 (490)	Post Yielding & Rotation in Soil	282.8 (31.9)
MGSATB-3	SYP 8x8 (203 x 203)	54 (1,372)	18.2 (29.3)	7.2 (32.0)	9.2* (41.0)*	NA	14.7 (65.2)	10.9** (277)	Post Fracture	94.6 (10.7)
MGSATB-4	SYP 8x8 (203 x 203)	54 (1,372)	18.7 (30.1)	7.3 (32.4)	10.6 (47.0)	11.9* (53.0)*	25.4 (112.9)	13.7** (348)	Post Fracture	180.9 (20.4)
MGSATB-5	Steel W6x15 (W152x22.3)	54 (1,372)	21.9 (35.2)	15.4 (68.6)	16.9 (75.3)	16.9 (75.3)	22.4 (99.5)	21.4 (545)	Post Yielding & Rotation in Soil	351.0 (39.7)
MGSATB-6	Steel W6x15 (W152x22.3)	54 (1,372)	21.7 (34.9)	16.2 (71.9)	17.9 (79.7)	18.0 (80.2)	22.3 (99.3)	19.4 (493)	Post Yielding & Rotation in Soil	343.9 (38.9)
MGSATB-7	SYP 8x8 (203 x 203)	54 (1,372)	21.4 (34.4)	10.9 (48.4)	7.5* (33.2)*	NA	17.3 (76.9)	7.9** (201)	Post Fracture	73.0 (8.3)
MGSATB-8	SYP 8x8 (203 x 203)	54 (1,372)	21.9 (35.2)	12.7 (56.4)	6.9* (30.5)*	NA	24.6 (109.4)	5.7** (145)	Post Fracture	66.8 (7.5)
MGSATB-9	SYP 8x10 (203 x 254)	54 (1,372)	19.9 (32.0)	7.5* (33.2)*	NA	NA	15.7 (69.8)	4.8** (122)	Post Fracture	37.3 (4.2)
MGSATB-10	SYP 10x10 (254 x 254)	54 (1,372)	20.5 (33.0)	25.6 (114.0)	28.2 (125.5)	NA	36.7 (163.3)	11.2 (284)	Rotation in Soil	307.4 (34.7)
MGSATB-11	SYP 8x10 (203 x 254)	54 (1,372)	20.6 (33.2)	21.6 (95.9)	25.1 (111.5)	NA	30.9 (137.4)	12.9 (328)	Rotation in Soil	311.7 (35.2)

* Fracture had already been initiated.

** Displacement associated with the end of fracture.

Table 7 (continued). Dynamic Testing Results

Test No.	Post Type	Embed. Depth in. (mm)	Bogie Speed mph (km/h)	Average Force			Peak Force kip (kN)	Max Disp. in. (mm)	Failure Type	Max Energy kip-in. (kJ)
				@ 5" kip (kN)	@ 10" kip (kN)	@ 15" kip (kN)				
MGSATB-12	SYP 8x10 (203 x 254)	54 (1,372)	19.4 (31.2)	18.1 (80.4)	20.8 (92.7)	NA	25.6 (113.7)	13.6 (345)	Rotation in Soil	275.5 (31.1)
MGSATB-13	SYP 8x10 (203 x 254)	48 (1,219)	20.2 (32.6)	13.7 (60.9)	14.6 (65.1)	15.1 (67.4)	19.1 (85.0)	20.5 (522)	Rotation in Soil	298.8 (33.8)
MGSATB-14	SYP 8x10 (203 x 254)	48 (1,219)	19.7 (31.7)	15.6 (69.3)	17.2 (76.7)	17.1 (75.9)	20.5 (91.2)	17.0 (432)	Rotation in Soil	283.5 (32.0)
MGSATB-15	SYP 8x10 (203 x 254)	48 (1,219)	21.0 (33.8)	20.0 (88.9)	24.5 (109.2)	20.8 (92.6)	31.5 (140.1)	16.8 (427)	Rotation in Soil	324.5 (36.7)
MGSATB-16	SYP 8x10 (203 x 254)	48 (1,219)	20.2 (32.5)	20.1 (89.3)	19.3* (85.9)*	NA	30.7 (136.5)	10.4** (264)	Post Fracture	194.4 (22.0)
MGSATB-17	SYP 8x10 (203 x 254)	48 (1,219)	19.6 (31.5)	23.4 (104.2)	24.7 (109.7)	NA	32.1 (142.8)	12.3 (312)	Rotation in Soil	285.6 (32.3)
MGSATB-18	SYP 6x10 (152 x 254)	52 (1,321)	21.0 (33.8)	14.7 (65.6)	17.7 (78.8)	18.4 (81.9)	21.8 (96.8)	18.0 (457)	Rotation in Soil	352.2 (36.7)
MGSATB-19	SYP 6x10 (152 x 254)	52 (1,321)	19.7 (31.7)	11.8 (52.6)	11.5* (51.3)*	NA	17.0 (75.8)	13.1** (333)	Post Fracture	124.3 (14.0)
MGSATB-20	SYP 6x10 (152 x 254)	52 (1,321)	24.5 (39.5)	5.5* (24.6)*	NA	NA	13.9 (61.9)	4.2** (107)	Post Fracture	28.5 (3.2)

* Fracture had already been initiated.

** Displacement associated with the end of fracture.

4.2.1 W6x15 (W152x22.3) Steel Posts, 7 ft (2.1 m) Long

Four tests were conducted on 7-ft (2.1-m) long W6x15 (W152x22.3) steel posts in order to establish the force deflection characteristics of the steel posts utilized in the MGS approach transition. As previously discussed, two posts were installed in moderately compacted soil, while two were installed in heavily compacted soil. After 10 in. (254 mm) of deflection, all posts provided similar loads with plastic bending occurring just below ground line, as shown in Figure 45. However, the two posts in heavily compacted soil provided higher peak forces and more constant forces over the first 10 in. (254 mm) of deflection.

Since these higher forces would increase the probability of fracture in an equivalent wood post, the heavily compacted soil was deemed critical. Therefore, results from test nos. MGSATB-5 and MGSATB-6 were averaged together to form a baseline, or target resistance force, for the equivalent wood post design. The average resistance force from these two tests was 17.4 kips (77.5 kN) and 17.5 kips (77.7 kN) at deflections of 10 in. (254 mm) and 15 in. (381 mm), respectively. The deflection magnitudes were based on BARRIER VII simulations conducted during the design and analysis of the steel post version of the MGS approach transition [3], which showed these larger transition posts deflected up to 15 in. (381 mm) during a TL-3 impact.

The plastic deformation observed in all four steel posts was significant when searching for an equivalent wood post. Since wood posts lack this ductility, the wood posts should have a larger/stronger cross section to reduce the risk of fracture. Further, it was recognized that the embedment depth of an equivalent wood post may vary from that of the steel post due to changes in the post cross section. Therefore, multiple post sections and lengths were tested in an attempt to determine an equivalent wood post.

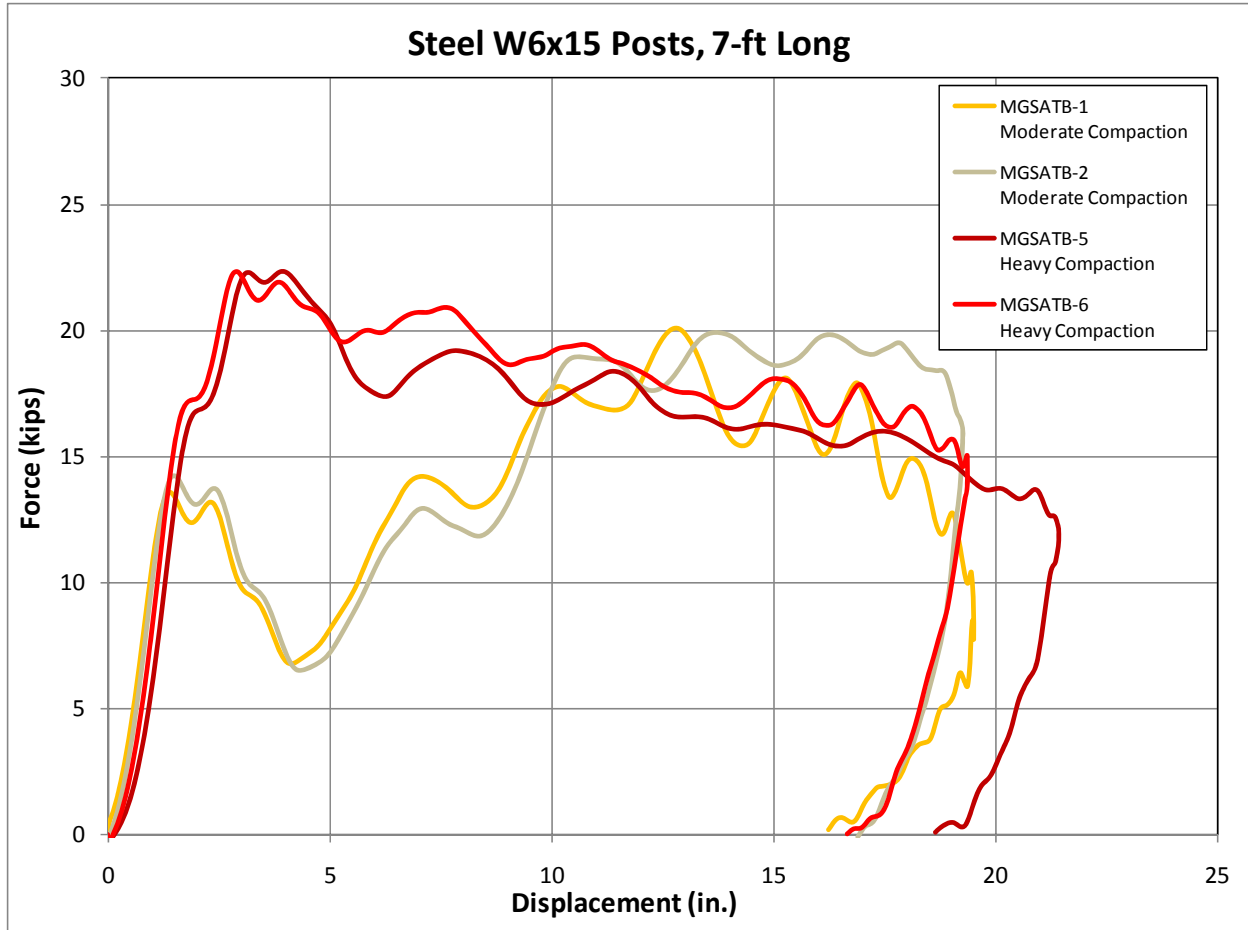


Figure 45. Force vs. Deflection Comparison, 7-ft (2.1-m) Long W6x15 (W152x22.3) Steel Posts

4.2.2 8-in. x 8-in. (203 mm x 203 mm) Wood Posts, 7 ft (2.1 m) Long

Four tests were conducted on 7-ft (2.1-m) long, 8-in. x 8-in. (203-mm x 203-mm) wood posts. Two posts were installed in moderately compacted soil, while the other two were installed in heavily compacted soil. Regardless of soil compaction, each test resulted in post fracture. Although the individual deflections at time of fracture varied, three out of four posts had fractured prior to 10 in. (254 mm) of deflection, thus restricting the total energy absorption of the post. As a result, the 8 in. x 8 in. (203 mm x 203 mm) cross section was determined to be too weak to provide equivalent resistance to the steel post when used as a 7-ft (2.1-m) long wood post.

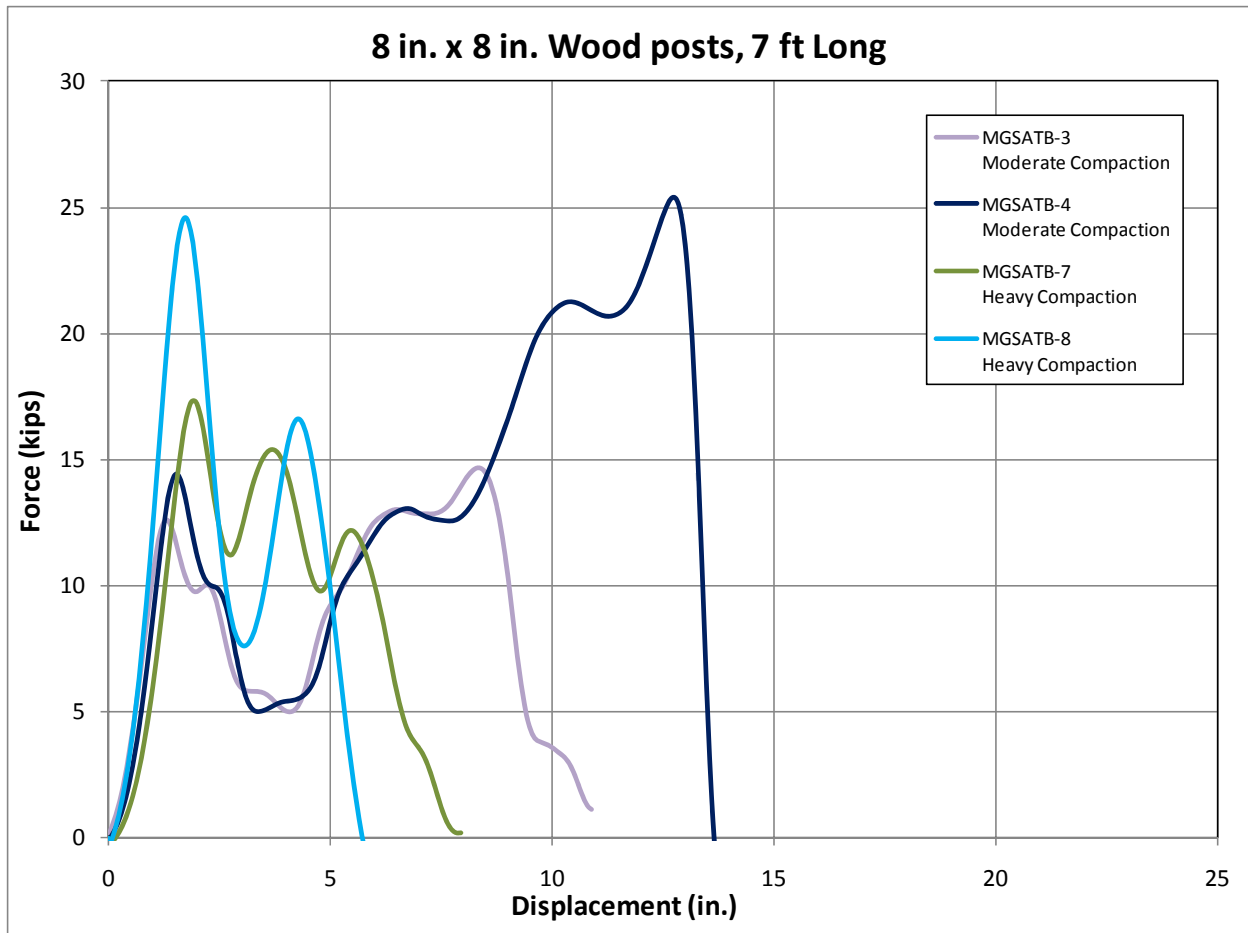


Figure 46. Force vs. Deflection Comparison, 7-ft (2.1-m) Long 8-in. x 8-in. (203-mm x 203-mm) Wood Posts

4.2.3 Wood 8-in. x 10-in. and 10-in. x 10-in. Posts, 7 ft Long

Three 8-in. x 10-in. (203-mm x 254-mm) wood posts and one 10-in. x 10-in. (254-mm x 254-mm) wood post were tested with embedment depths of 54 in. (1,372 mm). These two post sections were grouped together because the test results were similar. With the exception of one 8-in. x 10-in. (203-mm x 254-mm) post that fractured prematurely, these posts recorded resistance forces well above the targeted 17.4 kips (77.5 kN) design load determined from the W6x15 (W152x22.3) steel posts. In fact, calculated average force loads over 10 inches (254 mm) of deflection for the 8-in. x 10-in. (203-mm x 254-mm) wood posts and the 10-in. x 10-in. (254-mm x 254-mm) wood post were 23.0 kips (102.1 kN) and 28.2 kips (125.5 kN), respectively.

Thus, both of these post sizes exceeded the resistance of the 7-ft (2.1-m) long W6x15 (W152x22.3) steel post.

These 8-in. (203-mm) and 10-in. (254-mm) wide posts displaced more soil than the W6x15 (W152x22.3) steel post. This was the result of two main factors. First, the wood posts were wider than the steel posts, which meant more soil would be involved in the inertial resistance at the onset of post rotation. This created higher resistance forces at the beginning of the impact event. Second, the steel posts bent after impact which indicated the soil resistance to rotation was greater than the bending strength of the W6x15 (W152x22.3) cross section. Wood posts cannot yield in the same manner as steel posts; thus, the energy had to be absorbed by soil displacement. To minimize the amount of soil displacement/resistance, either the embedment depth or the post width had to be reduced.

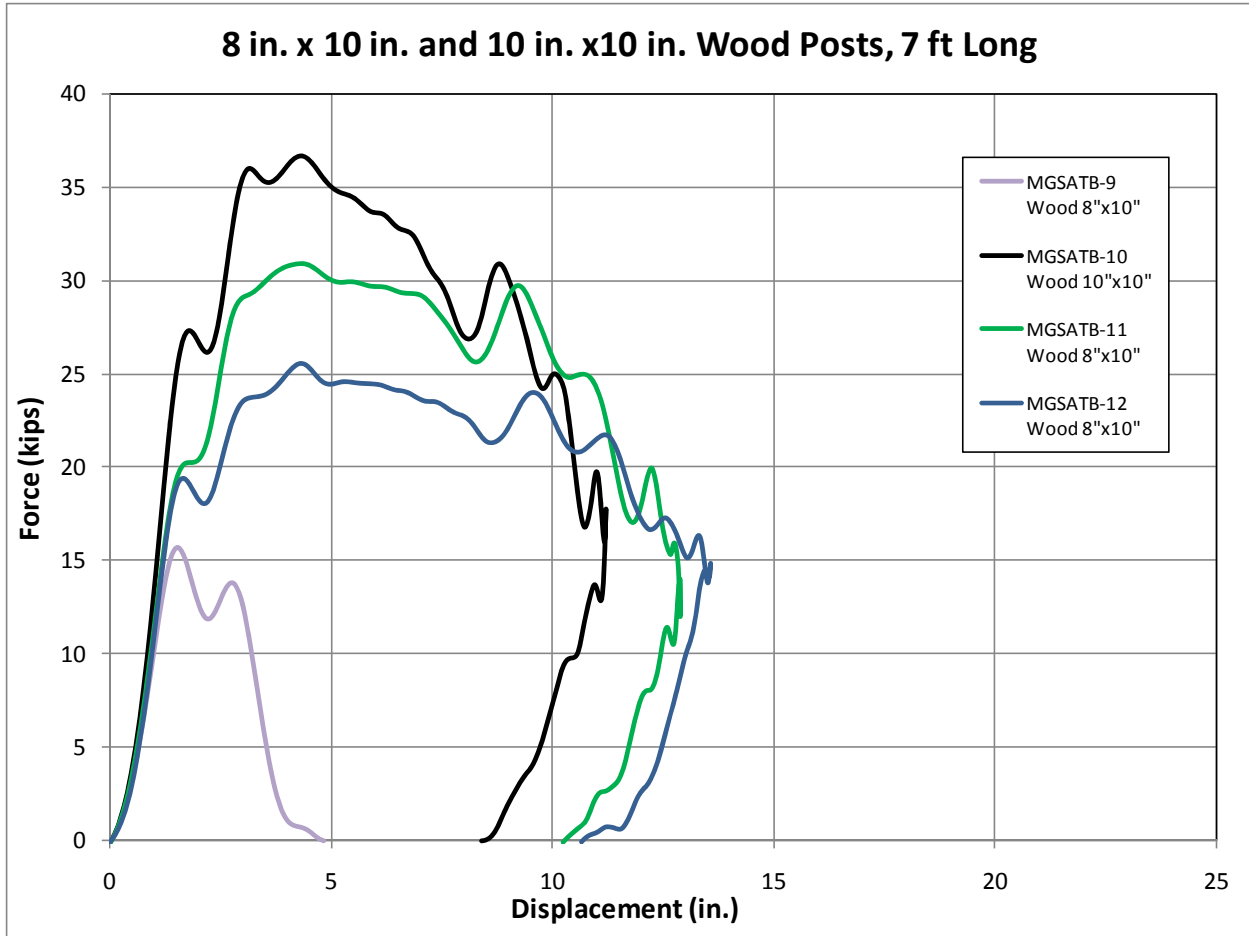


Figure 47. Force vs. Deflection Comparison, 7-ft (2.1-m) 8-in. x 10-in (203-mm x 254-mm). and 10-in. x 10-in. (254-mm x 254-mm) Wood Posts

4.2.4 6-in. x 10-in. (152-mm x 254-mm) Wood Posts, 7 ft (2.1 m) Long

Three tests were conducted on 6-in. x 10-in. (152-mm x 254-mm) wood posts with 52 in. (1,321 mm) embedment. Test no. MGSATB-18 provided favorable results as the resistance force remained relatively constant ranging from 17 to 21 kips (76 to 93 kN) throughout the test, as shown in Figure 48. The average force over 15 in. (381 mm) of deflection was 18.4 kip (81.9 kN), which closely resembled the average force for the W6x15 (W152x22.3) steel posts of 17.5 kips (77.7 kN). However, the next two bogie tests resulted in post fracture. Therefore, the 6-in. x 10-in. (152-mm x 254-mm) wood posts were determined to have inadequate bending strength to transfer the required forces.

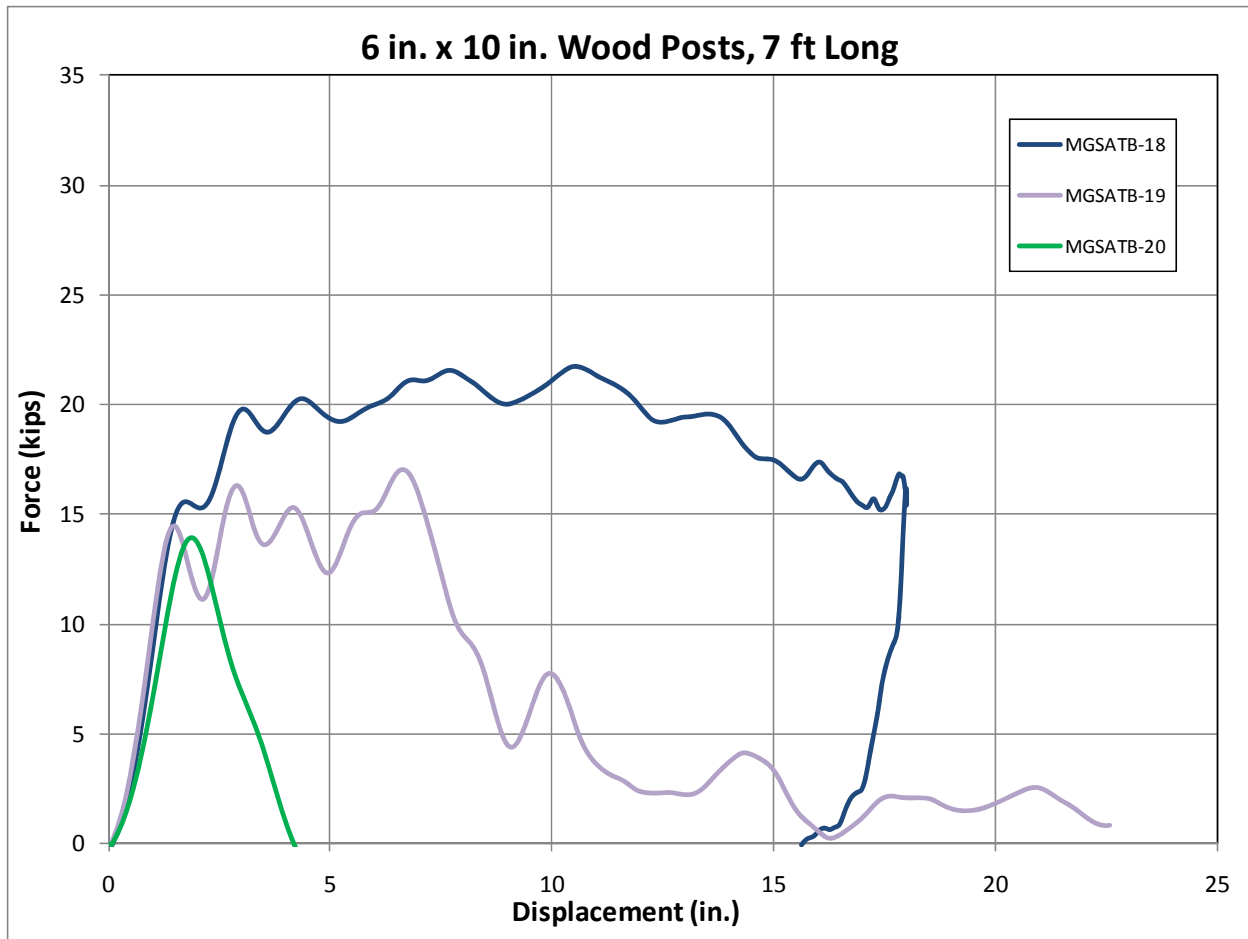


Figure 48. Force vs. Deflection Comparison, 7-ft (2.1-m) Long 6-in. x 10-in. (152-mm x 254-mm) Wood Posts

4.2.5 8-in. x 10-in. (203-mm x 254-mm) Wood Posts, 6.5 ft (2.0 m) Long

Five tests were conducted on 8-in. x 10-in. (203-mm x 254-mm) wood posts with 48 in. (1,219 mm) embedment. Only one post fractured, although another one showed the early stages of fracture and was slightly bent. Not including the results from test no. MGSATB-16 in which the post fractured, the average force over 15 in. (381 mm) of deflection 17.7 kips (78.6 kN). This value was very similar to the targeted design load of 17.5 kips (77.7 kN) over 15 in. (381 mm) of deflection.

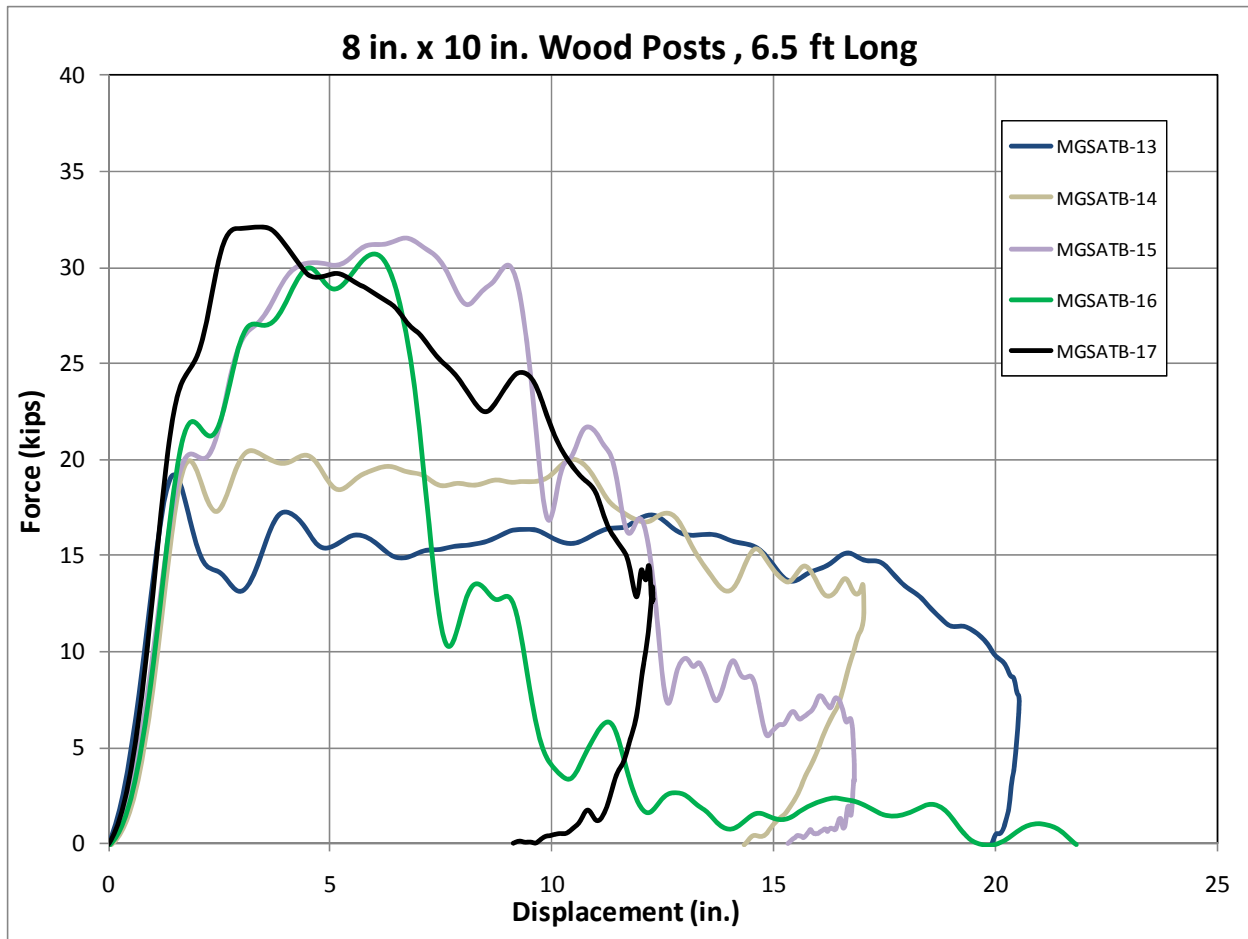


Figure 49. Force vs. Deflection Comparison, 6.5-ft (2.0-m) Long 8-in. x 10-in. (203-mm x 254-mm) Wood Posts

4.3 Bogie Testing Conclusions

The objective of the bogie testing program was to identify a wood post that provided similar force vs. deflection, or energy absorption, characteristics to the 7-ft (2.1-m) W6x15 (W152x22.3) steel posts utilized in the original MGS approach transition system. Variability in wood strength proved to be a difficult hurdle as multiple posts of the same cross section, embedment depth, and wood grade would occasionally result in different failure mechanisms, i.e., rotation through the soil or post fracture. The majority of the posts that fractured were found to contain defects in the wood such as knots, checks, and splits. Although Grade 1 Southern Yellow Pine posts were utilized during all of the tests, wood defects are inevitable in timber

posts, especially with the larger cross sectional dimensions. Therefore, posts utilized in actual installations would be expected to have some natural defects that may lead to premature post fracture. Thus, the possibility of post fracture had to be accounted for in the design process.

Posts that fracture absorb far less energy and do not provide any resistance after fracture, typically within the first few inches of deflection. From a guardrail transition design perspective, this lack of resistance can have negative effects on the safety performance of the system in this sensitive region of the barrier. In a study conducted by Jowza [12], transitions with missing posts were shown to have increased propensity for both vehicle snag and vehicle instabilities due to pocketing. Similar performance results are expected for a transition system in which a post fractured prematurely. Therefore, posts that showed a propensity for fracture before rotating were removed from consideration as equivalent posts to the W6x15 (W152x22.3) steel posts.

Post fracture was prevalent in tests conducted on 7-ft (2.1-m) long versions of 8-in. x 8-in. (203 mm x 203 mm) and 6-in. x 10-in. (152 mm x 254 mm) wood posts. As a result, these posts were not recommended for use in the MGS approach transition. However, this does not mean that these post sizes should not be used in any guardrail transition. Previous approach transition systems have been designed using posts with these or similar dimensions, and full-scale crash testing has verified the safety performance of these systems with no signs of post fracture. The success of these full-scale tests and the lack of post fracture suggest that posts deflecting in close proximity to one another in a barrier system distribute the load and reduce the stress on individual posts, thus reducing the likelihood of fracture. However, without the luxury of a full-scale crash test to verify the performance of these posts when functioning in the MGS approach transition system, the design recommendations had to be based on the bogie test results.

The individual test results for each post size were averaged together in order to compare the various posts. The 6.5-ft (2.0-m) long 8-in. x 10-in. (203-mm x 254-mm) wood posts provide average force characteristics that best match those of W6x15 (W152x22.3) steel posts when the soil was heavily compacted, as shown in Table 8. At 15 in. (381 mm) of deflection, the 8-in. x 10-in. (203-mm x 254-mm) wood posts averaged 17.7 kips (78.8 kN), only 1.1 percent higher than the steel posts. Although the average force of 8-in. x 10-in. (203-mm x 254-mm) wood posts showed an increase of 15.5 percent over the steel post at 10 in. (254 mm) of deflection, the average forces were relatively close. Further, the researchers would rather error conservatively toward stiff as opposed to being too soft and opening up the probability of snagging on the bridge rail. Therefore, at the conclusion of the bogie testing program, the 8-in. x 10-in. (203-mm x 254-mm) wood post with an embedment depth of 48 in. (1,219 mm) best resembled the performance of the W6x15 (W152x22.3) steel transition post and was recommended for further analysis in the MGS approach transition.

Table 8. Bogie Test Result Comparison by Post Size

Post Type	Length ft (m)	Soil Compaction	Fracture Occurrence	Average Force		% Change From W6x15 (Equivalent Soil)	
				@ 10"	@ 15"	@ 10"	@ 15"
				kip (kN)	kip (kN)		
Steel W6x15	7 (2.1)	Moderate	NA	10.9 (48.5)	13.4 (59.5)	-	-
SYP 8"x8"	7 (2.1)	Moderate	2 / 2	9.9 (44.0)	11.8 (62.7)	-9.2%	-11.9%
Steel W6x15	7 (2.1)	Heavy	NA	17.4 (77.5)	17.5 (77.7)	-	-
SYP 8"x8"	7 (2.1)	Heavy	2 / 2	7.2 (31.8)	NA	-58.6%	NA
SYP 8"x10"	7 (2.1)	Heavy	1 / 3	23.0 (102.1)	NA	32.2%	NA
SYP 10"x10"	7 (2.1)	Heavy	0 / 1	28.2 (125.5)	NA	62.1%	NA
SYP 6"x10"	7 (2.1)	Heavy	2 / 3	14.6 (65.0)	18.4 (81.9)	-16.1%	5.1%
SYP 8"x10"	6.5 (2.0)	Heavy	1 / 5	20.1 (89.3)	17.7 (78.6)	15.5%	1.1%

5 BARRIER VII ANALYSIS OF WOOD POST SYSTEM

As detailed in the previous chapter, wood posts were selected to provide similar resistance characteristics to that of the steel posts utilized in the original steel-post stiffness transition system. To verify the post change would not adversely affect the safety performance of the stiffness transition, BARRIER VII computer simulation analysis was undertaken. The evaluation began with the calibration of the steel-post stiffness transition model against previous full-scale crash test results. Next, the steel-post model was subjected to MASH TL-3 impact conditions with the 2270P vehicle throughout the length of the stiffness transition. The wood post characteristics were implemented into the BARRIER VII model, and the wood-post system was subjected to the same TL-3 impacts along the system length. Finally, the results from identical impacts into the steel- and wood-post stiffness transitions were compared and conclusions were made regarding the wood-post system.

5.1 Calibration of Steel Post Transition Model

During the development of the steel-post MGS stiffness transition, a BARRIER VII model was created and utilized to predict the safety performance of the system. This existing model was subjected to the documented impact conditions of test no. MWTSP-2 [3] and the results of the simulation were compared to those of the full-scale crash test. After a few minor changes to the BARRIER VII input deck (i.e., the coefficient of friction and the initial stiffness of the posts), the simulation results and the full-scale crash test results were found to be very similar, as shown in Table 9. Therefore, the calibrated steel-post transition model was deemed to provide accurate performance results regarding the behavior of both the 2270P vehicle and the stiffness transition system. The BARRIER VII input deck and a layout drawing of the barrier system are shown in Appendix E.

Table 9. Comparison of Test No. MWTSP-2 and BARRIER VII Simulation Results

	Test No. MWTSP-2	BARRIER VII Simulation	% Change From Tested Values
Maximum Deflection			
Deflection	30.7 in.	31.6 in.	3.1%
Location in Model	Post 10	Post 10	-
Vehicle Parallel Heading			
Time	0.246 sec	0.257 sec	4.5%
Speed	41.5 mph	38.1 mph	-8.2%
Vehicle Exit			
Time	0.506 sec	0.525 sec	3.8%
Speed	37.3 mph	36.6 mph	-1.9%
Exit Angle	22 deg	18.4 deg	-16.4%
Maximum Pocketing			
Pocket Angle	29.6 deg	28.9 deg	-2.4%
Location in Model	Post 12 – Post 13	Post 12 – Post 13	-

5.2 Wood-Post Transition Model

The wood-post stiffness transition model was developed from the steel-post transition model. The only difference was the individual post resistances were modified as described in the following sections. The wood-post transition BARRIER VII model is shown in Appendix E.

5.2.1 6-in. x 8-in. (152-mm x 203-mm) Wood Post, 6 ft (1.8 m) Long

The strong axis resistance (lateral direction) for the 6-in. x 8-in. (152-mm x 203-mm) wood posts was based on the results of bogie test nos. GWB-14 and GWB-15, as discussed in Section 2.1. The average resistance force through 16 in. (406 mm) of deflection during these two tests was 10.8 kips (48.2 kN). Thus, with a height to the impact point, or center of rail, of 24⁷/₈ in. (632 mm), the plastic rotation moment was set to 270.0 kip-in. (30.5 kN-m). The initial stiffness,

also taken from an average of these two bogie tests, was calculated to be 7.5 kip/in. (13.1 kN/cm).

Since post movement in the longitudinal direction would involve the 8-in. (203-mm) face of the post, the longitudinal resistance was based on the results of the 8-in. x 10-in. (203-mm x 254-mm) wood posts documented in Chapter 4. The average forces from these tests were then extrapolated to represent an embedment depth of 40 in. (1,016 mm), as shown below.

8 in. x 10 in. post embedded 48 in. (test nos. MGSATB-13 through MGSATB-17)

Average force: $F_{48} = 20.1$ kips

$$F_{40} = F_{48} * (EMB_{40}/EMB_{48})^2 = 20.1 * (40/48)^2$$

$$F_{40} = 13.96 \text{ kips}$$

8 in. x 10 in. post embedded 54 in. (test nos. MGSATB-11 and MGSATB-12)

Average force: $F_{54} = 23.0$ kips

$$F_{40} = F_{54} * (EMB_{40}/EMB_{54})^2 = 23.0 * (40/54)^2$$

$$F_{40} = 12.62 \text{ kips}$$

Average of both values

$$F_{40} = 13.3 \text{ kips}$$

Using the average force of 13.3 kips (59.2 kN), the plastic rotation moment was set to 331 kip-in. (37.4 kN-m).

5.2.2 8 in. x 10 in. (203-mm x 254-mm) Wood Post, 6.5 (2.0 m) ft Long

The strong axis resistance (lateral direction) for the 6.5-ft (2.0-m) long 8-in. x 10-in. (152-mm x 203-mm) wood posts was based on the results of bogie test nos. MGSATB-13 through MGSATB-17. The average resistance force through 15 in. (381 mm) of deflection was calculated to be 17.7 kips (78.8 kN). Note, the posts that fractured prior to 15 in. (381 mm) of deflection were not included in the average resistance force. Similar to W-beam rail, the center of the thrie beam rail was $24\frac{7}{8}$ in. (632 mm) high, and the plastic rotation moment was set to 440 kip-in. (49.7 kN-m).

Since post movement in the longitudinal direction would involve the 10-in. (254-mm) face of the post, the longitudinal resistance was based on the results of the 10-in. x 10-in. (254-mm x 254-mm) wood post evaluated in test no. MGSATB-10. Similar to the process shown in the previous section, the average resistance force was extrapolated to represent an embedment of 48 in. (1,219 mm), as shown below.

$$\begin{aligned} &10 \text{ in.} \times 10 \text{ in.} \text{ post embedded } 54 \text{ in. (test no. MGSATB-10)} \\ &\text{Average force: } F_{54} = 28.2 \text{ kips} \\ &F_{48} = F_{54} * (EMB_{48}/EMB_{54})^2 = 22.8 * (48/54)^2 \\ &F_{48} = 22.3 \text{ kips} \end{aligned}$$

Using the average force of 22.3 kips (99.2 kN), the plastic rotation moment was set to 555 kip-in. (62.7 kN-m). The initial stiffness in each direction was approximated from the bogie tests.

5.2.3 General Comments

The BARRIER VII resistance forces of the 6-in. x 8-in. (152-mm x 203-mm) wood posts were calculated to be significantly higher than the original W6x9 (W152x13.4) steel posts. The increase in the lateral direction is due to the torsional capacity of the post. Steel posts in a barrier system tend to twist due to the axial rail loads. As a result, the posts bend at loads lower than the maximum plastic moment due to a mechanism similar to lateral torsional buckling. This phenomenon was accounted for in the steel-post system by introducing a 13 percent reduction in strength to posts in the BARRIER VII model. On the contrary, the solid cross section of the wood posts greatly increases the twist resistance of the post. Thus, the reduction factor was not applied to the 6-in. x 8-in. (152-mm x 203-mm) wood posts. A solid wood post has more bending strength in the longitudinal direction than the weak axis of a wide-flange section.

Similarly, the larger wood transition posts located adjacent to the bridge rail have higher resistance values than the steel counterparts. The 8-in. x 10-in. (203-mm x 254-mm) wood posts were conservatively selected to meet/exceed the resistance of the W6x15 (W152x22.3) steel posts while minimizing the risk of post fracture.

5.3 Evaluation Criteria

Since the wood-post MGS stiffness transition would not be evaluated through full-scale crash testing, but with computer simulations, the evaluation criteria were conservatively established. At a minimum, the wood-post transition system was required to perform as well as the steel-post transition system for the following three criteria: (1) maximum deflection, (2) maximum pocketing angle, and (3) vehicle snag on posts. These performance characteristics were the same ones used to compare the various configurations during the development of the original steel-post stiffness transition. Thus, the wood-post transition system was evaluated in the same manner.

5.4 BARRIER VII Analysis and Results

The steel- and wood-post MGS stiffness transition models were subjected to the same impact matrix consisting of 45 individual impacts each for a total of 90 simulations. The individual impact points were spaced 9³/₈ in. (238 mm) apart and ranged from 150 in. (3,810 mm) upstream of the stiffness transition to 75 in. (1,905 mm) upstream of the bridge rail. The impacts were spaced throughout the MGS stiffness transition to provide an evaluation of the entire system. All simulated impacts complied to MASH test designation no. 3-61 with a 5,000 lb (2,270 kg) pickup truck impacting at 62 mph (100 km/h) and an angle of 25 degrees. The results from all 90 BARRIER VII simulations are summarized in Table 10 with more detailed results shown in Appendix F.

Table 10. Summary of BARRIER VII Simulation Results

Impact Location			Maximum Deflection			Maximum Pocket Angle			Worst Case Snag		
Node No.	Distance U.S. of Bridge Rail (in.)	Posts By Location	Steel (in.)	Wood (in.)	Change From Steel	Steel (deg.)	Wood (deg.)	Change From Steel	Steel (in.)	Wood (in.)	Change From Steel
81	487 1/2	6"x8"	32.4	26.3	-18.9%	22.7	21.0	-7.6%	7.84	5.80	-26.0%
82	478 1/8		32.6	25.9	-20.4%	22.7	21.1	-6.8%	7.78	6.66	-14.4%
83	468 3/4		32.7	26.2	-20.0%	22.6	21.5	-4.7%	7.96	6.64	-16.6%
84	459 3/8		32.7	26.0	-20.5%	22.1	21.5	-2.9%	7.88	5.99	-24.0%
85	450		32.3	23.8	-26.2%	21.4	19.7	-8.0%	7.57	5.67	-25.1%
86	440 5/8		29.1	23.8	-18.4%	19.6	19.0	-3.0%	7.13	5.68	-20.3%
87	431 1/4		29.4	23.6	-19.7%	19.9	18.8	-5.6%	6.86	5.66	-17.5%
88	421 7/8		29.4	23.4	-20.3%	20.5	18.9	-8.2%	7.41	5.87	-20.8%
89	412 1/2	6"x8"	29.8	23.3	-21.6%	21.8	18.7	-14.5%	7.65	5.84	-23.7%
90	403 1/8		29.7	23.4	-21.4%	22.3	18.5	-17.0%	7.65	5.96	-22.1%
91	393 3/4		29.9	23.3	-22.1%	23.5	18.7	-20.4%	7.24	5.82	-19.6%
92	384 3/8		29.6	22.8	-22.9%	24.3	18.6	-23.5%	7.07	5.66	-19.9%
93	375		29.2	21.2	-27.4%	24.2	17.1	-29.5%	6.83	5.29	-22.5%
94	365 5/8		26.8	21.3	-20.6%	22.6	18.0	-20.6%	6.33	4.87	-23.1%
95	356 1/4		26.7	20.3	-24.1%	22.8	18.0	-21.1%	6.10	4.74	-22.3%
96	346 7/8		26.0	19.0	-26.8%	22.8	17.0	-25.7%	5.77	4.51	-21.8%
97	337 1/2	6"x8"	24.5	18.7	-23.5%	21.6	17.3	-19.8%	5.33	4.40	-17.4%
98	328 1/8		23.8	18.0	-24.4%	21.5	17.4	-19.0%	5.14	3.99	-22.4%
99	318 3/4		23.1	17.1	-25.8%	21.3	16.8	-21.0%	5.55	3.70	-33.3%
100	309 3/8		23.0	16.8	-26.9%	21.5	17.2	-20.2%	5.47	3.98	-27.2%
101	300	6"x8"	22.4	16.7	-25.1%	21.0	16.8	-20.2%	5.31	4.12	-22.4%
102	290 5/8		21.7	15.6	-28.1%	20.0	16.0	-19.7%	5.58	4.30	-22.9%
103	281 1/4		21.3	15.4	-27.7%	19.2	15.9	-17.0%	5.40	4.59	-15.0%
104	271 7/8		20.5	15.1	-26.2%	18.2	15.5	-15.1%	5.89	4.90	-16.8%
105	262 1/2	6"x8"	20.0	14.6	-27.0%	18.2	14.9	-18.3%	7.19	4.72	-34.4%
106	253 1/8		19.9	14.0	-29.7%	17.8	14.0	-21.4%	7.50	4.92	-34.4%
107	243 3/4		18.5	13.1	-29.2%	15.9	13.6	-14.3%	7.67	6.51	-15.1%
108	234 3/8		18.1	13.0	-28.0%	14.7	12.8	-12.9%	7.53	6.94	-7.8%
109	225	6"x8"	16.8	12.7	-24.7%	13.9	12.4	-10.9%	7.65	7.19	-6.0%
110	215 5/8		15.2	11.9	-21.8%	12.7	11.7	-8.2%	7.63	7.32	-4.1%
111	206 1/4		14.5	11.3	-21.6%	11.5	10.7	-7.1%	7.46	7.32	-1.9%
112	196 7/8		13.8	10.7	-22.5%	10.9	9.8	-9.7%	7.01	7.11	1.4%
113	187 1/2	6"x8"	12.9	10.0	-22.2%	10.1	8.7	-14.0%	6.68	6.45	-3.4%
114	178 1/8		12.7	9.8	-23.1%	9.9	8.6	-12.9%	6.79	6.54	-3.7%
115	168 3/4	6"x8"	12.5	9.5	-23.5%	10.2	8.8	-13.5%	6.71	6.74	0.4%
116	159 3/8		12.3	9.6	-21.7%	11.5	8.7	-24.6%	6.27	6.47	3.2%
117	150	6"x8"	12.1	9.6	-20.8%	13.8	9.1	-34.0%	6.48	6.26	-3.4%
118	140 5/8		12.4	10.0	-19.2%	16.1	11.7	-27.1%	6.67	6.53	-2.1%
119	131 1/4	6"x8"	12.6	10.6	-15.5%	17.3	14.2	-18.3%	6.90	6.71	-2.8%
120	121 7/8		12.5	10.9	-13.4%	17.7	15.2	-14.4%	6.78	6.63	-2.2%
121	112 1/2	8"x10"	12.6	10.6	-15.7%	17.4	19.9	14.3%	6.33	6.47	2.2%
122	103 1/8		12.7	11.2	-11.9%	16.9	14.7	-13.1%	5.53	5.69	2.9%
123	93 3/4		12.2	11.1	-8.9%	15.9	14.1	-11.4%	4.46	4.53	1.6%
124	84 3/8		11.5	10.2	-11.4%	14.7	12.7	-13.4%	2.94	3.25	10.5%
125	75	8"x10"	10.2	9.2	-9.3%	13.0	11.5	-11.2%	1.20	1.46	21.7%

The wood-post MGS stiffness transition outperformed the original steel-post transition system in all three of the evaluation criteria. The maximum deflections for the wood-post system were consistently 15 to 30 percent lower than the original steel-post system. This deflection reduction was the result of the wood posts having a higher stiffness and resistance to rotation than their steel counterparts. The wood-post system also consistently showed a 5 to 25 percent reduction in the maximum pocketing angle. Thus, the wood post system is expected to reduce the risk of vehicle instability. Finally, the propensity for wheel snag was found to be lower for the wood-post system. The reduction in system deflection significantly reduced the estimated wheel snag for the 6-in. x 8-in. (152-mm x 203-mm) wood post. However, the wheel snag estimations for the larger 8-in. x 10-in. (203-mm x 254-mm) wood transition posts were found to be closer to (or slightly higher) the estimations for the steel W6x15 (W152x22.3) steel posts. Thus, the potential benefits (as far wheel snag are concerned) a deflection reduction were offset by the reduction in embedment depth. Although a slight increase in potential wheel snag was predicted at a limited number of locations, the increases in magnitude were minimal as they never exceeded 0.31 in. (7.9 mm). Therefore, the potential for wheel snag was not considered a major concern and the wood-post MGS stiffness transition system was expected to perform satisfactorily for all safety criteria.

6 DESIGN DRAWINGS

The design drawings for the wood post MGS stiffness transition are shown in Figures 50 through 55. Note the post numbers in these drawings begin at 5 and end at 18 in order to match the post numbering scheme contained in the steel post MGS stiffness transition design details [3]. The steel post system drawings included the upstream anchorage posts as they were part of the full-scale testing installations. These upstream posts were deemed unnecessary to detail the wood post version of the system. However, the numbering scheme of the transition posts was held constant so that posts from both systems could be compared on a number to number basis.

The wood post MGS stiffness transition consisted of only two different types of guardrail posts. Post nos. 5 through 15 (along with all MGS line posts upstream of this location) were 6-ft (1.8-m) long 6-in. x 8-in. (152-mm x 203-mm) wood posts. These posts were all embedded 40 in. (1,016 mm) into the soil and utilized 12-in. (305-mm) deep blockouts. However, the spacing between the posts decreased from 75 in. (1,903 mm) at the upstream end of the system to 37½ in. (953 mm) and 18¾ in. (476 mm) at the downstream end, as shown in Figure 50. Post nos. 16 through 18 were 6.5-ft (2.0-m) long 8-in. x 10-in. (203-mm x 254-mm) wood posts. These posts had an embedment depth of 48 in. (1,219 mm), a 37½ in. (953 mm) center to center spacing, and utilized 8-in. (203-mm) deep blockouts.

The rail elements utilized in the wood post MGS stiffness transition remained unchanged from the steel post version of the system. Standard 12 gauge (2.66-mm thick) W-beam guardrail was used upstream of post no. 9. A 75-in. (1,903-mm) long, 10 gauge (3.42-mm thick) asymmetrical W-beam to thrie beam transition element spanned between post nos. 9 and 11. A 75-in. (1,903-mm) long, 12 gauge (2.66-mm thick) section of thrie beam spanned between post nos. 11 and 14. Finally, nested 12 gauge (2.66-mm thick) thrie beam was utilized between post no 14 and the bridge rail.

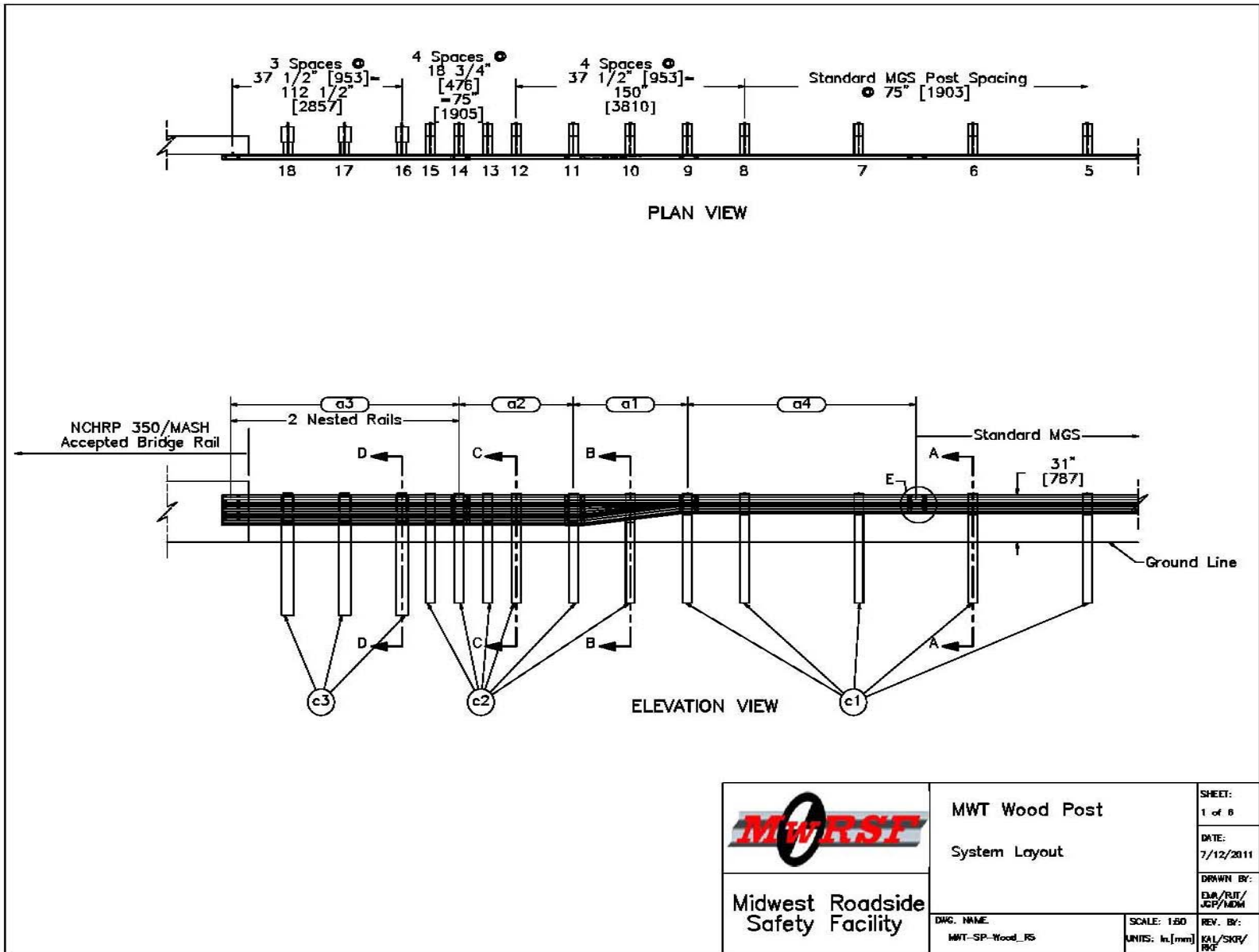


Figure 50. Design Details, Wood Post MGS Stiffness Transition System Layout

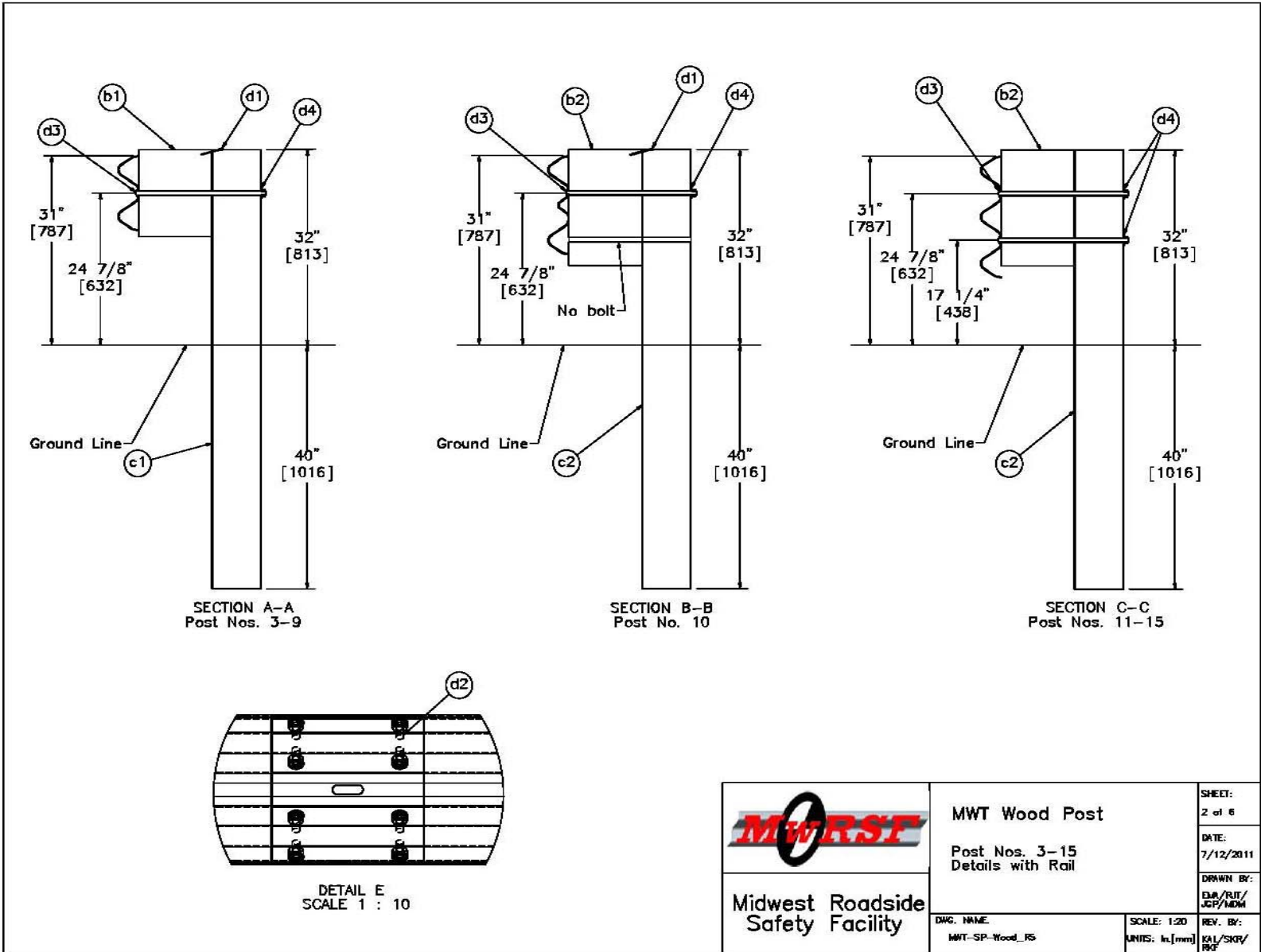


Figure 51. Post Nos. 3 through 15 Rail Attachment Details

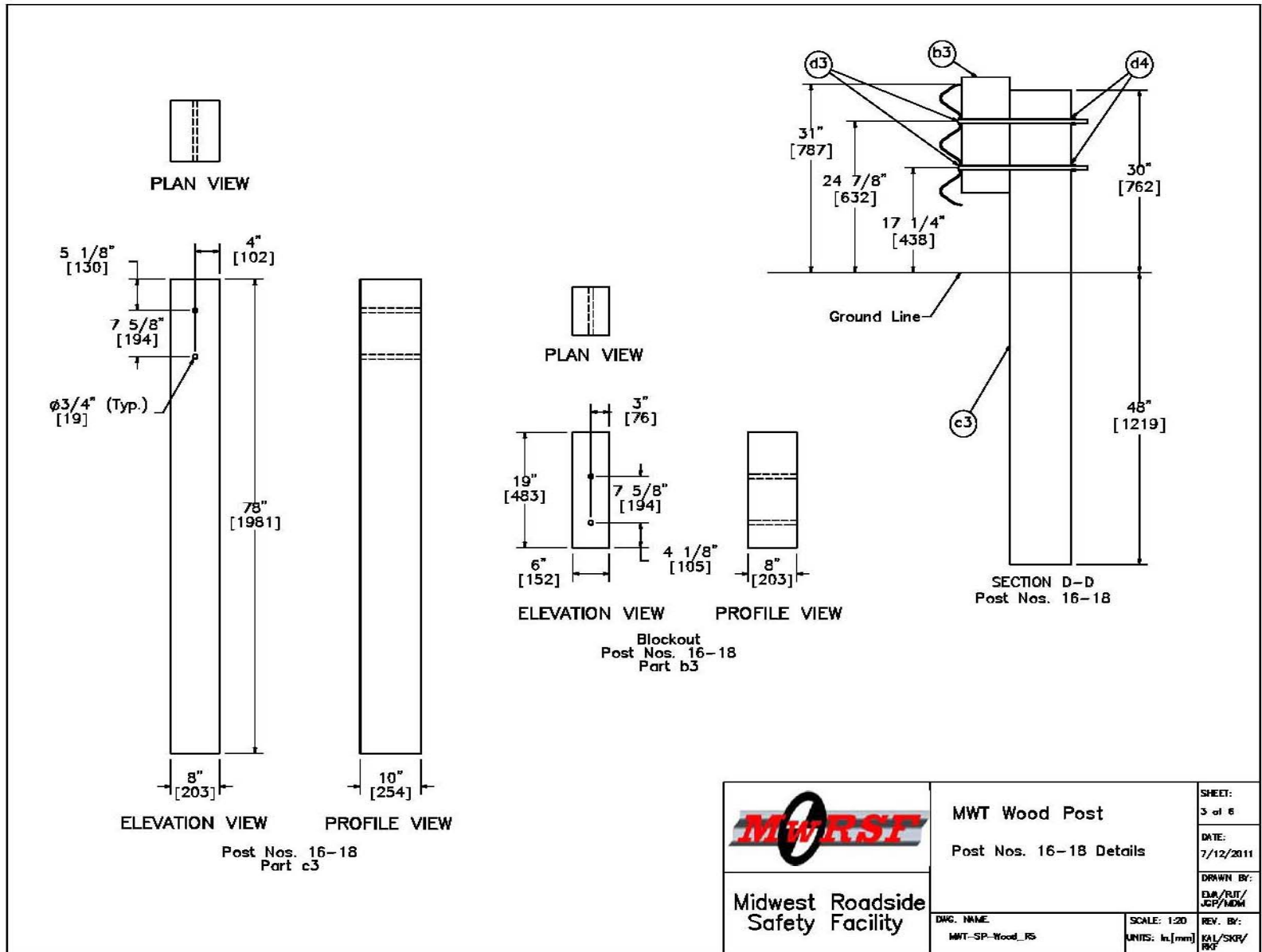


Figure 52. Post Nos. 16 through 18 Design Details

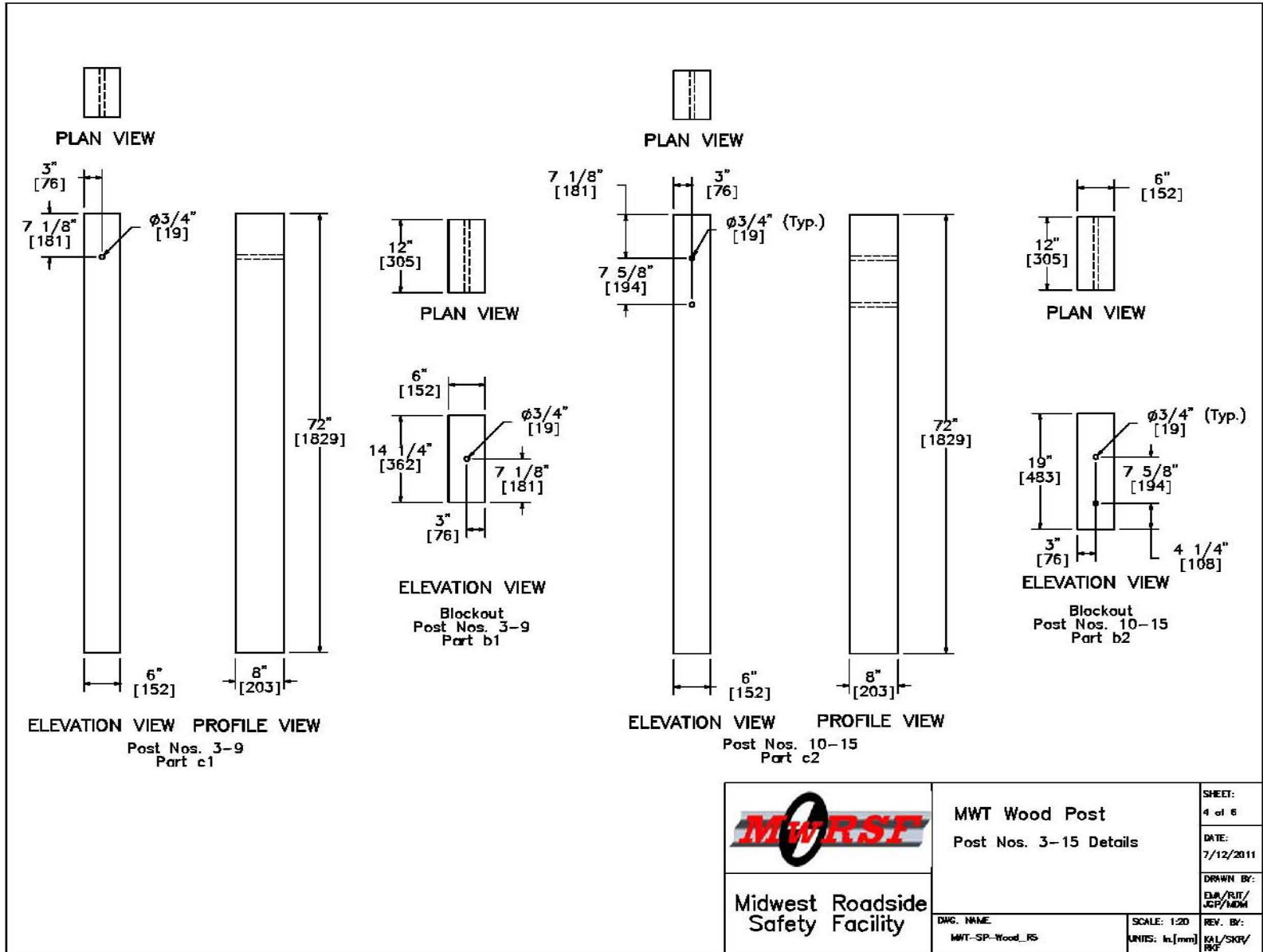


Figure 53. Post Nos. 3-15 Design Details

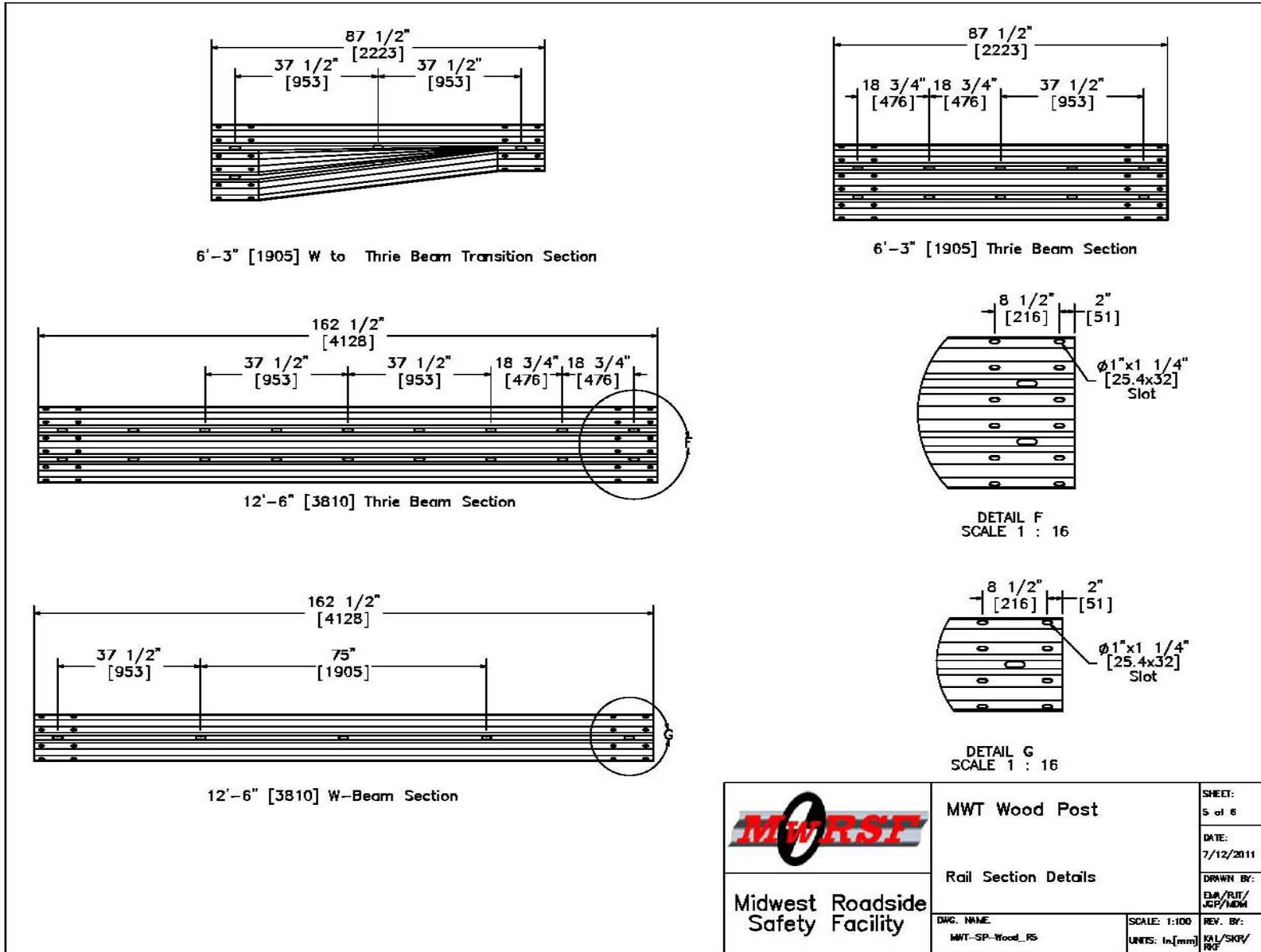


Figure 54. Rail Sections Details

Item No.	Description	Material Specification	Hardware Guide
a1	6'-3" [1905] W-Beam to Thrie-Beam Transition Section	10 gauge AASHTO M180	RWT01b
a2	6'-3" [1905] Thrie Beam Section - 1/2 Post Spacing	12 gauge AASHTO M180	RTM02a
a3	12'-6" [3810] Thrie Beam Section - 1/2 Post Spacing	12 gauge AASHTO M180	RTM04a
a4	12'-6" [3810] W-Beam MGS Section	12 gauge AASHTO M180	RWM04a
b1	6x12x14 1/4" [152x305x362] Blockout - Post Nos. 3-9	SYP Grade No. 1 or better	PDB11a
b2	6x12x19" [152x305x483] Blockout - Post Nos. 10-15	SYP Grade No. 1 or better	-
b3	6x8x19" [152x203x483] Blockout - Post Nos. 16-18	SYP Grade No. 1 or better	-
c1	6x8" [152x203] 72" [1829] long - Post Nos. 3-9	SYP Grade No. 1 or better	PDE02
c2	6x8" [152x203] 72" [1829] long - Post Nos. 10-15	SYP Grade No. 1 or better	PDE02
c3	8x10" [203x254] 78" [1981] long - Post Nos. 16-18	SYP Grade No. 1 or better	-
d1	16D Double Head Nail	-	-
d2	5/8" Dia. x 1 1/2" [M16x38] Long Guardrail Bolt	ASTM A563	FBB01
d3	5/8" Dia. x 21" [M16x533] Long Guardrail Bolt	ASTM A563	FBB07
d4	5/8" [16] Dia. Flat Washer	F436 Gr. 1	FWC16a


	MWT Wood Post Bill of Materials	SHEET: 6 of 6
	Midwest Roadside Safety Facility	DATE: 7/12/2011
DWG. NAME: MWT-SP-Wood_RS	SCALE: None UNITS: In./mm	DRAWN BY: EMW/RIT/ JGF/MDM
		REV. BY: KAL/SKR/ RKF

Figure 55. Bill of Materials

7 SUMMARY, CONCLUSIONS, AND RECOMMENDATIONS

The objective of this study was to identify a wood-post MGS approach transition system that is equivalent to the steel-post MGS stiffness transition. A literature study on previous bogie testing and comparisons between wood and steel guardrail posts suggested that 6-ft (1.8-m) long, 6-in. x 8-in. (152-mm x 203-mm) wood posts and W6x9 (W152x13.4) steel posts have similar force vs. displacement characteristics. However, very little component testing had been previously conducted on larger transition posts. Thus, a bogie testing program was undertaken to determine the behavior of W6x15 (W152x22.3) steel posts and wood posts of various cross sections and embedment depths. Early in this bogie-testing program, the propensity for wood-post fracture in stiff soil was observed. As a result, the wood-post replacements were conservatively selected such that the cross section had excess strength capacity to minimize the risk of post fracture. Ultimately, 6.5 ft (2.0 m) long 8-in. x 10-in. (203-mm x 254-mm) wood posts provide similar resistance to rotation and were selected as the replacement for the 7-ft (2.1-m) long W6x15 (W152x22.3) steel transition posts.

BARRIER VII computer simulations were utilized to evaluate the behavior of the wood-post transition system. First, a steel-post BARRIER VII transition model was calibrated against the results of full-scale crash test no. MWTSP-2. Next, the characteristics of the 6-in. x 8-in. (152-mm x 203-mm) and 8-in. x 10-in. (203-mm x 254-mm) wood posts replaced the steel-posts to create a wood-post transition system model. Both the steel- and wood-post versions of the model were then subjected to simulated MASH TL-3 impacts at 45 different impact points throughout the length of the MGS stiffness transition. The results of this BARRIER VII analysis showed that the proposed wood-post transition system consistently provided reductions in maximum deflection, vehicle pocketing angle, and propensity for wheel snag. Thus, the

introduction of wood posts to the MGS stiffness transition did not adversely affect the safety performance of the MGS stiffness transition system.

The steel-post MGS stiffness transition was found to satisfy all of the TL-3 safety performance criteria of MASH through a full-scale crash testing program. Since the BARRIER VII analysis showed the wood-post transition system behaved similarly and without increases in deflections, pocketing, or snag, it is believed that the wood-post transition system would also satisfy the TL-3 performance criteria of MASH. Therefore, the wood-post MGS stiffness transition was recommended for use as a TL-3 safety barrier.

The original steel post system was developed utilizing a very stiff thrie beam transition which represented a worst-case, critical scenario. Upon satisfying all MASH criteria and being deemed crashworthy, the steel-post system was also recommended for attachment to various thrie beam transition systems which were less stiff and less critical. Similar to the steel post stiffness transition, the upstream stiffness transition of the wood-post stiffness transition developed herein should be applicable to most other thrie beam approach guardrail transition designs. Details for attaching the upstream stiffness transition to other thrie beam transition systems are presented in Chapter 8.

The wood posts utilized in the bogie testing program presented herein and the posts contained in the literature review were Southern Yellow Pine. Thus, the development of the wood-post transition system was based upon the material strength of Southern Yellow Pine timber. As a result, the posts used in wood-post MGS stiffness transition should be fabricated from Southern Yellow Pine or another species that provides equal or greater strength.

Placement of the upstream end anchorage too close to the stiffness transition may negatively affect system performance and result in excessive barrier deflections, vehicle pocketing, wheel snagging on posts, vehicle-to-barrier override, or other vehicle instabilities.

Therefore, the following implementation guidelines should be followed. Note these guidelines were the same for the steel-post MGS stiffness transition.

1. A recommended minimum length of 12 ft – 6 in. (3.8 m) for standard MGS is to be installed between the upstream end of the asymmetrical W-beam to thrie beam transition section and the interior end of an acceptable TL-3 guardrail end terminal. This segment includes one half-post spacing for Design K and three half-post spacings for Design L.
2. A recommended minimum barrier length of 46 ft – 10½ in. (14.3 m) is to be installed beyond the upstream end of the asymmetrical W-beam to thrie beam transition section, which includes standard MGS, a crashworthy guardrail end terminal, and an acceptable anchorage system. This segment includes one half-post spacing for Design K and three half-post spacings for Design L.
3. For flared guardrail applications, a minimum length of 25 ft (7.6 m) is recommended between the upstream end of the asymmetrical W-beam to thrie beam transition section and the start of the flared section (i.e. bend between flare and tangent sections). This segment includes one half-post spacing for Design K and three half-post spacings for Design L.

It is unknown as to whether a non-blocked version of the MGS will perform in an acceptable manner when installed adjacent to the new stiffness transition. The safety performance of the non-blocked MGS in conjunction with the new stiffness transition can only be verified through the use of full-scale crash testing. As such, it is recommended that a minimum of 25 ft (7.6 m) of standard MGS with spacer blocks be placed adjacent to the new stiffness transition prior to transitioning to other non-blocked, 31-in. (787-mm) tall, W-beam guardrail systems.

The new stiffness transition was developed and evaluated for use with a thrie beam approach guardrail transition where all posts were installed on level terrain. Therefore, this stiffness transition should be implemented with a minimum of 2 ft (0.61 m) of level or gently-sloped fill placed behind the posts, unless special design provisions are made to account for decreased post-soil resistance.

8 STIFFNESS TRANSITION ADAPTATION RECOMMENDATIONS

The upstream stiffness transition within this study was developed while attached to a very stiff thrie beam approach guardrail transition. However, it is believed that this stiffness transition can be adapted to other wood-post, thrie beam approach guardrail transitions to mitigate concerns for vehicle pocketing and vehicle instabilities. Several examples of adapting the new stiffness transition to other approach guardrail transitions are provided below. The original approach guardrail transitions should only be used in conjunction with the bridge rail types for which they were designed, tested, or approved.

8.1 Adaptation for Transition to TL-4 Glulam Bridge Rail

The approach transition to TL-4 glulam bridge rail, the newly developed wood-post stiffness transition evaluated herein, and the adaptation of these two systems connected together are shown in Figure 56. The original approach guardrail transition was 19 ft – 6¼ in. (6.0 m) long [13-16], while the adapted stiffness transition system is configured to be 28 ft – 10¾ in. (8.8 m) long, as measured from the centerline of the first post at half-post spacing to the upstream end of the glulam bridge rail. For the adapted system, an additional 6-ft 3-in. (1.9-m) long segment of 12-gauge (2.66-mm thick) thrie beam was placed downstream of the W-to-Thrie transition element. The three furthest upstream 8-in. x 8-in. (203-mm x 203-mm) wood posts from the original transition were removed. Four, 6-ft (1.8-m) long, 6-in. x 8-in. (152-mm x 203-mm) wood posts were placed at quarter post spacing and adjacent to the remaining 8-in. x 8-in. (203-mm x 203-mm) wood posts. Upstream from these posts, four, 6-ft (1.8-m) long, 6-in. x 8-in. (152-mm x 203-mm) wood posts were placed at half-post spacing. The first post at half-post spacing was located 37½ in. (953 mm) upstream of the centerline of the splice between the MGS and the asymmetrical stiffness transition element.

8.2 Adaptation for Iowa Transition to New Jersey Safety Shape Concrete Parapet

The Iowa approach guardrail transition to New Jersey safety shape concrete parapet, the newly developed stiffness transition evaluated herein, and the adaptation of the two systems connected together are shown in Figure 57. The original approach guardrail transition was 18 ft – 9 in. (5.7 m) long [17-20], while the adapted stiffness transition system is configured to be 28 ft – 1½ in. (8.6 m) long, as measured from the centerline of the first post at half-post spacing to the centerline of the splice between the thrie beam and the concrete parapet. In the adapted system, an additional 6-ft 3-in. (1.9-m) long segment of 12-gauge (2.66-mm thick) thrie beam was placed downstream of the W-to-Thrie transition element. Four 6-ft (1.8-m) long, 6-in. x 8-in. (152-mm x 203-mm) wood posts were placed at a quarter-post spacing and upstream from the 7-ft (2.1-m) long, 6-in. x 8-in. (152-mm x 203-mm) wood posts. Upstream from these posts, four 6-ft (1.8-m) long, 6-in. x 8-in. (152-mm x 203-mm) wood posts were placed at half-post spacing. The first post at half-post spacing was located 37½ in. (953 mm) upstream of the centerline of the splice between the MGS and the asymmetrical stiffness transition element.

8.3 Adaptations to Other Thrie Beam Transitions

Although not specifically shown, the new wood post stiffness transition described herein can be adapted to other thrie beam approach guardrail transitions. Small adjustments in rail height for the upstream stiffness transition may be necessary to match previously-approved approach guardrail transitions, such as those with heights of 31⅝ in. (803 mm).

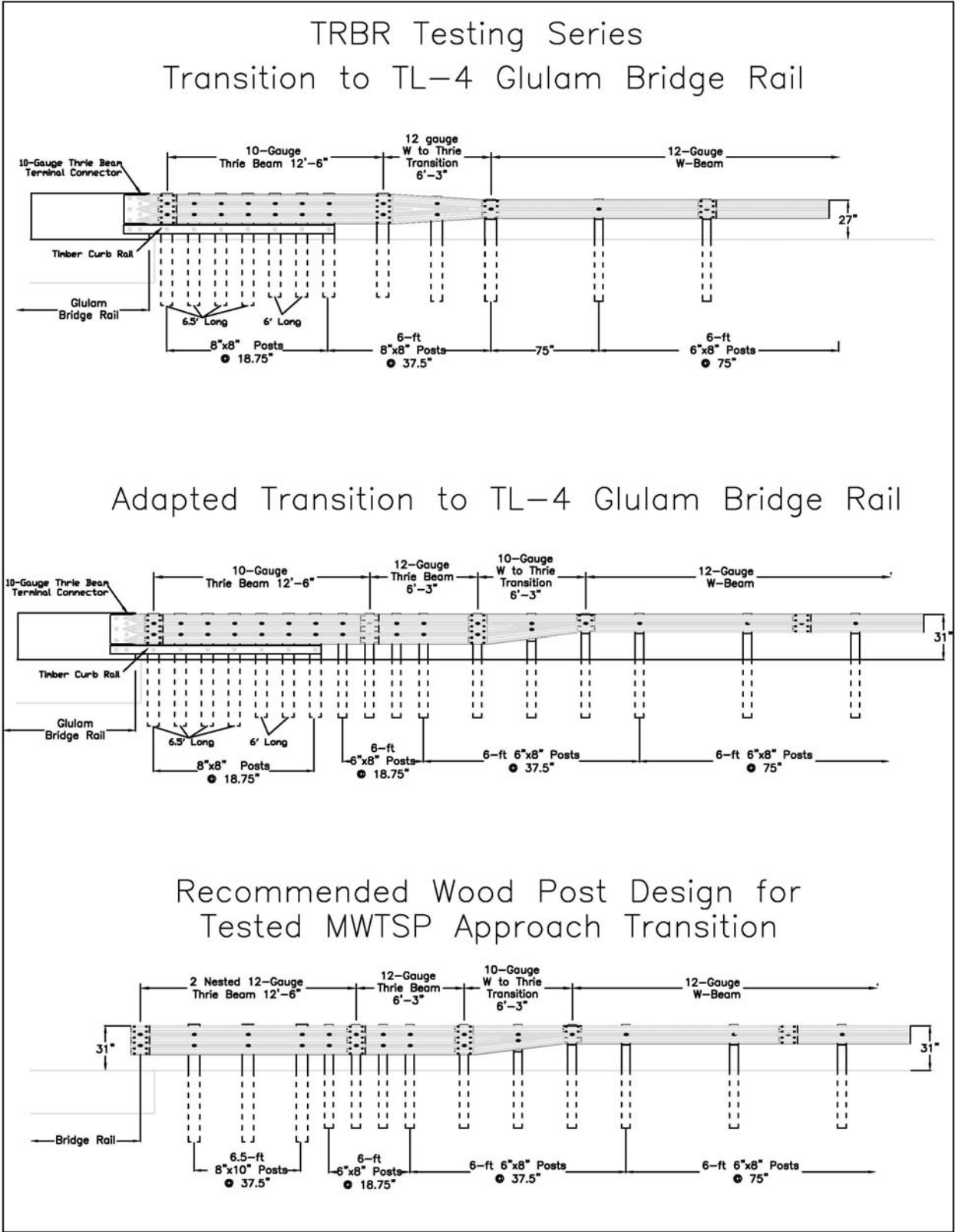


Figure 56. Approach Transition to TL-4 Glulam Bridge Rail [13-16]

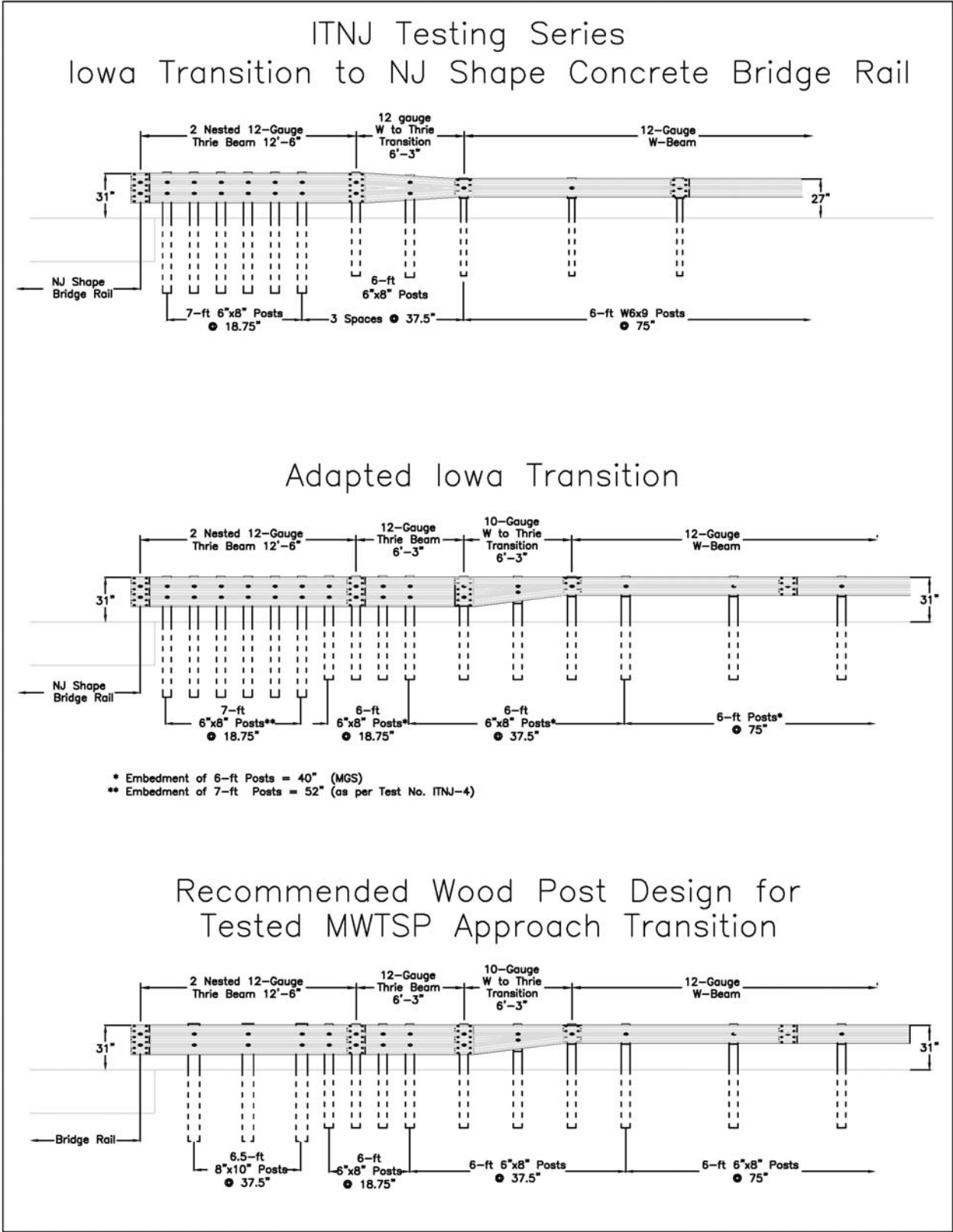


Figure 57. Approach Iowa Transition to NJ Shape Concrete Parapet [17-20]

9 REFERENCES

1. Polivka, K.A., Eller, C.M., Faller, R.K., Sicking, D.S., Rohde, J.R., Reid, J.D., Bielenberg, B.W., Allison, E.M., *Development of the Midwest Guardrail System (MGS) W-Beam to Thrie Beam Transition Element*, Final Report to the Midwest States Regional Pooled Fund Program, Transportation Research Report No. TRP-03-167-07, Project No. SPR-3(017)-Year 16, Midwest Roadside Safety Facility, University of Nebraska-Lincoln, Lincoln, NE, November 26, 2007.
2. Polivka, K.A., Faller, R.K., Sicking, D.L., Reid, J.D., Rohde, J.R., and Holloway, J.C., *Crash Testing of Missouri's W-Beam to Thrie beam Transition Element*, Final Report to the Midwest States Regional Pooled Fund Program, Transportation Research Report No. TRP-03-94-00, Project No. SPR-3(017)-Year 9, Midwest Roadside Safety Facility, University of Nebraska-Lincoln, Lincoln, NE, September 12, 2000.
3. Rosenbaugh, S.K., Lechtenberg, K.A., Faller, R.K., Sicking, D.L., Bielenberg, R.W., and Reid, J.D., *Development of the MGS Approach Guardrail Transition Using Standardized Steel Posts*, Final Report to the Midwest States Regional Pooled Fund Program, Research Report No. TRP-03-210-10, Project No. SPR-3(017) and TPF-5(193)-Years 18 and 19, Midwest Roadside Safety Facility, University of Nebraska-Lincoln, December 21, 2010.
4. *Manual for Assessing Safety Hardware (MASH)*, American Association of State Highway and Transportation Officials (AASHTO), Washington, D.C., 2009.
5. *A Guide to Standardized Highway Barrier Hardware*, Task Force 13 Report, AASHTO-AGC-ARTBA Joint Committee, Washington, D.C., 1995.
6. Kuipers, B.D. and Reid, J.D., *Testing of W152x23.8 (W6x16) Steel Posts - Soil Embedment Depth Study for the Midwest Guardrail System (Non-Proprietary Guardrail System)*, Final Report to the Midwest States Regional Pooled Fund Program, Transportation Research Report No. TRP-03-136-03, Midwest Roadside Safety Facility, University of Nebraska - Lincoln, June 12, 2003.
7. Dey, G., Faller, R.K., Hascall, J.A., Bielenberg, R.W., Polivka, K.A., and Molacek, K., *Dynamic Impact Testing of W152x13.4 (W6x9) Steel Posts on a 2:1 Slope*, Final Report to the Midwest States Regional Pooled Regional Pooled Fund Program, Transportation Research Report No. TRP-03-165-07, Project No. SPF-3(017)-Year 15, Midwest Roadside Safety Facility, University of Nebraska - Lincoln, March 23, 2007.
8. Homan, D.M., Thiele, J.C., Faller, R.K., Rosenbaugh, S.K., Rohde, J.R., Arens, S.W., Lechtenberg, K.A., Sicking, D.L., and Reid, J.D., *Investigation and Dynamic Testing of Wood and Steel Posts MGS on a Wire-Faced MSE Wall*, Draft Report to the Federal Highway Administration, Research Report No. TRP-03-231-11, Midwest Roadside Safety Facility, University of Nebraska Lincoln, June 2011.

9. Polivka, K.A., Faller, R.K., Sicking, D.L., Rohde, J.R., Bielenberg, B.W., and Reid, J.D., *Performance Evaluation of the Midwest Guardrail System – Update to NCHRP 350 Test No. 3-11 with 28” C.G. Height (2214MG-2)*, Final Report to the National Cooperative Highway Research Program (NCHRP), Transportation Research Report No. TRP-03-171-06, Midwest Roadside Safety Facility, University of Nebraska-Lincoln, October 11, 2006.
10. Stolle, C.J., Lechtenberg, K.A., Faller, R.K., Rosenbaugh, S.K., Sicking, D.L., and Reid, J.D., *Evaluation of the Midwest Guardrail System (MGS) with White Pine Wood Posts*, Final Report to the Wisconsin Department of Transportation, Transportation Research Report No. TRP-03-241-11, Midwest Roadside Safety Facility, University of Nebraska-Lincoln, March 28, 2011.
11. *Instrumentation for Impact Test - Part 1: Electronic Instrumentation*. SAE J211/1, SAE - Society of Automotive Engineers, Inc., 2007.
12. Jowza, E., Rosenbaugh, S.K., Faller, R.K., Sicking, D.L., and Reid, J.D., *Retrofits for Existing Approach Guardrail Transitions*, Draft Report in Progress, Midwest Roadside Safety Facility, University of Nebraska-Lincoln, March 2011.
13. Polivka, K.A., Faller, R.K., Rosson, B.T., Ritter, M.A., Fowler, M.D., and Keller, E.A., *Two Test Level 4 Bridge Railing and Transition Systems for Transverse Glue-Laminated Timber Decks*, Draft Report to the U.S. Department of Agriculture, Transportation Research No. TRP-03-71-01, Midwest Roadside Safety Facility, University of Nebraska - Lincoln, January 30, 2002.
14. Faller, R.K., Ritter, M.A., Rosson, B.T., Fowler, M.D., and Duwadi, S.R., *Two Test Level 4 Bridge Railing and Transition Systems for Transverse Timber Deck Bridges*, Transportation Research Record No. 1696, Transportation Research Board, Washington, D.C., 2000, pg 334-351.
15. Fowler, M.D., *Design and Testing of a Test Level 4 Bridge Railing for Transverse Glulam Timber Deck Bridges*, M.S. Thesis, University of Nebraska-Lincoln, May 1997.
16. Baxter, J.R., *FHWA NCHRP Report No. 350 Approval Letter B-138 of TL-2 and TL-4 Railings and Transitions for Timber Bridge Decks*, To R. K. Faller, Midwest Roadside Safety Facility, August 4, 2005.
17. Faller, R.K., Reid, J.D., Rohde, J.R., Sicking, D.L., and Keller, E.A., *Two Approach Guardrail Transitions for Concrete Safety Shape Barriers*, Final Report to the Midwest States Regional Pooled Fund Program, Transportation Research Report No. TRP-03-69-98, Project No. SPR-3(017)-Year 6, Midwest Roadside Safety Facility, University of Nebraska - Lincoln, May 15, 1998.
18. Faller, R.K., Reid, J.D., and Rohde, J.R., *Approach Guardrail Transition for Concrete Safety Shape Barriers*, Transportation Research Record No. 1647, Transportation Research Board, Washington, D.C., November 1998, pg 111-121.

19. Horne, D.A., *FHWA NCHRP Report No. 350 Approval Letter B-47 of Steel Post and Wood Post Thrie Beam Transitions to Concrete Parapets*, To R. K. Faller, Midwest Roadside Safety Facility, March 6, 1998.
20. Horne, D.A., *FHWA NCHRP Report No. 350 Approval Letter B-47A of Conditional Acceptance of Steel Post and Wood Post Thrie Beam Transitions to Vertical Wall*, To D. L. Sicking, Midwest Roadside Safety Facility, May 28, 1999.

10 APPENDICES

Appendix A. Soil Batch Sieve Analyses

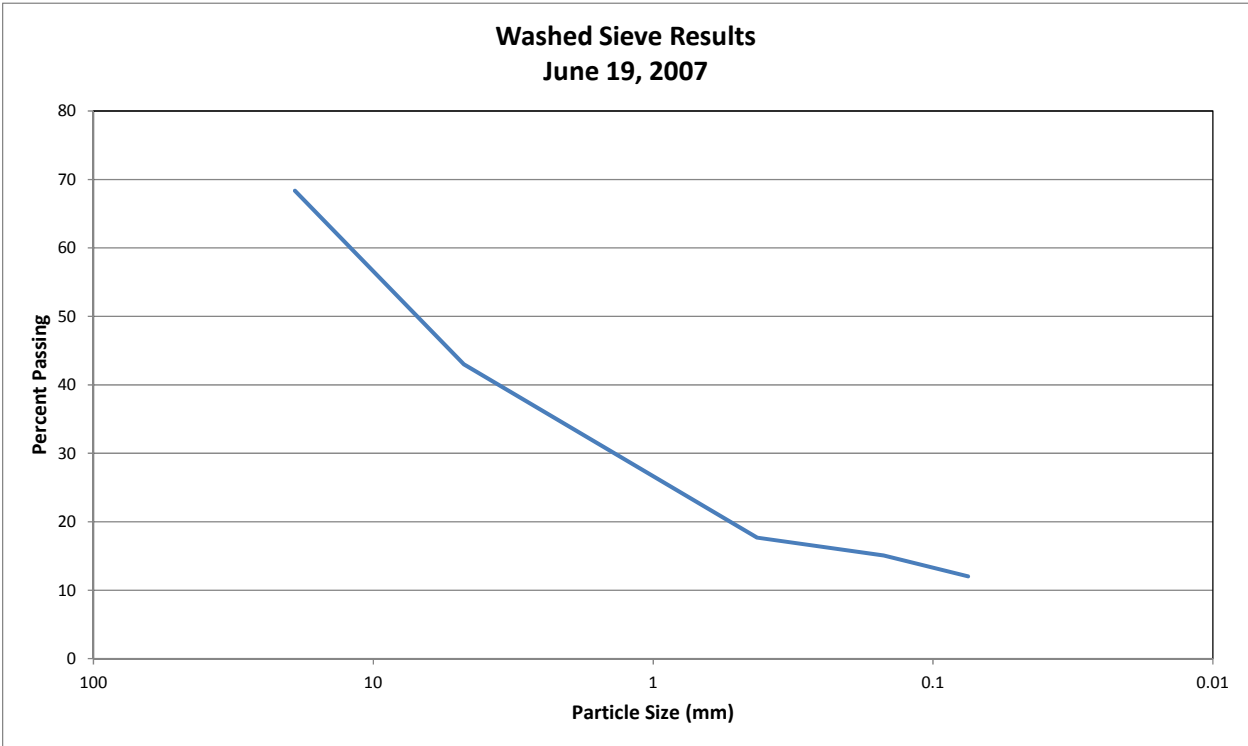


Figure A-1. Sieve Analysis for MGSATB-1 through MGSATB-4

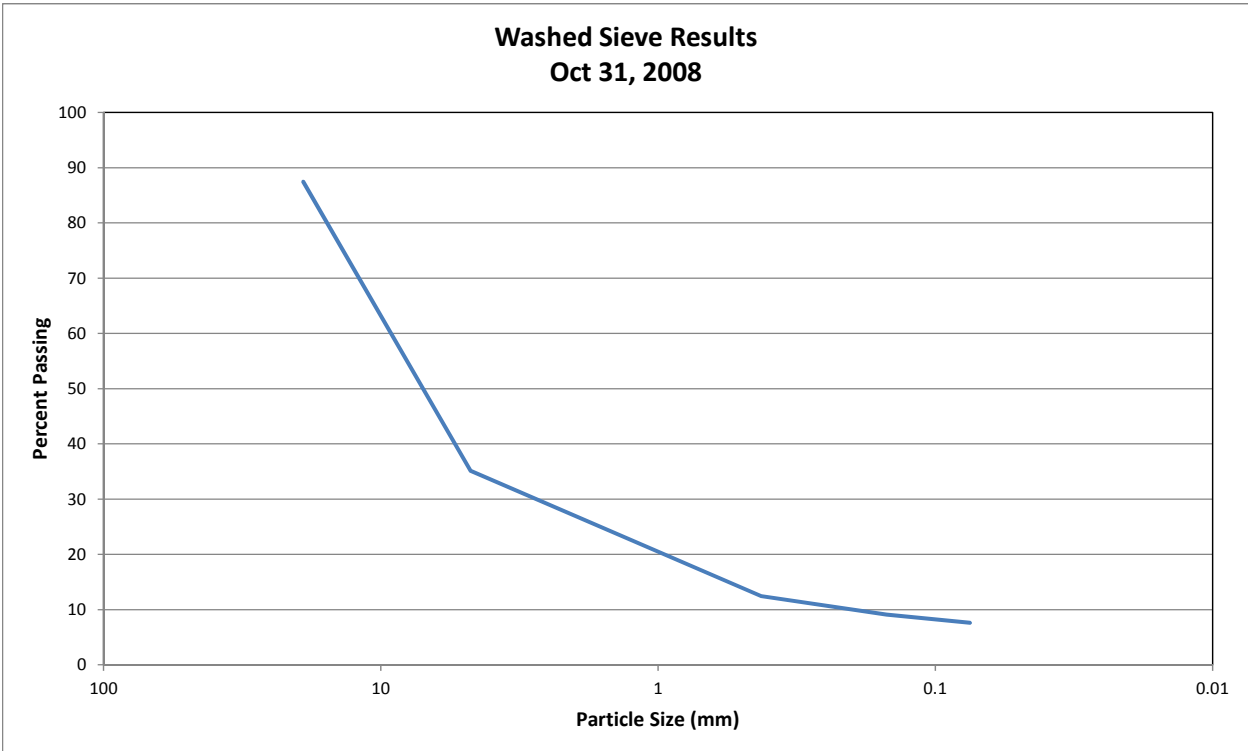


Figure A-2. Sieve Analysis for MGSATB-5 through MGSATB-8

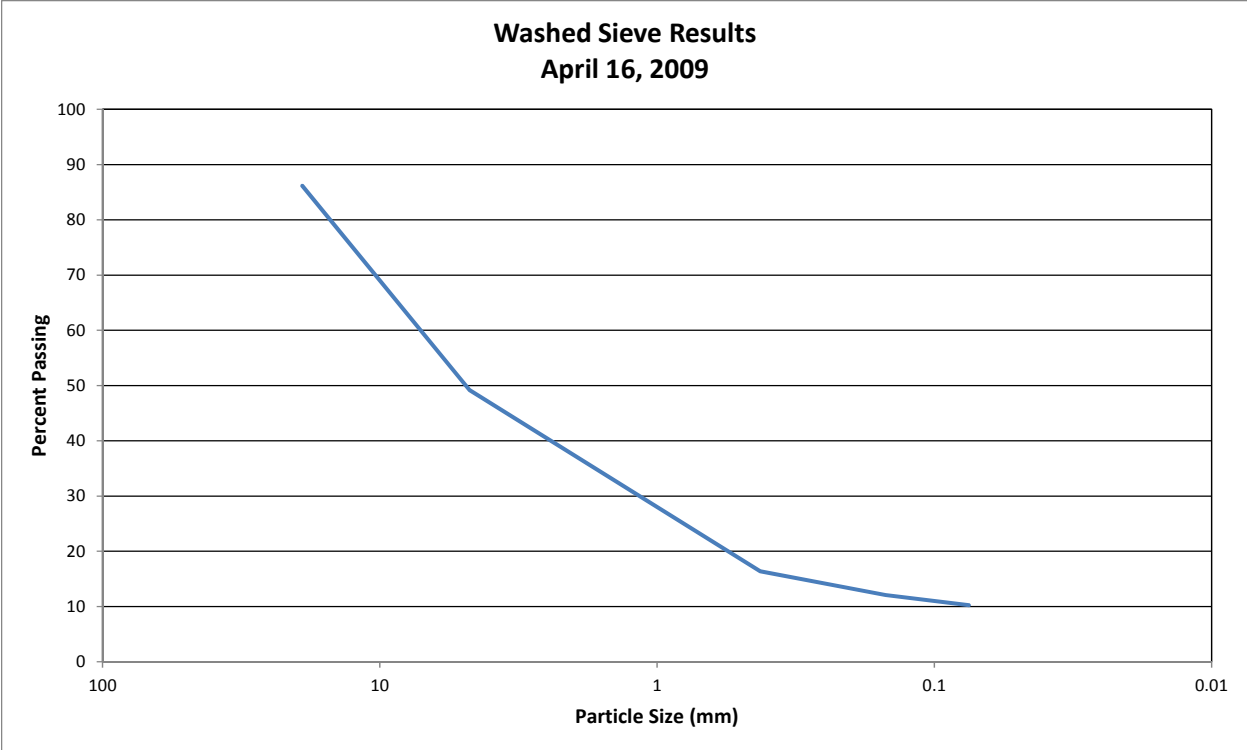


Figure A-3. Sieve Analysis for MGSATB-9 Through MGSATB-17.

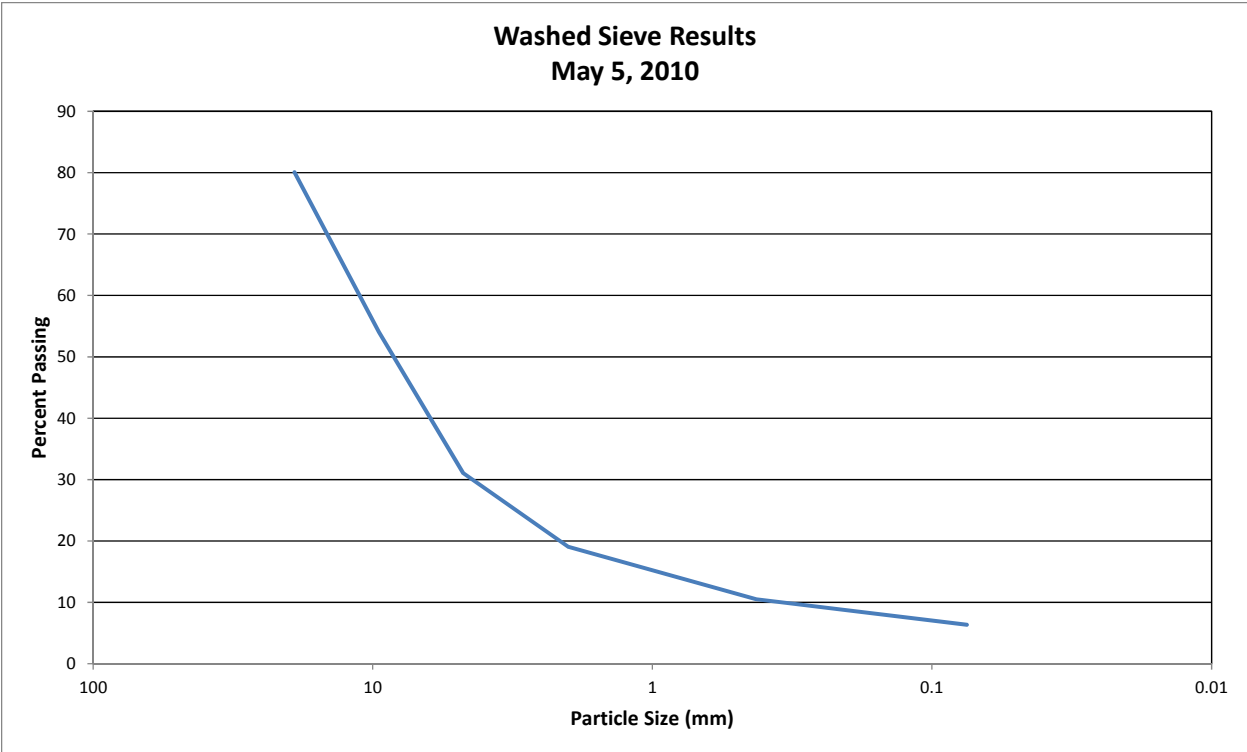


Figure A-4. Sieve Analysis for MGSATB-18 Through MGSATB-20.

Appendix B. EDR-3 Equivalency to Approved Transducer

At the time of testing, only the manufacturer, IST, had the capabilities to calibrate the EDR-3 unit because it is a self contained transducer utilizing IST software. Since IST is not an ISO 17025 accredited laboratory, the EDR-3 was not viewed as a transducer calibrated to ISO 17025. Additionally, both MASH and SAE J211-1 recommend a minimum sampling rate of at least 10 times the Channel Frequency Class (CFC). With the recommended CFC 1000 pre-sampling filter to prevent aliasing errors in the sampling process, the minimum sampling rate was recommended to be 10,000 Hz. The EDR-3 does not satisfy this limit as it records data at 3,200 Hz.

Although the EDR-3 has a lower than recommended sampling frequency and was not ISO 17025 calibrated, it has historically provided accurate and precise data when compared to MASH compliant transducers that have been ISO 17025 calibrated and high-speed video analysis results of physical testing. Thus, MwRSF has viewed the EDR-3 as an equivalent transducer and has continued using it during physical impact testing. Appendix B of SAE J211-1 entitled "Transducer Equivalency" states that to establish equivalence, tests must be performed to ensure that the transducer under consideration yields similar results for the application of interest. Further, transducers may be placed side-by-side in actual test conditions as the basis of comparison. Consequently, MwRSF has compared the EDR-3 to the ISO 17025 calibrated and MASH compliant DTS unit to establish equivalency.

The DTS was calibrated on July 10, 2010 by a laboratory in the process of becoming ISO 17025 accredited and was able to provide reverse traceability. The EDR-3 was directly compared to the DTS unit utilizing impact testing at the MwRSF test site that occurred after the calibration. Comparisons with the results from two bogie impact tests, test nos. MGSATB-18 and OCF-6, and one full-scale crash test, test no. DB-1 are shown in this appendix. During these tests, the

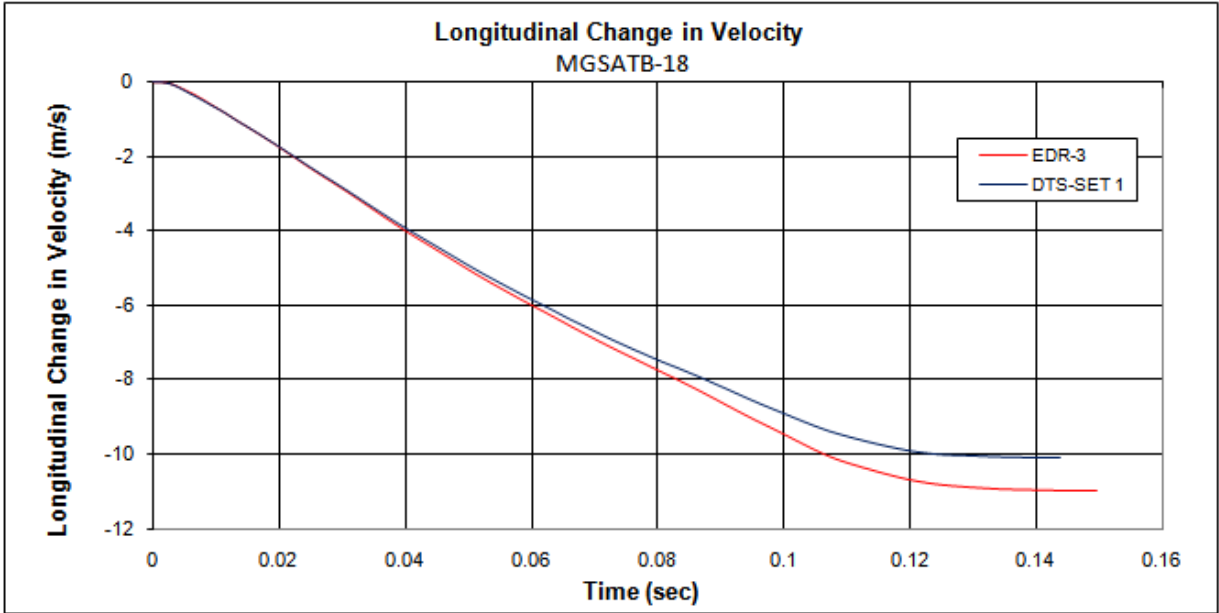
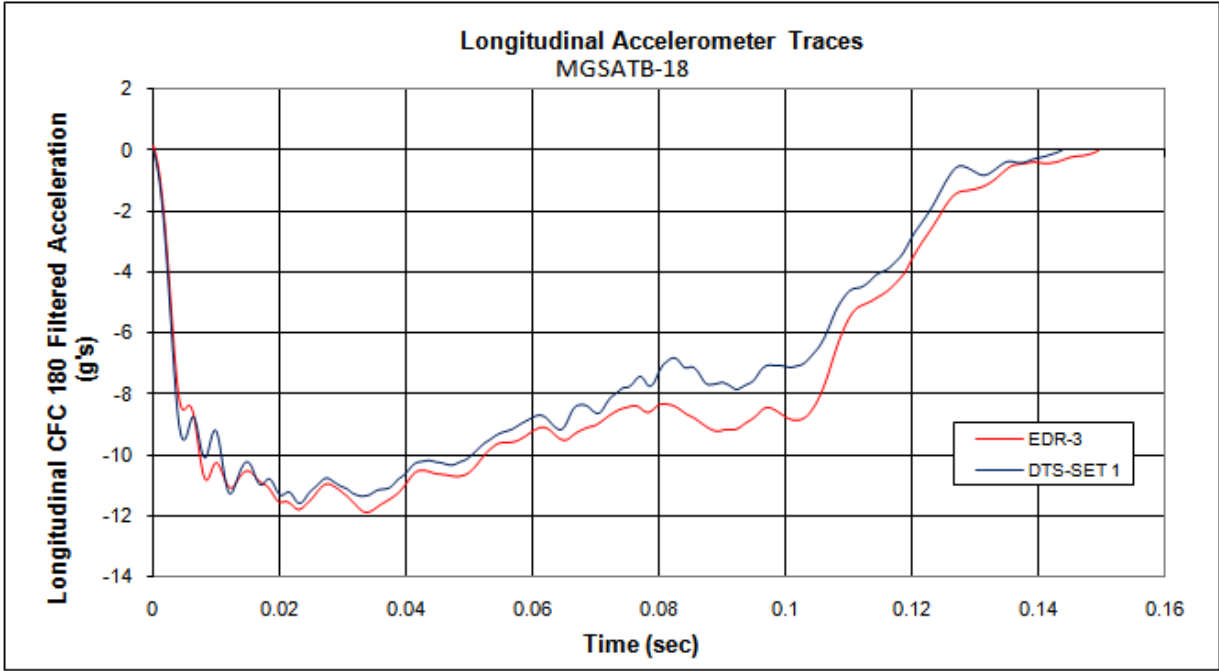
EDR-3 and DTS transducers were placed next to each other on the impacting vehicle, allowing for a direct comparison. Only the longitudinal accelerometer traces were analyzed from the full-scale test since only longitudinal accelerations were used during the project contained herein.

According to MwRSF procedure, the accelerometers would be considered equivalent if the following criteria were met.

- (1) The acceleration traces were similar in shape and magnitude, e.g., major peaks and valleys match throughout the impact event on an acceleration vs. time plot.
- (2) The total change in velocity (area under the acceleration vs. time curves) should differ by less than 10 percent over the entire impact event.

The two criteria were satisfied in the noted impact tests, as shown in the following figures. Therefore, the EDR-3 was deemed equivalent to the DTS and approved for use.

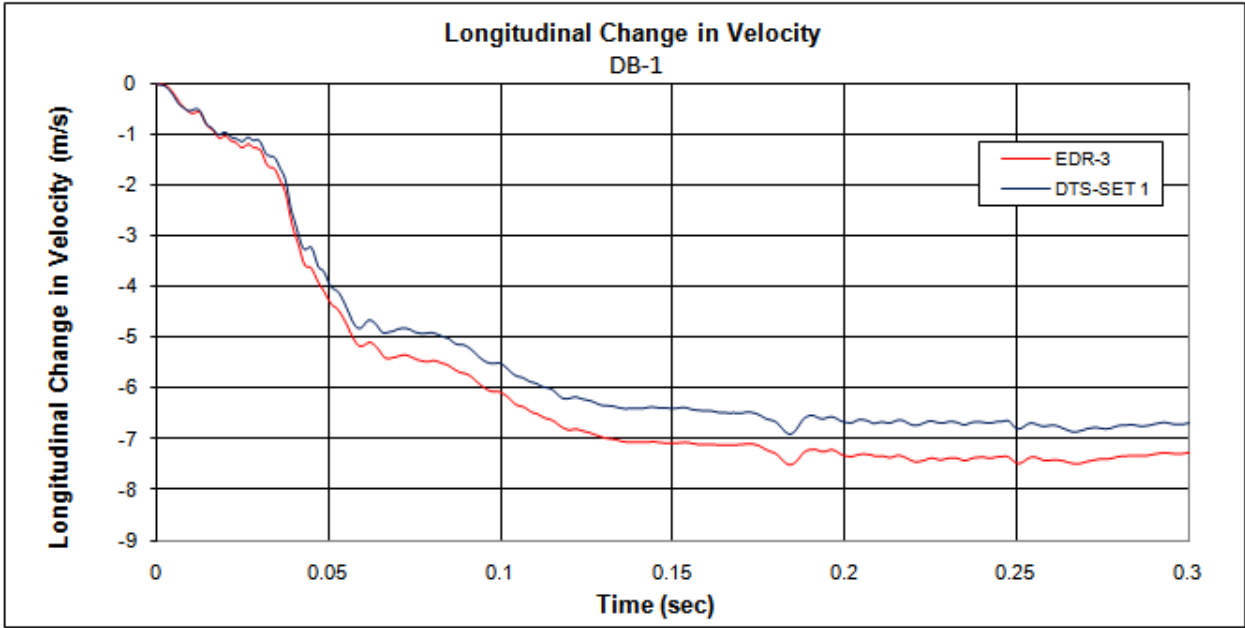
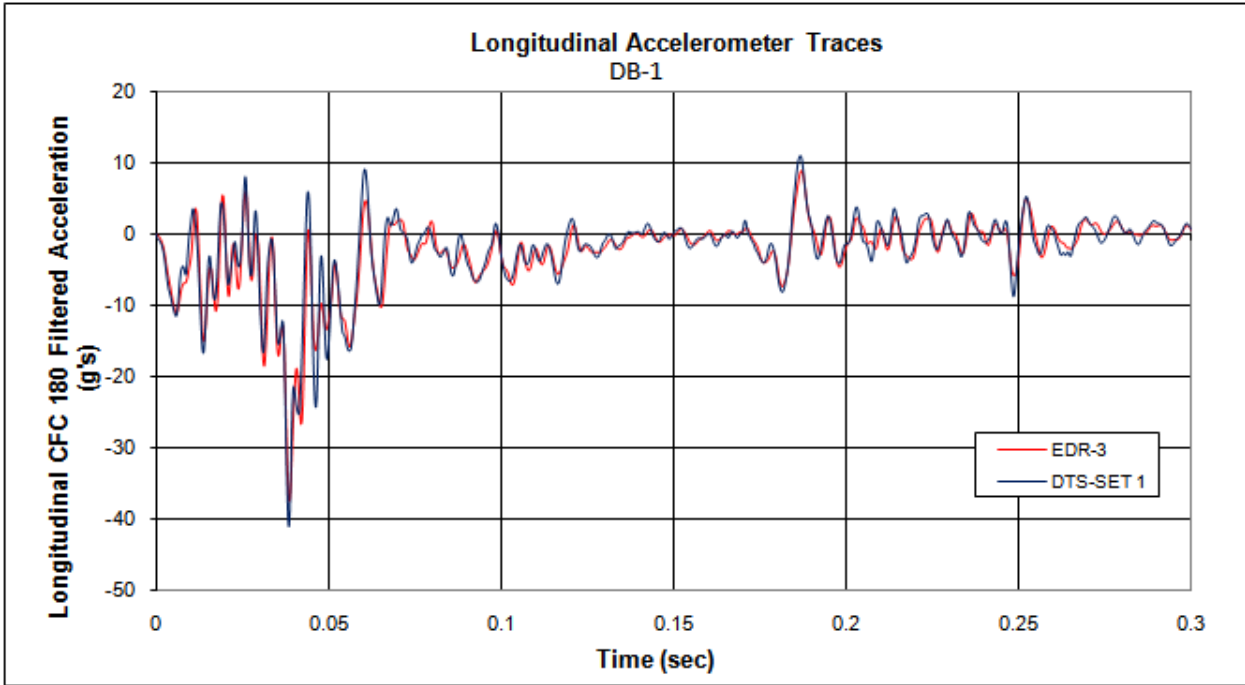
Test: MGSATB-18 Date: 7/28/2010 Test Type: Bogie-Post Testing



	DTS	EDR-3	% Difference
Final ΔV :	10.12	10.97	8.40%

Figure B-1. EDR-3 and DTS Equivalency Comparisons, Test No. MGSATB-18

Test: DB-1 Date: 8/3/2010 Test Type: Full-Scale Crash Test



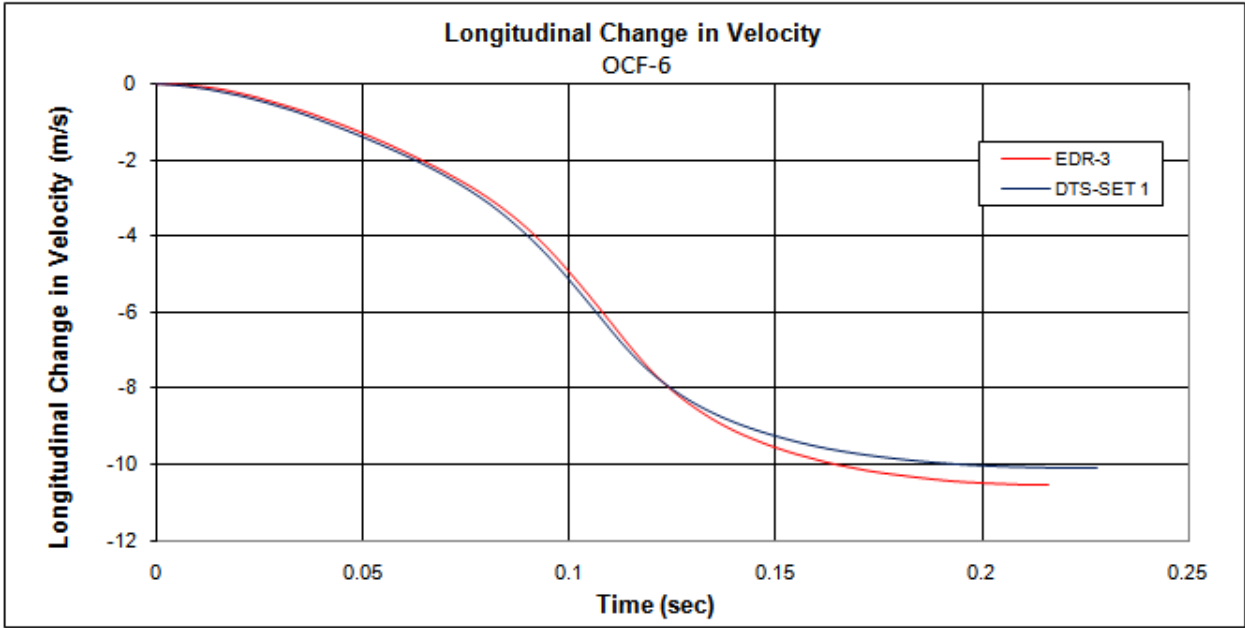
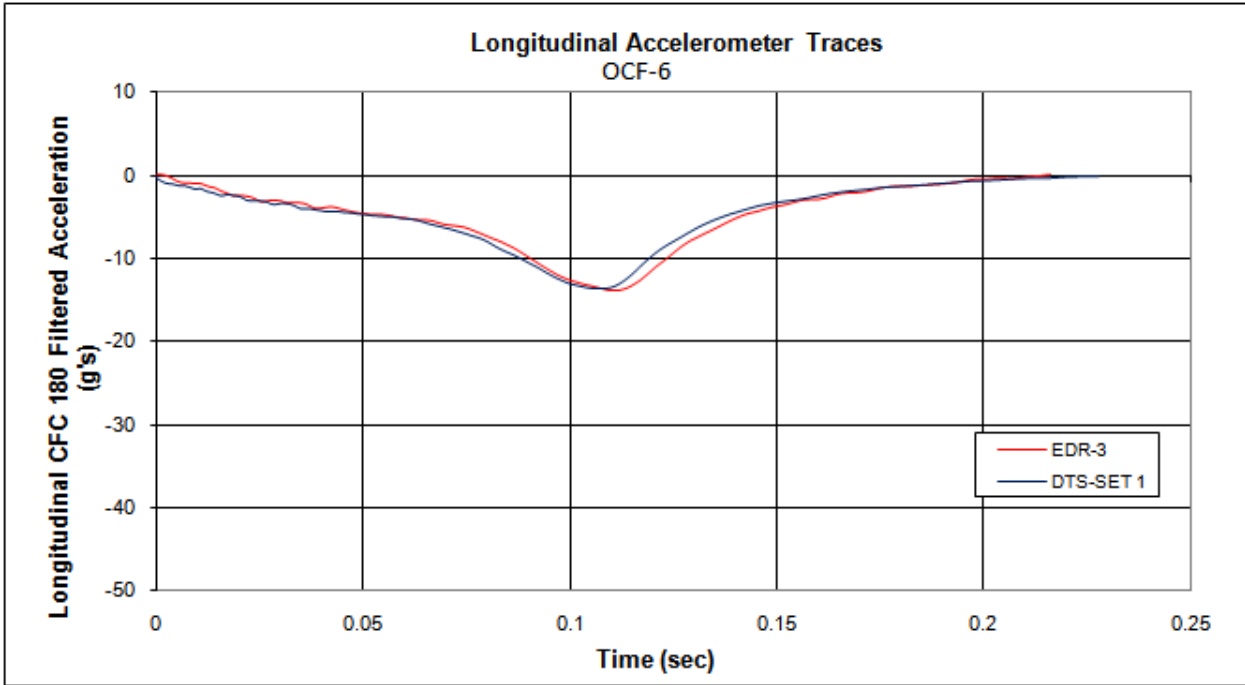
	DTS	EDR-3	% Difference
Final ΔV :	6.71	7.27	8.35%

Figure B-2. EDR-3 and DTS Equivalency Comparisons, Test No. DB-1

Test: OCF-6

Date: 8/16/2010

Test Type: Bogie-Foam Crush



	DTS	EDR-3	% Difference
Final ΔV :	10.12	10.53	4.05%

Figure B-3. EDR-3 and DTS Equivalency Comparisons, Test No. OCF-6

Appendix C. Material Specifications

CERTIFIED MATERIAL TEST REPORT

CHAPARRAL STEEL
300 Ward Rd.
Midlothian, TX
76065-9651
(972) 775-8241

CHAPARRAL

Bill To: STEEL AND PIPE SUPPLY
P.O. BOX 1688
MANHATTAN
66502
KS
US

Ship To: 2
STEEL AND PIPE SUPPLY
1050 FORT GIBSON ROAD
CATOOSA
OK
US

Order Date: 02/28/2007
PO No: 45/85145
Mill Order No: 3266337
Load No: 1095374
Manifest No: 1811250

MWT Base Testing

SIZE: W 6 X 15# / W150 X 22.5

GRADE: 992/572-50

LENGTH: 50 FT / 15.24 M

SPECIFICATIONS: ASTM A6-05a, A992-06a, A572-06

HEAT NO: 22389380

CHEMICAL ANALYSIS

C	Mn	P	S	Si	Cu	Ni	Cr	Mo	Sn	V	Al	Nb	CE
.08	.93	.005	.034	.24	.24	.09	.12	.028	.008	.001	.005	.014	.29

PHYSICAL PROPERTIES

<u>Yield Strength</u>		<u>Tensile Strength</u>		<u>Specimen Area</u>		<u>Elongation</u>		<u>Bend Test</u>	<u>ROA</u>
KSI	MPa	KSI	MPa	Sq In	Sq cm	%	Gage Length	Dia. Result	%
55.2	380.6	73.8	508.8	0.341	2.20	24.4	8 In 200 mm		
54.9	378.5	73.3	505.4	0.338	2.18	24.9	8 In 200 mm		

All manufacturing processes of this product, including electric arc melting and continuous casting, occurred in the U.S.A. CMTR complies with DIN EN 10204 3.1.B

"I hereby certify that the contents of this report are correct and accurate. All tests and operations performed by this material manufacturer or its sub-contractors, when applicable, are in compliance with the requirements of the material specifications and applicable purchaser designated requirements."

Signed: Tom L. Harrington Date: Mar. 12, 2007 Signed: _____ Date: _____
Tom L. Harrington: Quality Assurance Manager Notary Public (if applicable) Page: 1 of 1

106

Figure C-1. Material Test Report for W6x15 (W152x22.3) Steel Posts used in MGSATB-5 and MGSATB-6

November 28, 2011
MWRSF Report No. TRP-03-243-11

Appendix D. Bogie Test Results

The results of the recorded data from each accelerometer used during the dynamic bogie test are provided in the summary sheets found in this appendix. Summary sheets include acceleration, velocity, and displacement versus time plots as well as force and energy versus displacement plots.

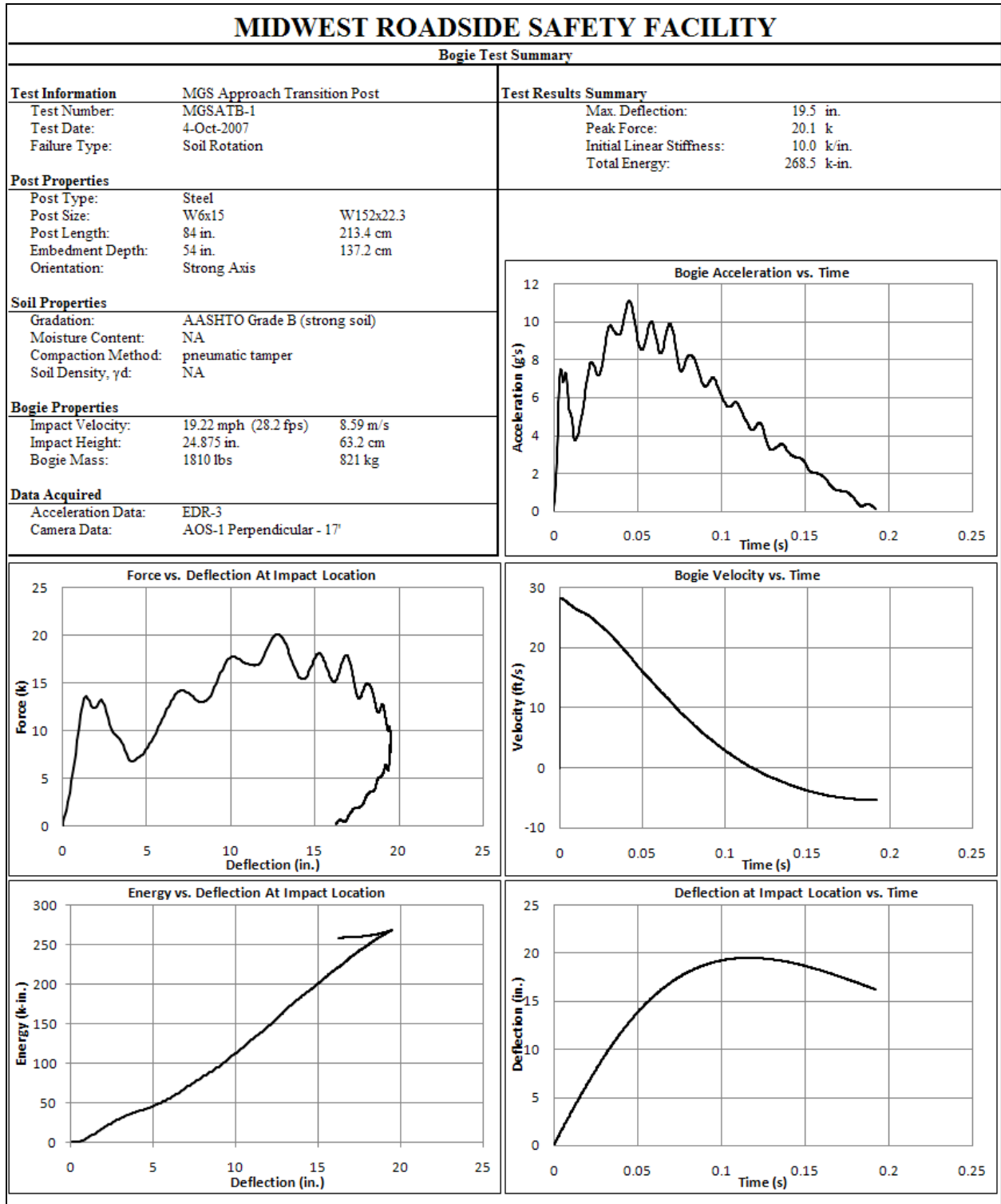


Figure D-1. Results of Test No. MGSATB-1 (EDR-3)

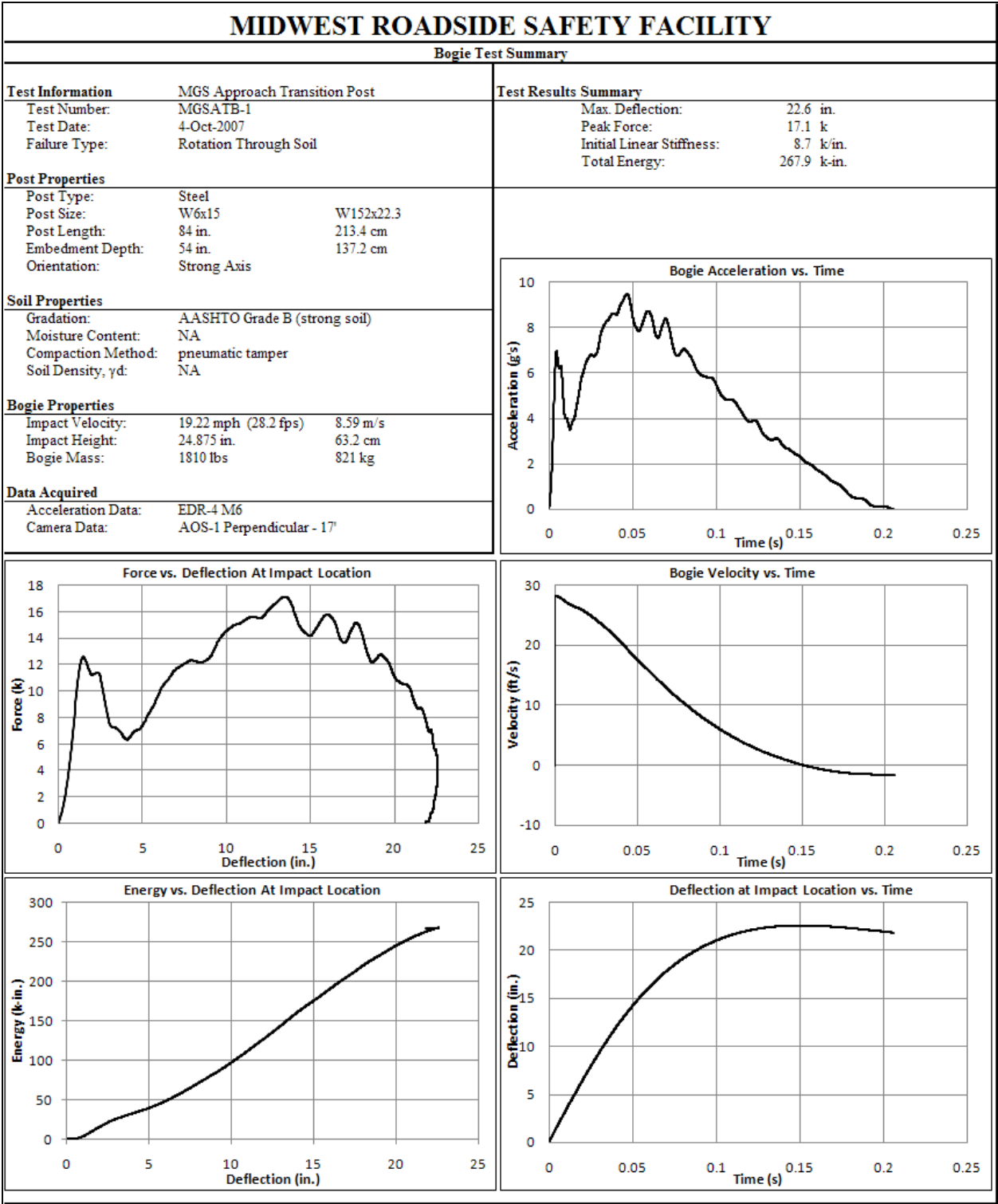


Figure D-2. Results of Test No. MGSATB-1 (EDR-4)

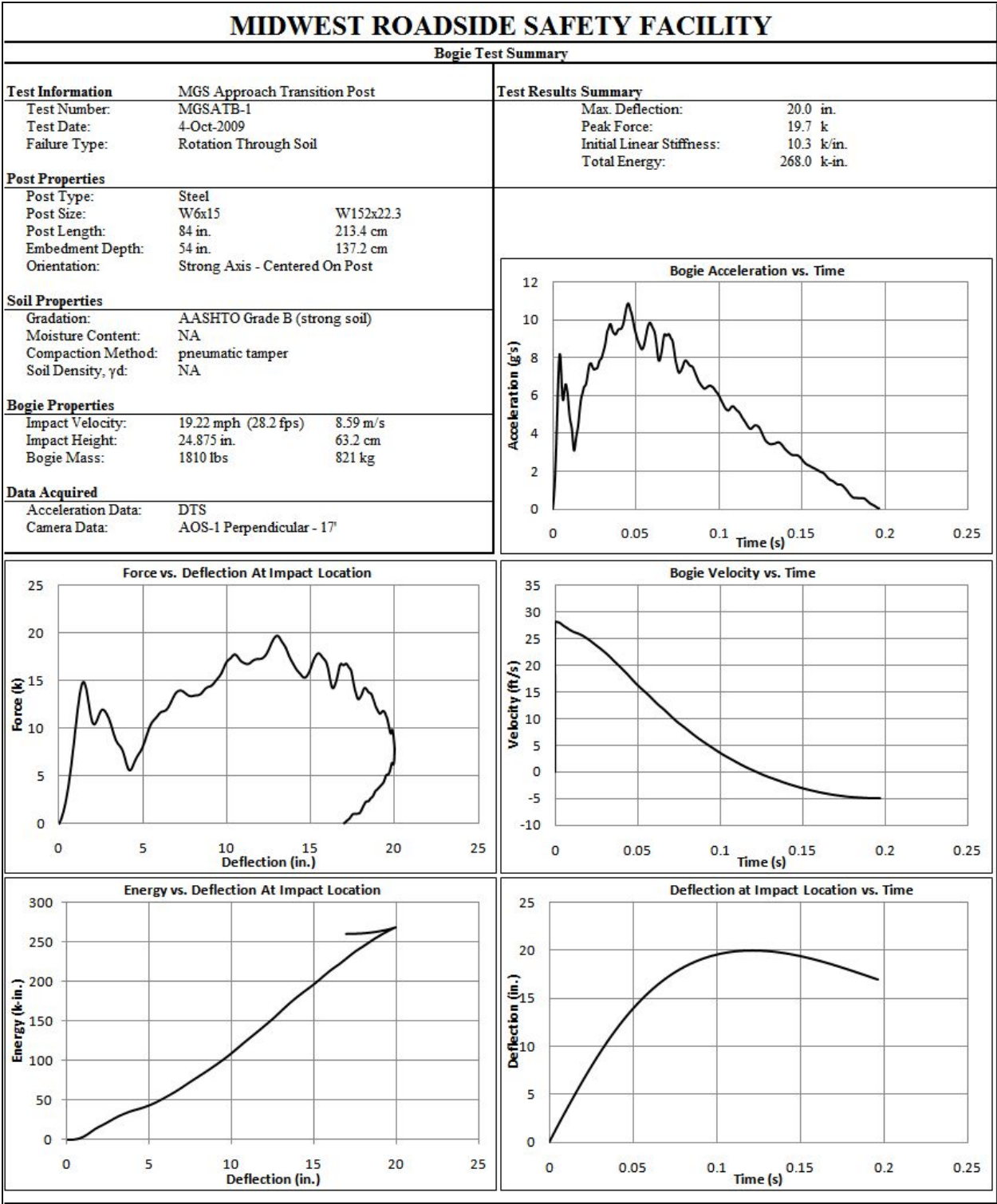


Figure D-3. Results of Test No. MGSATB-1 (DTS)

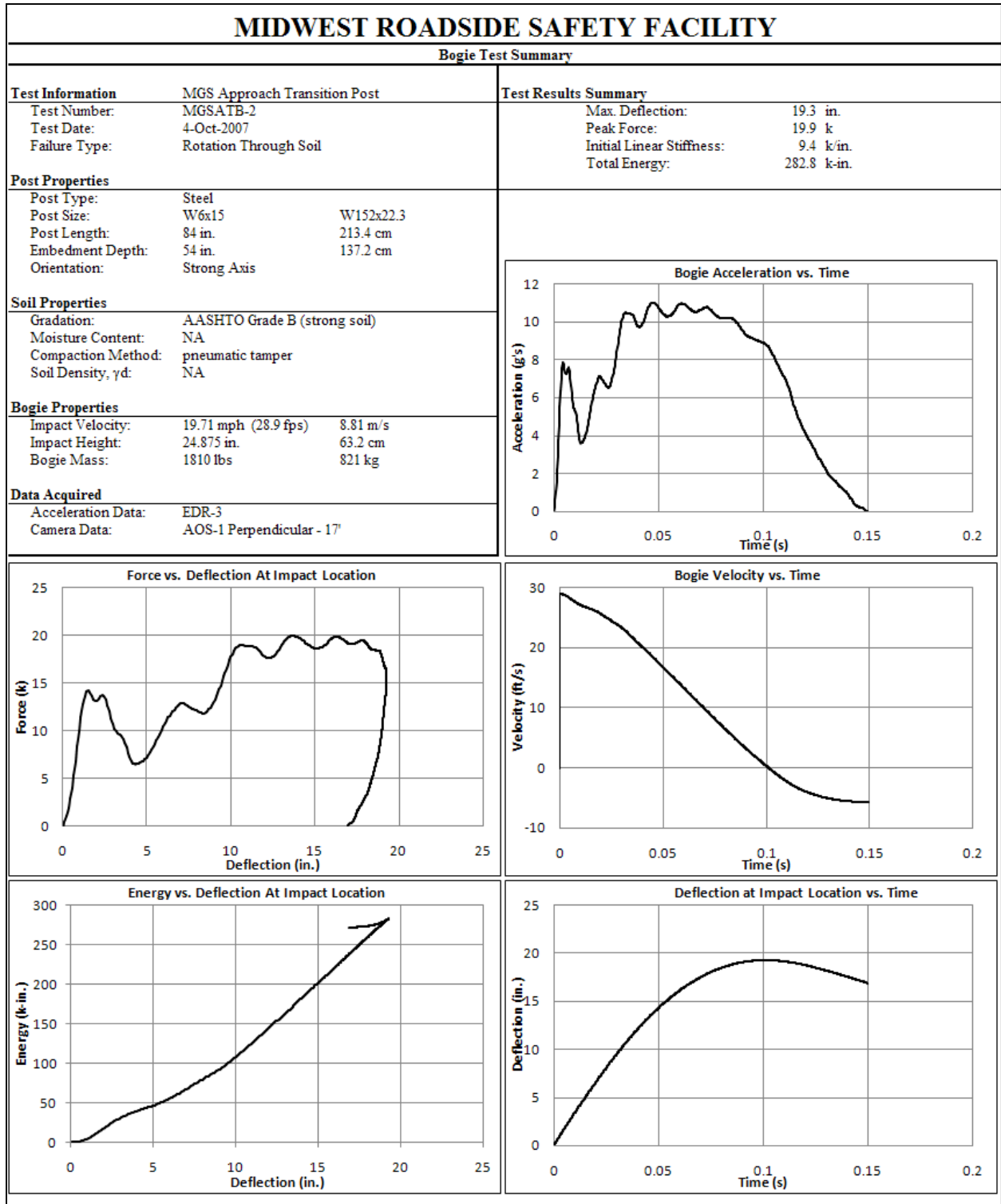


Figure D-4. Results of Test No. MGSATB-2 (EDR-3)

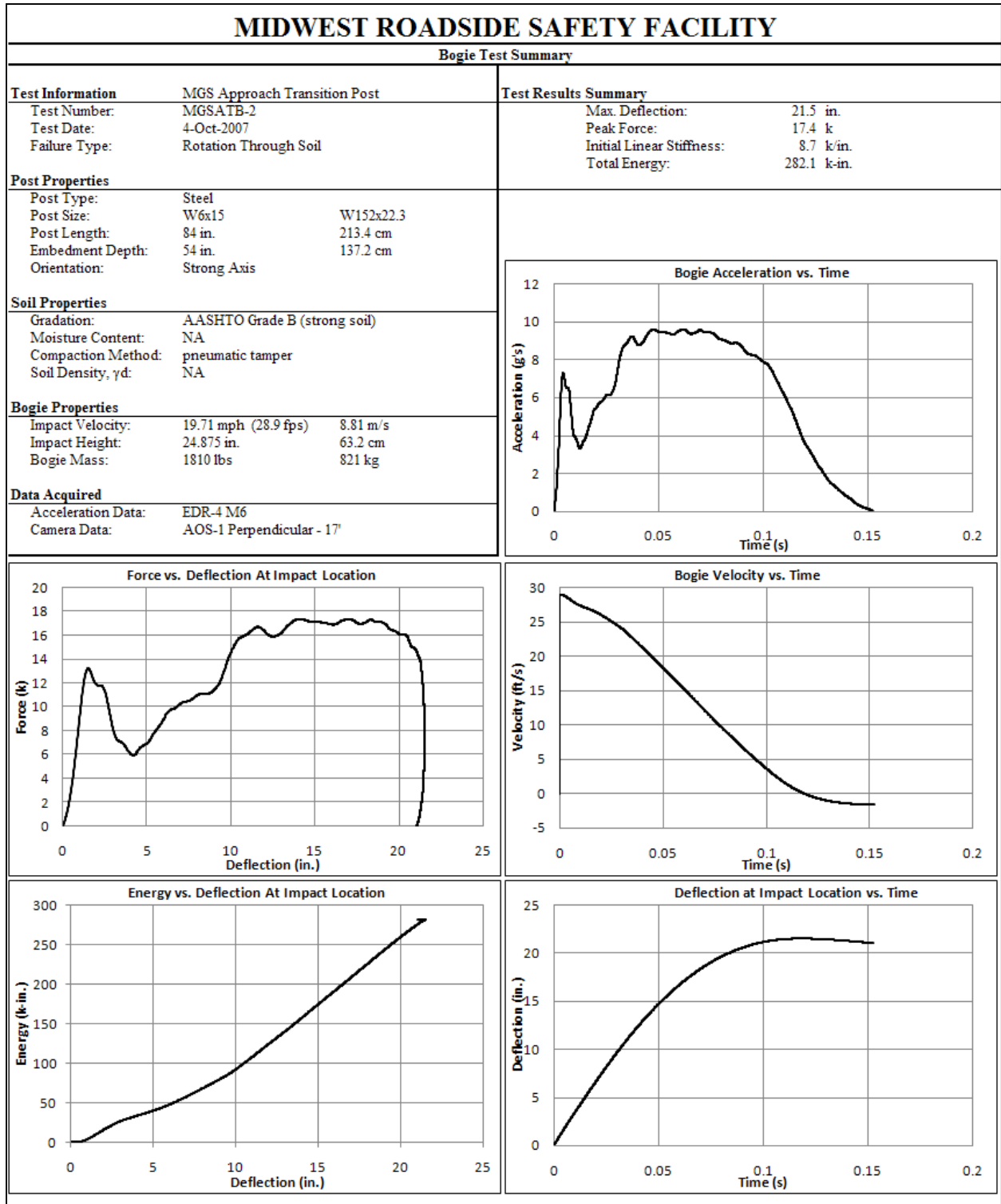


Figure D-5. Results of Test No. MGSATB-2 (EDR-4)

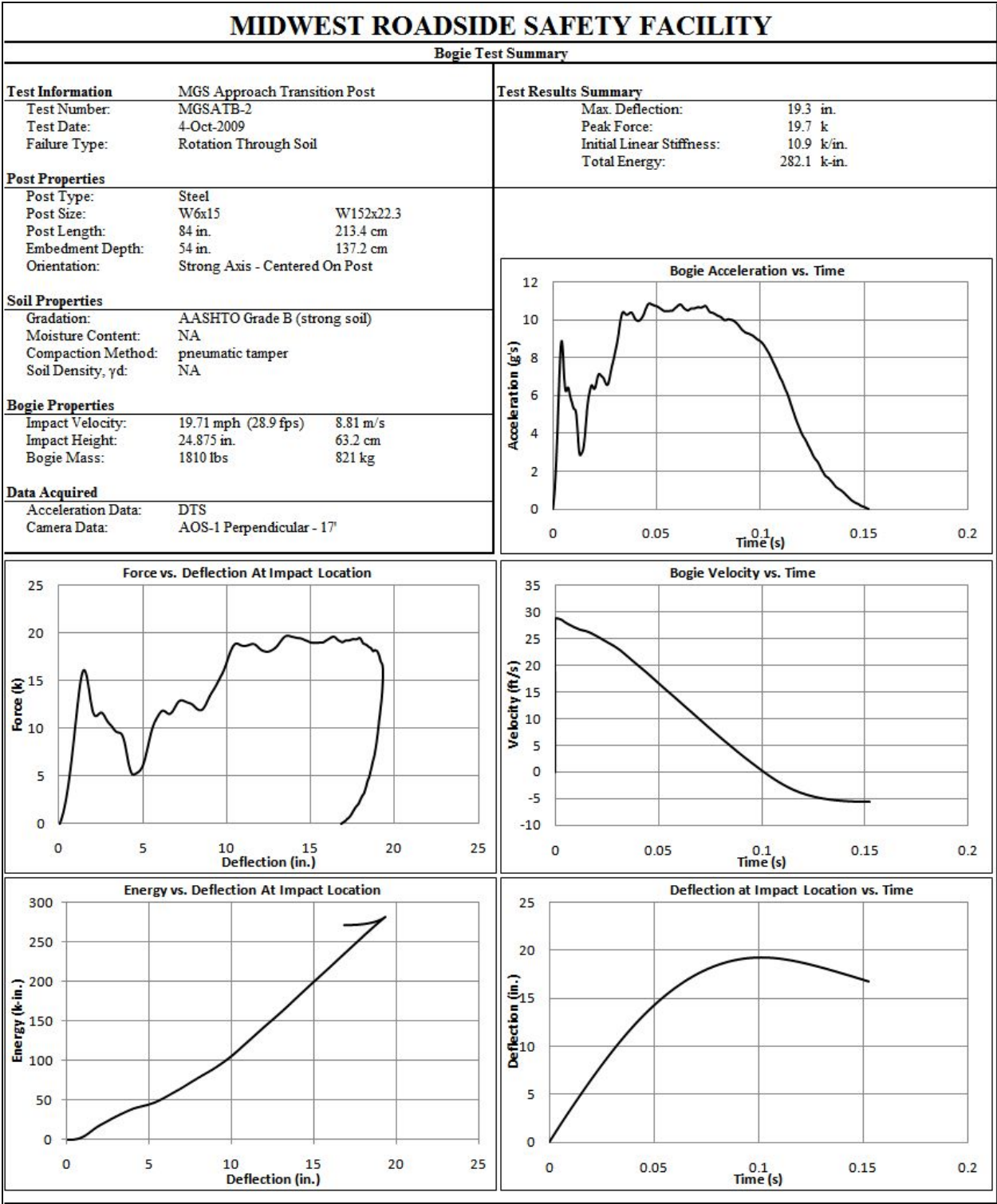


Figure D-6. Results of Test No. MGSATB-2 (DTS)

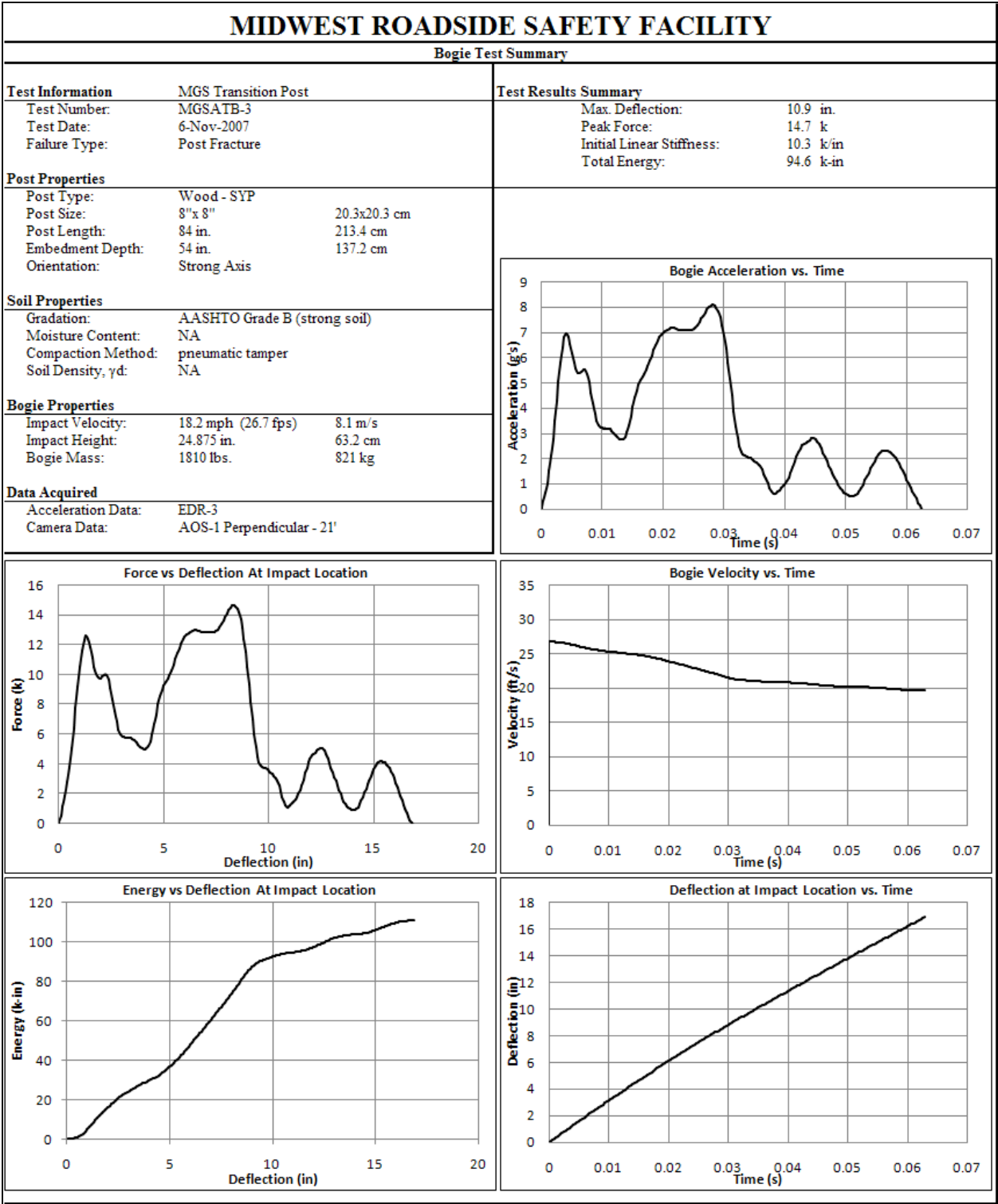


Figure D-7. Results of Test No. MGSATB-3 (EDR-3)

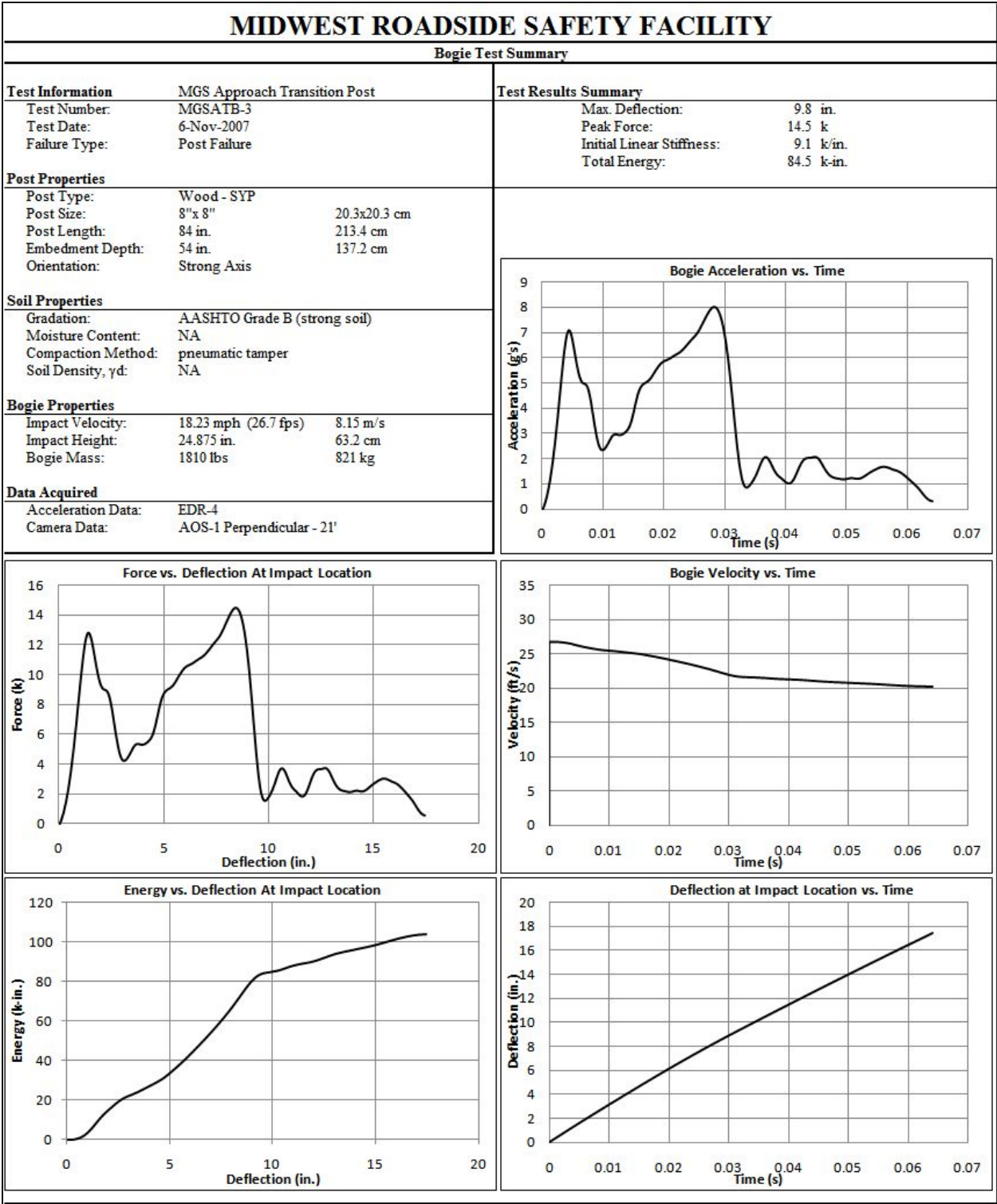


Figure D-8. Results of Test No. MGSATB-3 (EDR-4)

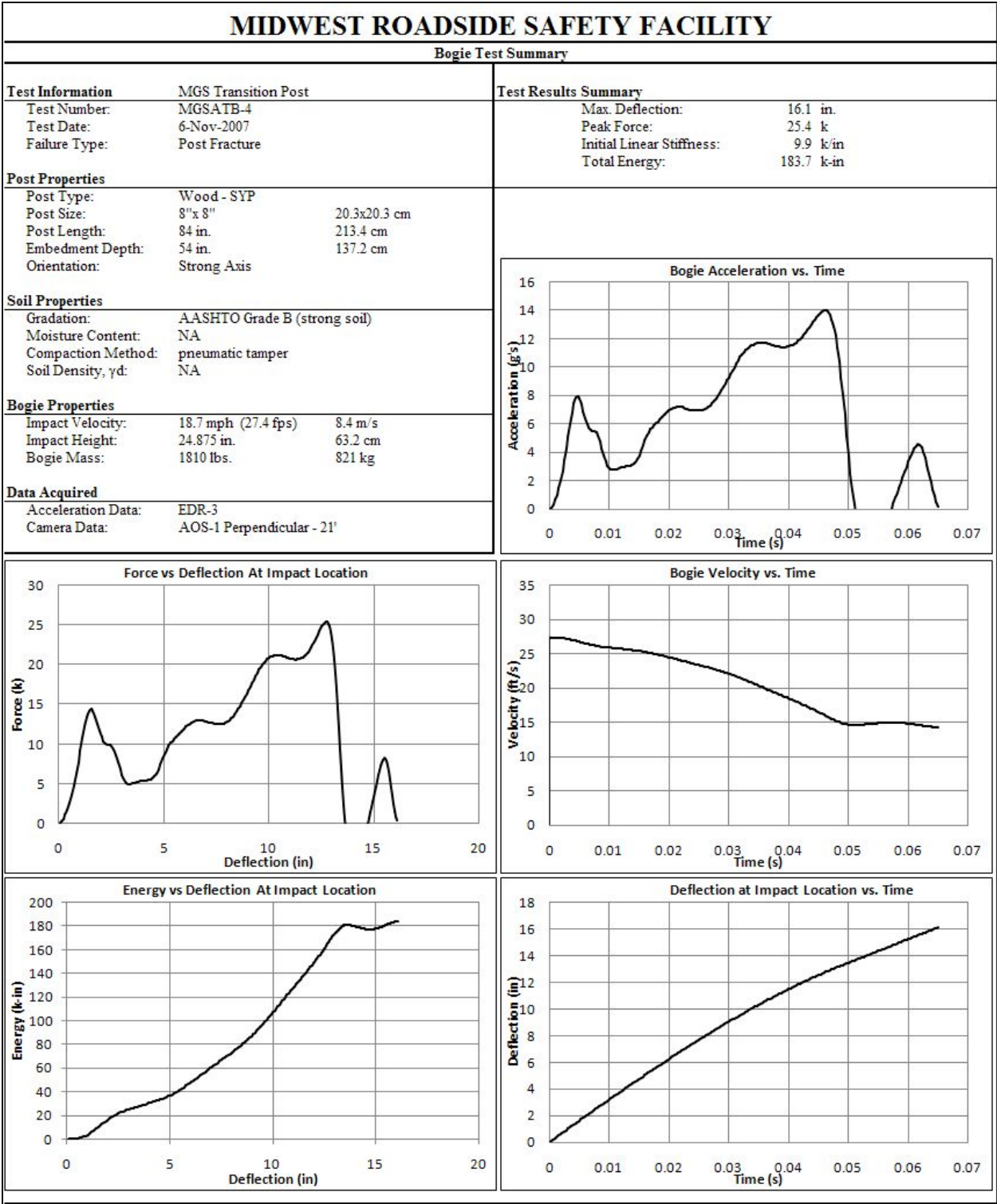


Figure D-9. Results of Test No. MGSATB-4 (EDR-3)

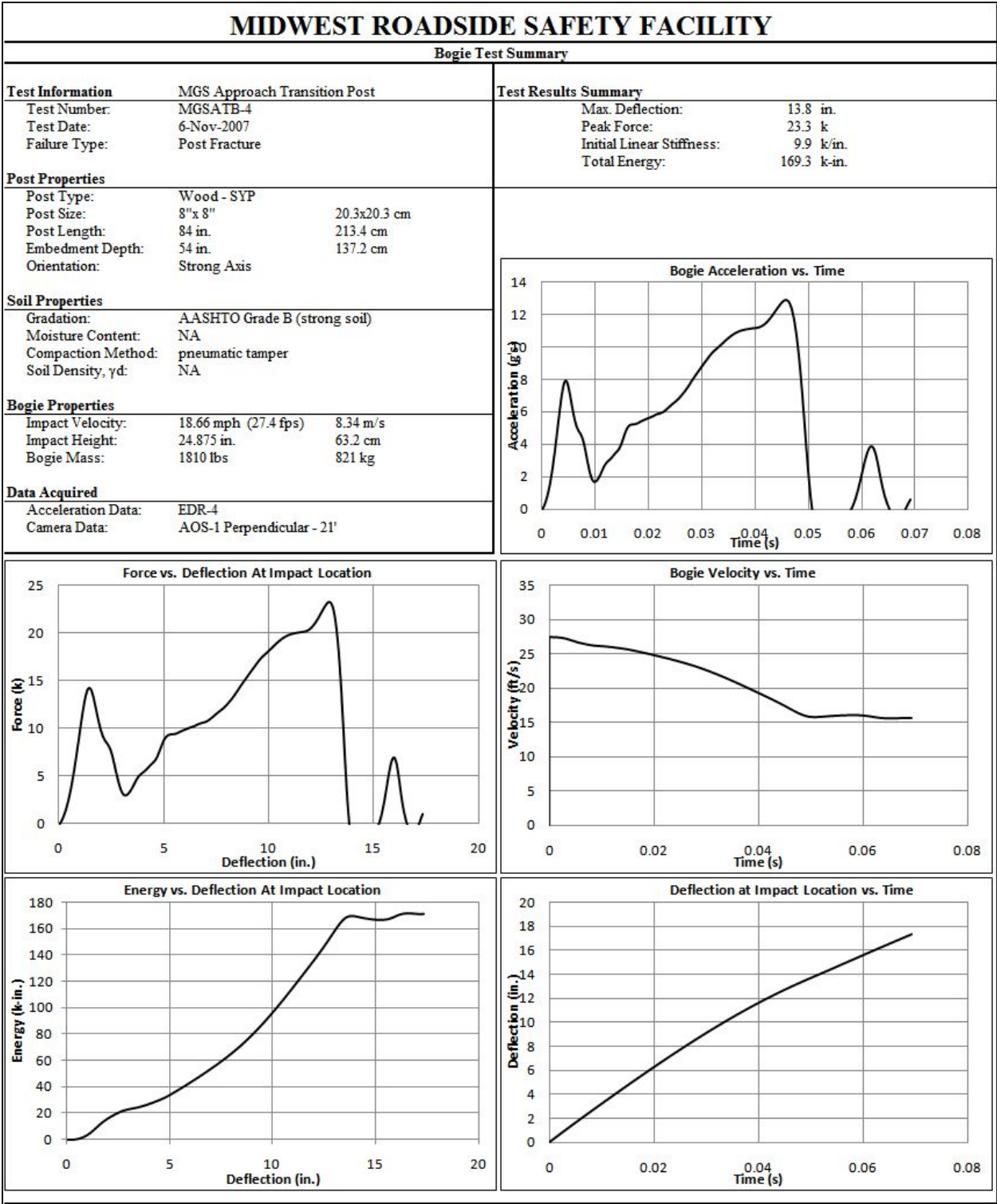


Figure D-10. Results of Test No. MGSATB-4 (EDR-4)

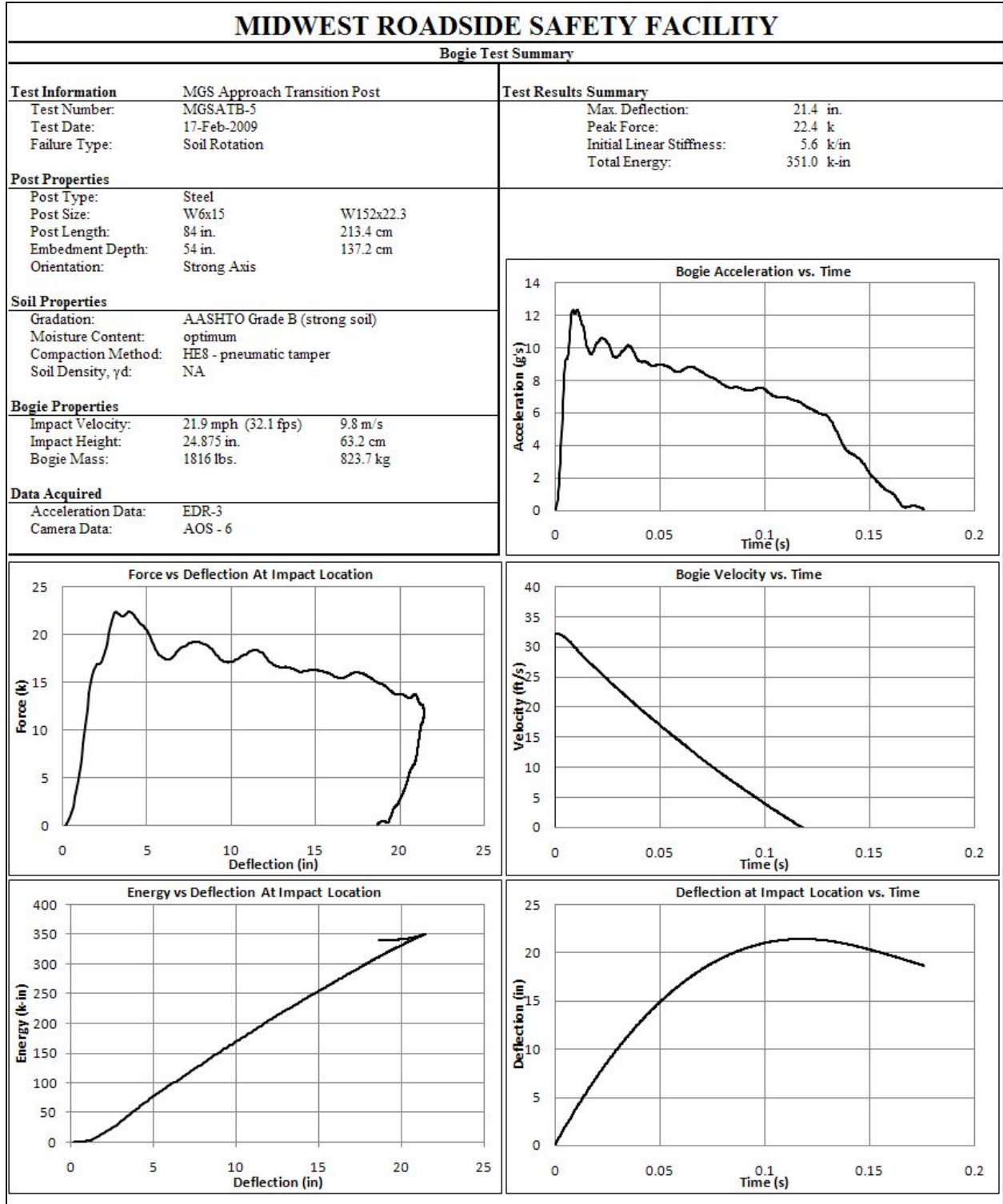


Figure D-11. Results of Test No. MGSATB-5 (EDR-3)

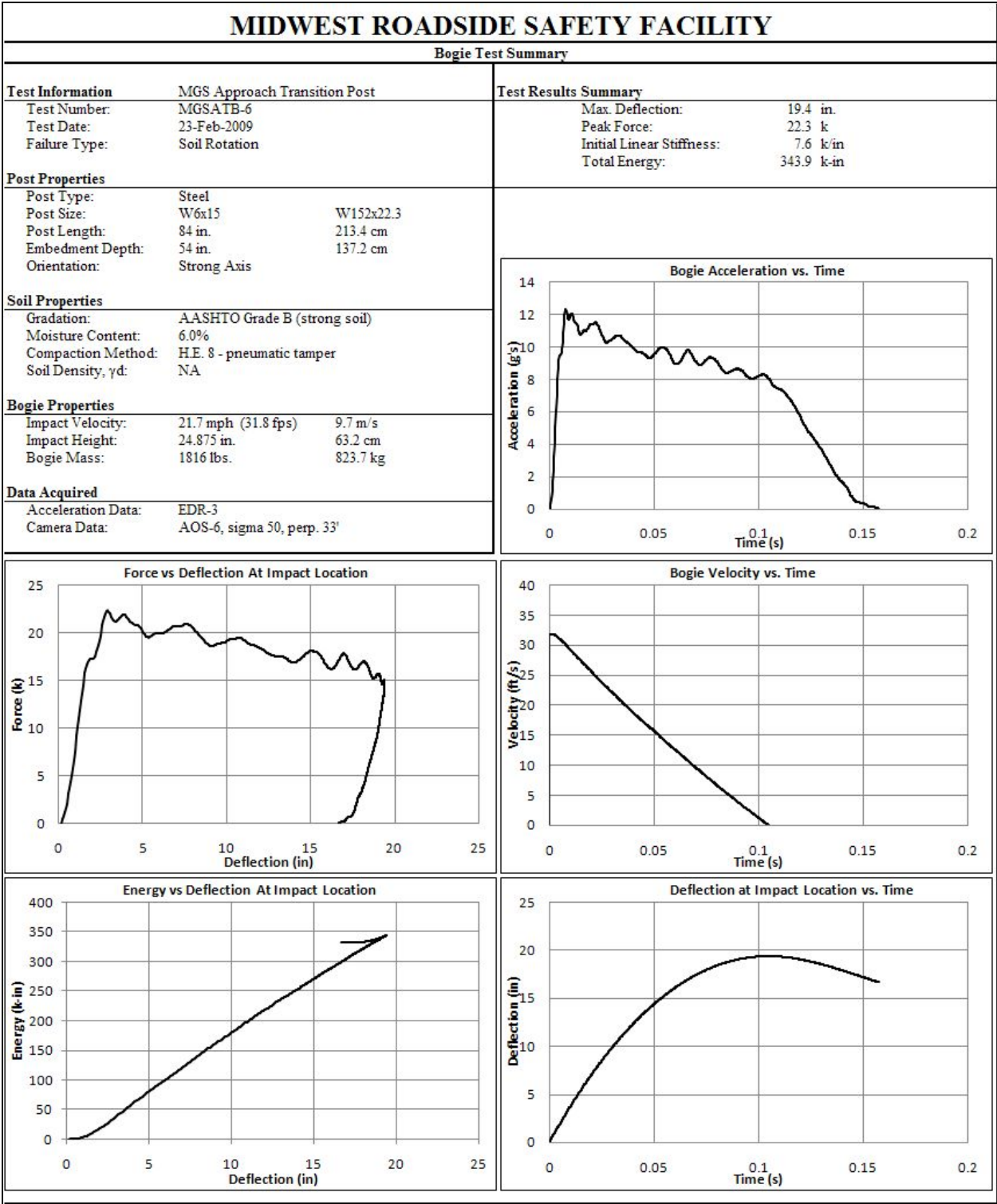


Figure D-12. Results of Test No. MGSATB-6 (EDR-3)

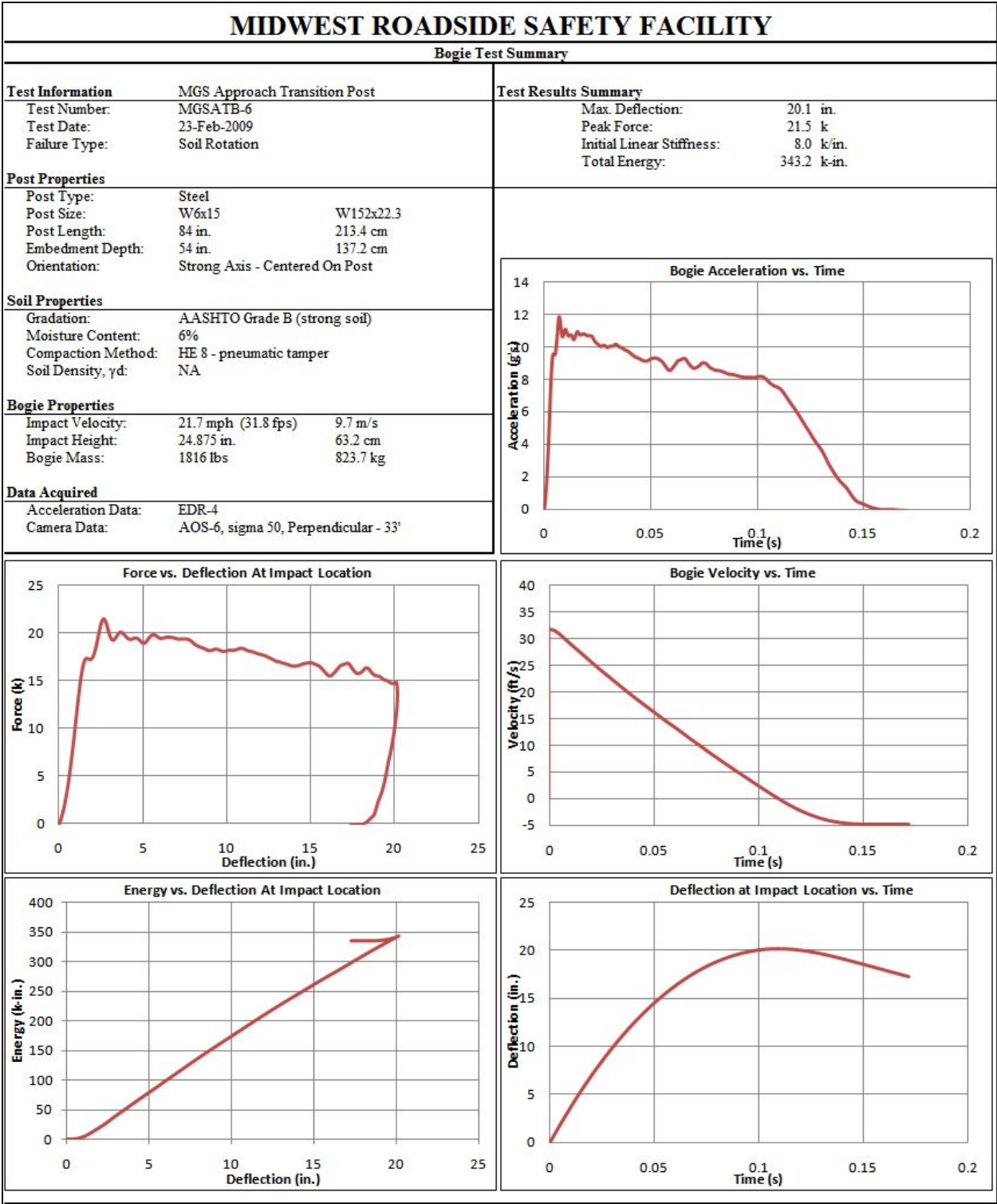


Figure D-13. Results of Test No. MGSATB-6 (EDR-4)

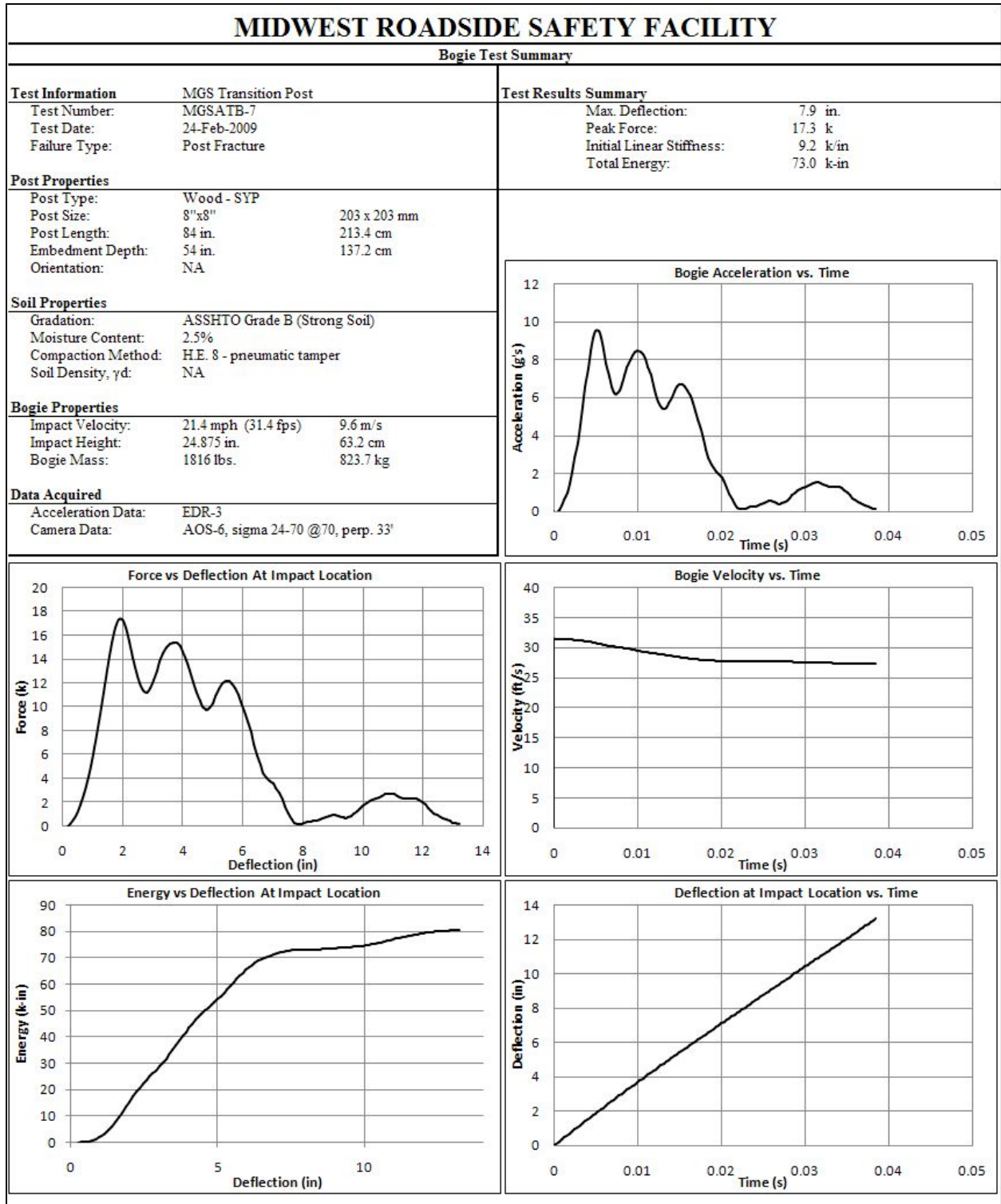


Figure D-14. Results of Test No. MGSATB-7 (EDR-3)

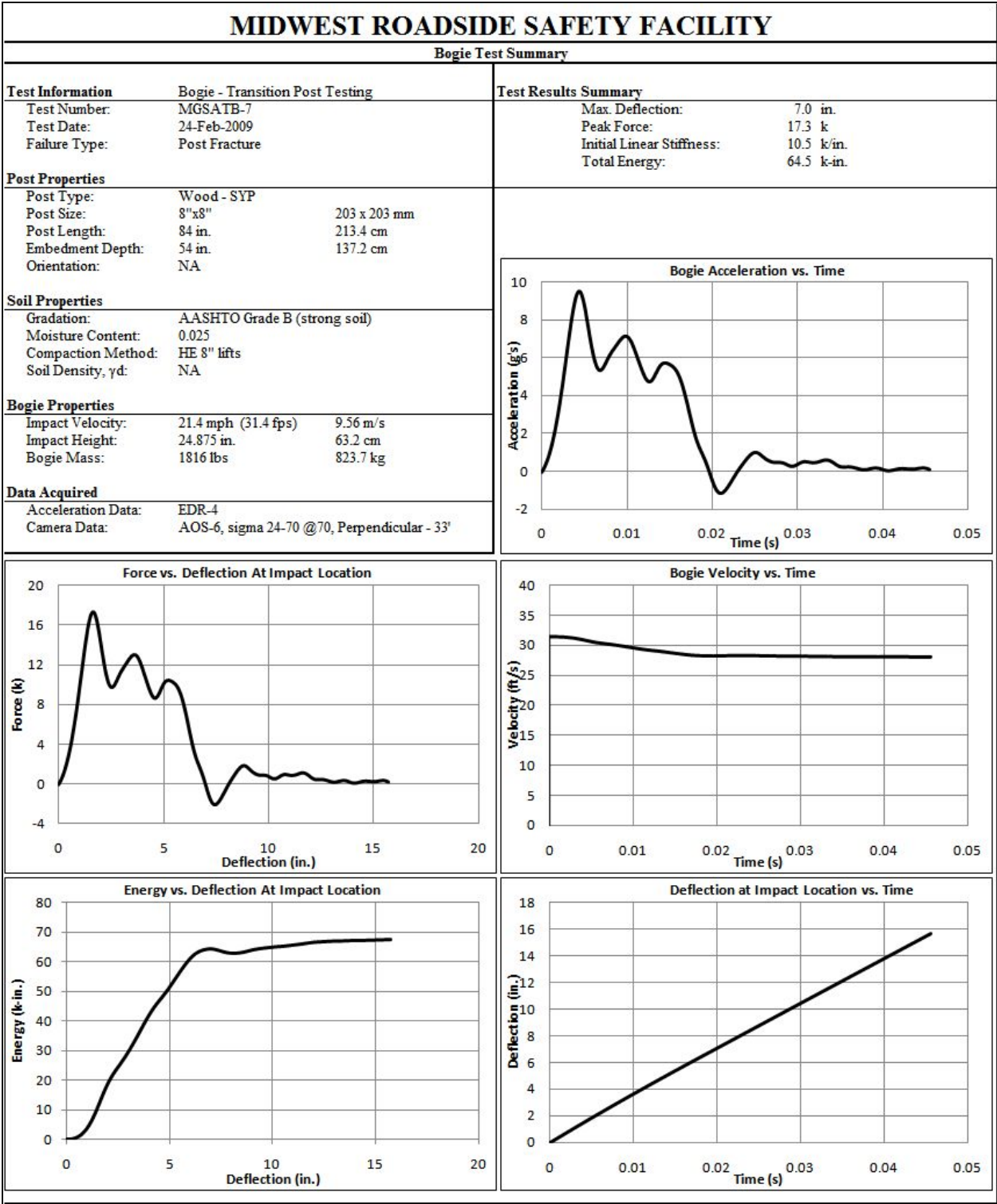


Figure D-15. Results of Test No. MGSATB-7 (EDR-4)

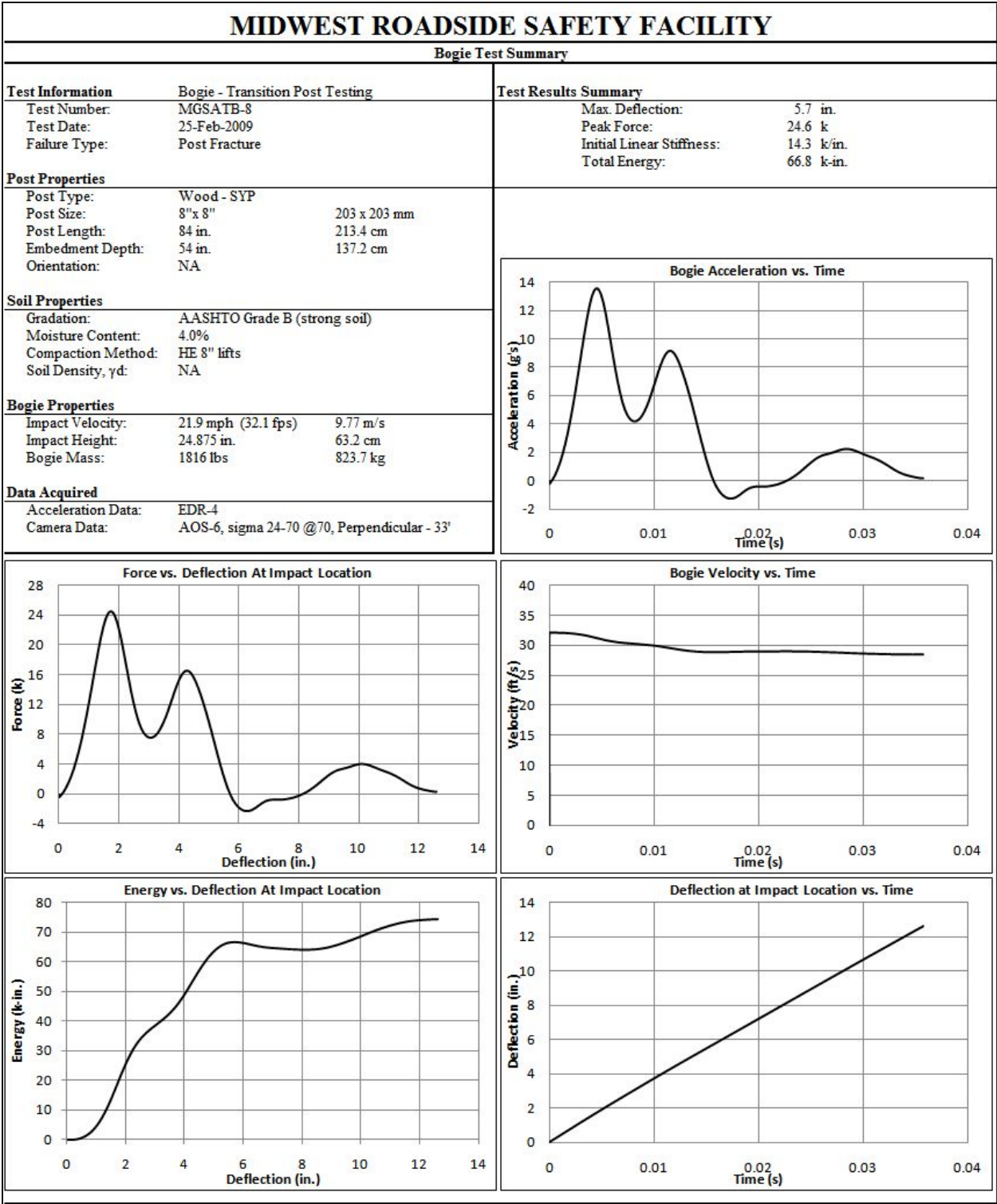


Figure D-16. Results of Test No. MGSATB-8 (EDR-4)

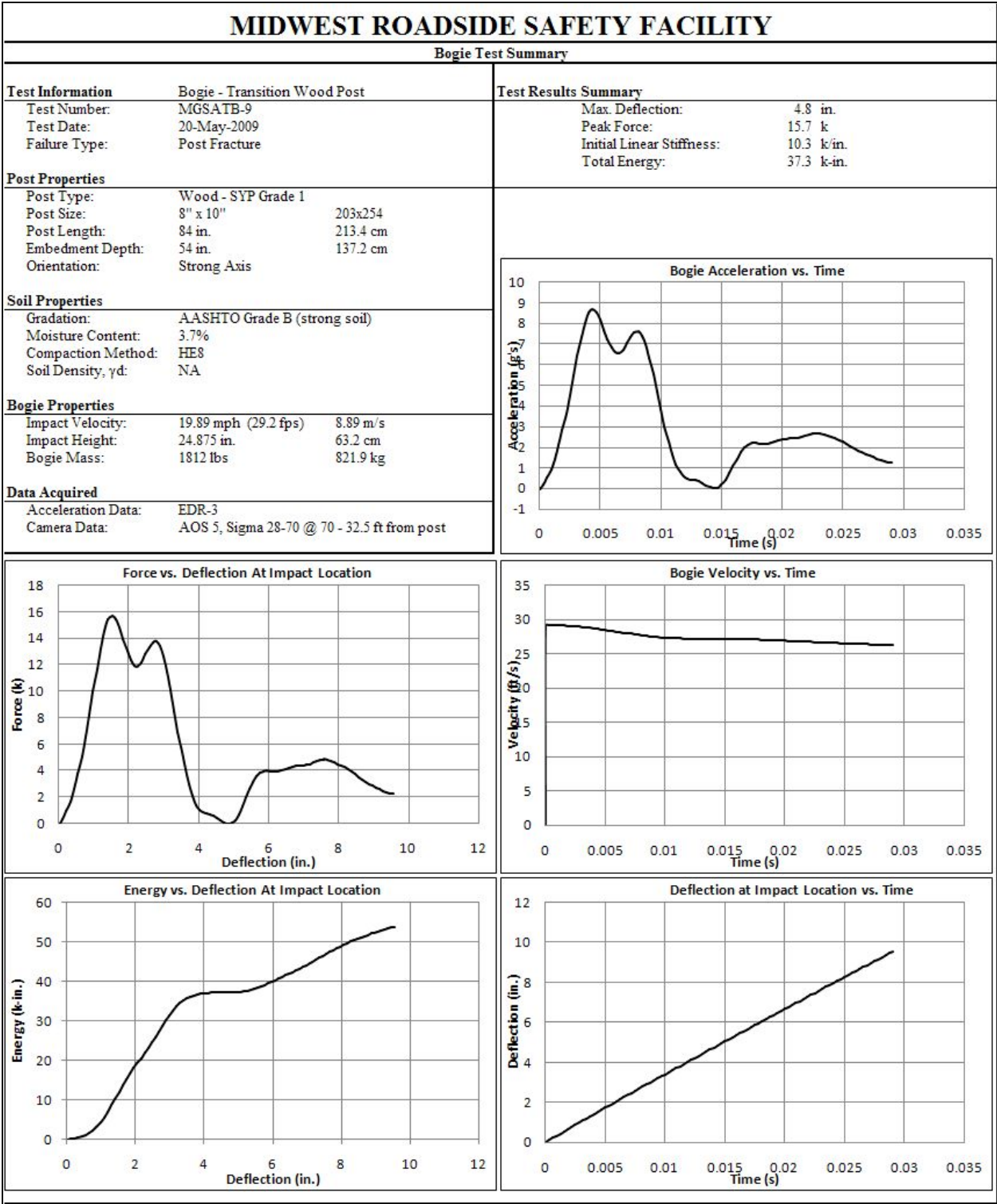


Figure D-17. Results of Test No. MGSATB-9 (EDR-3)

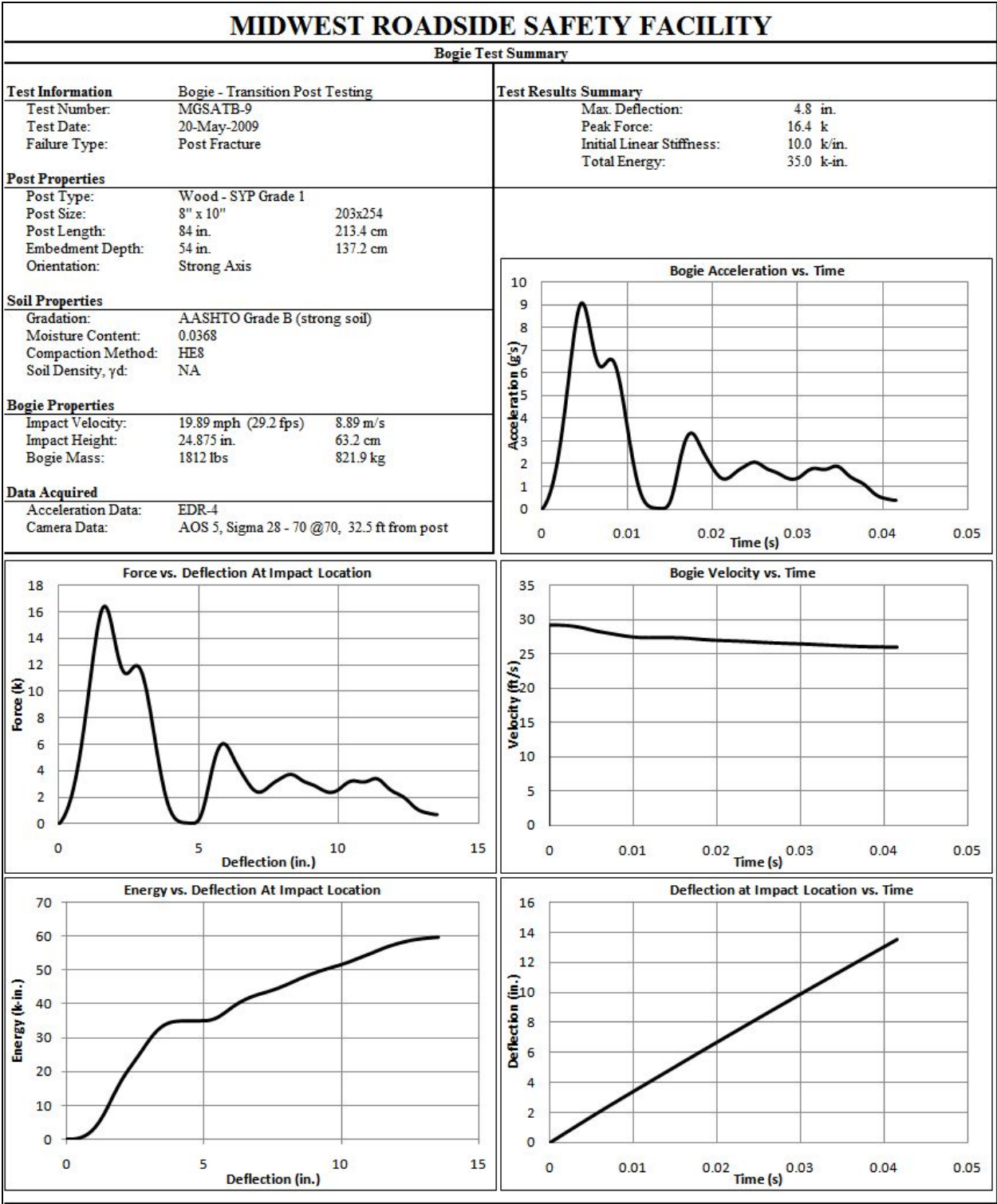


Figure D-18. Results of Test No. MGSATB-9 (EDR-4)

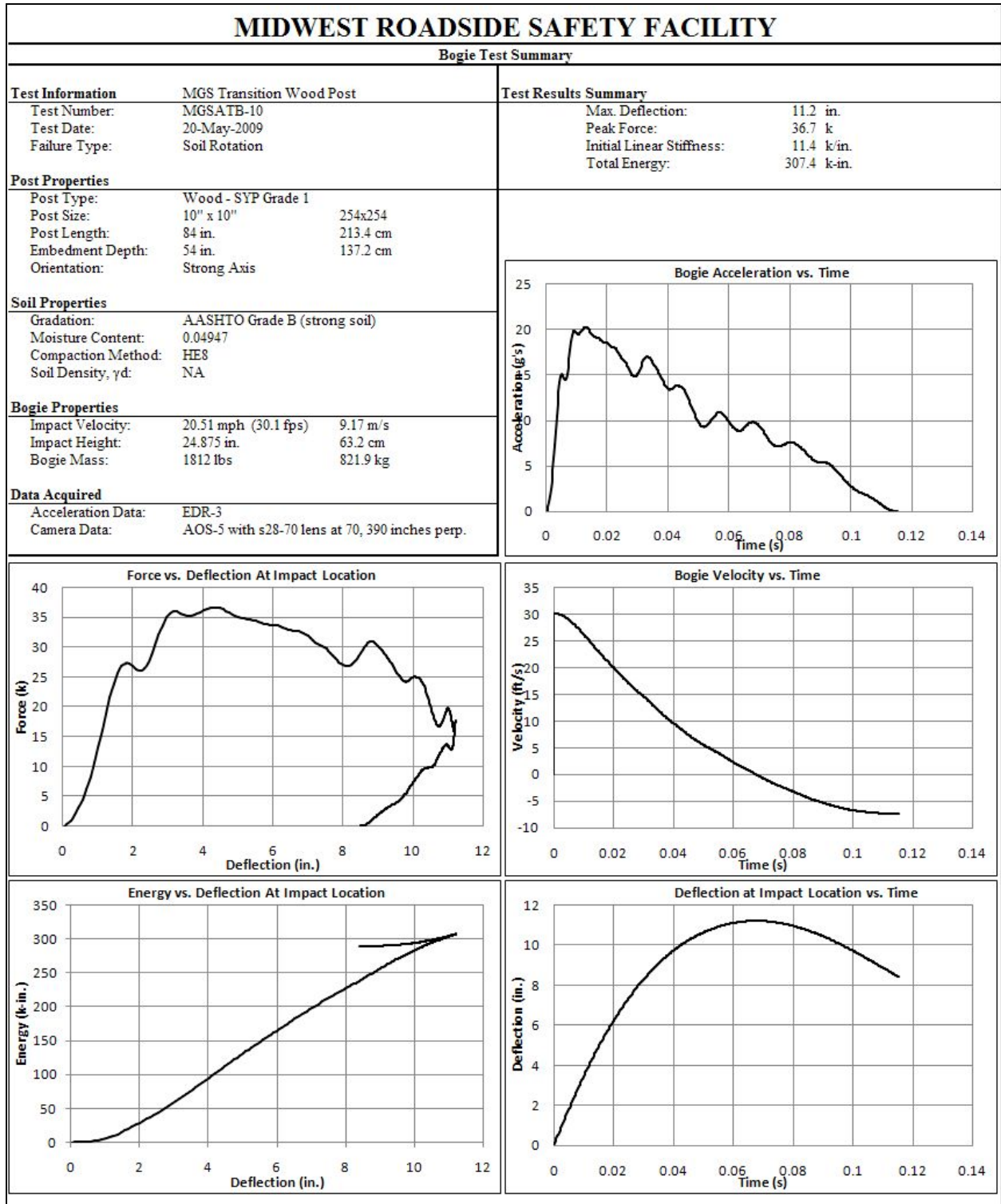


Figure D-19. Results of Test No. MGSATB-10 (EDR-3)

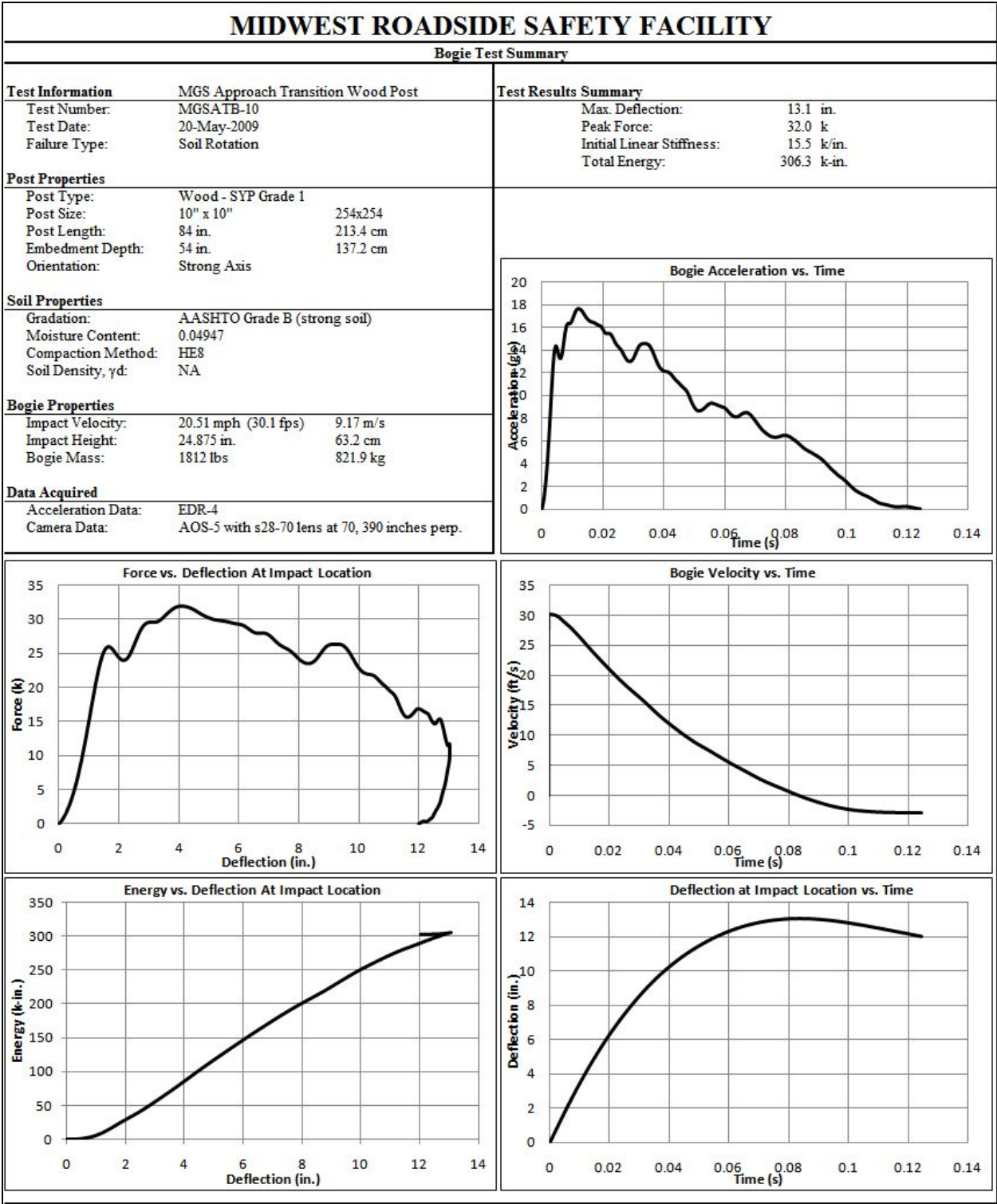


Figure D-20. Results of Test No. MGSATB-10 (EDR-4)

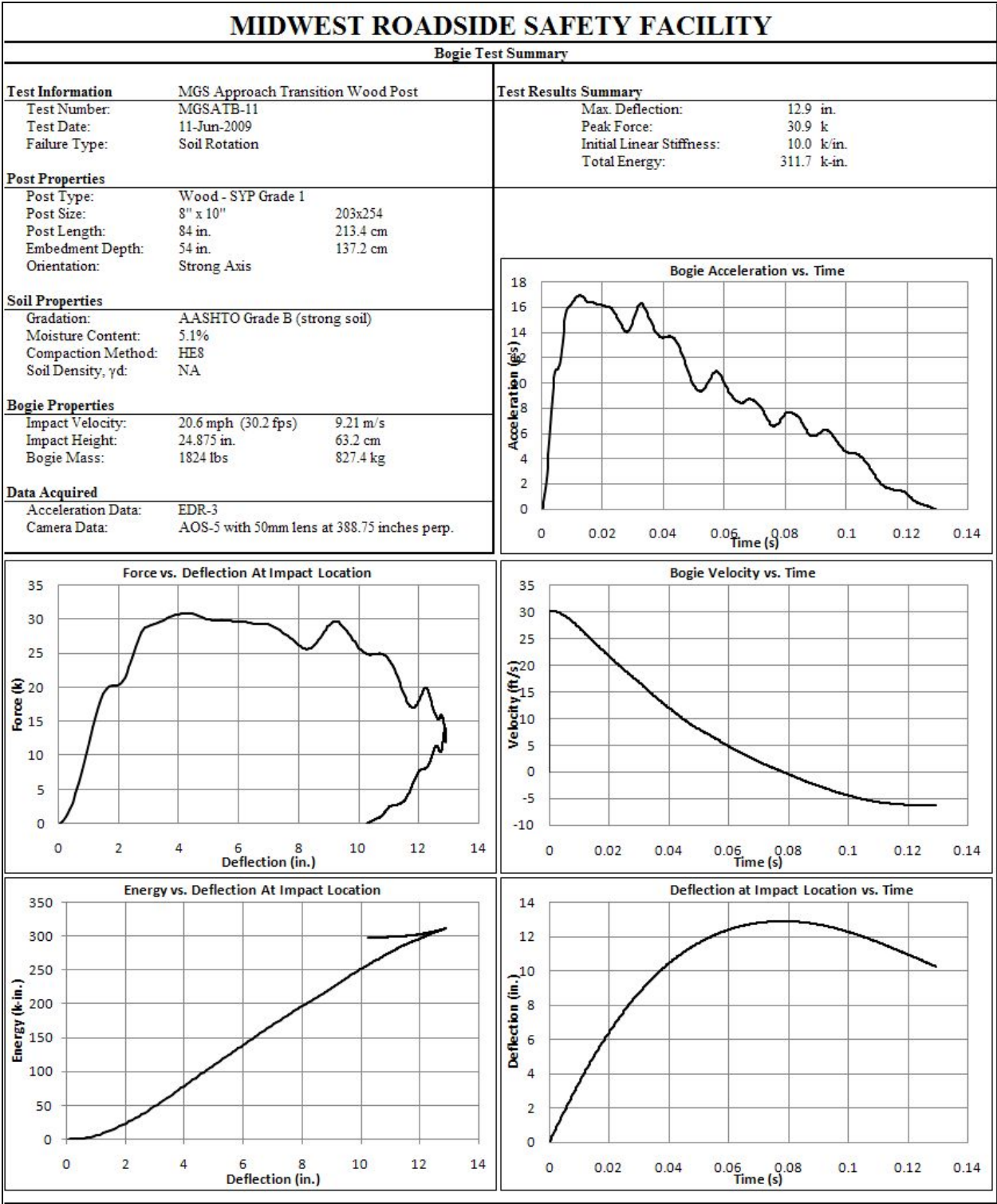


Figure D-21. Results of Test No. MGSATB-11 (EDR-3)

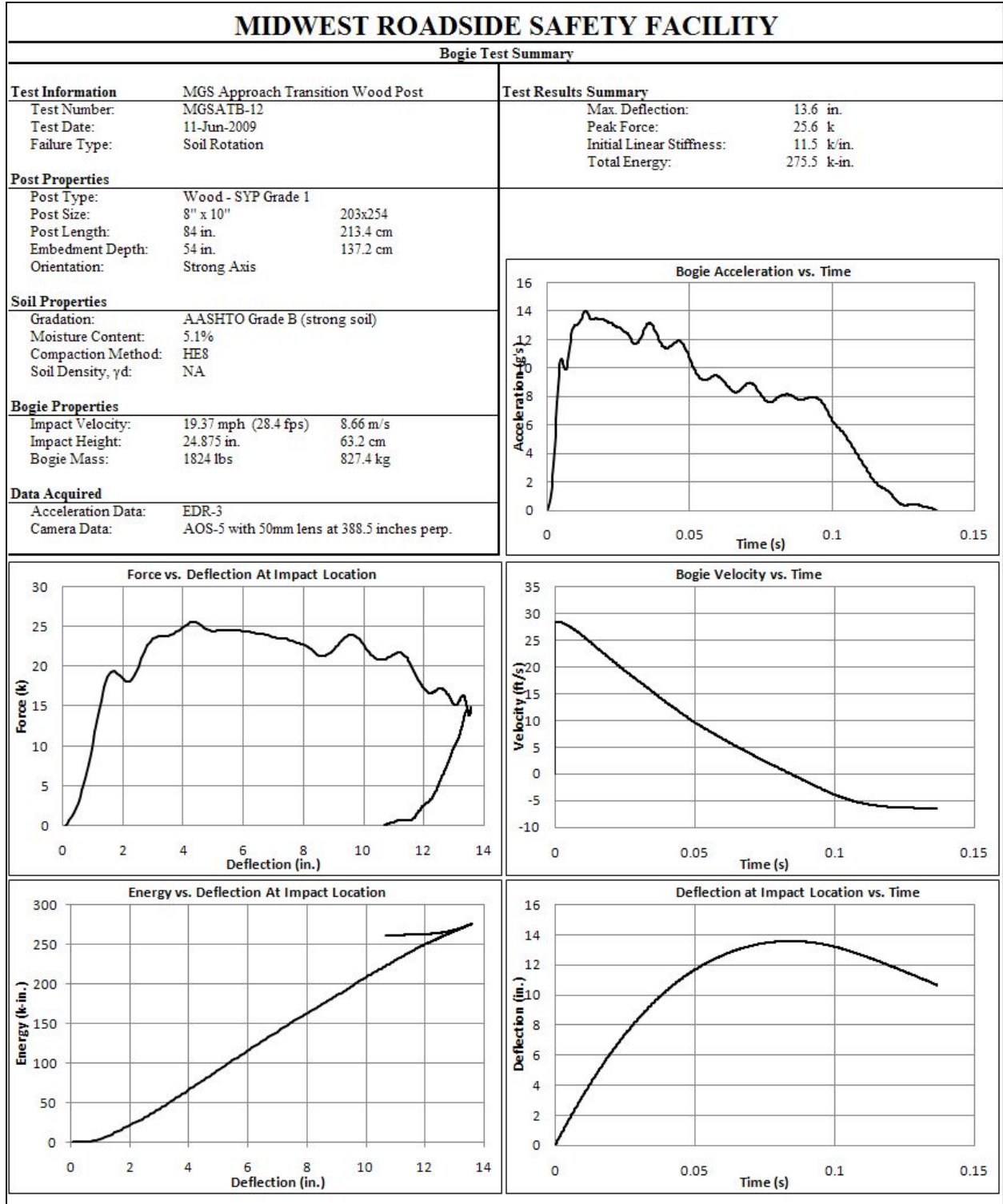


Figure D-22. Results of Test No. MGSATB-12 (EDR-3)

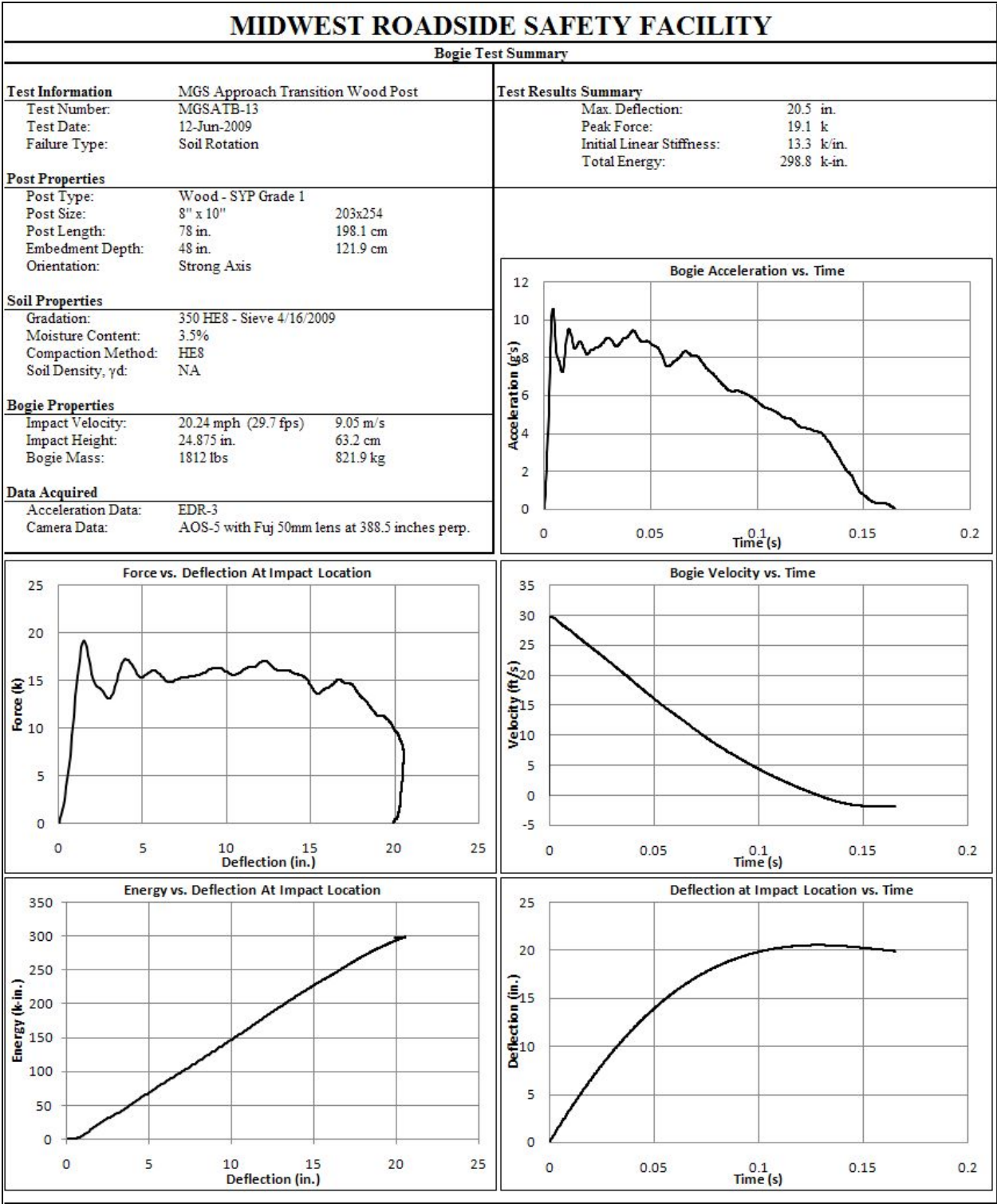


Figure D-23. Results of Test No. MGSATB-13 (EDR-3)

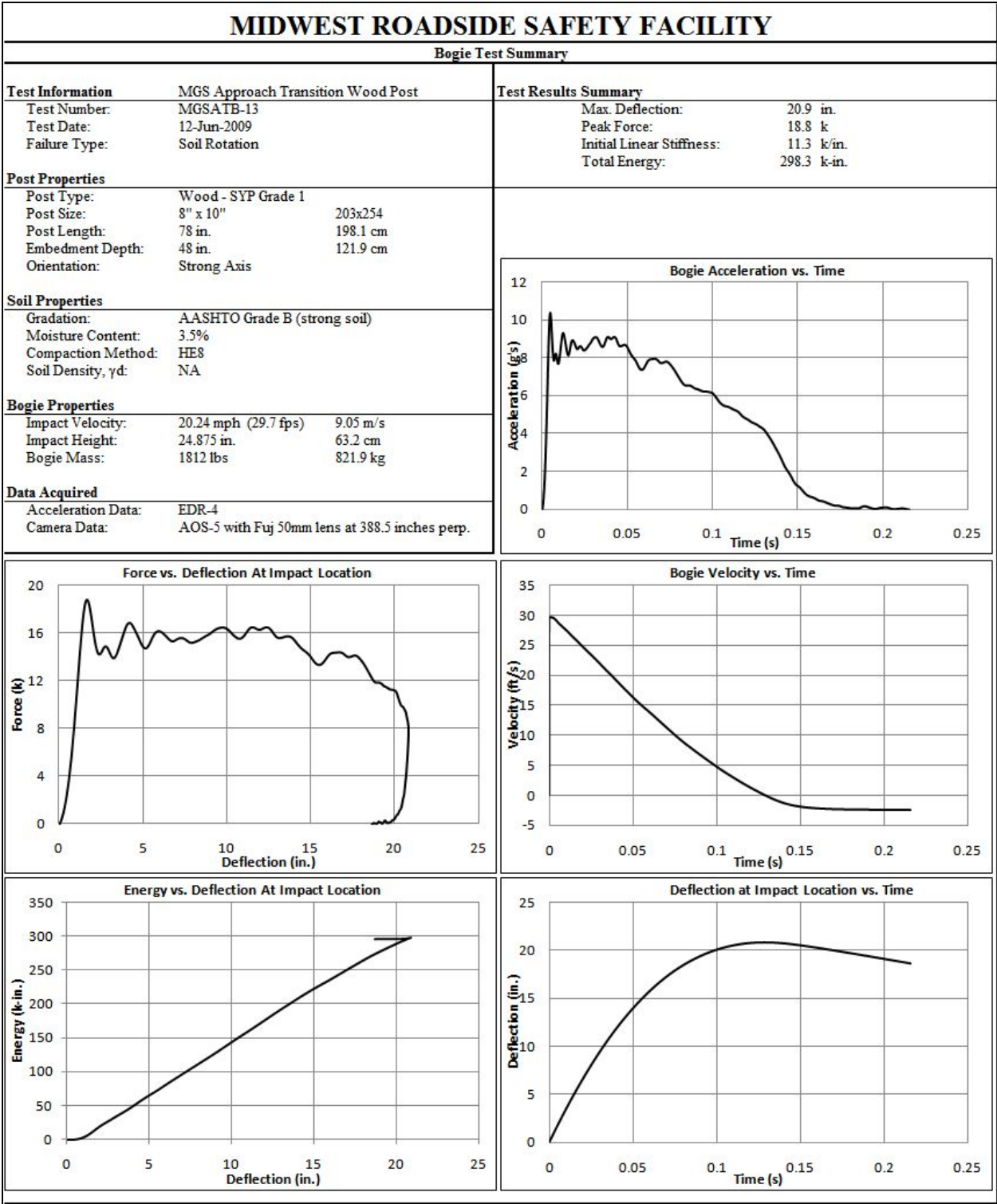


Figure D-24. Results of Test No. MGSATB-13 (EDR-4)

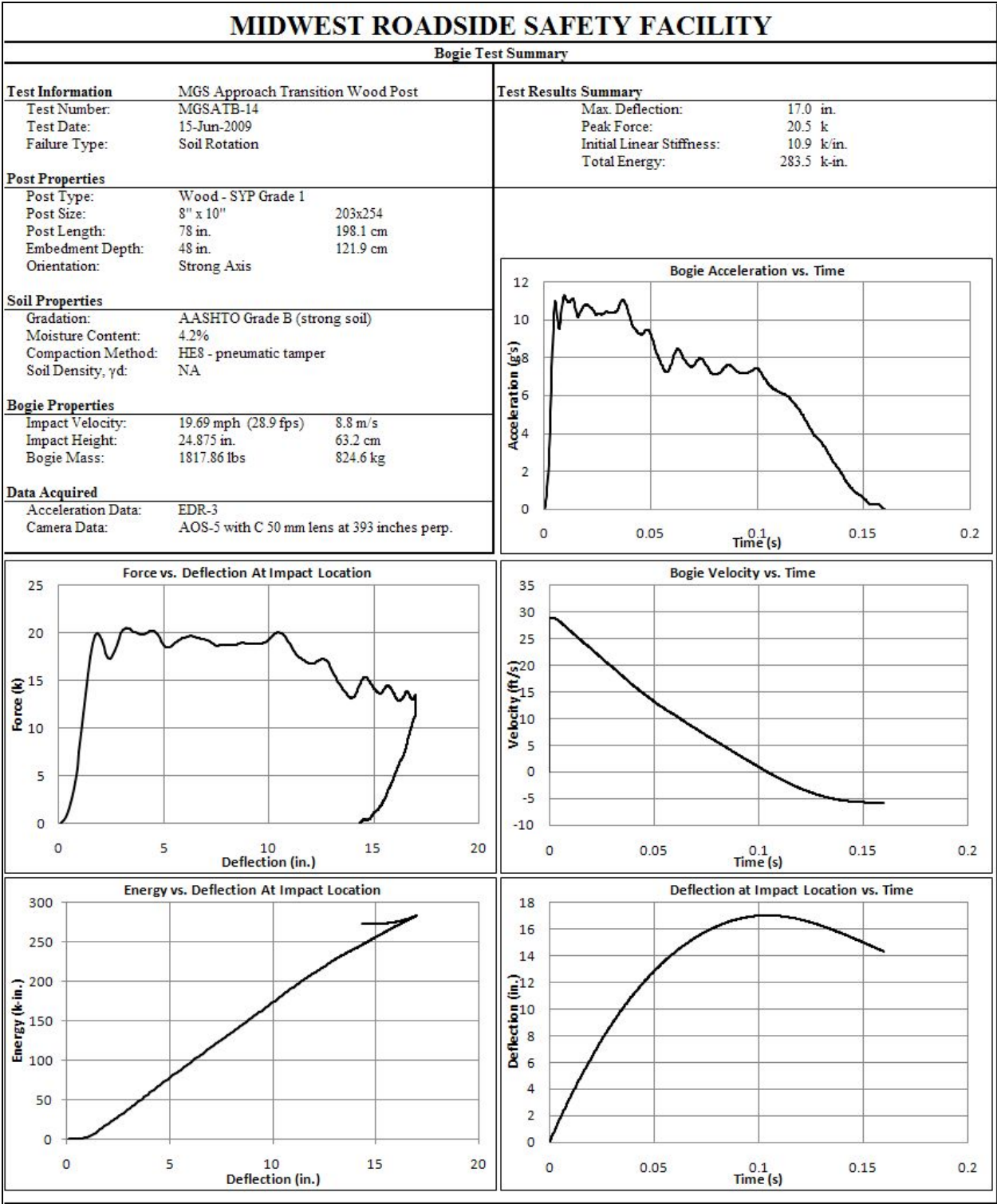


Figure D-25. Results of Test No. MGSATB-14 (EDR-3)

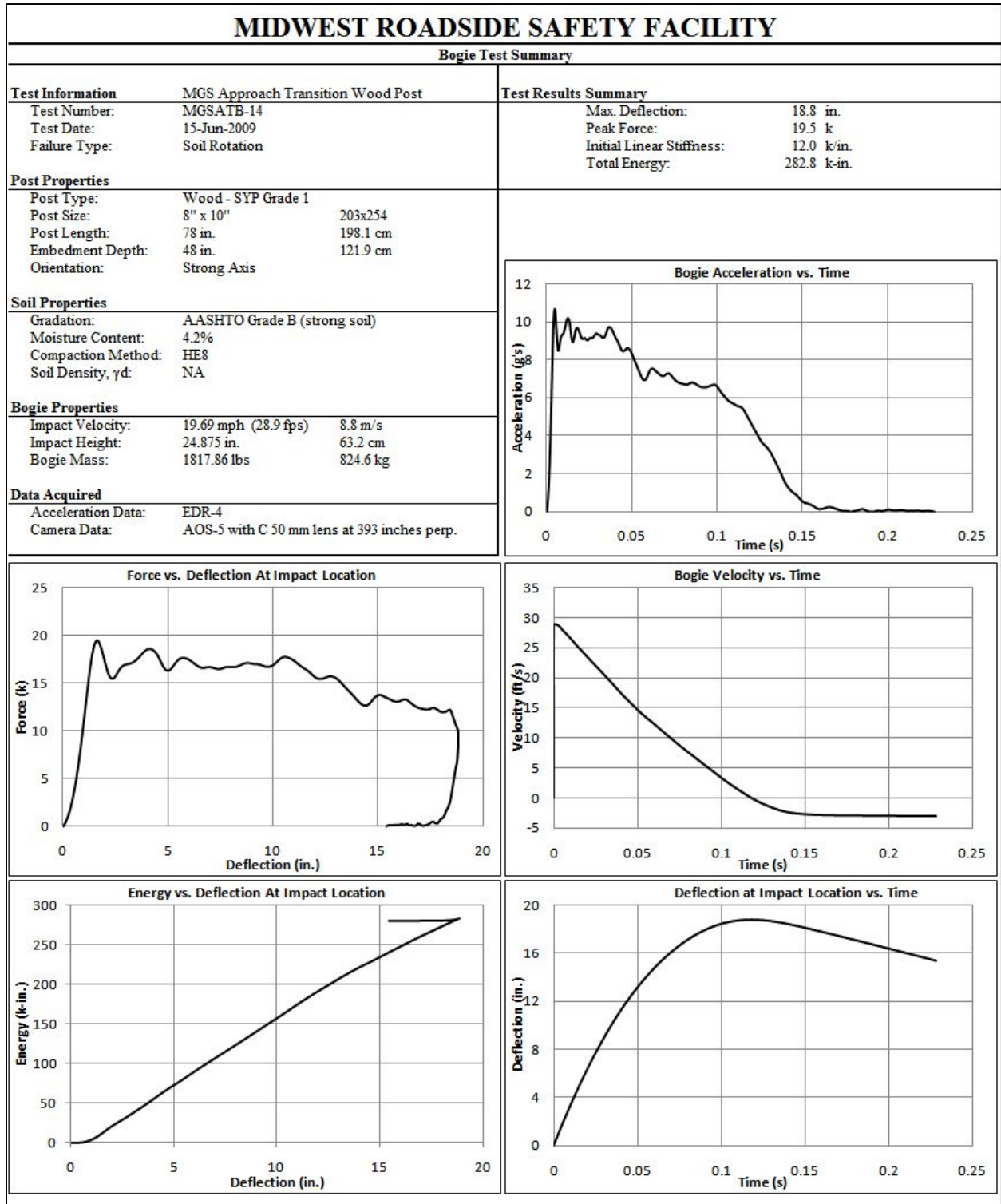


Figure D-26. Results of Test No. MGSATB-14 (EDR-4)

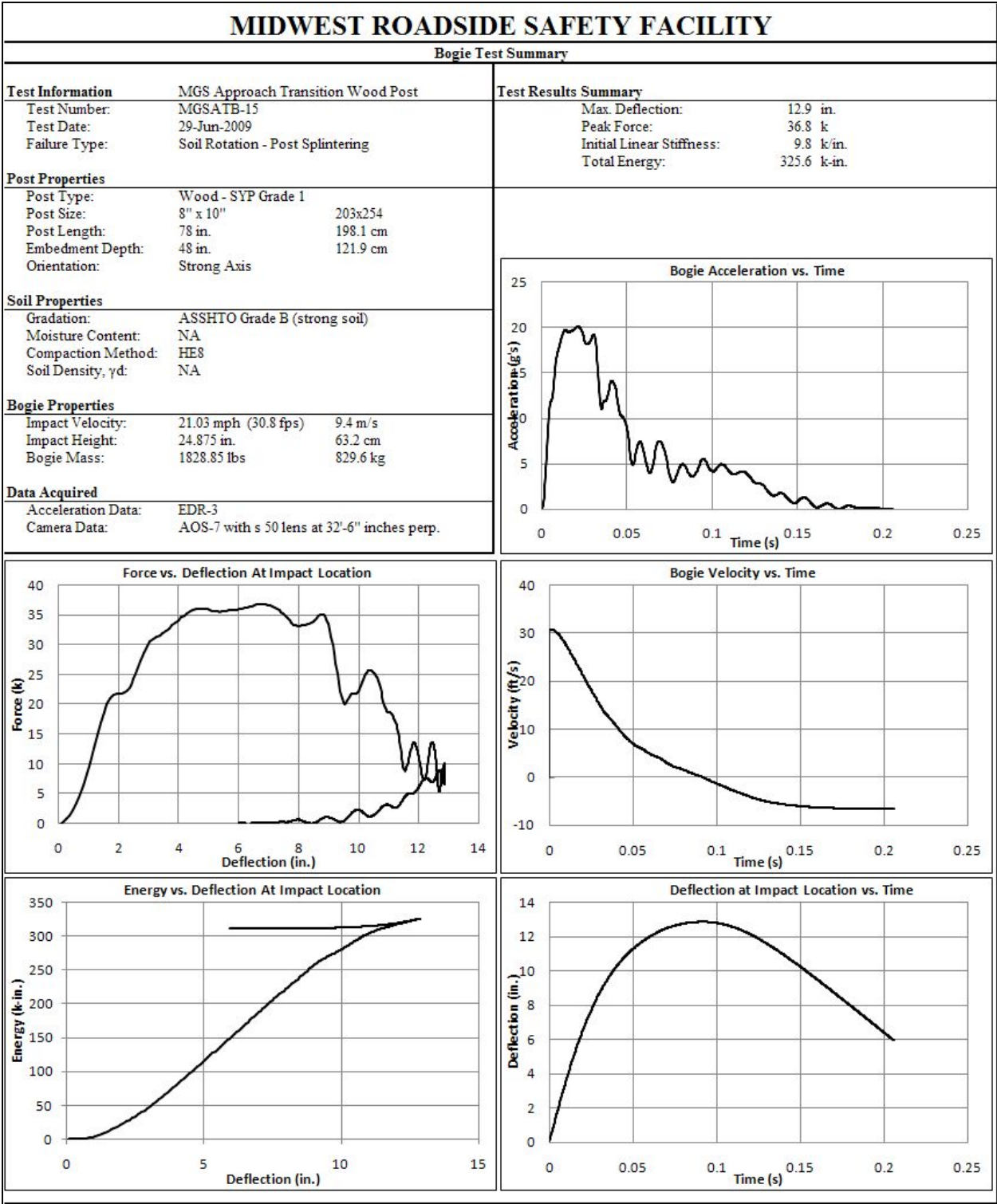


Figure D-27. Results of Test No. MGSATB-15 (EDR-3)

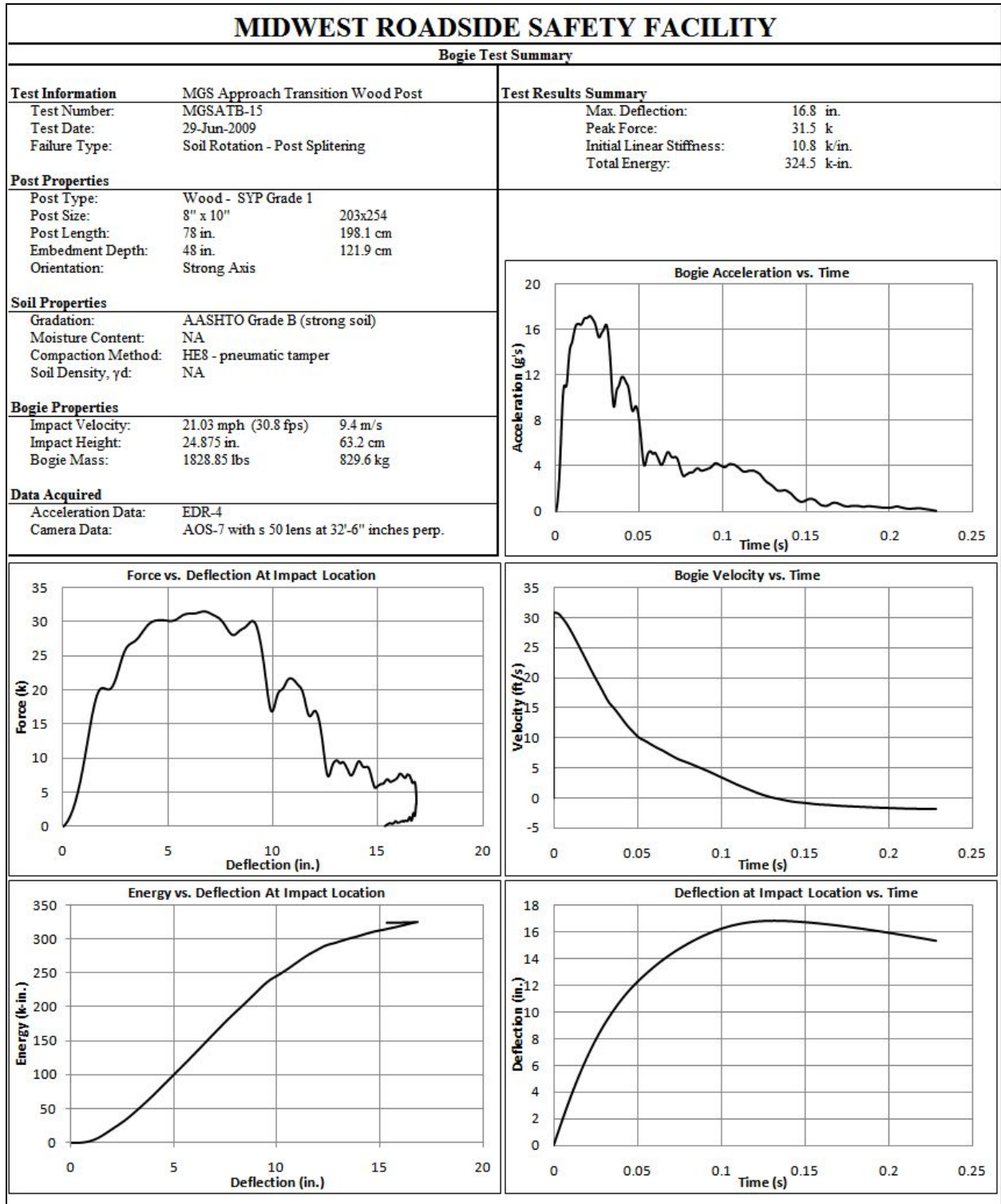


Figure D-28. Results of Test No. MGSATB-15 (EDR-4)

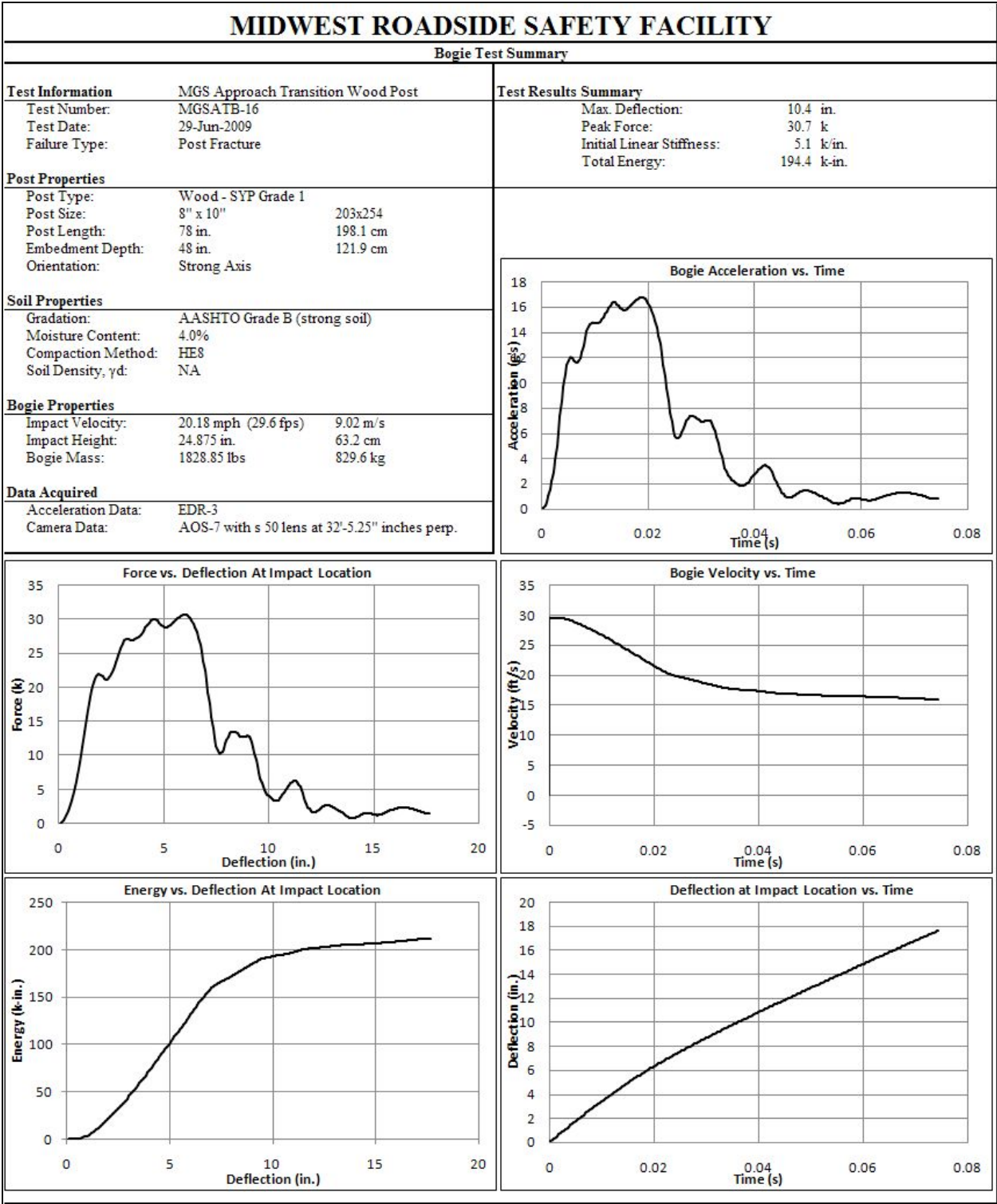


Figure D-29. Results of Test No. MGSATB-16 (EDR-3)

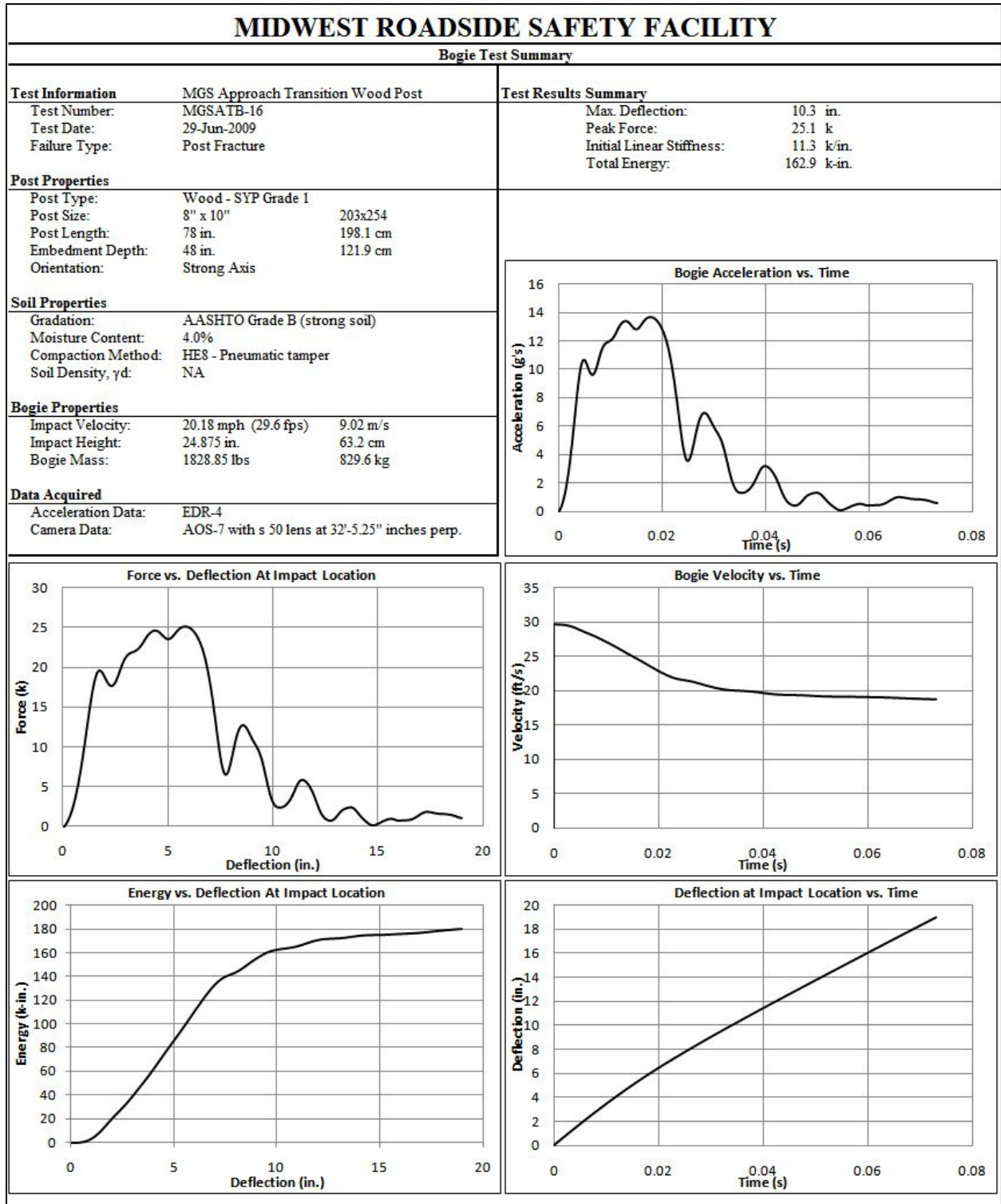


Figure D-30. Results of Test No. MGSATB-16 (EDR-4)

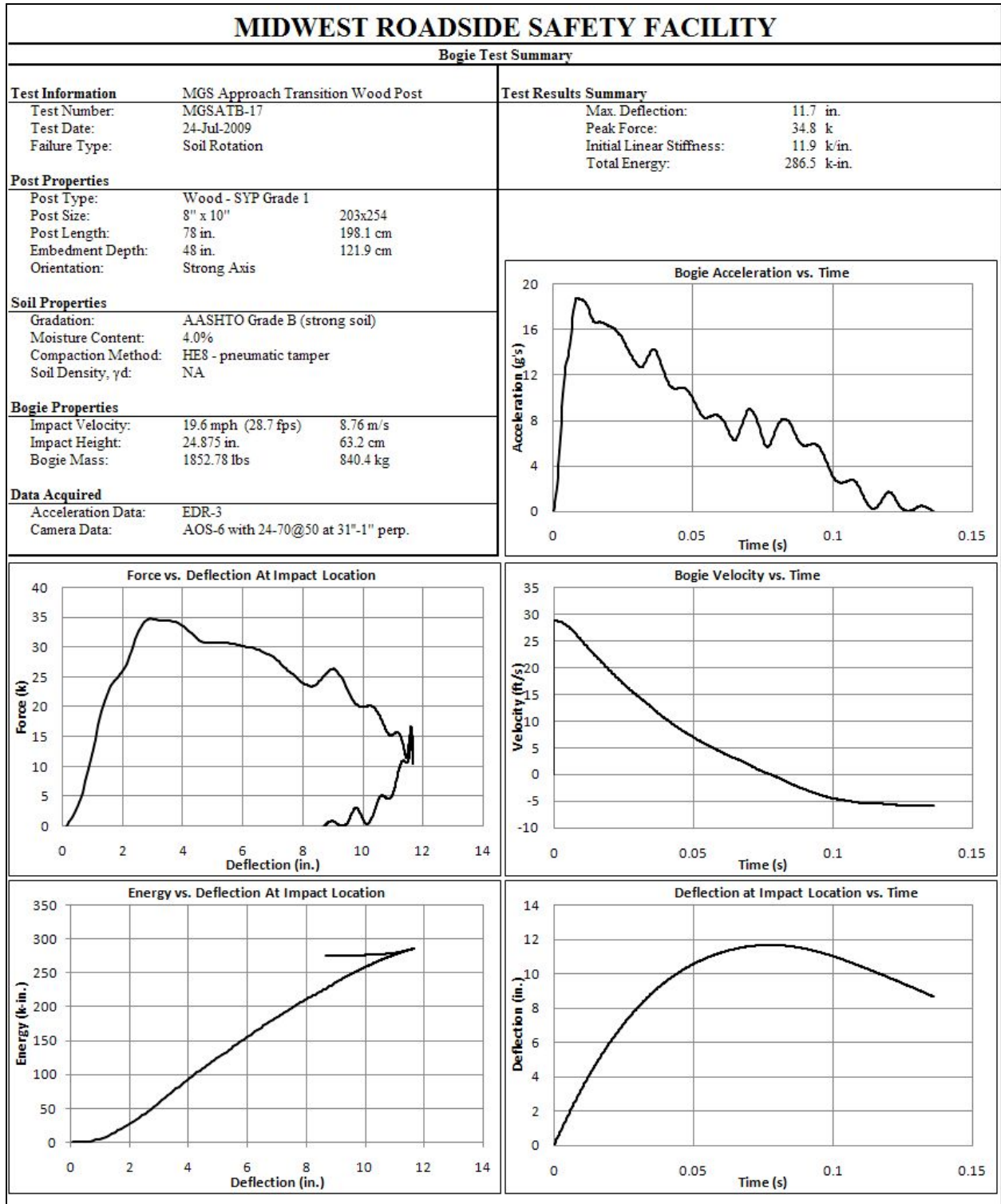


Figure D-31. Results of Test No. MGSATB-17 (EDR-3)

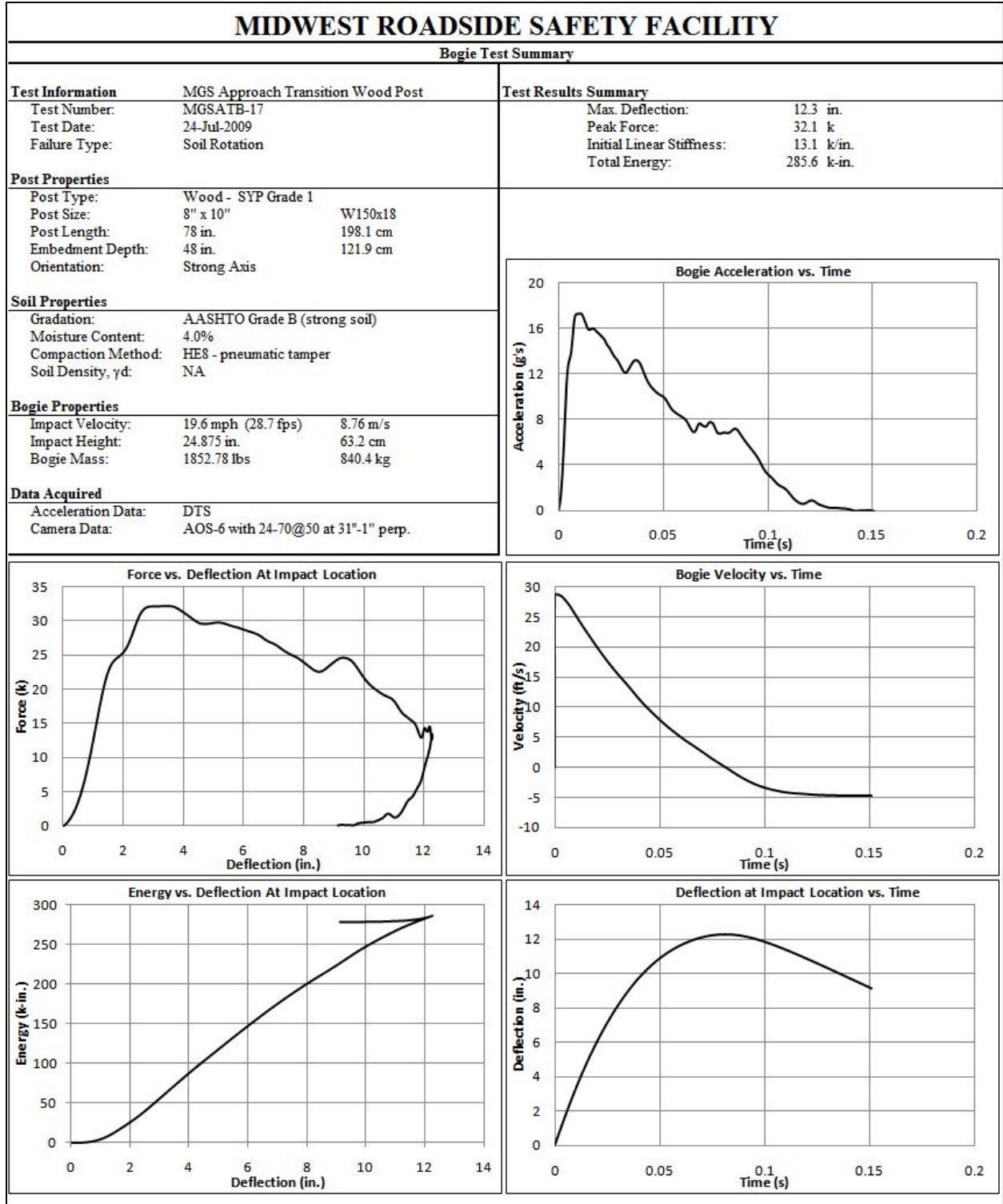


Figure D-32. Results of Test No. MGSATB-17 (DTS)

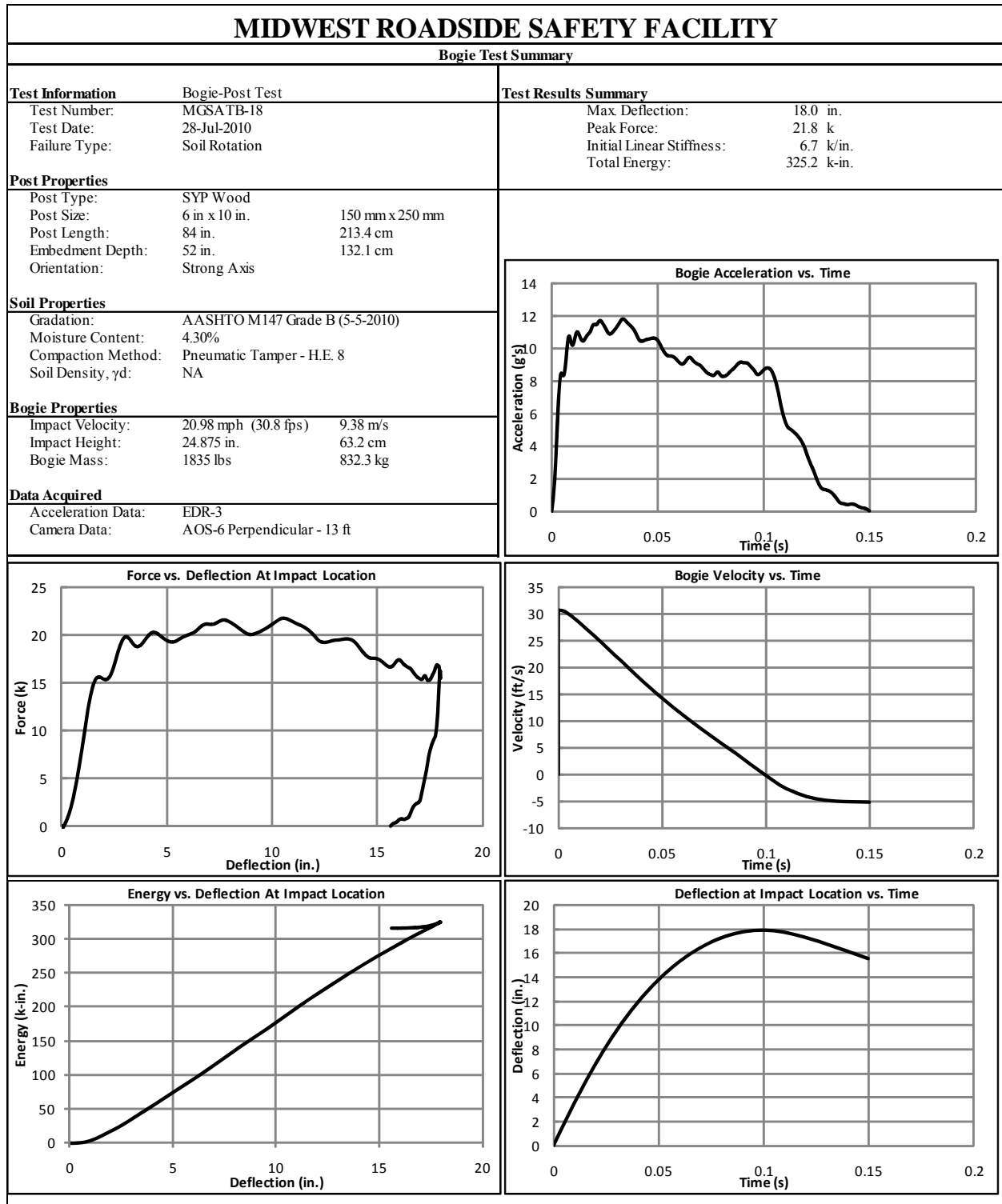


Figure D-33. Results of Test No. MGSATB-18 (EDR-3)

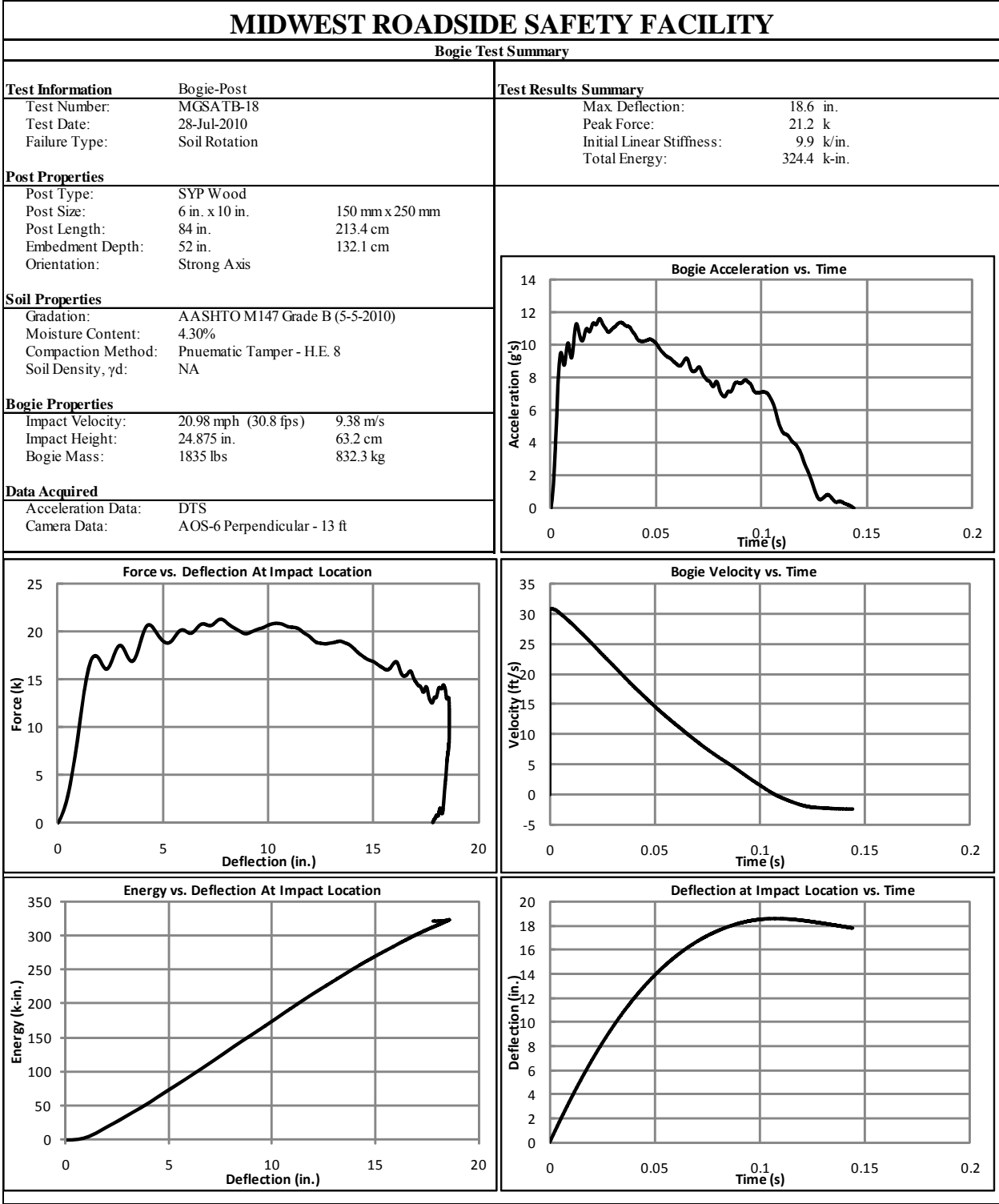


Figure D-34. Results of Test No. MGSATB-18 (DTS)

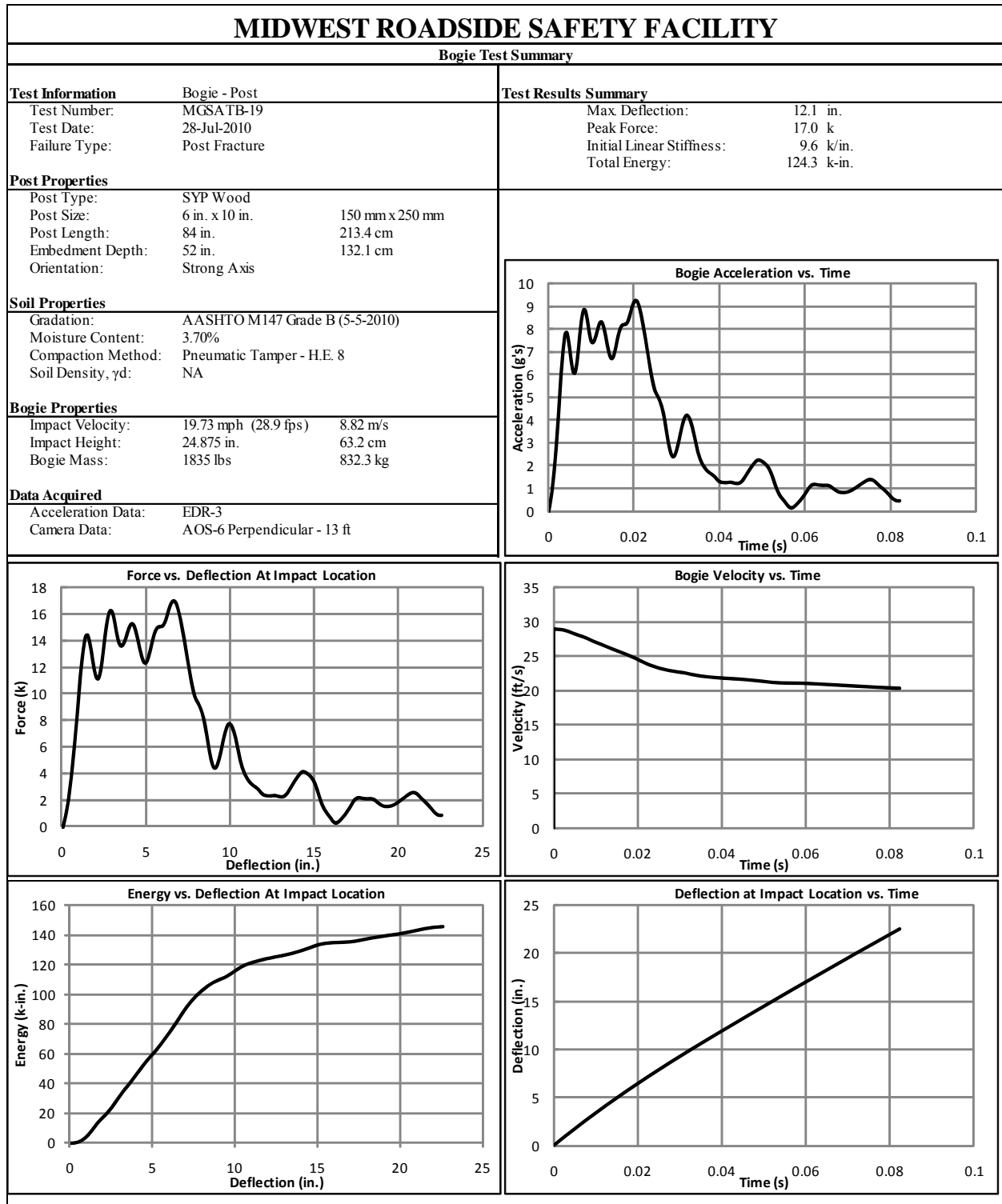


Figure D-35. Results of Test No. MGSATB-19 (EDR-3)

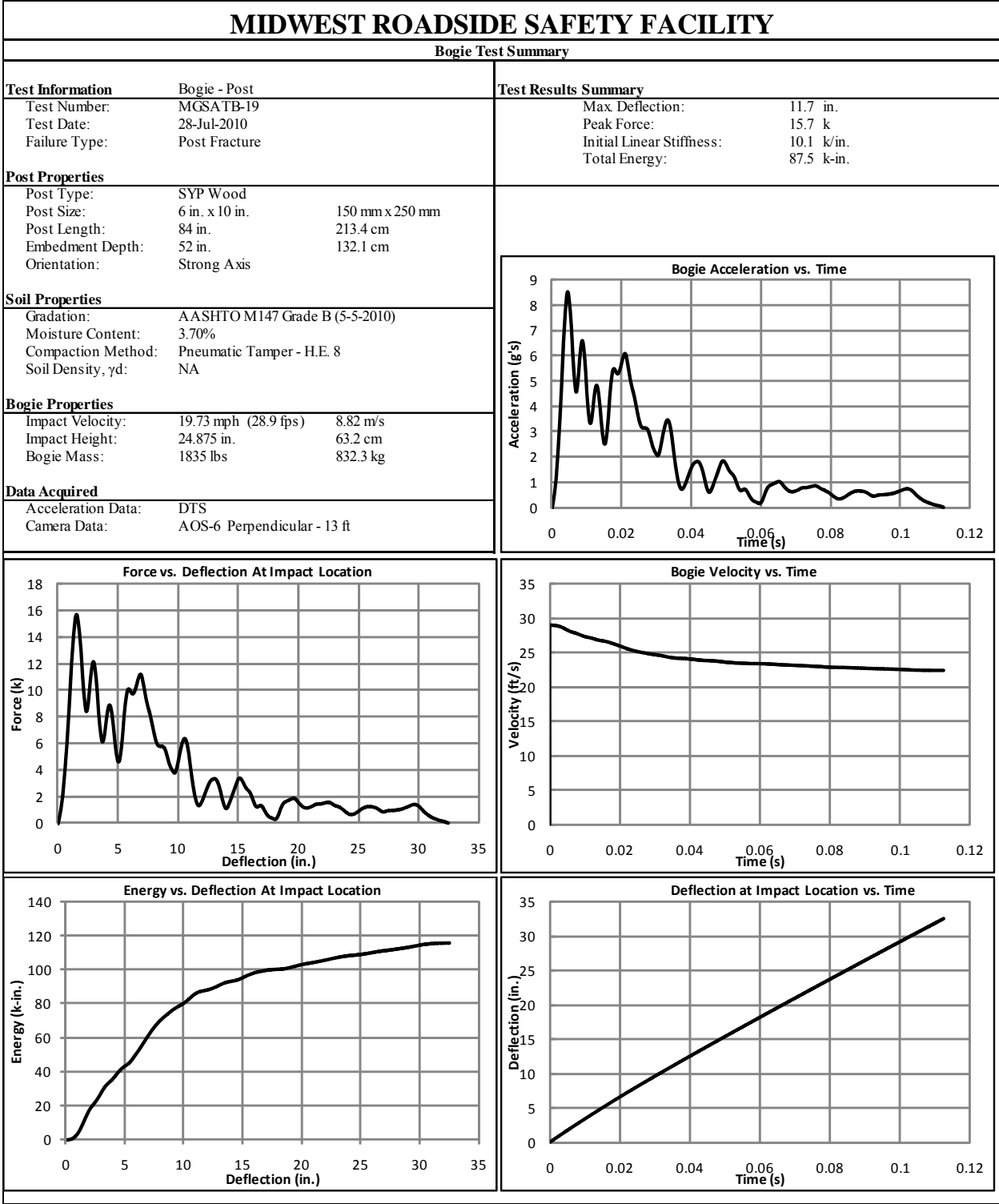


Figure D-36. Results of Test No. MGSATB-19 (DTS)

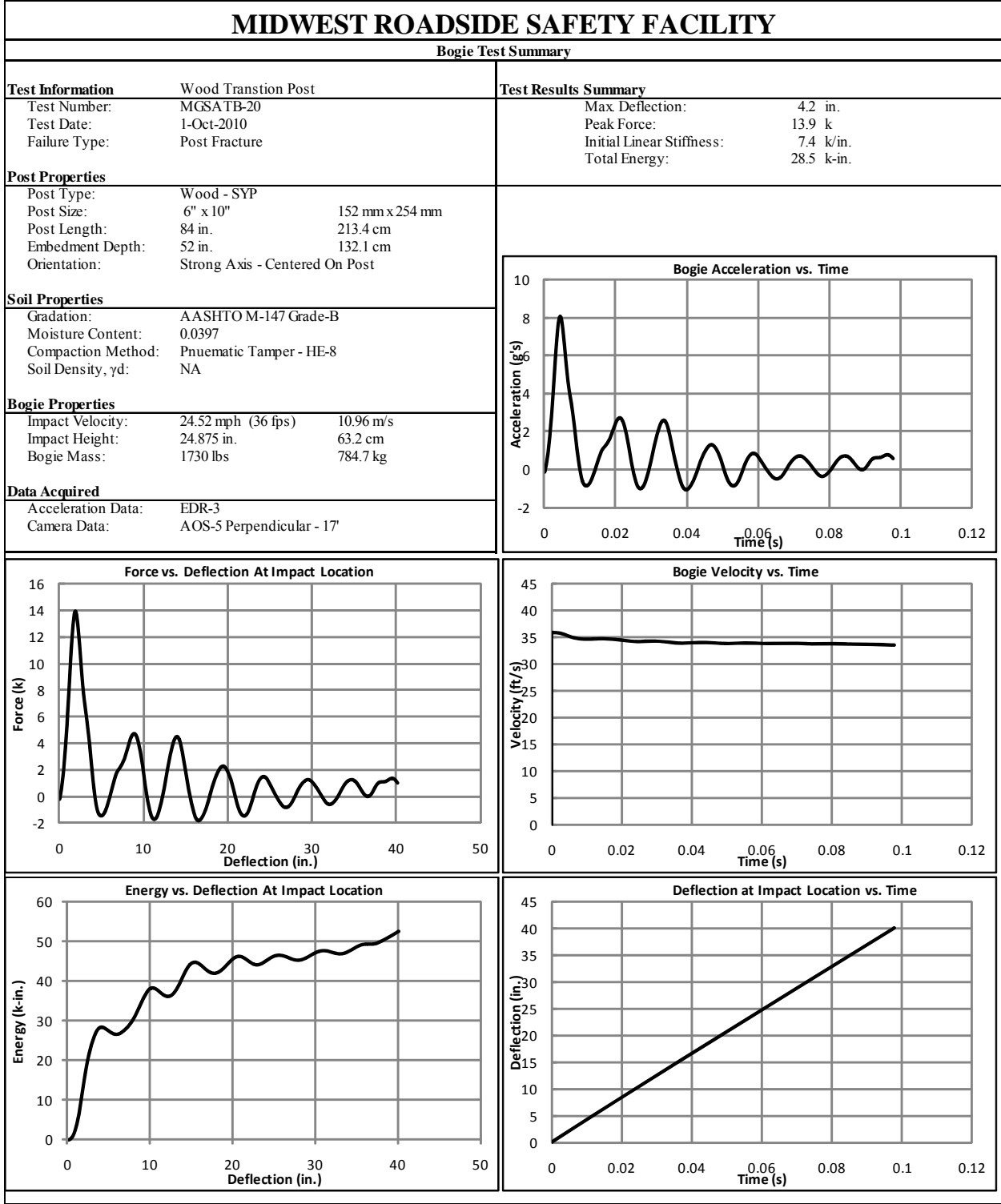


Figure D-37. Results of Test No. MGSATB-20 (EDR-3)

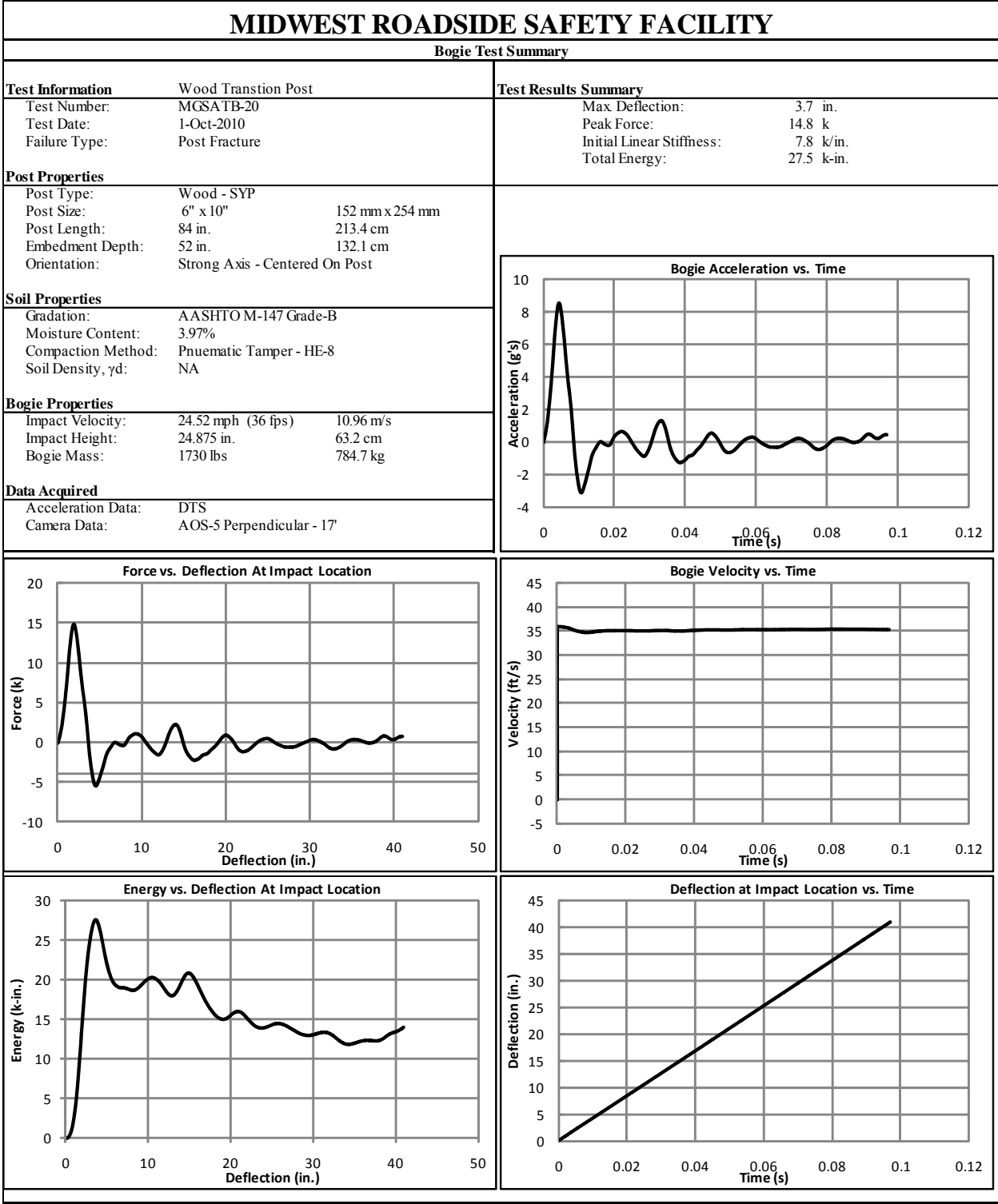


Figure D-38. Results of Test No. MGSATB-20 (DTS)

Appendix E. BARRIER VII Input Decks

The following pages contain a BARRIER VII input data file for both the calibrated steel post model and the wood post model. To aid in visualizing the system, a layout drawing for the stiffness transition was included in this appendix following the sample input decks.

4	24.875	0.0	3.40	5.14	105.0	171.00	384.00	0.05	W6x15 BY 7-FT STEEL POST		
5	15.0	35.0	18.0	18.0	129.0	200.0	612.5	362.90	804.60	0.05	W6x20 STEEL BRIDGE POST
1	20.0	45.0	6.0	6.0							
101	1	2	101								
101	101	102	1	103		0.0	0.0	0.0			
102	102	103	1	104		0.0	0.0	0.0			
103	103	104	1	105		0.0	0.0	0.0			
104	104	105	1	106		0.0	0.0	0.0			
105	105	106	1	107		0.0	0.0	0.0			
106	106	107	1	108		0.0	0.0	0.0			
107	107	108	1	109		0.0	0.0	0.0			
108	108	109	1	110		0.0	0.0	0.0			
109	109	110	1	111		0.0	0.0	0.0			
117	117	118	1	112		0.0	0.0	0.0			
133	133	134	1	111		0.0	0.0	0.0			
149	149	150	1	102		0.0	0.0	0.0			
165	1			301		0.0	0.0	0.0	0.0	0.0	
166	9			302		0.0	0.0	0.0	0.0	0.0	
167	17	176	8	303		0.0	0.0	0.0	0.0	0.0	
177	97	180	4	303		0.0	0.0	0.0	0.0	0.0	
181	113	184	2	303		0.0	0.0	0.0	0.0	0.0	
185	121	187	4	304		0.0	0.0	0.0	0.0	0.0	
188	133	190	8	305		0.0	0.0	0.0	0.0	0.0	
	5000.0	58310.0	20	6	4	0	25				
1		0.055	0.12	6.00		17.0					
2		0.057	0.15	7.00		18.0					
3		0.062	0.18	10.00		12.0					
4		0.110	0.35	12.00		6.0					
5		0.35	0.45	6.00		5.0					
6		1.45	1.50	15.00		1.0					
1	102.50	15.875	1	12.0	1	1	0	0			
2	102.50	27.875	1	12.0	1	1	0	0			
3	102.50	39.000	2	12.0	1	1	0	0			
4	88.75	39.000	2	12.0	1	1	0	0			
5	76.75	39.000	2	12.0	1	1	0	0			
6	64.75	39.000	2	12.0	1	1	0	0			
7	52.75	39.000	2	12.0	1	1	0	0			
8	40.75	39.000	2	12.0	1	1	0	0			
9	28.75	39.000	2	12.0	1	1	0	0			
10	16.75	39.000	2	12.0	1	1	0	0			
11	-13.25	39.000	3	12.0	1	1	0	0			
12	-33.25	39.000	3	12.0	1	1	0	0			
13	-53.25	39.000	3	12.0	1	1	0	0			
14	-73.25	39.000	3	12.0	1	1	0	0			
15	-93.25	39.000	3	12.0	1	1	0	0			

16	-125.35	39.000	4	12.0	1	1	0	0
17	-125.35	-39.000	4	12.0	0	0	0	0
18	102.50	-39.000	1	12.0	0	0	0	0
19	62.40	33.90	5	1.0	1	1	0	0
20	-77.85	33.90	6	1.0	1	1	0	0
1	62.40	33.90		0.0	608.			
2	62.40	-33.90		0.0	608.			
3	-77.85	33.90		0.0	492.			
4	-77.85	-33.90		0.0	492.			
1	102.50	39.00						
2	-125.35	39.00						
3	-125.35	-39.00						
4	102.50	-39.00						
5	5.00	2.50						
6	5.00	-2.50						
7	-5.00	-2.50						
8	-5.00	2.50						
9	78.03	39.12						
10	78.03	28.69						
11	46.78	28.69						
12	46.78	39.12						
13	78.03	-28.69						
14	78.03	-39.12						
15	46.78	-39.12						
16	46.78	-28.69						
17	-62.22	39.12						
18	-62.22	28.69						
19	-93.47	28.69						
20	-93.47	39.12						
21	-62.22	-28.69						
22	-62.22	-39.12						
23	-93.47	-39.12						
24	-93.47	-28.69						
25	0.00	0.00						
3	750.000	0.0	25.00	62.14	0.0	0.0	1.0	

EQUIVALENT WOOD POST MODEL INPUT FILE

MGS Approach Transition - Wood Posts: No Fracture

165	2	1	1	190	20	2	0														
0.0001		0.0001		0.750	3000	0		1.0	1												
10	10	50	50	10	500	10															
1		0.00		0.0																	
165	1537.50			0.0																	
1	165	163	1		0.0																
1	165		0.23																		
165	164	163	162	161	160	159	158	157	156												
155	154	153	152	151	150	149	148	147	146												
145	144	143	142	141	140	139	138	137	136												
135	134	133	132	131	130	129	128	127	126												
125	124	123	122	121	120	119	118	117	116												
115	114	113	112	111	110	109	108	107	106												
105	104	103	102	101	100	99	98	97	96												
95	94	93	92	91	90	89	88	87	86												
85	84	83	82	81	80	79	78	77	76												
75	74	73	72	71	70	69	68	67	66												
65	64	63	62	61	60	59	58	57	56												
55	54	53	52	51	50	49	48	47	46												
45	44	43	42	41	40	39	38	37	36												
35	34	33	32	31	30	29	28	27	26												
25	24	23	22	21	20	19	18	17	16												
15	14	13	12	11	10	9	8	7	6												
5	4	3	2	1																	
100	12																				
1		2.29		1.99		9.375	30000.0	6.92	99.5	68.5	0.05									12-GAUGE W-BEAM	
2		1.00		1.00		9.375	30000.0	1.000	1.000	1.000	0.05									END SECTION - NOTHING	
3		3.114		2.650		9.375	30000.0	9.216	132.5	91.25	0.05									10-GAUGE W-TO-THRI E BEAM	
4		3.341		2.830		9.375	30000.0	9.847	141.5	97.75	0.05									10-GAUGE W-TO-THRI E BEAM	
5		3.569		3.010		9.375	30000.0	10.478	150.5	104.25	0.05									10-GAUGE W-TO-THRI E BEAM	
6		3.796		3.190		9.375	30000.0	11.109	159.5	110.75	0.05									10-GAUGE W-TO-THRI E BEAM	
7		4.024		3.370		9.375	30000.0	11.741	168.5	117.25	0.05									10-GAUGE W-TO-THRI E BEAM	
8		4.251		3.550		9.375	30000.0	12.372	177.5	123.75	0.05									10-GAUGE W-TO-THRI E BEAM	
9		4.479		3.730		9.375	30000.0	13.003	186.5	130.25	0.05									10-GAUGE W-TO-THRI E BEAM	
10		4.706		3.910		9.375	30000.0	13.634	195.5	136.75	0.05									10-GAUGE W-TO-THRI E BEAM	
11		3.76		3.10		9.375	30000.0	10.81	155.0	109.5	0.05									12-GAUGE THRI E BEAM	
12		7.52		6.20		9.375	30000.0	21.62	310.0	219.0	0.05									12-GAUGE NESTD THRI E BEAM	
300	6																				
1		24.875		0.00		6.0	6.0	100.0	675.0	675.0	0.05										Sim. Strong Anchor Post
	100.0		100.0		15.0		15.0														
2		24.875		0.00		3.0	3.0	100.0	150.0	225.00	0.05										Second BCT Post
	50.0		50.0		15.0		15.0														
3		24.875		0.0		4.0	7.50	54.0	331.00	270.00	0.05										6"x8" BY 6-FT WOOD POST
	15.0		15.0		15.0		15.0														

150

4	24.875	0.0	15.0	12.0	105.0	555.00	440.00	0.05	8"x10" BY 6.5' WOOD POST
5	35.0	35.0	18.0	18.0	129.0	200.0	612.5	362.90	804.60 0.05
6	24.875	0.0	4.0	7.50	54.0	130.00	270.00	0.05	6"x8" WOOD POST (U. S.)
1	1	2	100	1	101	0.0	0.0	0.0	
101	101	102	1	103	0.0	0.0	0.0	0.0	
102	102	103	1	104	0.0	0.0	0.0	0.0	
103	103	104	1	105	0.0	0.0	0.0	0.0	
104	104	105	1	106	0.0	0.0	0.0	0.0	
105	105	106	1	107	0.0	0.0	0.0	0.0	
106	106	107	1	108	0.0	0.0	0.0	0.0	
107	107	108	1	109	0.0	0.0	0.0	0.0	
108	108	109	1	110	0.0	0.0	0.0	0.0	
109	109	110	116	1	111	0.0	0.0	0.0	
117	117	118	132	1	112	0.0	0.0	0.0	
133	133	134	148	1	111	0.0	0.0	0.0	
149	149	150	164	1	102	0.0	0.0	0.0	
165	1				301	0.0	0.0	0.0	0.0 0.0
166	9				302	0.0	0.0	0.0	0.0 0.0
167	17	176	8		306	0.0	0.0	0.0	0.0 0.0
177	97	180	4		303	0.0	0.0	0.0	0.0 0.0
181	113	184	2		303	0.0	0.0	0.0	0.0 0.0
185	121	187	4		304	0.0	0.0	0.0	0.0 0.0
188	133	190	8		305	0.0	0.0	0.0	0.0 0.0
	5000.0	58310.0	20	6	4	0	25		
1	0.055	0.12			6.00		17.0		
2	0.057	0.15			7.00		18.0		
3	0.062	0.18			10.00		12.0		
4	0.110	0.35			12.00		6.0		
5	0.35	0.45			6.00		5.0		
6	1.45	1.50			15.00		1.0		
1	102.50	15.875	1		12.0	1	0	0	
2	102.50	27.875	1		12.0	1	1	0	0
3	102.50	39.000	2		12.0	1	1	0	0
4	88.75	39.000	2		12.0	1	1	0	0
5	76.75	39.000	2		12.0	1	1	0	0
6	64.75	39.000	2		12.0	1	1	0	0
7	52.75	39.000	2		12.0	1	1	0	0
8	40.75	39.000	2		12.0	1	1	0	0
9	28.75	39.000	2		12.0	1	1	0	0
10	16.75	39.000	2		12.0	1	1	0	0
11	-13.25	39.000	3		12.0	1	1	0	0
12	-33.25	39.000	3		12.0	1	1	0	0
13	-53.25	39.000	3		12.0	1	1	0	0

14	-73.25	39.000	3	12.0	1	1	0	0
15	-93.25	39.000	3	12.0	1	1	0	0
16	-125.35	39.000	4	12.0	1	1	0	0
17	-125.35	-39.000	4	12.0	0	0	0	0
18	102.50	-39.000	1	12.0	0	0	0	0
19	62.40	33.90	5	1.0	1	1	0	0
20	-77.85	33.90	6	1.0	1	1	0	0
1	62.40	33.90		0.0	608.			
2	62.40	-33.90		0.0	608.			
3	-77.85	33.90		0.0	492.			
4	-77.85	-33.90		0.0	492.			
1	102.50	39.00						
2	-125.35	39.00						
3	-125.35	-39.00						
4	102.50	-39.00						
5	5.00	2.50						
6	5.00	-2.50						
7	-5.00	-2.50						
8	-5.00	2.50						
9	78.03	39.12						
10	78.03	28.69						
11	46.78	28.69						
12	46.78	39.12						
13	78.03	-28.69						
14	78.03	-39.12						
15	46.78	-39.12						
16	46.78	-28.69						
17	-62.22	39.12						
18	-62.22	28.69						
19	-93.47	28.69						
20	-93.47	39.12						
21	-62.22	-28.69						
22	-62.22	-39.12						
23	-93.47	-39.12						
24	-93.47	-28.69						
25	0.00	0.00						
3	750.000	0.0	25.00	62.14	0.0	0.0	1.0	

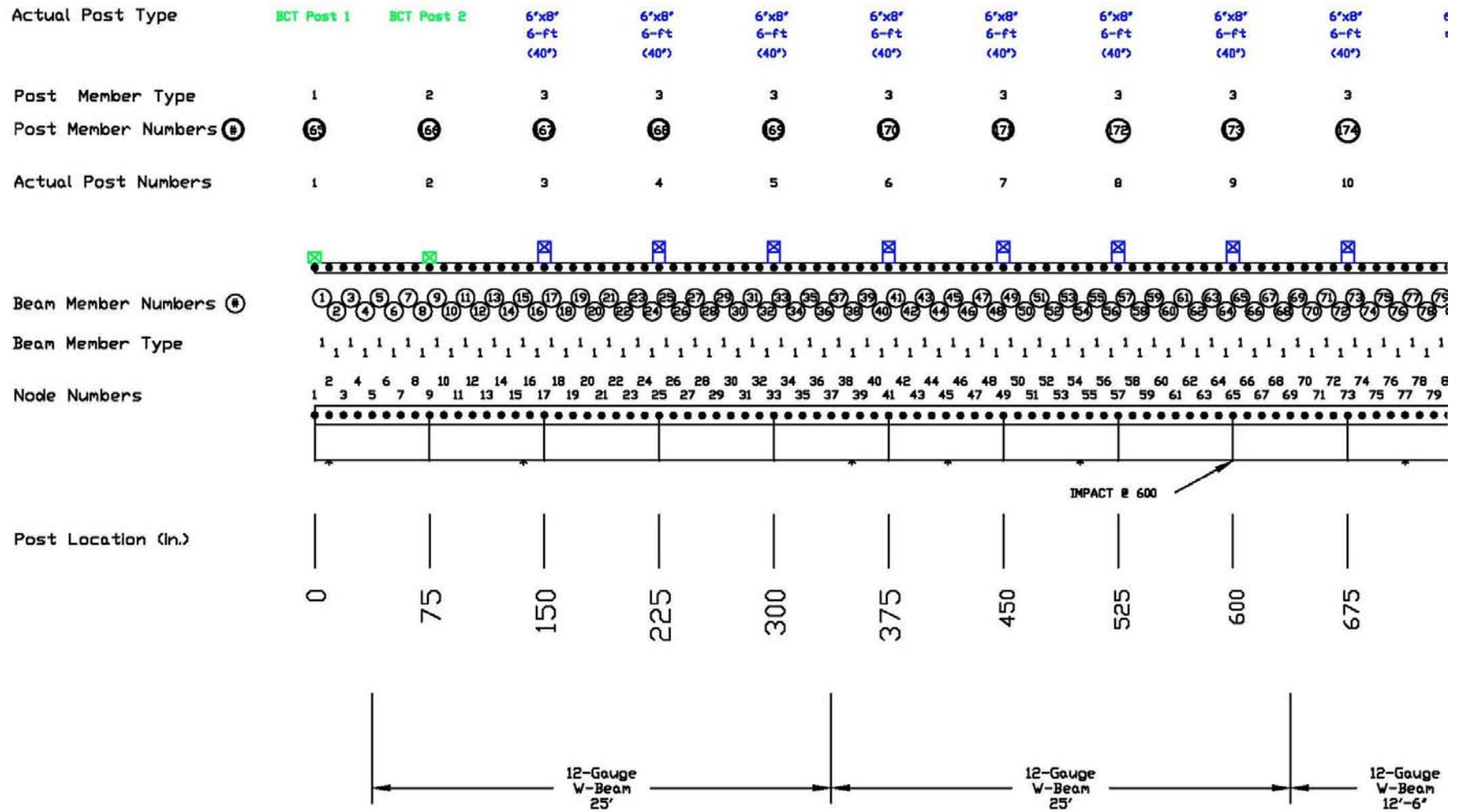


Figure E-1. System Layout Drawing of BARRIER VII Model

Appendix F. Tabulated BARRIER VII Simulation Results

Table F-1. BARRIER VII Results for Calibrated Steel Post Transition Model

Impact Location		Max. Pocket Angle		Maximum Deflection		Worst Case Snag Points				Parallel Time
Node No.	Dist. U.S. of Impact (in.)	(deg.)	@ Node	(in.)	@ Node	Post #	Snag (in)	Post #	Snag (in)	(sec)
81	487.5	22.7	97	32.41	96	97	7.84	-	-	0.258
82	478.125	22.7	97	32.57	96	97	7.78	-	-	0.259
83	468.75	22.6	97	32.68	97	101	7.96	-	-	0.260
84	459.375	22.1	97	32.65	98	101	7.88	-	-	0.259
85	450	21.4	97	32.27	99	101	7.57	-	-	0.258
86	440.625	19.6	106	29.14	100	101	7.13	-	-	0.250
87	431.25	19.9	106	29.41	101	101	6.86	-	-	0.251
88	421.875	20.5	110	29.41	101	105	7.41	-	-	0.253
89	412.5	21.8	110	29.77	103	105	7.65	-	-	0.254
90	403.125	22.3	111	29.74	104	105	7.65	-	-	0.254
91	393.75	23.5	111	29.85	104	105	7.24	-	-	0.252
92	384.375	24.3	112	29.56	105	109	7.07	-	-	0.250
93	375	24.2	111	29.24	106	109	6.83	-	-	0.248
94	365.625	22.6	112	26.78	106	109	6.33	-	-	0.240
95	356.25	22.8	112	26.74	107	109	6.10	-	-	0.238
96	346.875	22.8	113	25.99	107	113	5.77	-	-	0.235
97	337.5	21.6	113	24.46	108	113	5.33	-	-	0.230
98	328.125	21.5	113	23.84	109	113	5.14	-	-	0.228
99	318.75	21.3	113	23.10	110	113	5.55	-	-	0.227
100	309.375	21.5	113	23.01	111	113	5.47	-	-	0.226
101	300	21.0	113	22.35	112	115	5.31	121	2.48	0.224
102	290.625	20.0	113	21.67	112	115	5.58	121	4.14	0.224
103	281.25	19.2	114	21.25	114	117	5.34	121	5.40	0.224
104	271.875	18.2	117	20.50	114	117	5.31	121	5.89	0.222
105	262.5	18.2	117	19.95	116	117	5.65	121	7.19	0.223
106	253.125	17.8	117	19.94	116	117	5.36	121	7.50	0.223
107	243.75	15.9	117	18.45	116	119	5.02	121	7.67	0.219
108	234.375	14.7	117	18.08	117	119	4.62	121	7.53	0.216
109	225	13.9	117	16.79	118	119	4.21	121	7.65	0.214
110	215.625	12.7	117	15.24	118	119	3.68	121	7.63	0.212
111	206.25	11.5	117	14.46	119	119	3.00	121	7.46	0.212
112	196.875	10.9	122	13.84	120	119	2.18	121	7.01	0.211
113	187.5	10.1	123	12.87	122	119	0.92	125	6.68	0.207
114	178.125	9.9	124	12.70	122	-	-	125	6.79	0.205
115	168.75	10.2	126	12.47	123	-	-	125	6.71	0.204
116	159.375	11.5	129	12.28	124	-	-	125	6.27	0.201
117	150	13.8	129	12.14	126	-	-	129	6.48	0.198
118	140.625	16.1	129	12.43	126	-	-	129	6.67	0.195
119	131.25	17.3	129	12.56	127	-	-	129	6.90	0.197
120	121.875	17.7	129	12.54	128	-	-	129	6.78	0.201
121	112.5	17.4	129	12.58	130	-	-	129	6.33	0.207
122	103.125	16.9	130	12.72	130	-	-	129	5.53	0.214
123	93.75	15.9	130	12.20	131	-	-	129	4.46	0.220
124	84.375	14.7	130	11.53	131	-	-	129	2.94	0.224
125	75	13.0	130	10.15	131	-	-	129	0.80	0.224

Table F-2. BARRIER VII Results for Wood Post Transition Model

Impact Location		Max. Pocket Angle		Maximum Deflection		Worst Case Snag Points				Parallel Time
Node No.	Dist. U.S. of Impact (in.)	(deg.)	@ Node	(in.)	@ Node	Post #	Snag (in)	Post #	Snag (in)	(sec)
81	487.5	21.0	97	26.30	94	97	5.80	-	-	0.239
82	478.125	21.1	97	25.93	94	97	6.66	-	-	0.241
83	468.75	21.5	97	26.15	95	97	6.64	-	-	0.242
84	459.375	21.5	97	25.96	96	97	5.99	-	-	0.240
85	450	19.7	97	23.80	97	97	5.67	-	-	0.234
86	440.625	19.0	98	23.79	98	101	5.68	-	-	0.233
87	431.25	18.8	101	23.61	98	101	5.66	-	-	0.235
88	421.875	18.9	101	23.44	100	101	5.87	-	-	0.236
89	412.5	18.7	101	23.33	101	101	5.84	-	-	0.237
90	403.125	18.5	105	23.38	102	105	5.96	-	-	0.237
91	393.75	18.7	106	23.26	102	105	5.82	-	-	0.235
92	384.375	18.6	106	22.79	103	105	5.66	-	-	0.234
93	375	17.1	106	21.23	104	105	5.29	-	-	0.228
94	365.625	18.0	110	21.25	104	105	4.87	-	-	0.228
95	356.25	18.0	110	20.30	105	109	4.74	-	-	0.224
96	346.875	17.0	110	19.02	106	109	4.51	-	-	0.219
97	337.5	17.3	111	18.72	107	109	4.40	-	-	0.217
98	328.125	17.4	111	18.02	108	109	3.99	-	-	0.213
99	318.75	16.8	111	17.13	108	109	3.70	-	-	0.210
100	309.375	17.2	112	16.82	110	113	3.98	-	-	0.209
101	300	16.8	112	16.74	112	113	4.12	-	-	0.209
102	290.625	16.0	112	15.57	111	113	4.30	-	-	0.208
103	281.25	15.9	113	15.36	112	115	4.59	-	-	0.209
104	271.875	15.5	113	15.12	112	115	4.90	121	2.11	0.210
105	262.5	14.9	113	14.56	112	115	4.72	121	3.93	0.210
106	253.125	14.0	113	14.02	114	117	4.62	121	4.92	0.209
107	243.75	13.6	117	13.07	114	117	4.77	121	6.51	0.209
108	234.375	12.8	117	13.01	116	119	4.38	121	6.94	0.209
109	225	12.4	117	12.65	116	119	3.98	121	7.19	0.208
110	215.625	11.7	117	11.92	117	119	3.61	121	7.32	0.206
111	206.25	10.7	117	11.33	118	119	3.02	121	7.32	0.205
112	196.875	9.8	120	10.72	119	119	2.25	121	7.11	0.204
113	187.5	8.7	122	10.01	120	119	1.18	121	6.45	0.202
114	178.125	8.6	123	9.76	122	-	-	125	6.54	0.201
115	168.75	8.8	124	9.54	123	-	-	125	6.74	0.200
116	159.375	8.7	125	9.62	124	-	-	125	6.47	0.199
117	150	9.1	126	9.62	124	-	-	125	6.26	0.200
118	140.625	11.7	129	10.04	126	-	-	129	6.53	0.197
119	131.25	14.2	129	10.61	127	-	-	129	6.71	0.193
120	121.875	15.2	129	10.86	128	-	-	129	6.63	0.195
121	112.5	19.9	129	10.61	130	-	-	129	6.47	0.200
122	103.125	14.7	130	11.20	130	-	-	129	5.69	0.206
123	93.75	14.1	130	11.11	130	-	-	129	4.53	0.214
124	84.375	12.7	130	10.21	131	-	-	129	3.35	0.219
125	75	11.5	130	9.21	131	-	-	129	1.46	0.220

END OF DOCUMENT